UNIVERSITY OF BIRMINGHAM

Metallo-supramolecular cylinders and their peptide conjugates. Synthesis, dynamics and DNA recognition.

Lucia Cardo

A thesis submitted in partial fulfilment of the requirements for the degree of Doctor of Philosophy in Chemistry

University of Birmingham, School of Chemistry

July 2010

Acknowledgements.

I would like to thank my supervisor, Prof. Michael J. Hannon, who gave me the opportunity to join his group for my PhD four years ago. He has always been present for help, suggestions and support and my experience in his group has been very significant for my scientific formation. I wish to thank all the people that I have met in the Hannon group, those who helped me in the past, and those with whom I have shared a great time in the lab in the last years. Particularly, I wish to thank Victoria Sadovnikova for carrying out cell tests and for being such a great and patient 'personal trainer' in Bioscience, and Siriporn Phongtongpasuk for taking care of the PAGE experiments. To all of you my best wishes for a successful future.

I would like to thank the Analytical Department of the School of Chemistry for the technical support received during the last four years, particularly Neil Spencer and Peter Ashton for their availability. A special thanks to Graham Burns, not only for his help in HPLC, but also for his friendship, the countryside pubs and because with him I have met the real spirit of the Midlands.

I have not forgotten that my formation as a chemist started in Italy, and I wish to thank all the people from the Department of Chemistry of the 'Federico II' University of Napoli who have contributed to improve my skills and helped me with important advice. I believe that in Napoli I mainly learnt how to be a chemist and in Birmingham how to be a scientist, and both are necessary aspects.

I wish to thank all the friends from the level 3, 4, 6 and 7 of the Department of Chemistry of the University of Birmingham, with whom I shared lot of laughs, beers, amazing football (played and watched) and barbecues. I am very lucky because I cannot mention all the great people that I have met here and have made my time in Birmingham so unique and unforgettable. But few of them were particularly special for me. Susana, who shared with me fun, tough times, very important moments and was always present for me as only special friends can do. Bhaven, whose sincere friendship, help, support and the simple idea of having him around were extremely important for me. Then I am very glad that I have met Luca and we became so good friends, and I wish to thank him not only for being my 'hero' for every computer issue, but also for sharing with me a lot of inspiring discussions about chemistry, 'complains' about Italian politics and jokes about our future as 'farmers'. And I wish

to thank Mino, for being simply Mino, for the many laughs, chats, dinners and movies shared together.

I wish to thank Carlos and Gino. I can simply say that they have been and they are like family for me, and my life in England would not have been so special without them around me. And my life would not be the same without the love and support of my parents and my sister Mariangela, to whom I wish to dedicate this work. A last thought goes to my city, Napoli, and saying this I mean people, culture, art, spirit. All this is part of me, my origins and my strength, and it will always be with me wherever I go.

Declaration.

The experimental work, observations and recommendations reported in this thesis are those of the author unless specifically stated and have not previously been submitted as part of a degree at the University of Birmingham or any other institution.

List of papers published from this Thesis.

1. Design and DNA-binding of metallo-supramolecular cylinders conjugated to peptides. L. Cardo and M. J. Hannon *Inorg. Chim. Acta* **2009**, 362, 784-792.
2. Understanding the dynamic behaviour of the di-nuclear Fe(II) supramolecular cylinder. L. Cardo, C.L. Painting and M.J. Hannon (*manuscript to be submitted*).
3. Arginine residues conjugated to di-nuclear Fe(II) cylinders mediate the diastereoselectivily of the hybrids and improve their DNA binding and cytotoxicity. L. Cardo, V. Sadovnikova, S. Phongtongpasuk and M.J. Hannon (*manuscript to be submitted*).
4. Probing the interaction of imine based supramolecular cylinders with TRISPHAT using NMR. C.R. Pearmund, L. Cardo, F. Tuna, J. Lacôur and M.J. Hannon (*manuscript to be submitted.*).

Contents

Abbreviations.

3WJ	Three way junction
Arg	Arginine
bipy	2,2'-bipyridine
bp	base pairs
br	broaden
CD	Circular Dichroism
CD_3CN	Acetonitrile-d_3
CD_3OD	Methyl-d_3 alcohol-d
chrysi	chrysene-5,6-quinone diimine
ct	calf thimus
d	doublet
ΔG‡	Free energy of activation
DCM	Dichloromethane
dd	double doublet
DIEA	N,N’-diisopropylethylamine
DMEM	Dulbecco’s modified Eagle's medium
DMF	Dimethylformamide
DNA	Deoxyribonucleic acid
DMSO	Dimethyl sulfoxide
D_2O	Deuterium oxide
dt	double triplet
EDTA	Ethylenediaminetetracetic acid
EEDQ	2-Ethoxy-1-ethoxycarbonyl-1,2-dihydroquinoline
EI-MS	Electronic Impact Mass Spectrometry
ESI-MS	Electrospray Ionisation Mass Spectrometry
Et_2O	Diethyl ether
EtOAc	Ethyl Acetate
EtOH	Ethanol
FBS	Foetal bovine serum
Fmoc	Fluorenylmethyloxycarbonyl
FTIR	Fourier Transform Infrared
Gly	Glycine
HEPES	4-(2-hydroxyethyl)-1-piperazineethanesulfonic acid
HMBC	Heteronuclear Multiple Bond Correlation
HMG	High Mobilty Group
HP	Hydrogen peroxide
HSQC	Heteronuclear Single Quantum Coherence
HBTU	2-(1H-Benzotriazole-1-yl)-1,1,3,3-tetramethylaminium hexafluorophosphate
HRMS	High Resolution Mass Spectrometry
Hz	Hertz

IC_{50}	half maximal inhibitory concentration
ICD	Induced Circular Dichroism
ILD	Induced Linear Dichroism
K	Kelvin
λ_{max}	maximum of wavelength
LD	Linear Dichroism
m	medium (in IR data)
m	multiplet (in NMR data)
MeOH	Methanol
MLCT	Metal to Ligand Charge Transfer
MTT	3-(4,5-Dimethylthiazol-2-yl)-2,5-diphenyltetrazolium bromide
NMR	Nuclear Magnetic Resonance
phen'	5-(amidoglutary1)-1,l0-phenanthroline
phi	9,l0-phenanthrenequinone diimine
phzi	benzo[*a*]phenazine-5,6-quinone diimine
PBS	Phosphate Buffered Saline
PCR	Polymerase Chain Reaction
PNA	Peptide Nucleic Acid
ppm	parts per million
py	pyridine
rac	racemic
R,R-Me_2trien	2R,9R-2,9- diamino-4,7-diazadecane
RNA	Ribonucleic acid
RP-HPLC	Reverse Phase High Performance Liquid Chromatography
Rt	Room Temperature
R_T	Retention time
s	singlet (NMR data)
s	strong (IR data)
Ser	Serine
t	triplet
tBu	tert-Butyl
td	triple doublet
Tc	Coalescence temperature
terpy	2,6-bis(2-pyridyl)pyridine
TEA	Thriethanolamine
TFA	Trifluoroacetic acid
TIS	Triisopropylsilane
TRISPHAT	*tris*(tetrachlorobenzenediolato) phosphate(V)
UV-vis	Ultraviolet-visible spectroscopy
vt	variable temperature
w	weak

Abstract

The work described in this thesis focuses on two main topics: i) the study of the dynamic behaviour of metallo-supramolecular cylinders, that are known for their major groove DNA binding properties, and ii) the synthesis and DNA binding studies of the cylinders conjugated to short peptides and amino acids. In Chapter 1 an overview of the DNA molecular recognition by synthetic agents and biomolecules is presented, with a section dedicated to the selective recognition of DNA.

In Chapter 2 the study of the dynamic behaviour of the Fe(II) supramolecular cylinder is explored. The behaviour of the complex at variable temperature conditions was analysed by NMR, UV-Vis and CD. Thermal experiments with the complex in the presence of DNA are also presented.

In Chapter 3 a versatile procedure for the conjugation of short amino acids and peptides to Fe(II), Cu(I) and Ag(I) cylinders has been established and the influence of the attached peptides on the chirality of the resulting hybrids has been investigated.

In Chapter 4 the DNA binding properties of the conjugated cylinders are explored by CD, LD and gel electrophoresis experiments and the cytotoxic activity of the Fe(II) conjugates against cancer cell lines was investigated by MTT tests.

CHAPTER 1

DNA RECOGNITION.

During the last 50 years, following the initial studies that established DNA and RNA structures[1-5], great efforts in the scientific world have been focused on achieving a greater knowledge about 'how' the information in DNA encodes all the biological events in any living organism. Such knowledge requires understanding of the structures, functions, interactions, and evolutions of all the genes composing a genome. New branches of molecular biology, such as genomics, proteomics and genetic engineering, have been introduced and have exponentially developed such that in just a few decades big scientific aims, such as the "Human Genome Project", have been solved. In this context, the parallel and rapid expansion of informatic technologies has been crucial, giving origin to new methodologies such as bioinformatics, which is one of the major tools used in analysing and processing data from genomics and proteomics.

Now, in the post genomic environment, the goal is to understand the processing of the genetic code and 'how' to stimulate, manipulate or prevent this processing. In this context the study of DNA recognition is an interesting and widely explored approach, because it offers potential for controlling gene expression, creating new therapeutic and diagnostic devices, and investigating molecular recognition in general.

1.1 Structural properties of DNA.

DNA is composed of polymers whose monomeric units are called *nucleotides*. Each nucleotide is composed of a five-carbon sugar (2'-deoxyribose), one phosphate group attached to the 5' position of the sugar and one nitrogenous base, of purine or pyrimidine nature, attached to the 1' position of the sugar (Figure 1.1.a)). Only four bases are part of the nucleotides of the DNA: adenine (A) and guanine (B) (the purine bases), cytosine (C) and thymine (T) (the pyridine bases). Usually, each nucleotide is identified by the base that is attached to it. The nucleotides are joined together to form a chain by formation of phosphodiester bonds between the third and

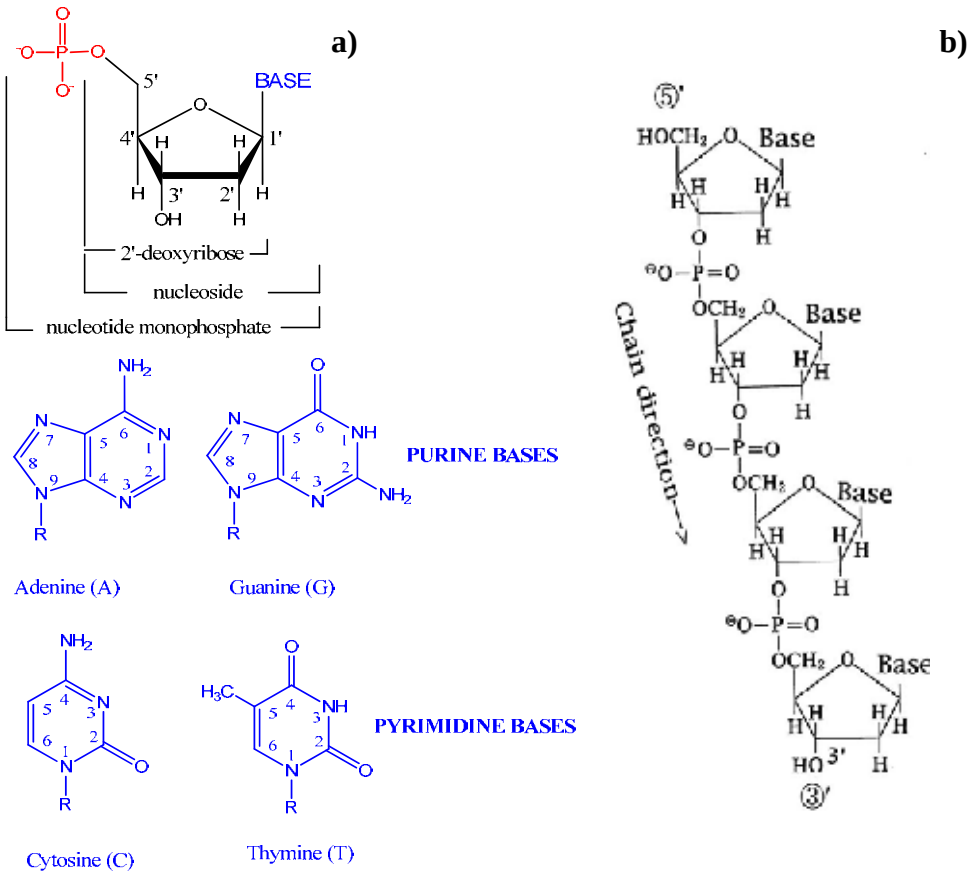

Figure 1.1. a) Composition of the nucleotides with the IUPAC numbering system given for the sugar and bases[6]. **b)** A chain of polymeric DNA.

fifth carbon atoms of adjacent sugar rings (Figure 1.1.b)). One chain of DNA with a given sequence of nucleotides is the *primary structure* of the DNA. In living organisms, DNA rarely exists as single strands, but it is organised in double stranded or "duplex" *secondary* structures. In these structures the two strands wrap around each other forming a double helix with the phosphate groups directed to the external hydrophilic environment. The bases are directed to the heart of the helix and a specific pattern of hydrogen bonds between base pairs is formed. This is also known as *complementary* or *Watson-Crick base pairing*, in which A interact with T and G with C (Figure 1.2). The base pairs are approximately perpendicular to the axis of the double helix and they are stacked parallel to each other, forming face-face π–π interactions. Grooves are traced between the two twisting strands of the helix, but the two strands are not directly opposite to each other along the hydrogen bonds vector so that the two grooves have different sizes. In fact they are known as the

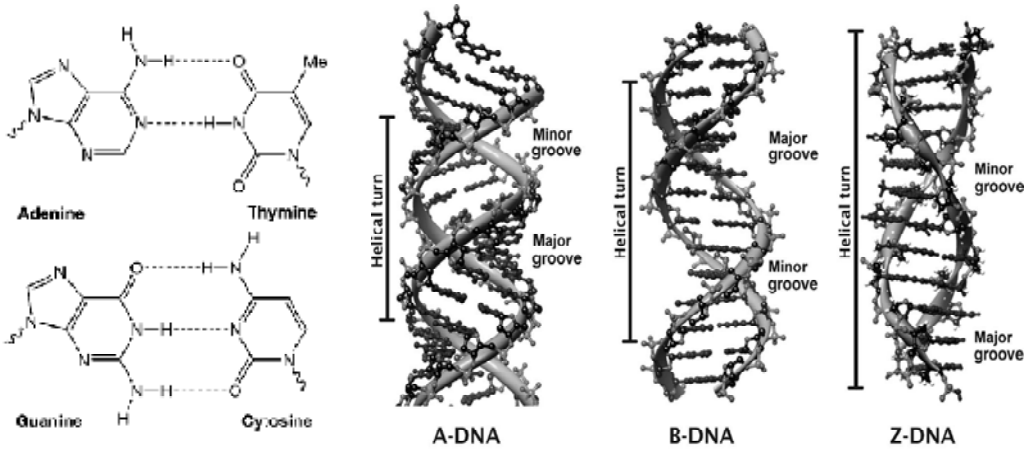

Figure 1.2. The Watson-Crick hydrogen bond patterns between base pairs (left) and the three known structures of double helix, A, B and Z-DNA (right). Figure adapted from ref. [7]).

	DNA form		
Structural Characteristic	A	B	Z
Helical sense	Right-handed	Right-handed	Left-handed
Diameter	25.5 Å	23.7 Å	18.4 Å
Repeating unit	1 bp	1 bp	2 bp
Rotation per repeating unit (t_g)	32.7°	35.9°	-60°
bp* per turn (mean)	10.7	10.5	12
Tilt of bp relative to helical axis	+19°	-1°	-9°
Rise/bp along axis	2.56 Å	3.38 Å	3.71 Å
Pitch/turn of helix	28.2 Å	35.5 Å	44.6 Å
Mean propeller twist	+18°	+16°	0°
Minor groove	Wide and shallow	Narrow and deep	Narrow and deep
Major groove	Deep and narrow	Deep and wide	Shallow

Table 1.1. Structural parameters of the three principal conformation of DNA (adapted from reference [8]).
* *base pairs*

major and *minor* groove.

There are three types of DNA double helix that have been crystallised, known as A, B and Z-DNA (right of Figure 1.2). A and B-DNA are right-handed helices whilst Z-DNA is left-handed. Some of the structural parameters that differentiate the three

structures are reported in Table 1.1. 90% of the DNA in living organisms is in B conformation and molecules of water and different cations (especially K^+ and Na^+) are also involved in this structure. Z-DNA has also been observed in living cells,[9-12] whilst it seems that the DNA can assume the A conformation at low levels of hydration, as during a crystallographic experiment, or when forming certain hybrids with RNA.[13]

Alternative conformations of DNA also exist and in some cases have important biological roles. *Quadruplex DNA* or *G quadruplexes* are four stranded structures formed by G rich strands of DNA. These structures are stabilized by sets of Hoogsteen hydrogen bonds between guanines and the interaction with positive cations (especially K^+) located at the heart of the tetrads (Figure 1.3).[14-20] Great interest is now focused on G quadruplex since they have been found in telomeric DNA at the end of the chromosomes and involved in DNA replication. *DNA Triple-helix* formation is possible between a homopyrimidine-homopurine Watson-Crick duplex and a third strand of DNA, either pyrimidine or purine rich, that lays in the major groove of the former duplex. The third strand forms Hoogsteen or reverse Hoogsteen hydrogen bonds if it is pyrimidine or purine rich respectively (Figure 1.4.a)). A possible biological role of triplex DNA has emerged in the area of gene regeneration.[21,22] Several *branched* DNA structures are also possible and play important biological functions.[23-25] The simplest example involves only three strands of DNA and it is known as DNA *three way junction* or *Y-shaped junction* (Figure 1.4.b).[25,26] This conformation is possible when the two strands of a fragment of duplex DNA present frayed ends (non complementary sequences) so that the pairing between bases cannot occur. But a third strand that is complementary to the frayed ends of the duplex can stabilise the formation of a three way junction structure. These assemblies are formed transiently during DNA replication (replication fork)[27,28] and they are very common RNA structures;[29-31] they are also associated with some human genetic diseases, such as myotonic dystrophy type 1 and Huntington's disease;[32] they are present in the inverted terminal repeats of certain viral genomes and are intermediates during phage genetic recombination.[33-35] *Four way junctions*, also known as *Holliday junctions* (Figure 1.4.c)) are the key intermediates in nearly all recombination process,[36,37] whilst higher levels of branched DNA are not so common in cells but they are widely employed in

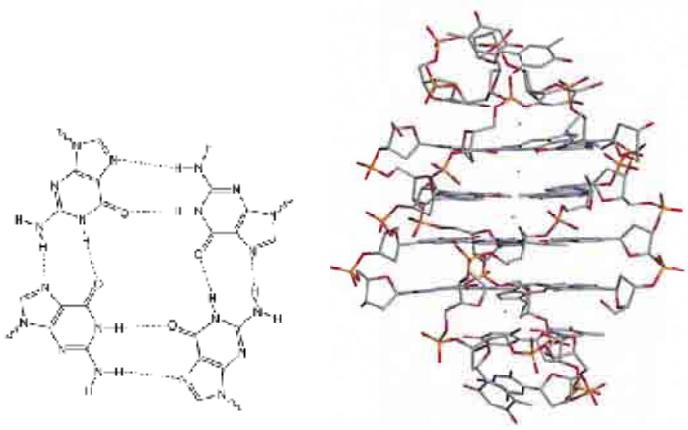

Figure 1.3. Hoogsteen hydrogen bonds between guanine bases and an example of G-quadruplex structure (X-ray, PDB ref. 1JPQ) with stacked sets of square arrangement of guanines and five potassium ions in the centre of the structure (Figure taken from ref. [18]).

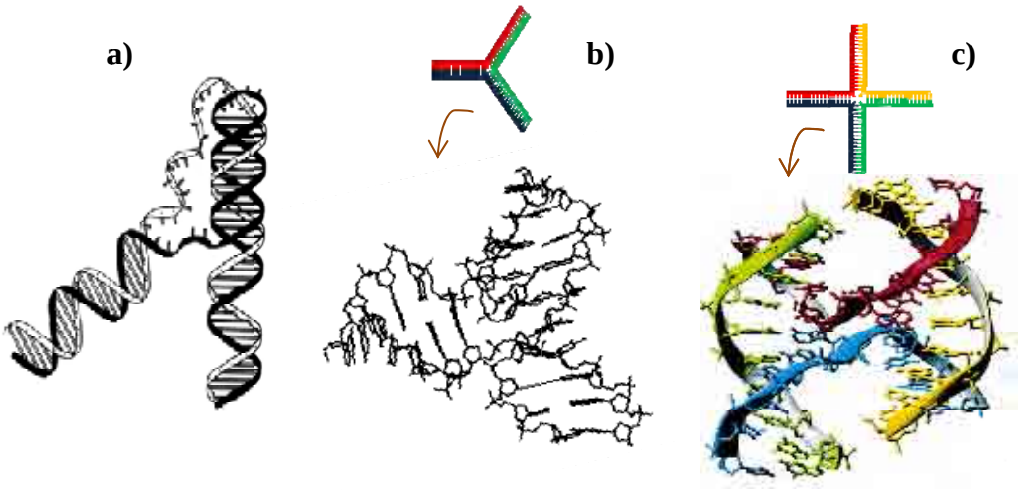

Figure 1.4.a) Model of an intramolecular triplex (figure taken from ref. [22] Example of structures of **b)** a three way junction (by NMR, figure taken from ref. [26]) and **c)** a Holliday junction (by X-ray, figure taken from ref. [36]).

nanotechnology.[38]

Errors in the replication process or external influences may cause further modifications of the Watson-Crick double strand. *Mismatched base pairs* are relatively common and occur when non complementary base pairs are opposite within a double helix and are forced to form hydrogen bond interactions that are less stable than hydrogen bonds between complementary bases (Figure 1.5.a)).[39,40]

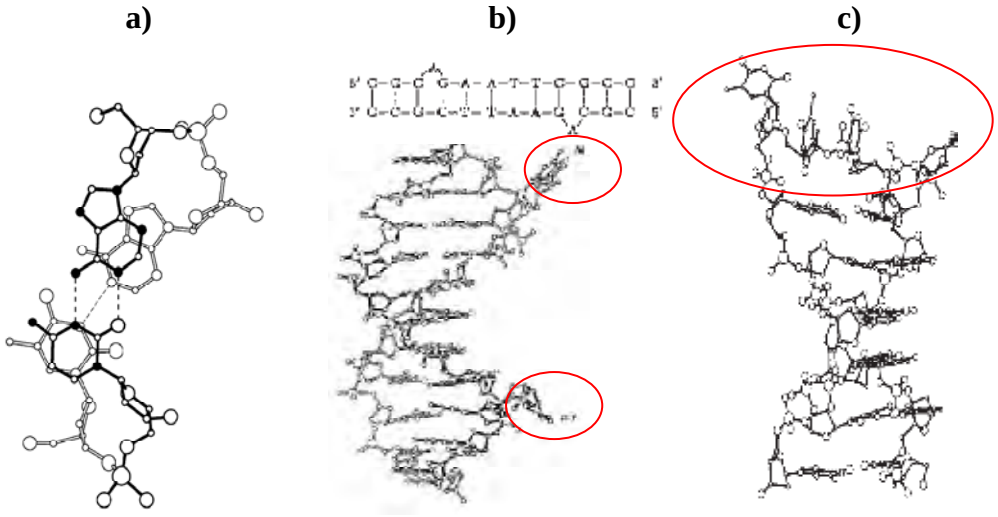

Figure 1.5. Crystallographic structures **a)** including a A-C base pair mismatch (structure taken from ref. [40]); **b)** of the tridecamer d(CGCAGAATTCGCG)$_2$ showing the extra adenosine looped out (structure taken from ref. [41]); **c)** of the hairpin conformation of the hexadecanucleotide CGCGCGTTTTCGCGCG (structure taken from ref. [42]).

Bulged double helixes are stretches of extra bases, within the double helix, that do not have the complementary stretch in the opposite strand so that are looped out of the duplex (Figure 1.5.b)).[41] Formation of *hairpin loops* can occur upon DNA intermolecular base pairing, although this is a very common characteristic of RNA (Figure 1.5.c).[42]

1.2 DNA recognition in biological systems.

All the necessary information for the life, functions and death of a living cell is mainly included in fragments of B-DNA (*genes*), inside the cell itself. Each gene contains specific instructions in the form of a "code" made of sequences of base pairs. The processing of an instruction occurs upon specific recognition events and "reading" of the corresponding code. DNA recognition is not only the basis for gene expression, but also the way in which possible genetic errors are identified and repaired. For this reason the understanding of the molecular recognition of DNA with other molecules, both biomolecules and synthetic agents, is the base for the discovery of new approaches to mimic such recognition or interfere with it.

Within biological systems, sequence specific code recognition is generally

achieved by particular surface motifs of proteins; the most important structures are the helix-turn-helix motifs, the zinc-fingers, the zipper motifs, the β-sheets and the β-hairpins.[43] More rarely, other biomolecules can recognise DNA, including oligonucleotides which can bind in the major groove forming DNA triplexes, as explained above. Since the 'reading' of the DNA involves a large number of non specific and specific DNA-binding proteins, DNA-protein interactions have been the objective of many studies.[44-48] Structural information is now available on over 400 distinct DNA-protein complexes, from a wide range of eukaryotic and prokaryotic sources, but this is a relatively small number compared to the total protein encoded by individual genomes. The determination of the human genome sequence in 2001[49] has led to estimate that of the ca. 30000 proteins in total, ca. 2300 are involved in nucleic acid binding, of which 6% are expected to be transcription factors.

The wide diversity of functions of DNA-binding proteins is in contrast with the relatively few ways that they use to interact with the DNA itself. Principally DNA-protein recognition occurs by non-covalent contacts, such as hydrogen-bonding, Van der Waals, hydrophobic and electrostatic interactions. Usually proteins bind DNA in the major groove, because it contains a higher number of possible H-bond interacting sites and more variety in the bases sequence, and because its dimensions are well-matched to hosting protein structural motifs. Nonetheless, the minor groove is also an important target for some regulatory and structural proteins. Indirect readout can also occur via the sugar-phosphate backbone or solely the phosphate group. Indeed, even when the phosphate groups do not participate directly in the binding with proteins, they provide DNA with an anionic nature which makes the whole structure a target for basic side chains, and the resulting electrostatic interactions are significant contributors to overall protein-DNA binding. Van der Waals interactions and water-mediated hydrogen bonds are recurrent themes in protein-DNA contacts, but usually they are not involved in any selective recognition event although they display an important role in stabilising the complexes.[50,51]

Although a very complicated combination of factors contributes in each gene recognition event, the *direct* DNA-protein contacts occur mainly through hydrogen bonds between amino acids side chains and the edges of the base pairs, involving their pattern of donor acceptors molecules.[52] The majority of interactions involve the O6 and/or N7 atoms of guanine bases forming hydrogen bonds with the charged ends

	Guanine	Cytosine	Adenine	Thymine
Arginine	98	8	19	24
Lysine	30	6	4	9
Serine	12	2	1	3
Asparagine	7	10	18	7
Glutamine	6	2	16	2
Glutamate	1	10	1	0

Table 1.2 Distribution of amino acid-base interactions observed from the analysis of a data set of 129 structures of protein-DNA complexes. For example 98 contacts between arginine and guanine have been observed (table adapted from ref. [52]).

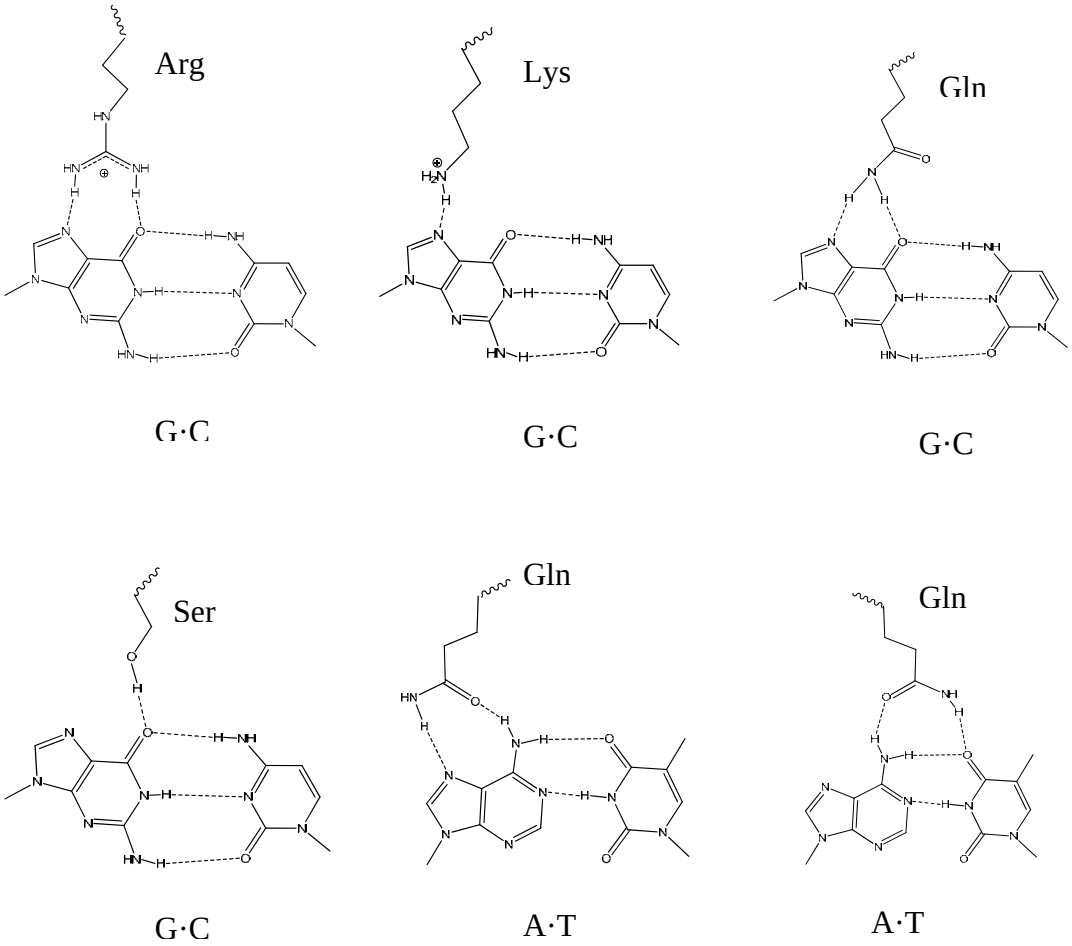

Figure 1.6. Examples of hydrogen-bonding patterns which can be observed in amino acid-base pairs interactions.[52]

of long flexible side chains from the basic residues arginine or lysine, the amide residues glutamine and asparagines or the hydroxyl group of a serine.[48,50,53-55] Table1.2 shows the distribution of amino acid-base interactions and Figure 1.6 some examples of observed patterns of hydrogen-bonding interactions.[52] Although table 1.2 shows that just few amino acids are the most recurrent in DNA-protein contacts, there is not a one-to-one correspondence between specific amino acid residues and a base pairs, and in addition to the simple mono or bidentate interactions as the type showed in Figure 1.6, many other type of interactions are also possible.

From the many DNA-protein complexes investigated, a few general characteristics have been understood concerning the nature of the interactions that can occur and the structures of the most recurrent DNA-protein complexes. But it is also understood that each gene recognition event involves a very complex combination of numerous factors: amino acid sequences, DNA base sequences, their reciprocal positions (that depend on DNA and protein motifs folding), the position of amino acids side chains in respect of the sugar backbone, molecules of water and different ions. All these are variables whose combination in space and time contributes to the uniqueness of each recognition event and any attempt of mimic or reproduce these systems is extremely difficult.

1.3 DNA-drug recognition.

Synthetic molecules that can act on the DNA and can modulate DNA processing have a great potential especially for the development of new drugs. The activity of a large number of clinically important drugs and antibiotics is based on the interaction with DNA and the subsequent inhibition of its template function. Since the 1960s it is known that there are essentially five distinct ways in which existing synthetic agents can bind the DNA:[7,56,57]

1. Binding covalently or through coordination bonds to DNA.
2. Interacting with DNA by a process termed *intercalation*.
3. Binding in the major groove, often with the formation of hydrogen bonds to the bases.
4. Binding in the minor groove, via hydrogen bonds with the bases.
5. Binding to the sugar-phosphate backbone.

Using any of these modes, the drug disturbs the natural interactions present in the Watson-Crick double helix (such as the hydrogen bonding of the base pair or the regular arrangement of the sugar-phosphate back bone), causing abnormal uncoiling or irregular bending and coiling in the DNA. As a result replication and/or transcription can be affected.

The modes of DNA binding described above concern mainly B-DNA, which is the most abundant conformation in cells. However, much interest now focuses on drugs able to target other DNA structures, such as quadruplex, triplex and junctions. These synthetic agents are potentially very selective since these structures occur only in specific times and/or parts of the genome in a cell.

1.3.1 Covalent bonding drugs.

Several drugs inhibit DNA replication and transcription forming covalent bonds or coordination bonds with DNA bases, usually involving nitrogen atoms of the bases. Pt(II) based drugs use this kind of interaction and they are among the most important antitumor compounds. Particularly, cis-platin was introduced in the clinic in 1978 and today it is still one of the leading compounds in cancer treatment.[58-64] Out of thousands of synthesized and evaluated Pt(II) complexes, only cis-platin and two other cis-platin derivatives, carboplatin and oxaliplatin, have been approved for worldwide clinical practice. Other cis-platin derivatives have been clinically approved as anticancer agents only in Japan (nedaplatin), China (lobaplatin) and South Korea (heptaplatin) (Figure 1.7).

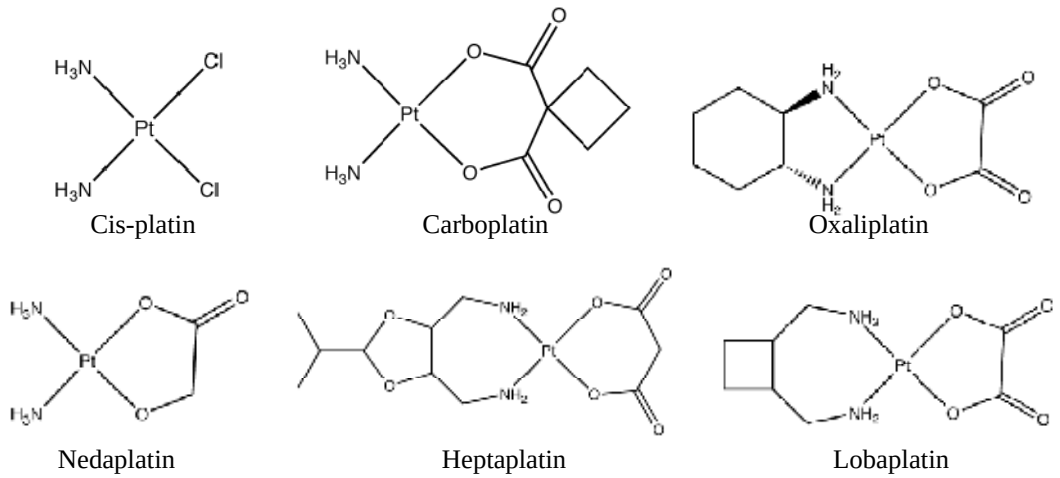

Figure 1.7. Cis-platin and its derivatives.

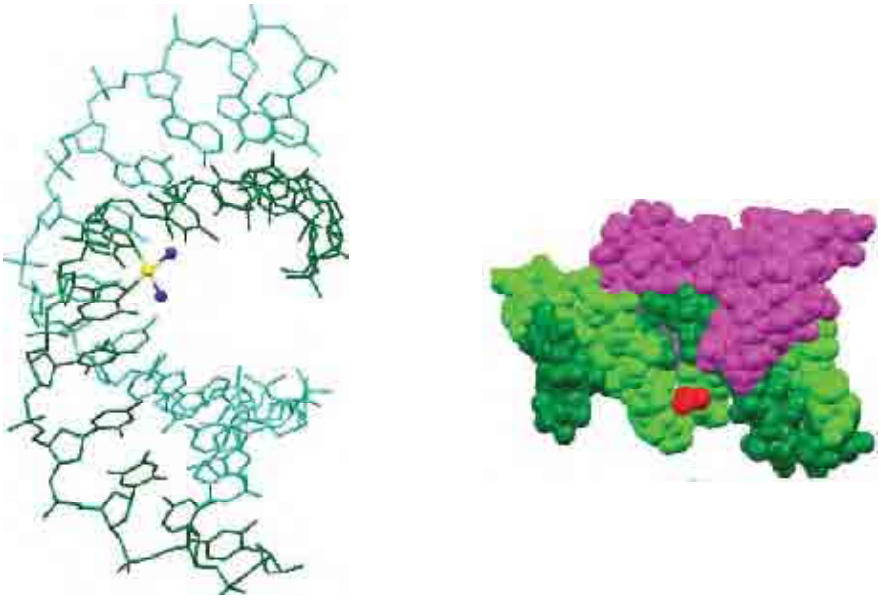

Figure 1.8. Bending of the DNA upon interaction with cis-platin (left, PBD ref. 1AIO, figure taken from ref. [63]) and DNA (green)-cis-platin (red) adduct recognised by the HMG ptotein (pink) in the major groove (right, PBD ref. 1CKT, figure taken from ref. [64])

When cis-platin binds to DNA, the two chlorides are displaced and the Pt(II) centre forms metal-coordination bonds with the N7 of two adjacent purine DNA bases (with a strong preference of G over A) on the same strand. This binding cause a bend of DNA of ~45 degree that affects the DNA functionality and that is recognised by the HMG proteins which bind the lesion and "protect" it from repair mechanisms (Figure 1.8). In general, many metallo-drugs that are today under clinical investigation (especially Pt and Ru based compounds) base their action on the formation of coordination bonds with purine bases upon displacement of one or two of the ligands of the first coordination sphere (ref. [59] and references therein).

Among organic compounds, chlorambucil[65,66] (Figure 1.9.a)) is a chemotherapy drug used for the treatment of lymphocytic leukemia, ovarian and breast carcinomas and Hodgkin's disease, often in combination with other drugs. It belongs to nitrogen mustards compounds[67] also known as DNA 'alkylating agents' because they cause alkylation of the nitrogen bases. Chlorambucil causes alkylation of the N7 of guanine bases. Other important examples of alkylating agents are the (+)CC1065 (whose clinical use in chemotherapy was abandoned due to its side effects) and its derivatives. The pyrrolidine ring subunit of (+)CC1065 forms a covalent bond with

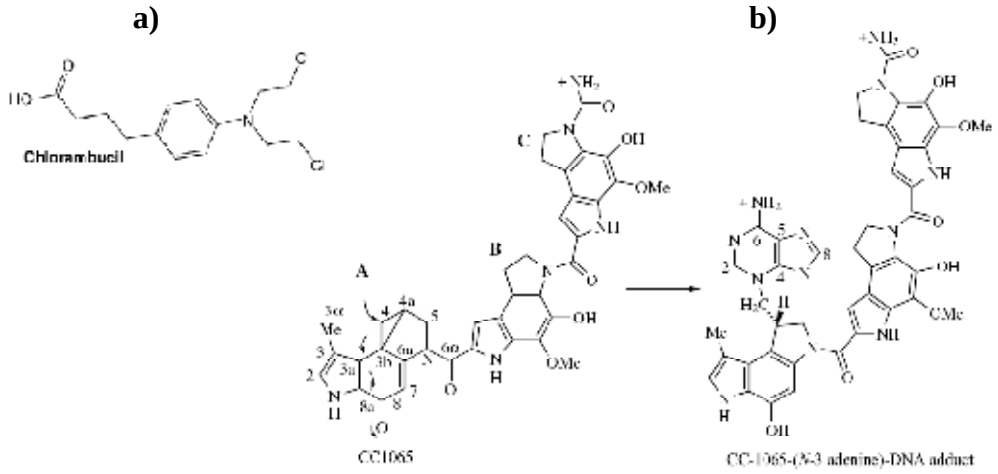

Figure 1.9. a) Chlorambucil. **b)** Structures of CC1065 and its adenine adduct. The natural drug assumes the (+) conformation at the C4a chiral centre. The synthetic enantiomer, (-)-CC1065, has different biological activity. The cyclopropane ring in subunit **A** opens on adduct formation, according to the mechanism indicated by the arrows (figure adapted from ref. [7]).

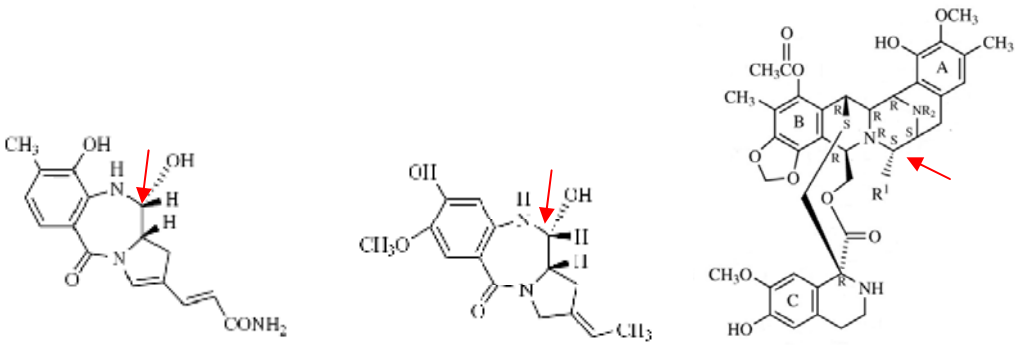

Figure 1.10. Structures of anthramycin (left), tomaymicin (centre) and ecteinascidins (right). Red arrows indicate the carbon atoms involved in the alkylation of the guanine residues.

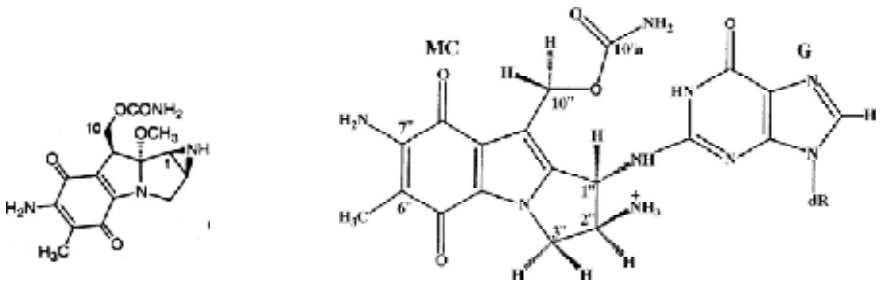

Figure 1.11. Structures of mitomycin C (MC) (left) and a monoalkylation adduct of MC with guanine (figure adapted from ref. [68]).

the adenine N3 upon opening the cyclopropane ring (Figure 1.9.b)).[69,70] Anthramycin, tomaymycin (belonging to the family of chemicals classified as pyrrolo[1,4]-benzodiazepines)[71] and ecteinascidins (Ets)[72] are anticancer drugs that form covalent bonds with the N2 (amine) of guanine residues in the minor groove (Figure 1.10). Mitomycins are a class of antitumor antibiotics currently in clinical use and over 1000 analogous have been studied (mitomycin C (MC) is shown in Figure 1.11). These compounds also bind the N2 of guanines, but unlike other drugs, they are reductive alkylating agents. Thus, a one-electron reduction produces a mono- functional adduct, whereas a two-electron reduction yields a bifunctional adduct with DNA (Figure 1.11).[68,73-75]

1.3.2 Intercalators.

The concept of *intercalation* was pioneered by Lerman during the 1960s.[76] During those years it was observed that polycyclic aromatic ring molecules, such as acridine dyes, can be sandwiched (intercalated) in the gap between two base pairs of the DNA double helix, forming face-face π–π interactions with the heterocyclic rings (above and below) of the base residues. Positive charges, usually present on intercalators, reinforce the binding with the DNA by ionic interaction with negatively charged sugar-phosphate backbone (Figure 1.12). The insertion of the drug between two bases causes an opening up of the gap and an unwinding effect of the twisted helix. Usually the maximum loading of an intercalator is one per two gaps of the helix, thus the free gap between the two loaded gaps ensures the necessary space for the elongation and the unwinding of the helix. Intercalating compounds are very popular as antibacterial and anticancer drugs. Together with the acridine dyes cited above, daunomycin, doxorubicin, and thalidomide are also very important *organic intercalators* employed in cancer therapy [77-79] and ethidium bromide is one of the most common fluorescent tag (nucleic acid stain) that are used in molecular biology[80] (Figure 1.13). With a similar principle of interaction, organic intercalators such as dibenzophenanthrolines and diazoniapolycycles (Figure 1.13) have been recently employed to selectively stabilise other DNA structures such as triplex-DNA.[81,82]

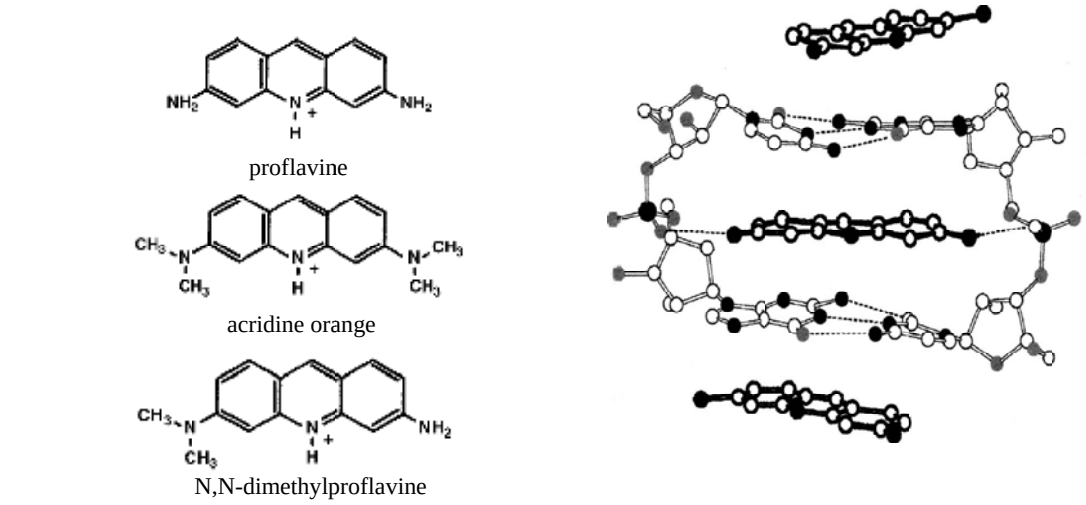

Figure 1.12. Examples of acridine dyes (left) and crystal structure of proflavine–d(CpG). The nitrogen and phosphorus atoms are black, and oxygen atoms are stippled. The dotted lines represent hydrogen bonds (figure adapted from ref. [83]).

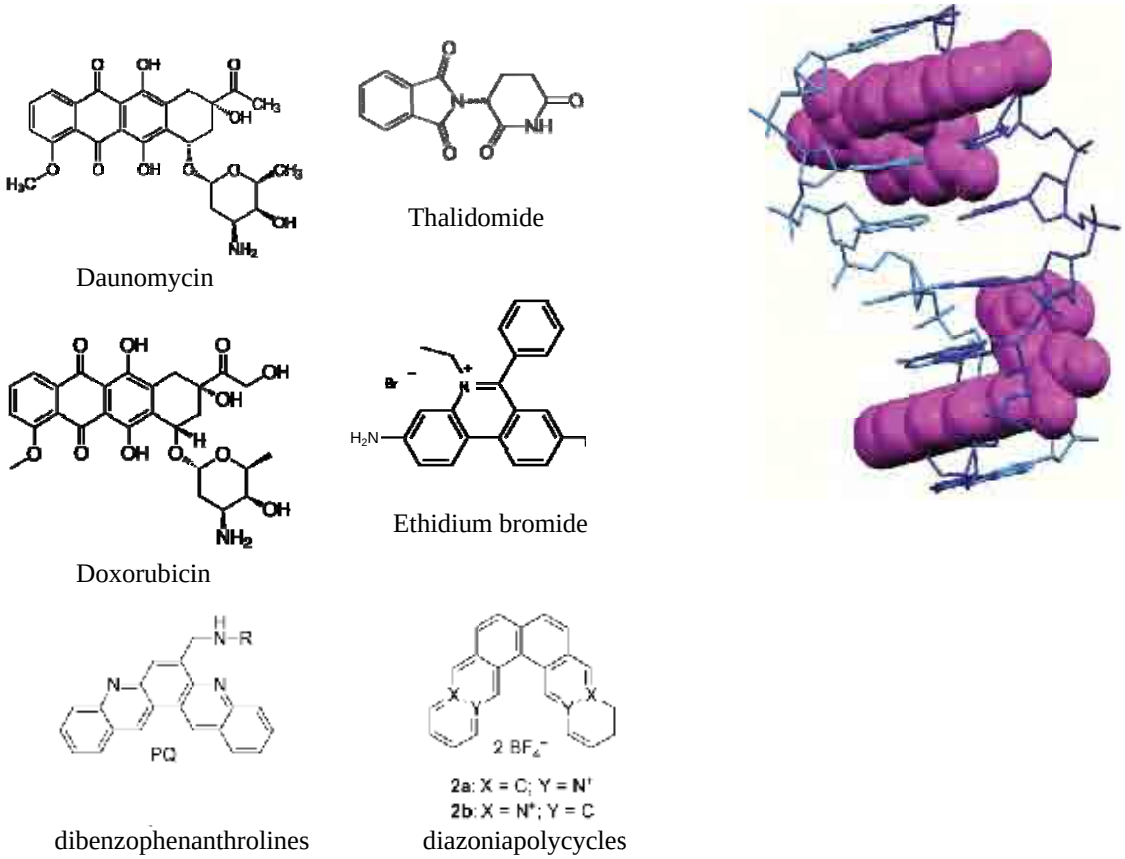

Figure 1.13. Organic intercalating drugs (left) and the X-ray structure of a DNA oligonucleotide with two doxorubicin drugs intercalated between the base pairs, with insertion from the minor groove side (right, PDB ref. 1D12, figure adapted from ref. [78]).

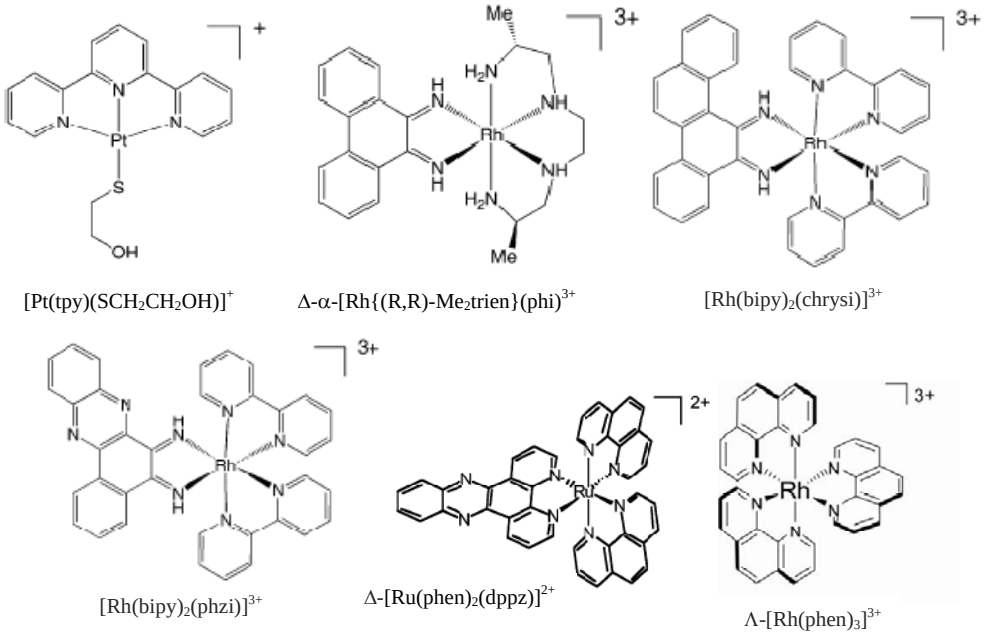

Figure 1.14. Examples of metallo-intercalators.

The idea of combining the properties of intercalating drugs with the use of transition metal complexes has led to the development of the class of *metallo-intercalator* agents. These compounds are stable, inert and water-soluble, and contain spectroscopically active metal centres. In this way, the positive charge imparted by the metal facilitates the interaction with the negative DNA backbone and the presence of the metal can provide the compound with additional properties. .[84-88] For example the luminescence of Ru(II) and Rh(III) based intercalators makes these compounds useful as probes of biological systems, whilst metal centres with oxidising properties (photo induced as in rhodium or chemically induced as in copper) impart DNA cleavage activity. Numerous synthetic intercalators based on metallo-complexes have been investigated and few representative examples are shown in Figure 1.14.[89-94] The terpyridine-Pt(II) complex $[Pt(tpy)(SCH_2CH_2OH)]^+$ was the first metallo-intercalator reported by Lippard.[95,96] Particularly intense has been the activity of Barton and co-workers in this field, especially concerning the study of Rh(III) and Ru(II) intercalators (Figure 1.15 a)).[89] Interestingly, Barton and co-workers demonstrated that is possible to design the size and the shape of the ligand in a way to exclude intercalation in the Watson-Crick duplex and target alternative structures. For example $[Rh(bipy)_2(chrysi)]^{3+}$ and $[Rh(bipy)_2(phzi)]^{3+}$ are

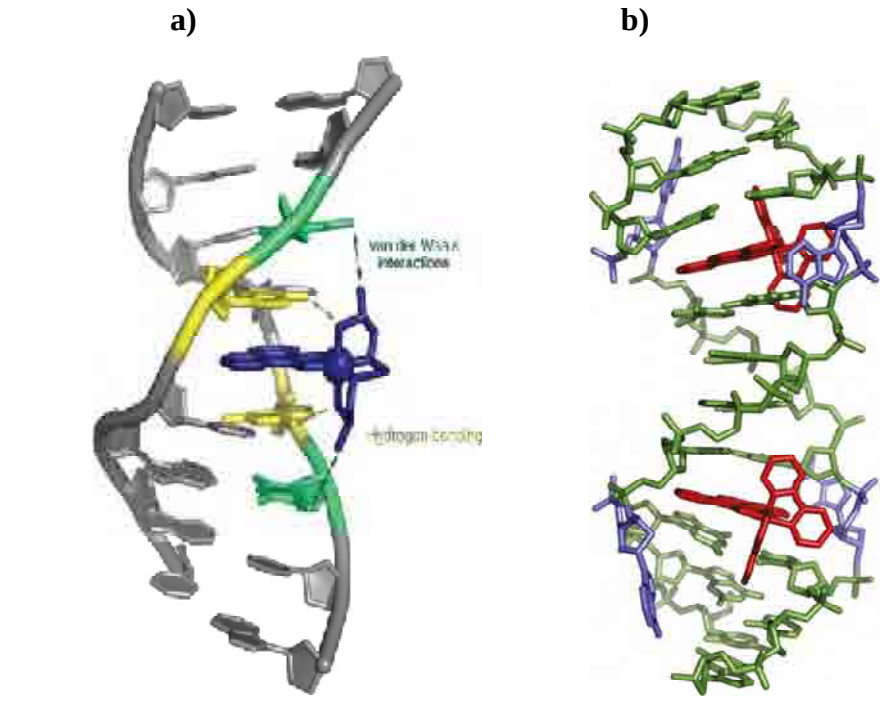

Figure 1.15.a) Crystal structure of Δ–α–[Rh{(R,R)-Me_2trien}(phi)]$^{3+}$ bound to its target sequence 5'-TGCA-3' (PDB ref. 454D, figure taken from ref. [89]) **b)** Crystal structure of two Δ-$Rh(bpy)_2(chrysi)^{3+}$ molecules (red) are inserted, one in each AA mismatch of oligonucleotide 5'-CGGAAATTACCG-3' (green). The ejected adenosines are coloured blue (PDB ref. 3GSK, figure taken from ref [97]).

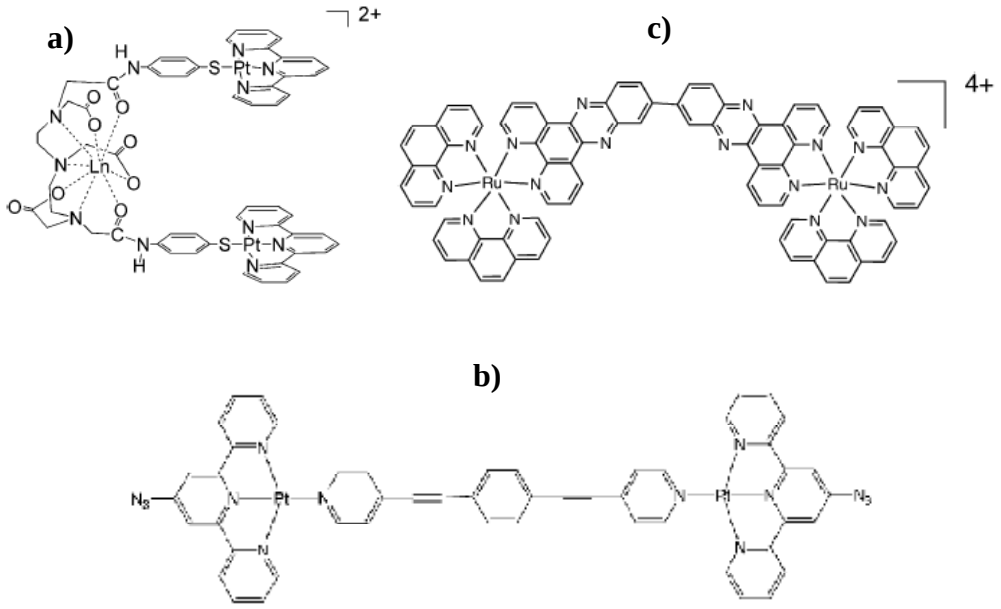

Figure 1.16. a) Pikramenou's and **b)** Lowe's bis-intercalators. **c)** Lincoln's threading intercalator.

too big to be inserted in the gap of a Watson-Crick duplex but they fit in the gaps of a bulged helix originating from base pair mismatches.[94,97-99]

Due to the importance of metallo-intercalators among DNA binding agents, more sophisticated variations of these compounds have been proposed such as *bis-intercalators* and *threading intercalators*.[84,100-102] For example Pikramenou and co-workers have studied a Ln-Pt_2 complex bearing two Pt(terpy) groups as intercalating units folded in a hairpin fashion by a neodymium aminocarboxylate centre (Figure 1.16.a)[103]. The two intercalating Pt(terpy) units are oriented in a way to intercalate the same DNA double strand and allowing a gap to be left between them. These caused an increase of DNA stiffening compared to mono-intercalators. The rigid tetracationic bis-intercalator based on Pt(terpy) in Figure 1.16.b) was designed by Lowe and co-worker to obtain DNA intramolecular cross-linking.[104-106] The bis-intercalator $[\Delta,\Delta-\mu-(bidppz)\text{-}(phen)_4Ru_2]_4$ proposed by Lincoln and Nordén (Figure 1.14.c))[56,107] is different from the others because the two dppz intercalating units are not exposed but linked inside the drug, so that the intercalation occurs after that part of the molecule threads through DNA.

1.3.3 Major and minor groove binders.

Groove-binding drugs are molecules that can fit within DNA grooves forming non covalent interactions (hydrogen bonds, $\pi-\pi$ interactions, Van der Waals forces) mainly with the base pairs of the duplex. Most of the known and clinically used groove-binding drugs are long and flexible organic molecules and they usually bind the minor groove. Goodsell and Dickerson demonstrated that minor groove binders tend to have a characteristic structure containing between two and five aromatic heterocycles linked by amide or vinyl groups and flanked at each end by cationic groups.[108] Baraldi et al. reported a selection concerning all the most important DNA-minor groove binders which, in some case, show a good level of sequence specificity and several biological activities, especially with antiprotozoal, antiviral and antibacterial properties.[109-114] Natural compounds netropsin and distamycine (Figure 1.17)[115-119] are the most studied natural antibiotics that bind the AT-rich minor grooves of B-DNA. The binding includes hydrogen bonds formation between the amide NH of the drugs and the N3 of adenines and O2 of thymines, van de Waals

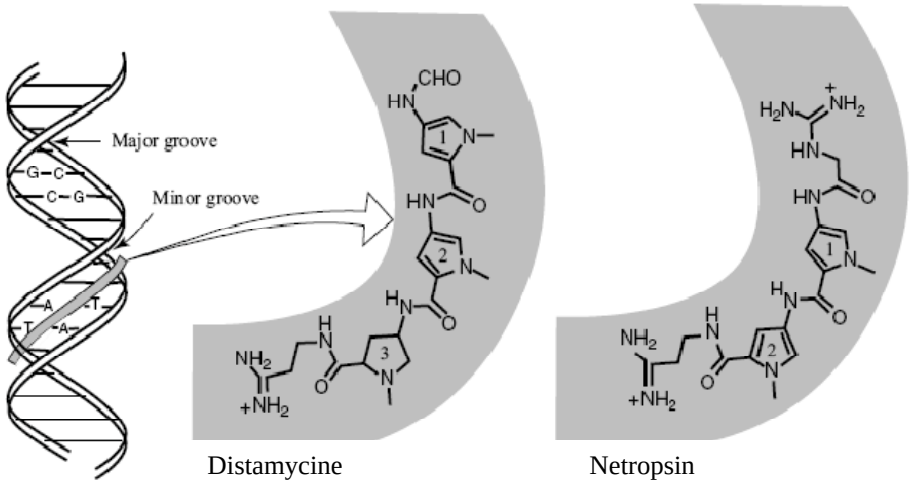

Figure 1.17 Conceptual drawing of minor groove binding, and structures of distamycin and netropsin (Figure adapted from ref. [7]).

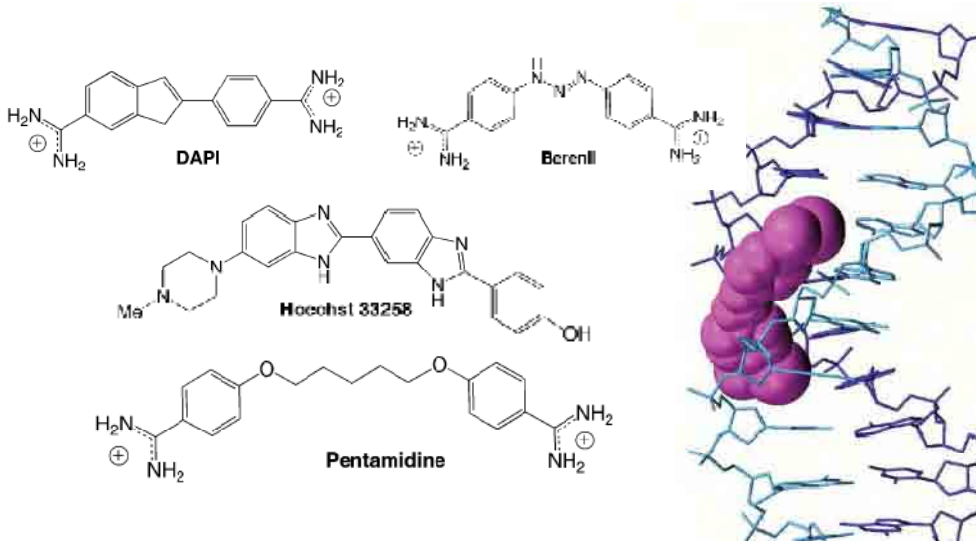

Figure 1.18. AT rich-minor groove binders and the structure of Berenil (pink) in a DNA minor groove (PDB ref. 1D63, figures taken from ref. [7,56]).

and electrostatic interactions. At least four base pairs within the minor groove are involved in the binding with the drug. Particularly important in this field was the contribution of Dervan and co-workers for the understanding of how distamycine-type compounds can recognise different AT rich sequences.[7,120,121]

In Figure 1.18 other well known synthetic minor groove binders are shown. DAPI and Hoechst 33258 are used mainly as fluorescent dyes. Berenil is used in veterinary

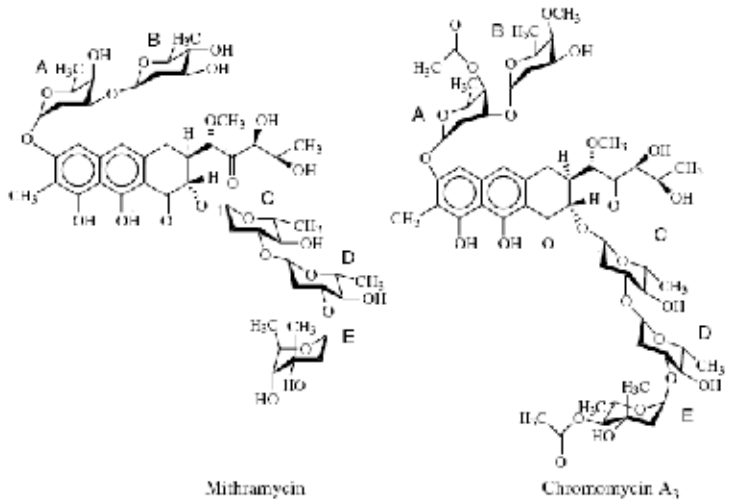

Figure 1.19. GC rich-minor groove binders.[7,56]

medicine for the treatment of the trypanosomiasis class of parasitic diseases (e.g. sleeping sickness). Pentamidine is also a diarylamidine anti-parasitic agent and it is used in the clinic to treat sleeping sickness and also pneumonia, particularly in HIV-positive patients. All these compounds bind AT rich minor grooves because the absence of the amino group of the guanine residues makes the groove slightly narrower than GC rich minor grooves. This allow a better fit of the drug inside the groove without causing particularly changes to the width of the groove.[56]

The two natural compounds chromomycin A3 and mithramycin (Figure 1.19) are antitumor antibiotics and consist of an aglycon ring (chromophore) to which the disaccharide (A-B), the trisaccharide (C-D-E) and a hydrophilic side chain are attached. Unlike the AT-groove-binding drugs, chromomycin (A3) and mithramycin bind to the GC-rich region causing conformational changes of the B-DNA structure: the resulting minor groove is wider and shallower so that these drugs tend to convert B-DNA in A-DNA.[113,122-126]

Most of the organic drugs (either synthetic of natural) that interact non covalently with DNA, target the minor groove. This occurs because the major groove is too wide to provide the right contacts with relatively small organic molecules. Most of the attempts of targeting the major groove are based on the use of synthetic biomolecules (such as oligonucleotides, peptides, synthetic protein motifs), agents that mimic biomolecules (peptide nucleic acids, PNA) or minor groove binders

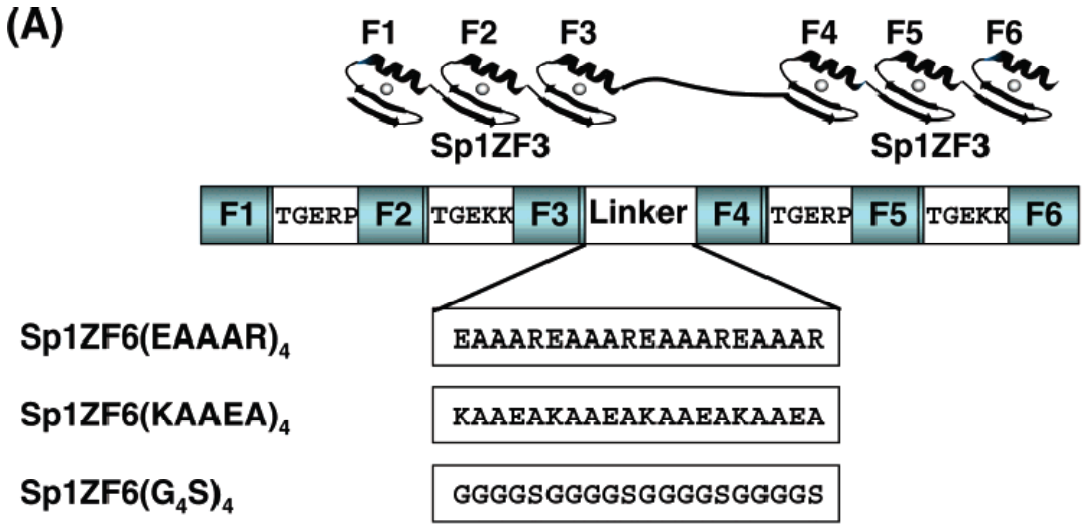

Figure 1.20. Schematic representation of the three 6 zinc finger peptides designed by Imanishi and co-workers. Each of them contain a linker with a different amino acid sequence (Figure taken from ref. [127]).

conjugated with other elements that allow the binding in the major groove. As it has been described in section 1.2, the major groove is the main target in the natural recognition of DNA. However, the reproduction of that combination of factors that determines the specific DNA recognition, typical of protein motifs, is very complicated. Libraries of peptides may be prepared, with rounds of selection and amplification used to identify the best binder for a given sequence. Particular successes have been achieved with synthetic peptides containing zinc finger motifs.[51] Some useful result can be obtained by modifying the residues of an established protein unit to affect its specificity[55] or by connecting multiple protein motifs in tandem. For example Imanishi and co-workers designed artificial peptides containing 6 zinc fingers units. The three zinc fingers units indicated as SP1ZF3 in Figure 1.20 correspond to the DNA binding domain of a transcription factor so that the whole system contain two DNA binding domains connected by a α-helix linker peptide. Three 6 zinc fingers peptides with three different linkers were studied. The amino acid sequence of the linkers determines the reciprocal position of the two DNA binding domains and each 6 zinc finger peptide recognise differently discontinue DNA binding sites.[127]

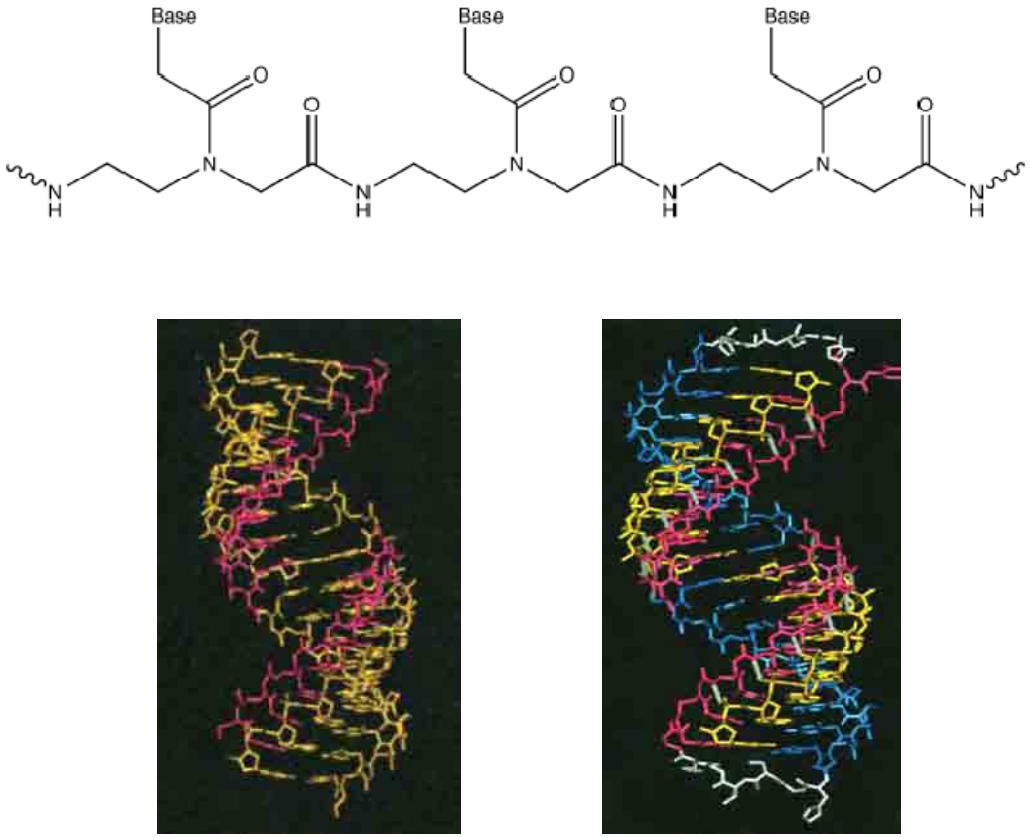

Figure 1.21. General structure of PNA (top) and structure of a $(DNA)_2(PNA)$ triplex (bottom left) and and a $(DNA)(PNA)_2$ triplex (bottom right). DNA chains are in yellow (PDB ref. 1PNN, figure taken from ref. [128]).

Major groove recognition by synthetic oligonucleotides has been widely investigated in the last decades based on the possibility of oligonucleotides to form triple helix with homopyrimidine-homopurine Watson-Crick duplex, as described in section 1.1 and Figure 1.4.a).[56,129] However, one of the limits of using oligonucleotides concerns their negative charge that makes the interaction with the DNA major groove relatively weak. This can be overcome using peptide nucleic acid (PNA), which are synthetic polymers whose backbone is composed of repeating N-(2-aminoethyl)-glycine units linked by peptide bonds (Figure 1.21). The backbone is linked to various purine and pyrimidine bases by methylene carbonyl bonds. PNAs are depicted like peptides, with the N-terminus at the first (left) position and the C-terminus at the right. PNAs were introduced by Nielsen and co-workers, in 1991[130] and since then a remarkable number of studies have been dedicated to the characterisation and applications of these polymers.[128,131-134] Bases of PNA chains

can form both Watson-Crick and Hoogsten hydrogen bonds and in fact they bind DNA duplex in the major groove forming $(DNA)_2(PNA)$ triplexes. However this is not the most stable structure, thus DNA double helix is opened up by PNA strands forming more stable $(DNA)(PNA)_2$ triple helixes (Figure 1.21, bottom). The use of both oligonucleotides and PNAs for medical and biotechnological purposes has been widely explored in the last decades, not only as major groove binders. This will be further discussed in section 1.4.

1.3.4 Sugar-backbone binding.

The sugar-backbone of DNA offers a hard oxygen-rich polyanion surface that can be involved in both electrostatic interactions and hydrogen bonds with either drugs or natural proteins. The most representative example of backbone binding drug is a class of multinuclear complexes of Pt(II) developed by Farrell.[135,136] In these compounds Pt(II) centres are coordinated by inert amine ligands, so that formation of

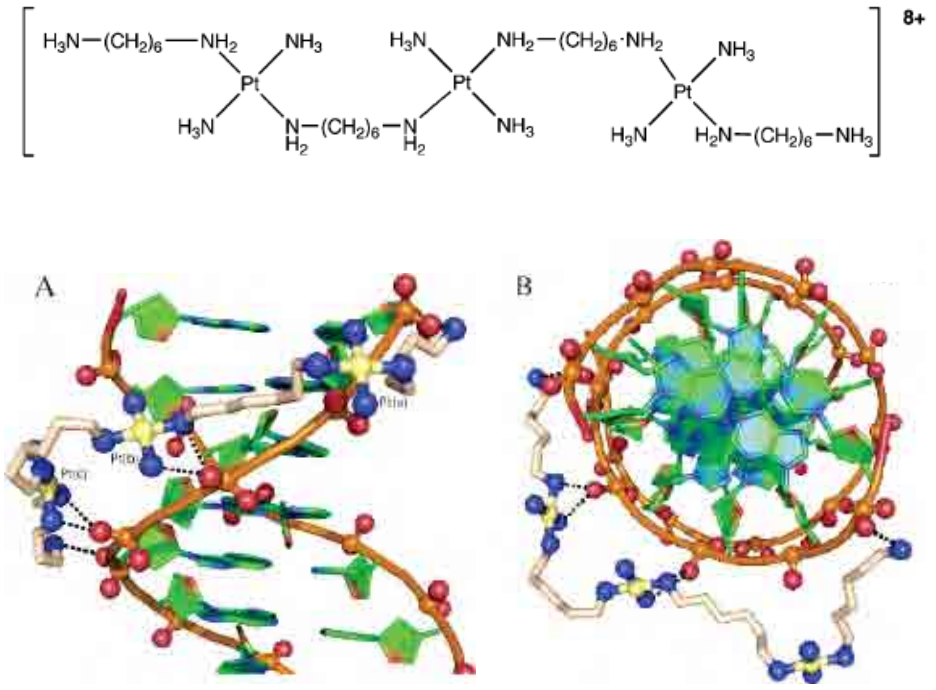

Figure 1.22. Chemical structure of the trinuclear platinum(II) compound, TriplatinNC (top) and Backbone Tracking (bottom). Hydrogen bonds between TriplatinNCa and DNA are indicated by dashed lines. Two Phosphate Clamps are shown. View perpendicular (A) and along (B) the helical axis (PDB ref. 2DYW, figure adapted from ref [137]).

Pt-DNA covalent bonds (as it occurs in Pt-Cl based drugs) is excluded and the compounds can only form hydrogen bonds and electrostatic interactions. The structure of the adduct that the tri-nuclear platinum compound TriplatinumNC forms with DNA was analysed by Komeda[137] and is shown in Figure 1.22. The amino groups of the Pt(II) compound forms bidentate complexes with the oxygen of the phosphate groups (NH···O···HN) that have been named 'phosphate clamps' and this way of binding the DNA along the sugar-backbone is known as 'back-bone tracking'.

1.4 Selective DNA recognition.

The recognition of specific DNA regions is one of the main issues that allow a DNA binding agent to find application as a successful drug. Thousands of compounds that can bind DNA and affect its functionality, do not have a future at clinical level, because they are unable to discriminate those parts of DNA and or/type of cells that are involved in a given disease. For example, all the agents used in chemotherapy are known for their grave side effects and this originates from the inability of these compounds to act exclusively against cancer cells. Thus, DNA selective recognition is still a subject of major interest and in the last decades many strategies have been explored in this area.

1.4.1 Sequence selectivity.

In section 1.2 it has been highlighted that, in Nature, protein motifs are the main molecules that selectively recognise DNA, but also that the *de novo* design of those motifs, including all the pattern of factors that are involved in each recognition event, is extremely complex. Something analogous occurs for oligonucleotides or PNAs. In theory, a certain bases sequence of DNA could be recognised by a complementary synthetic oligonucleotide, as mentioned in section 1.3.3, and for this reason oligonucleotides are considered a very significant tool in therapeutics design. They can be employed according to three different strategies: the *antisense strategy*, in which the oligonucleotide targets a single strand of nucleic acid, most commonly of mRNA, thus to affect the transcription of the related protein; the *antigene strategy*

aims to use oligonucleotides to target DNA double helices to form triple helices as described above; the *aptamer strategy* is based on the design of oligonucleotides that are recognised by DNA binding proteins, such as transcription factors, thus to obstruct the gene recognition activity of the proteins. However, the use of 'naked' oligonucleotides fails often for several reasons: their poor cellular uptake, their lack of stability in intracellular fluid (due to the high possibility of being recognised and modified by nuclease proteins) and their low binding affinity to the target (in part due to their negative charge). The use of PNAs can surely obviate the problems concerning the charge and these artificial polymers are not hydrolysed by nuclease enzymes. But the low cell uptake is an issue for PNAs as well as the fact that the DNA is organised in complex coiled structures (chromosomes) and the target sequence could be not easily available for the recognition.

On the other hand, DNA binding agents, either organic, inorganic or metallo-organic compounds, can bind the DNA more efficiently, causing more effective modifications, such as coiling, unwinding, bending, rupture of the DNA, but they lack sequence selectivity most of the time. For this reason, one of the most explored strategies for the achievement of selective DNA recognition aims to combine the efficiency of DNA binding agents, with the selective DNA recognition potential of either peptides, oligonucleotides or PNAs. This has led to a wide production and analysis of a huge number of *bioconjugates*. Barton and co-workers demonstrated that Rh(III) based intercalators conjugated to peptides exhibited a DNA recognition selectivity that depended on the amino acids sequence of the conjugated peptide. For example the intercalator $[Rh(phi)_2(phen')]^{3+}$ was conjugated to a 13 residues peptide in α-helix conformation and the resulting peptide-intercalator system showed DNA site recognition to the sequence 5'-CCA-3' that depended on the presence of the glutamate at the position 10 (Figure 1.23 a)).[138] The DNA sequence selectivity of this peptide-complex system involved different DNA sequences by single amino acid modification of the peptide sequence.[139-141] With a similar approach a *de novo* designed Zn(II) metallo-peptide, known as the active site of metal containing hydrolase enzymes, was conjugated to the intercalator $[Rh(phi)_2bpy']$ and this system showed selective DNA nuclease activity.[142]

Most recently the same strategy has been investigated for Ru(II) and Pt(II) complexes, due the large importance of this compounds especially in

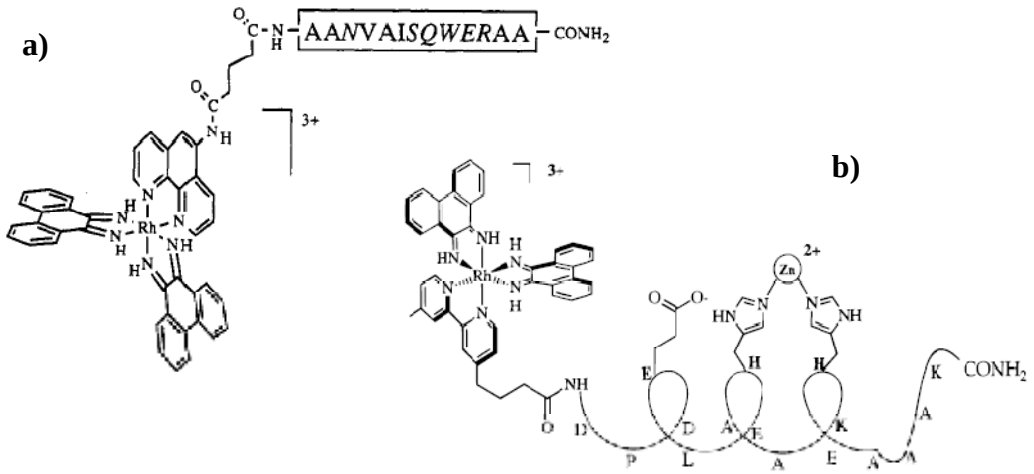

Figure 1.23. Barton's peptide metallo-intercalator. **a)** Peptide $[Rh(phi)_2(phen')]^{3+}$ conjugate as example of glutamate switch (figure taken from ref.[138]) **b)** Peptide-$[Rh(phi)_2(bpy')]^{3+}$ as artificial selective DNA nuclease (figure taken from ref [142]).

chemotherapy.[143] In Reedijk laboratories mono and di-nuclear cisplatin based complexes have been conjugated to peptides for the first time via solid phase synthesis[144,145] and in Hadjiliadis group a similar synthetic approach led to the development of Ru(II) complexes conjugated with peptide and amino acids, whose DNA binding affinity depended on the type of amino acid appended.[146-148] Obviously, the idea of assembling DNA binders with DNA recognition motifs does not concern metal complexes only. Mascareñas and co-workers demonstrated that DNA sequence-selective binding can be achieved with the rational design of minor grove binder-peptide hybrids.[149] They chose a minimal DNA binding domain of a zinc transcription factor from *Drosophila melanogaster*. This domain is a zinc finger unit that binds its consensus DNA sequence (GAGAG) by means of a trivalent interaction involving a classical zinc-finger module and two basic regions, that are indicated as BR1 and BR2 in figure 1.24.a). The 65 amino acids minimal domain alone does not bind the DNA. Two different distamycin-like tripyrrole units were anchored at the Arg44 of the zinc finger, in a position in which the folding of the zinc finger conformation was not compromised and aiming to a major-minor groove binding combination (Figure 1.24.b) and c)). DNA binding studies showed that both hybrids bind the DNA, involving also the zinc finger unit, and the hybrid 2a showed

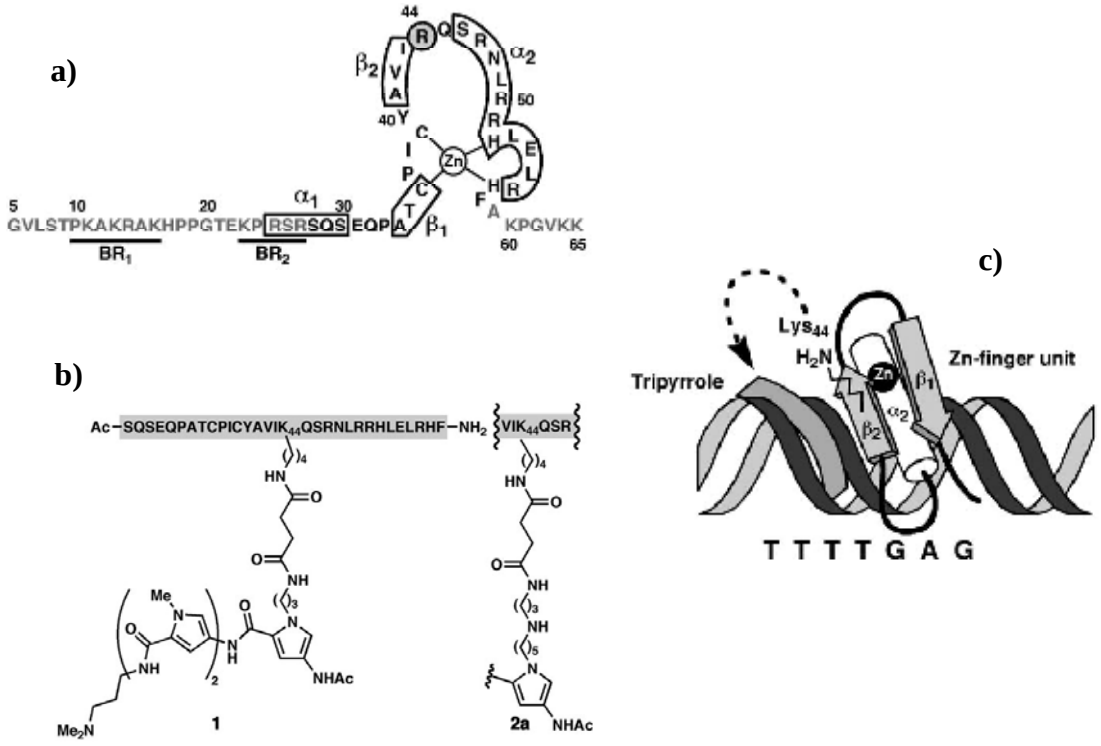

Figure 1.24 Mascareñas design of zinc finger-tripyrrole hybrid **a)** Sequence of the minimal DNA binding domain of the GAGA factor, showing the location of the two basic regions (BR1 and BR2) as well as the secondary-structure elements. **b)** Two tripyrrole-peptide hybrids investigated (1 and 2a). **c)** Representation of the designed bipartite major-minor groove recognition (Figure adapted from ref. [149]).

selective binding for a GAG sequence adjacent to an A-rich minor groove.[149] It has been demonstrated that the approach of conjugating is effective also using oligonucleotides[150-154] and PNA.[155-160]

1.4.2 Structure specificity.

The design of synthetic agents that target tertiary structures of DNA, rather than specific sequences along the B-DNA, is a valid alternative to achieve selective DNA recognition. DNA structures such as G-quadruplex, DNA junctions or triplexes, occur only in specific moments or are located only in few regions of the entire genome, so their recognition would affect the genetic event in which they are involved. For example, the binding of G-quadruplex structures has been deeply

investigated in the last decades, since they have been found in telomeric DNA. Telomeres are stretches of DNA, located at the ends of the chromosomes, which are not replicated with the rest of the genome. The telomerase enzyme (not normally present in cells) is responsible for the synthesis of telomeres and can maintain their integrity and prevent their shortening. The telomerase enzyme is particularly active in cancer cells and because it can keep replicating telomeric DNA, the cell cannot reach crisis points of senescence and apoptosis.[161] It has been discovered that if the G-rich telomeric DNA folds in G-quadruplex structures, these are able to inhibit the telomerase.[162] Consequently synthetic agents that can induce the formation of G-quadruplex structures and stabilise them are considered very useful for applications in cancer therapy. Many organic and metallo-based compounds, that are known DNA duplex intercalators or groove binders, exhibit the ability of stabilising G-quadruplex.[163-165] An example is shown in Figure 1.25: the complex of daunomycin (known intercalator) with d(TGGGGT) has been crystallised showing that the daunomycin does not intercalate within stacked bases of the tetraplex; rather two layers of daunomycine molecules fill the interface between two quadruplex forming $\pi-\pi$ interactions.[165]

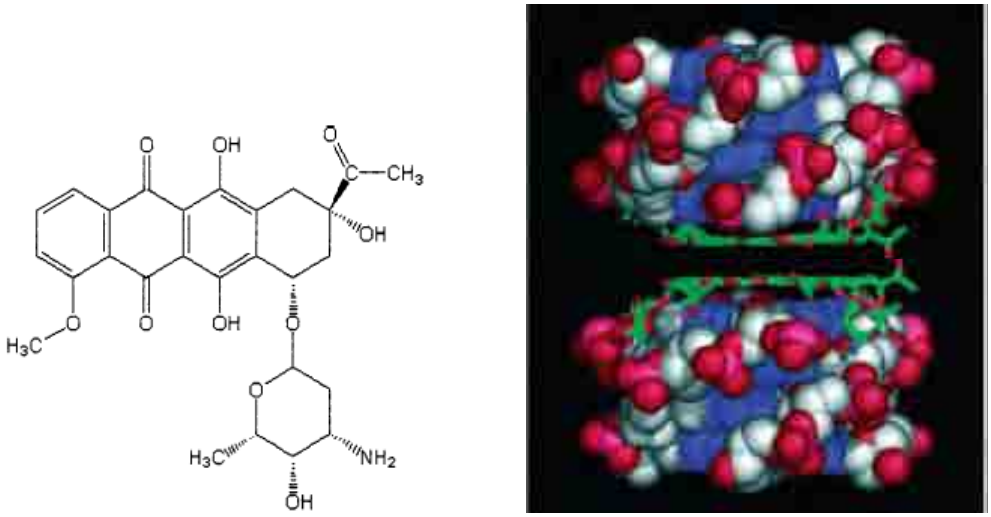

Figure 1.25. Structure of daunomycin (left) and crystal structure of the daunomycin-d(TGGGGT) complex, showing the arrangement in the crystal lattice of two quadruplexes, in van der Waals space-filling mode, and stacked end-to-end. The daunomycin molecules are shown in green ball-and-stick representation (PDB ref. 10OK, figure adapted from ref. [165]).

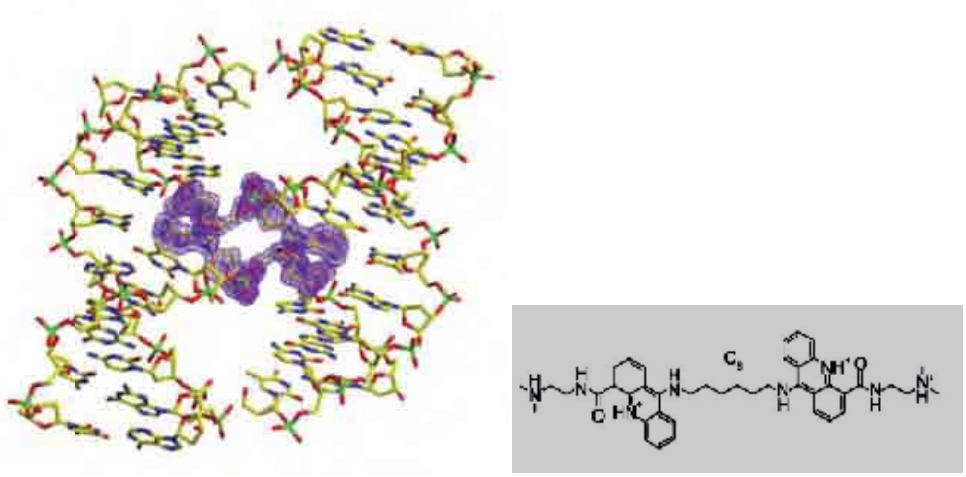

Figure 1.26. Bis-acridine based compound in the heart of a Holliday junction upon displacement of two adenine bases at the crossover region (PDB ref. 1NQS, figure adapted from ref. [166])

Also the recognition of either three way junctions or Holliday would give the possibility of interfere with specific moments or actions of the genome. Studies concerning agents that specifically recognise these structures are still in early stages[56]. Recently Cardin and co-workers demonstrated that a bis-acridine based compound fits in the heart of an Holliday junction upon displacement of the adenine bases A6(A) and A6(A') at the crossover region to allow the ligand chromophores to fit in (Figure 1.26).[166] Hannon and co-workers have developed a class of metallo-supramolecular cylinders that are able to recognise DNA three way junctions, and this will be described in Chapter 2 and 3.

1.5 Final remarks and aims of the thesis.

The understanding of DNA recognition by natural and synthetic molecules is one of the biggest challenges in the post-genomic era and one of the fundaments for the scientific development in the area of biotechnologies. In this chapter the most explored methods for the achievement of DNA recognition, specific and not specific, have been reviewed. The studies carried out in the last 30 years have allowed the understanding of the action of many drugs and placed the bases for the design of new

therapeutic and diagnostic agents. However there is still a lot to be discovered about the possibility of targeting specific structures of nucleic acids or specific genes. Chapter 2 will be dedicated to the description of a class of metallo-supramolecular helicates developed in Hannon laboratories and whose DNA binding properties have been explored in the last decade. These di-nuclear complexes bind the major groove of the DNA and this makes them particularly interesting, as most of the synthetic DNA binders are intercalators, minor groove binders or alkylating agents. Most interestingly, they bind the heart of DNA three way junctions. Studies concerning the dynamic behaviour of the most representative of these helicates will be discussed in the same chapter. As it has been highlighted above, the conjugation of DNA binders to DNA recognition motifs can provide several advantages, especially concerning the selective recognition of DNA. Thus the synthesis and characterisation of these helicates conjugated with short peptides and amino acids will be presented in Chapter 3 and Chapter 4 will be dedicated to the study of the DNA binding properties and cytotoxic activity of the conjugates.

1.6 References.

(1) Watson, J. D.; Crick, F. H. C. *Nature* **1953**, *171*, 737-738.
(2) Watson, J. D.; Crick, F. H. C. *Nature* **1953**, *171*, 964-967.
(3) Zamenhof, S.; Brawerman, G.; Chargaff, E. *Biochimica Et Biophysica Acta* **1952**, *9*, 402-405.
(4) Wilkins, M. H. F.; Stokes, A. R.; Wilson, H. R. *Nature* **1953**, *171*, 738-740.
(5) Franklin, R. E.; Gosling, R. G. *Nature* **1953**, *171*, 740-741.
(6) *International Union of Pure and Applied Chemistry. Nomenclature of Organic Chemistry*; J. Rigandy and S.P. Klesney, S. P. e., Ed.; Pergamon Press, Oxford, 1979.
(7) *Drug-DNA interactions. Structures and Spectra*; Nakamoto, K., Tsuboi, M., Strahan, G.D. , Ed.; Wiley, 2008.
(8) *Drug-DNA interactions. Structures and Spectra*; K. Nakamoto, M. T., G.D. Strahan, Ed.; Wiley, 2008.
(9) Gagna, C. E.; Lambert, W. C.; Kuo, H. R.; Farnsworth, P. N. *Journal of Histochemistry & Cytochemistry* **1997**, *45*, 1511-1521.
(10) Kwon, J. A.; Rich, A. *Proceedings of the National Academy of Sciences of the United States of America* **2005**, *102*, 12759-12764.
(11) Wang, G. L.; Christensen, L. A.; Vasquez, K. M. *Proceedings of the National Academy of Sciences of the United States of America* **2006**, *103*, 2677-2682.

(12) Wolfl, S.; Martinez, C.; Rich, A.; Majzoub, J. A. *Proceedings of the National Academy of Sciences of the United States of America* **1996**, *93*, 3664-3668.
(13) Ghosh, A.; Bansal, M. *Acta Crystallographica Section D-Biological Crystallography* **2003**, *59*, 620-626.
(14) *Quadruplex Nucleic Acids*; Neidle, S., Balasubramanian, S. , Ed.; RCS Publishing, 2006.
(15) Sen, D.; Gilbert, W. *Nature* **1988**, *334*, 364-366.
(16) Sundquist, W. I.; Klug, A. *Nature* **1989**, *342*, 825-829.
(17) Blackburn, E. H. *Nature* **1991**, *350*, 569-573.
(18) Haider, S.; Parkinson, G. N.; Neidle, S. *Journal of Molecular Biology* **2002**, *320*, 189-200.
(19) Kang, C.; Zhang, X. H.; Ratliff, R.; Moyzis, R.; Rich, A. *Nature* **1992**, *356*, 126-131.
(20) Burge, S.; Parkinson, G. N.; Hazel, P.; Todd, A. K.; Neidle, S. *Nucleic Acids Research* **2006**, *34*, 5402-5415.
(21) Mirkin, S. M.; Lyamichev, V. I.; Drushlyak, K. N.; Dobrynin, V. N.; Filippov, S. A.; Frankkamenetskii, M. D. *Nature* **1987**, *330*, 495-497.
(22) Hanvey, J. C.; Shimizu, M.; Wells, R. D. *Proceedings of the National Academy of Sciences of the United States of America* **1988**, *85*, 6292-6296.
(23) Lilley, D. M. J.; Clegg, R. M.; Diekmann, S.; Seeman, N. C.; vonKitzing, E.; Hagerman, P. *Journal of Molecular Biology* **1996**, *255*, 554-555.
(24) Altona, C.; Pikkemaat, J. A.; Overmars, F. J. J. *Current Opinion in Structural Biology* **1996**, *6*, 305-316.
(25) van Buuren, B. N. M.; Overmars, F. J. J.; Ippel, J. H.; Altona, C.; Wijmenga, S. S. *Journal of Molecular Biology* **2000**, *304*, 371-383.
(26) Ouporov, I. V.; Leontis, N. B. *Biophysical Journal* **1995**, *68*, 266-274.
(27) Rosche, W. A.; Trinh, T. Q.; Sinden, R. R. *Journal of Bacteriology* **1995**, *177*, 4385-4391.
(28) Singleton, M. R.; Scaife, S.; Wigley, D. B. *Cell* **2001**, *107*, 79-89.
(29) Guthrie, C.; Patterson, B. *Annual Review of Genetics* **1988**, *22*, 387-419.
(30) Wimberly, B. T.; Brodersen, D. E.; Clemons, W. M.; Morgan-Warren, R. J.; Carter, A. P.; Vonrhein, C.; Hartsch, T.; Ramakrishnan, V. *Nature* **2000**, *407*, 327-339.
(31) Ban, N.; Nissen, P.; Hansen, J.; Moore, P. B.; Steitz, T. A. *Science* **2000**, *289*, 905-920.
(32) Sinden, R. R. *Nature* **2001**, *411*, 757-758.
(33) Rettberg, C. C.; Prere, M. F.; Gesteland, R. F.; Atkins, J. F.; Fayet, O. *Journal of Molecular Biology* **1999**, *286*, 1365-1378.
(34) Minagawa, T.; Murakami, A.; Ryo, Y.; Yamagishi, H. *Virology* **1983**, *126*, 183-193.
(35) Jensch, F.; Kemper, B. *Embo Journal* **1986**, *5*, 181-189.
(36) Ortiz-Lombardia, M.; Gonzalez, A.; Eritja, R.; Aymami, J.; Azorin, F.; Coll, M. *Nature Structural Biology* **1999**, *6*, 913-917.
(37) Lilley, D. M. J.; Norman, D. G. *Nature Structural Biology* **1999**, *6*, 897-899.

(38) Seeman, N. C. *Current Opinion in Structural Biology* **1996**, *6*, 519-526.
(39) Brown, T.; Hunter, W. N.; Kneale, G.; Kennard, O. *Proceedings of the National Academy of Sciences of the United States of America* **1986**, *83*, 2402-2406.
(40) Hunter, W. N.; Brown, T.; Anand, N. N.; Kennard, O. *Nature* **1986**, *320*, 552-555.
(41) Joshuator, L.; Rabinovich, D.; Hope, H.; Frolow, F.; Appella, E.; Sussman, J. L. *Nature* **1988**, *334*, 82-84.
(42) Chattopadhyaya, R.; Ikuta, S.; Grzeskowiak, K.; Dickerson, R. E. *Nature* **1988**, *334*, 175-179.
(43) *Introduction to Protein Structure*; Branden, C., Tooze, J. , Ed.; Garland Publishing, Inc., 1991.
(44) *Nucleic acid structure and recognition*; Neidle, S., Ed., 2002; Vol. Oxford University Press. Oxford
(45) Jones, S.; van Heyningen, P.; Berman, H. M.; Thornton, J. M. *Journal of Molecular Biology* **1999**, *287*, 877-896.
(46) Pabo, C. O.; Nekludova, L. *Journal of Molecular Biology* **2000**, *301*, 597-624.
(47) Nobeli, I.; Laskowski, R. A.; Valdar, W. S. J.; Thornton, J. M. *Nucleic Acids Research* **2001**, *29*, 4294-4309.
(48) Luscombe, N. M.; Austin, S. E.; Berman, H. M.; Thornton, J. M. *Genome Biol* **2000**, *1*, REVIEWS001.
(49) International Human Genome Sequencing Consortium Nature, 2001, 409, 860.
(50) Arauzo-Bravo, M. J.; Fujii, S.; Kono, H.; Ahmad, S.; Sarai, A. *Journal of the American Chemical Society* **2005**, *127*, 16074-16089.
(51) Sarai, A.; Kono, H. *Annual Review of Biophysics and Biomolecular Structure* **2005**, *34*, 379-398.
(52) *Nucleic Acid Structure and Recognition*; Neidle, S., Ed.; Oxford University Press. Oxford 2002.
(53) Luscombe, N. M.; Laskowski, R. A.; Thornton, J. M. *Nucleic Acids Research* **2001**, *29*, 2860-2874.
(54) Nadassy, K.; Wodak, S. J.; Janin, J. *Biochemistry* **1999**, *38*, 1999-2017.
(55) Jantz, D.; Amann, B. T.; Gatto, G. J.; Berg, J. M. *Chemical Reviews* **2004**, *104*, 789-799.
(56) Hannon, M. J. *Chemical Society Reviews* **2007**, *36*, 280-295.
(57) *Small Molecules DNA and RNA Binders. From Synthesis to Nucleic Acid Complexes*; Demeunynck, M., Bailly, C., WilsonW. D. , Ed.; WILEY-VCH, 2003.
(58) Rosenber.B; Vancamp, L.; Trosko, J. E.; Mansour, V. H. *Nature* **1969**, *222*, 385-&.
(59) Hannon, M. J. *Pure and Applied Chemistry* **2007**, *79*, 2243-2261.
(60) *Cisplatin, Chemistry and Biochemistry of a Leading Anti-Cancer Drug*; Lippert, B., Ed.; Wiley-VCH, Weinheim, Germany, 1999.
(61) Guo, Z. J.; Sadler, P. J. *Advances in Inorganic Chemistry, Vol 49* **2000**, *49*, 183-306.

(62) Parkinson, J. A.; Chen, Y.; Murdoch, P. D.; Guo, Z. J.; Berners-Price, S. J.; Brown, T.; Sadler, P. J. *Chemistry-a European Journal* **2000**, *6*, 3636-3644.
(63) Takahara, P. M.; Rosenzweig, A. C.; Frederick, C. A.; Lippard, S. J. *Nature* **1995**, *377*, 649-652.
(64) Ohndorf, U. M.; Rould, M. A.; He, Q.; Pabo, C. O.; Lippard, S. J. *Nature* **1999**, *399*, 708-712.
(65) Mohamed, D.; Mowaka, S.; Thomale, J.; Linscheid, M. W. *Chemical Research in Toxicology* **2009**, *22*, 1435-1446.
(66) Oppitz, M. M.; Musch, E.; Malek, M.; Rub, H. P.; Vonunruh, G. E.; Loos, U.; Muhlenbruch, B. *Cancer Chemotherapy and Pharmacology* **1989**, *23*, 208-212.
(67) Bauer, G. B.; Povirk, L. F. *Nucleic Acids Research* **1997**, *25*, 1211-1218.
(68) Sastry, M.; Fiala, R.; Lipman, R.; Tomasz, M.; Patel, D. J. *Journal of Molecular Biology* **1995**, *247*, 338-359.
(69) Chidester, C. G.; Krueger, W. C.; Mizsak, S. A.; Duchamp, D. J.; Martin, D. G. *Journal of the American Chemical Society* **1981**, *103*, 7629-7635.
(70) Hurley, L. H.; Reynolds, V. L.; Swenson, D. H.; Petzold, G. L.; Scahill, T. A. *Science* **1984**, *226*, 843-844.
(71) Kopka, M. L.; Goodsell, D. S.; Baikalov, I.; Grzeskowiak, K.; Cascio, D.; Dickerson, R. E. *Biochemistry* **1994**, *33*, 13593-13610.
(72) Guan, Y.; Sakai, R.; Rinehart, K. L.; Wang, A. H. J. *Journal of Biomolecular Structure & Dynamics* **1993**, *10*, 793-818.
(73) Iyer, V. N.; Szybalski, W. *Science* **1964**, *145*, 55-&.
(74) Tomasz, M.; Chawla, A. K.; Lipman, R. *Biochemistry* **1988**, *27*, 3182-3187.
(75) Subramaniam, G.; Paz, M. M.; Kumar, G. S.; Das, A.; Palom, Y.; Clement, C. C.; Patel, D. J.; Tomasz, M. *Biochemistry* **2001**, *40*, 10473-10484.
(76) Lerman, L. S. *Journal of Molecular Biology* **1961**, *3*, 18-&.
(77) Martinez, R.; Chacon-Garcia, L. *Current Medicinal Chemistry* **2005**, *12*, 127-151.
(78) Frederick, C. A.; Williams, L. D.; Ughetto, G.; Vandermarel, G. A.; Vanboom, J. H.; Rich, A.; Wang, A. H. J. *Biochemistry* **1990**, *29*, 2538-2549.
(79) Ando, Y.; Fuse, E.; Figg, W. D. *Clinical Cancer Research* **2002**, *8*, 1964-1973.
(80) Huang, Q.; Fu, W. L. *Clinical Chemistry and Laboratory Medicine* **2005**, *43*, 841-842.
(81) Granzhan, A.; Ihmels, H. *Chembiochem* **2006**, *7*, 1031-1033.
(82) Holt, P. A.; Ragazzon, P.; Strekowski, L.; Chaires, J. B.; Trent, J. O. *Nucleic Acids Research* **2009**, *37*, 1280-1287.
(83) Neidle, S.; Achari, A.; Taylor, G. L.; Berman, H. M.; Carrell, H. L.; Glusker, J. P.; Stallings, W. C. *Nature* **1977**, *269*, 304-307.
(84) Gaus, K.; Wollschlager, K.; Zobel, A.; Korff, G.; Juodaityte, J.; Kleimann, C.; Sischka, A.; Anselmetti, D.; Sewald, N. *Journal of Peptide Science* **2008**, *14*, 192-192.
(85) Neto, B. A. D.; Lapis, A. A. M. *Molecules* **2009**, *14*, 1725-1746.

(86) Sun, Y.; Lutterman, D. A.; Turro, C. *Inorganic Chemistry* **2008**, *47*, 6427-6434.
(87) Yang, Q.; Yang, P.; Qian, X. H.; Tong, L. P. *Bioorganic & Medicinal Chemistry Letters* **2008**, *18*, 6210-6213.
(88) Zeglis, B. M.; Barton, J. K. *Nature Protocols* **2007**, *2*, 357-371.
(89) Zeglis, B. M.; Pierre, V. C.; Barton, J. K. *Chemical Communications* **2007**, 4565-4579.
(90) Erkkila, K. E.; Odom, D. T.; Barton, J. K. *Chemical Reviews* **1999**, *99*, 2777-2795.
(91) Greguric, A.; Greguric, I. D.; Hambley, T. W.; Aldrich-Wright, J. R.; Collins, J. G. *Journal of the Chemical Society-Dalton Transactions* **2002**, 849-855.
(92) Friedman, A. E.; Chambron, J. C.; Sauvage, J. P.; Turro, N. J.; Barton, J. K. *Journal of the American Chemical Society* **1990**, *112*, 4960-4962.
(93) Foxon, S. P.; Metcalfe, C.; Adams, H.; Webb, M.; Thomas, J. A. *Inorganic Chemistry* **2007**, *46*, 409-416.
(94) Hart, J. R.; Johnson, M. D.; Barton, J. K. *Proceedings of the National Academy of Sciences of the United States of America* **2004**, *101*, 14040-14044.
(95) Jennette, K. W.; Lippard, S. J.; Vassilia.Ga; Bauer, W. R. *Proceedings of the National Academy of Sciences of the United States of America* **1974**, *71*, 3839-3843.
(96) Bond, P. J.; Langridge, R.; Jennette, K. W.; Lippard, S. J. *Proceedings of the National Academy of Sciences of the United States of America* **1975**, *72*, 4825-4829.
(97) Zeglis, B. M.; Pierre, V. C.; Kaiser, J. T.; Barton, J. K. *Biochemistry* **2009**, *48*, 4247-4253.
(98) Brunner, J.; Barton, J. K. *Biochemistry* **2006**, *45*, 12295-12302.
(99) Hart, J. R.; Glebov, O.; Ernst, R. J.; Kirsch, I. R.; Barton, J. K. *Proceedings of the National Academy of Sciences of the United States of America* **2006**, *103*, 15359-15363.
(100) Kokoschka, M.; Bangert, J. A.; Stoll, R.; Sheldrick, W. S. *European Journal of Inorganic Chemistry*, 1507-1515.
(101) Nazif, M. A.; Bangert, J. A.; Ott, I.; Gust, R.; Stoll, R.; Sheldrick, W. S. *Journal of Inorganic Biochemistry* **2009**, *103*, 1405-1414.
(102) Xie, H.; Tansil, N. C.; Gao, Z. Q. *Frontiers in Bioscience* **2006**, *11*, 1147-1157.
(103) Glover, P. B.; Ashton, P. R.; Childs, L. J.; Rodger, A.; Kercher, M.; Williams, R. M.; De Cola, L.; Pikramenou, Z. *Journal of the American Chemical Society* **2003**, *125*, 9918-9919.
(104) Annan, N. K.; Cook, P. R.; Mullins, S. T.; Lowe, G. *Nucleic Acids Research* **1992**, *20*, 983-990.
(105) Mullins, S. T.; Annan, N. K.; Cook, P. R.; Lowe, G. *Biochemistry* **1992**, *31*, 842-849.
(106) Lowe, G.; Droz, A. S.; Park, J. J.; Weaver, G. W. *Bioorganic Chemistry* **1999**, *27*, 477-486.
(107) Onfelt, B.; Lincoln, P.; Norden, B. *Journal of the American Chemical Society* **2001**, *123*, 3630-3637.

(108) Goodsell, D.; Dickerson, R. E. *Journal of Medicinal Chemistry* **1986**, *29*, 727-733.
(109) Baraldi, P. G.; Bovero, A.; Fruttarolo, F.; Preti, D.; Tabrizi, M. A.; Pavani, M. G.; Romagnoli, R. *Medicinal Research Reviews* **2004**, *24*, 475-528.
(110) Pandya, P.; Islam, M. M.; Kumar, G. S.; Jayaram, B.; Kumar, S. *Journal of Chemical Sciences*, *122*, 247-257.
(111) Tevis, D. S.; Kumar, A.; Stephens, C. E.; Boykin, D. W.; Wilson, W. D. *Nucleic Acids Research* **2009**, *37*, 5550-5558.
(112) Wang, H.; Laughton, C. A. *Physical Chemistry Chemical Physics* **2009**, *11*, 10722-10728.
(113) Munde, M.; Ismail, M. A.; Arafa, R.; Peixoto, P.; Collar, C. J.; Liu, Y.; Hu, L. X.; David-Cordonnier, M. H.; Lansiaux, A.; Bailly, C.; Boykin, D. W.; Wilson, W. D. *Journal of the American Chemical Society* **2007**, *129*, 13732-13743.
(114) Jain, A. K.; Gupta, S. K.; Tawar, U.; Dogra, S. K.; Tandon, V. *Oligonucleotides* **2009**, *19*, 53-62.
(115) Kopka, M. L.; Yoon, C.; Goodsell, D.; Pjura, P.; Dickerson, R. E. *Proceedings of the National Academy of Sciences of the United States of America* **1985**, *82*, 1376-1380.
(116) Bailly, C.; Chaires, J. B. *Bioconjugate Chemistry* **1998**, *9*, 513-538.
(117) Dolenc, J.; Baron, R.; Oostenbrink, C.; Koller, J.; van Gunsteren, W. F. *Biophysical Journal* **2006**, *91*, 1460-1470.
(118) Freyer, M. W.; Buscaglia, R.; Cashman, D.; Hyslop, S.; Wilson, W. D.; Chaires, J. B.; Lewis, E. A. *Biophysical Chemistry* **2007**, *126*, 186-196.
(119) Mishra, K.; Bhardwaj, R.; Chaudhury, N. K. *Radiation Research* **2009**, *172*, 698-705.
(120) Dervan, P. B. *Bioorganic & Medicinal Chemistry* **2001**, *9*, 2215-2235.
(121) Dervan, P. B. *Science* **1986**, *232*, 464-471.
(122) Banville, D. L.; Keniry, M. A.; Shafer, R. H. *Biochemistry* **1990**, *29*, 9294-9304.
(123) Banville, D. L.; Keniry, M. A.; Kam, M.; Shafer, R. H. *Biochemistry* **1990**, *29*, 6521-6534.
(124) Gao, X. L.; Mirau, P.; Patel, D. J. *Journal of Molecular Biology* **1992**, *223*, 259-279.
(125) Sastry, M.; Patel, D. J. *Biochemistry* **1993**, *32*, 6588-6604.
(126) Barcelo, F.; Scotta, C.; Ortiz-Lombardia, M.; Mendez, C.; Salas, J. A.; Portugal, J. *Nucleic Acids Research* **2007**, *35*, 2215-2226.
(127) Yan, W.; Imanishi, M.; Futaki, S.; Sugiura, Y. *Biochemistry* **2007**, *46*, 8517-8524.
(128) Betts, L.; Josey, J. A.; Veal, J. M.; Jordan, S. R. *Science* **1995**, *270*, 1838-1841.
(129) Thuong, N. T.; Helene, C. *Angewandte Chemie-International Edition in English* **1993**, *32*, 666-690.
(130) Nielsen, P. E.; Egholm, M.; Berg, R. H.; Buchardt, O. *Science* **1991**, *254*, 1497-1500.
(131) Pooga, M.; Land, T.; Bartfai, T.; Langel, U. *Biomolecular Engineering* **2001**, *17*, 183-192.
(132) Ray, A.; Norden, B. *Faseb Journal* **2000**, *14*, 1041-1060.

(133) Nielsen, P. E. *Chem Biodivers*, *7*, 786-804.
(134) Totsingan, F.; Jain, V.; Bracken, W. C.; Faccini, A.; Tedeschi, T.; Marchelli, R.; Corradini, R.; Kallenbach, N. R.; Green, M. M. *Macromolecules*, *43*, 2692-2703.
(135) Harris, A.; Qu, Y.; Farrell, N. *Inorganic Chemistry* **2005**, *44*, 1196-1198.
(136) Harris, A. L.; Yang, X. H.; Hegmans, A.; Povirk, L.; Ryan, J. J.; Kelland, L.; Farrell, N. P. *Inorganic Chemistry* **2005**, *44*, 9598-9600.
(137) Komeda, S.; Moulaei, T.; Woods, K. K.; Chikuma, M.; Farrell, N. P.; Williams, L. D. *Journal of the American Chemical Society* **2006**, *128*, 16092-16103.
(138) Sardesai, N. Y.; Zimmermann, K.; Barton, J. K. *Journal of the American Chemical Society* **1994**, *116*, 7502-7508.
(139) Hastings, C. A.; Barton, J. K. *Biochemistry* **1999**, *38*, 10042-10051.
(140) Holmlin, R. E.; Dandliker, P. J.; Barton, J. K. *Bioconjugate Chemistry* **1999**, *10*, 1122-1130.
(141) Sardesai, N. Y.; Barton, J. K. *Journal of Biological Inorganic Chemistry* **1997**, *2*, 762-771.
(142) Fitzsimons, M. P.; Barton, J. K. *Journal of the American Chemical Society* **1997**, *119*, 3379-3380.
(143) Reedijk, J. *Macromolecular Symposia* **2008**, *270*, 193-201.
(144) van Zutphen, S.; Robillard, M. S.; van der Marel, G. A.; Overkleeft, H. S.; den Dulk, H.; Brouwer, J.; Reedijk, J. *Chemical Communications* **2003**, 634-635.
(145) Robillard, M. S.; Valentijn, A.; Meeuwenoord, N. J.; van der Marel, G. A.; van Boom, J. H.; Reedijk, J. *Angewandte Chemie-International Edition* **2000**, *39*, 3096-3099.
(146) Karidi, K.; Garoufis, A.; Hadjiliadis, N.; Reedijk, J. *Dalton Transactions* **2005**, 728-734.
(147) Karidi, K.; Reedijk, J.; Hadjiliadis, N.; Garoufis, A. *Journal of Inorganic Biochemistry* **2007**, *101*, 1483-1491.
(148) Myari, A.; Hadjiliadis, N.; Garoufis, A. *European Journal of Inorganic Chemistry* **2004**, 1427-1439.
(149) Vazquez, O.; Vazquez, M. E.; Blanco, J. B.; Castedo, L.; Mascarenas, J. L. *Angewandte Chemie-International Edition* **2007**, *46*, 6886-6890.
(150) Da Ros, T.; Spalluto, G.; Prato, M.; Saison-Behmoaras, T.; Boutorine, A.; Cacciari, B. *Current Medicinal Chemistry* **2005**, *12*, 71-88.
(151) Ma, D. D.; Rede, T.; Naqvi, N. A.; Cook, P. D. *Biotechnol Annu Rev* **2000**, *5*, 155-96.
(152) Carbone, G. M.; McGuffie, E.; Napoli, S.; Flanagan, C. E.; Dembech, C.; Negri, U.; Arcamone, F.; Capobianco, M. L.; Catapano, C. V. *Nucleic Acids Research* **2004**, *32*, 2396-2410.
(153) Privat, E.; Melvin, T.; Asseline, U.; Vigny, P. *Photochemistry and Photobiology* **2001**, *74*, 532-541.
(154) Choi, J. S.; Kang, C. W.; Jung, K.; Yang, J. W.; Kim, Y. G.; Han, H. Y. *Journal of the American Chemical Society* **2004**, *126*, 8606-8607.
(155) Mokhir, A.; Stiebing, R.; Kraemer, R. *Bioorganic & Medicinal Chemistry Letters* **2003**, *13*, 1399-1401.
(156) Zelder, F.; Kramer, R. *Journal of Inorganic Biochemistry* **2001**, *86*, 489-489.

(157) Govindaraju, T.; Kumar, V. A. *Tetrahedron* **2006**, *62*, 2321-2330.
(158) Miyajima, Y.; Ishizuka, T.; Yamamoto, Y.; Sumaoka, J.; Komiyama, M. *Journal of the American Chemical Society* **2009**, *131*, 2657-2662.
(159) Abes, S.; Turner, J. J.; Ivanova, G. D.; Owen, D.; Williams, D.; Arzumanov, A.; Clair, P.; Gait, M. J.; Lebleu, B. *Nucleic Acids Research* **2007**, *35*, 7396-7396.
(160) Oh, S. Y.; Ju, Y.; Park, H. *Molecules and Cells* **2009**, *28*, 341-345.
(161) Kim, N. W.; Piatyszek, M. A.; Prowse, K. R.; Harley, C. B.; West, M. D.; Ho, P. L. C.; Coviello, G. M.; Wright, W. E.; Weinrich, S. L.; Shay, J. W. *Science* **1994**, *266*, 2011-2015.
(162) *G-Quadruplex DNA: Methods and Protocols*; Baumann, P., Ed.; Humana Press, 2010.
(163) Arola, A.; Vilar, R. *Current Topics in Medicinal Chemistry* **2008**, *8*, 1405-1415.
(164) Reed, J. E.; Neidle, S.; Vilar, R. *Chemical Communications* **2007**, 4366-4368.
(165) Clark, G. R.; Pytel, P. D.; Squire, C. J.; Neidle, S. *Journal of the American Chemical Society* **2003**, *125*, 4066-4067.
(166) Brogden, A. L.; Hopcroft, N. H.; Searcey, M.; Cardin, C. J. *Angewandte Chemie-International Edition* **2007**, *46*, 3850-3854.

CHAPTER 2

METALLO-SUPRAMOLECULAR CYLINDERS: A NEW APPROACH FOR DNA MAJOR GROOVE RECOGNITION.

2.1 Non covalent DNA recognition and supramolecular chemistry.

Non covalent interactions (hydrogen bonding, metal coordination, hydrophobic and van der Waals forces, π–π interactions and electrostatic effects) play a major role in biological systems both regarding the multi dimensional assembly of biomolecules (such as proteins, RNA and DNA) and in the modes in which they "communicate" with their external environment and consequently the way their functions are processed and regulated.[1,2] Because of the key role of the non covalent bond in DNA recognition, this field is closely related to supramolecular chemistry, which is a branch of modern chemistry whose features and importance started to be understood during the 1980s thanks to the intense activity of Donald J. Cram, Jean-Marie Lehn and Charles J. Pedersen (Nobel Prizes, 1987). Supramolecular chemistry is known as the "chemistry beyond the molecule"[3] to distinguish it from the traditional molecular chemistry. The latter is mainly focused on making and breaking covalent bonds between atoms, while supramolecular chemistry concerns intermolecular interactions of non covalent nature to enforce the spontaneous but controlled generation of well-defined architectures[4].

The synthesis of a supramolecular compound does not have to be particularly intricate because the final molecule is the result of a natural self-assembly of smaller components. However the supramolecular chemist has to be particularly able in designing the right components capable of promoting the desired assembly and precluding the formation of unwanted structures. If this is achieved, it is possible to make slight modifications to these components or combine them in different ways to obtain a large number of final molecules to examine.

During the 1980-90's supramolecular chemistry was mainly focused on the design, construction and understanding of fascinating architectures, with the aim of establishing the general principles to create different supramolecular assemblies.

During this period a myriad of beautiful structures such as squares, triangles, boxes, grids, knots, helicates and many others, were designed and fully described[5]. However, during the mid 90s, it became evident that supramolecular chemistry was not only a way to create molecular constructions with nice forms, definite features and functions based on the "bottom up" approach, but also a method to understand and describe many physical, chemical and biological events[5]. Today supramolecular chemistry is a highly interdisciplinary field of science with applications in a very wide range of areas from material technologies to catalysis, from medicine to nanotechnologies.[6-8] For example a protein motif that recognises a specific sequence of DNA with consequent switching on or off a particular biological process, or a drug that interacts with its target producing a specific effect, or molecules that are able to be transferred throughout protein membranes, are all examples of events based on molecular recognition, which is one of the key concepts in supramolecular chemistry.

The study of synthetic molecules that recognise DNA via non covalent interactions, forming specific host-guest complexes that produce modifications of natural events, is the area of supramolecular chemistry on which this thesis focus.

2.2 Design of "cylinders": where metallo-supramolecular chemistry meets bioinorganic chemisty.

Starting from the end of 1990s, a key focus of the research in the Hannon group has been the design and synthesis of agents that probe DNA for potential applications in drug discovery and biotechnologies.

In natural systems the processing of DNA principally occurs by non covalent molecular recognition of the major groove of B-DNA by specific protein motifs. In Chapter 1 it has been explained that many sophisticated and complex factors, of a supramolecular nature, are involved in such recognition, not all of them completely explained and it is very difficult to replicate these systems by *de novo* design approach. However, it is known that "shapes" of protein motifs have a relevant role in the recognition.

The approach used by Hannon and co-workers was based on the idea to "mimic" the action of protein motifs by reproducing their shapes and dimensions rather than

their compositions. A further important aspect was the idea of employing a synthetic methodology which allowed a large number of synthetic agents to be prepared with the smallest possible synthetic effort, which could be an advantage in terms of costs and time. Metallo-supramolecular chemistry, which is a combination between coordination chemistry and supramolecular chemistry, was used as the key synthetic method. This method involves the use of ligand-metal ion interactions for the self assembly of the supramolecular product of desired architecture. The directionality inherent in the geometry of different metal ions, which can be controlled by changing the nature or the oxidation state of the metal, plays a crucial role in the spatial orientations of large organic molecules in the final supramolecular structure.

Helicates are among the most studied architectures in metallo-supramolecular chemistry. The term helicate, first introduced by J.M. Lehn in 1987, indicates helical architectures where one or more strands of organic ligands wrap around two or more metal ions, which are located along the axis of the helix itself[9]. The organic ligands must possess several binding sites that are able of coordinating to the metal ions, and they have to include appropriate rigid spacers between the binding domains to prevent two binding sites from the same ligand coordinating to the same metal centre (see schematic representation in Figure 2.1).

The most recurrent protein motifs that recognise the DNA major groove in natural systems have a typical cylindrical shape which promotes the formation of a perfect "host-guest" complex based, most of the time, on non covalent interactions. Examples are shown in Figure 2.2, all of which employ α-helix protein motifs for the

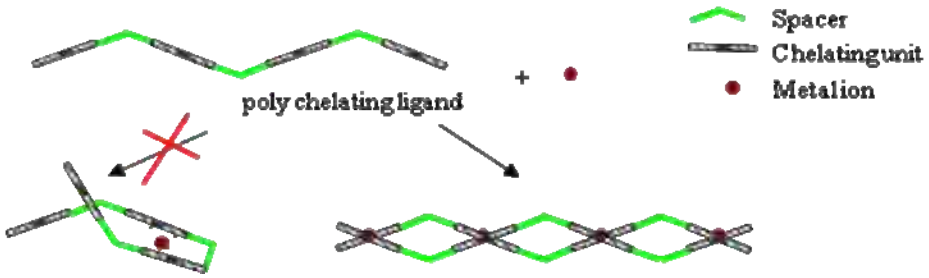

Figure 2.1. Schematic representation of the design of a poly nuclear double stranded helicate.

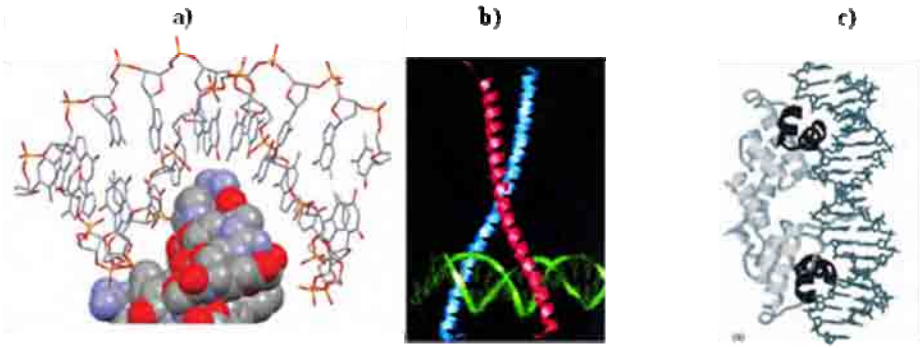

Figure 2.2. Examples of protein motifs that recognise DNA major groove: **a)** zinc finger, **b)** leucine zipper and **c)** helix-turn-helix (figures taken from ref. [10], [11] and [12] respectively).

recognition. Supramolecular helicates architectures can mimic, in terms of shape and dimensions, the cylindrical shape of those protein motifs. As potential DNA binders, the presence of the metal centres is particularly helpful, not only for their structural role, but also because the presence of cationic charges can energetically contribute to the interaction with the negatively charged DNA and they can eventually provide the potential drug with useful physical and/or chemical properties (depending on the metal). The wide range of metal ion coordination geometries available and the vast number of possible ligands, allows the identification of different "blocks" that could be combined in different ways to obtain a large set of helicate structures with different features.

Many studies, reported by Hannon et co-workers over the last decade, have demonstrated the ability of some of these helicates to recognise the DNA major groove by non covalent interactions,[13-22] opening new routes for the development of potential metallo-based drugs which are now receiving major attention in bioinorganic chemistry.[23] Because of their distinctive shape and the modality in which they recognise the DNA, these helicates have been termed "cylinders".

Interestingly, this approach makes use of metallo-supramolecular chemistry twice: as key method to design and synthesise a large array of different "cylinders" and as the discipline whose principles (in this particular case referred to the non covalent molecular recognition concept) are the base to design and understand the interaction between potential metallo-based drugs and their target binding site (DNA).

2.2.1 Triple stranded helicates-based "parent cylinders". DNA recognition and biological activity studies.

Ligands containing pyridine rings units, such as poly 2,2'-bipyridine-based ligands,[9] where the pyridine nitrogen is one of the coordinating sites, are the most common helicating ligands known in supramolecular chemistry. However, the preparation of poly-pyridyl ligands often requires long multistep organic synthesis from relatively expensive starting materials. A valid alternative is the use of poly-pyridylimine based ligands, whose characteristics can still ensure the formation of helicate architectures, but can be easily and inexpensively synthesised (one step reaction) by mixing pyridine aldehyde containing units and amino-based spacers to obtain Schiff bases.

One of the most important "cylinders", whose structure was first reported in 1997,[24] is based on the bispyridylimine ligand L1 showed in Figure 2.3 a). Reactions of this ligand with octahedral metal ions (such as Fe(II), Ni(II), Co(II), Zn(II), Ru(II)) led to the formation of dinuclear triple helicates of general formula $[M_2L1_3]^{4+}$ in which three strands of ligand wrap around the 2 metal centres (Figure 2.3 b)).[13,24,25]

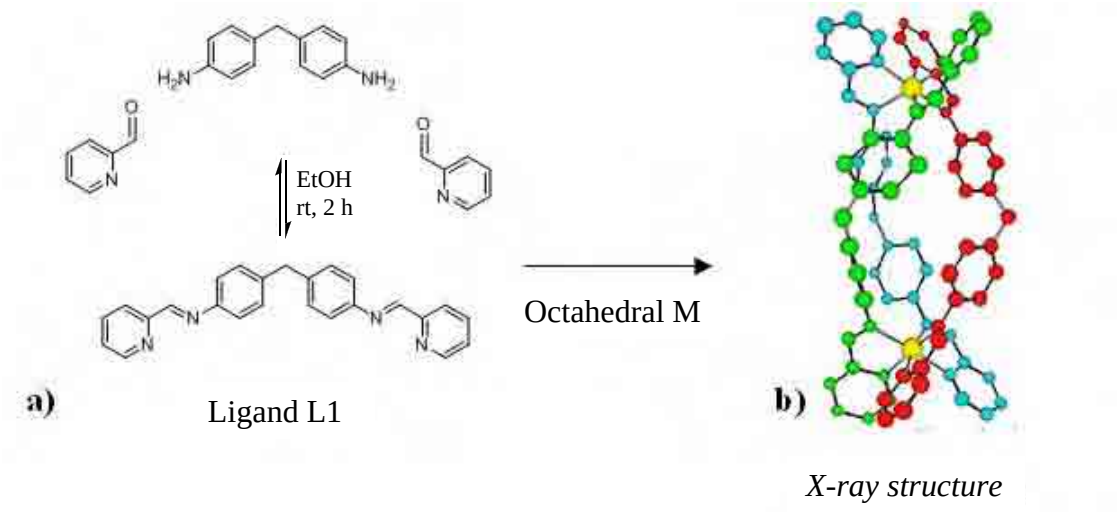

Figure 2.3. **a)** Scheme of synthesis of bispyridylimine based ligand L1, from which **b)** a triple stranded helicate ("cylinder") is obtained upon reaction with octahedral metals.

From a structural point of view the formation of these triple helicate complexes does not depend on the nature of the octahedral metal M (it forms with all the ones that have been investigated) and each N imine and N pyridine of the ligand are involved in the coordination of the metal centres. These new systems satisfy the design requirements to target the major groove of DNA via non covalent interactions: firstly they have the right dimensions (~2 nm length and ~1 nm diameter from X-ray studies) and shape (cylindrical, like the DNA-binding protein motifs) to exclude either binding in the minor groove or intercalation; secondly, they are saturated triple helicates (the metal centres are fully coordinated by the helical ligands[26] excluding metal coordination to the DNA bases) and the exposed surface, made of ligand strands, can easily form π-stacking (face to face or edge to face) interactions with the DNA.

Cylinders based on saturated triple stranded helicates of ligand L1 were the first to be investigated for binding to DNA in the Hannon group, and for this reason we refer to them as the "parent cylinders". Extensive DNA binding and biological studies have been carried out and are currently ongoing, in order to verify the potential of this new class of synthetic agents as potential drugs, with particular attention given to the triple stranded Fe(II) cylinder ($[Fe_2(L1)_3]^{4+}$)[13,15,18,22,27-30] and Ru(II) cylinder, ($[Ru_2(L1)_3]^{4+}$).[31,32] The Fe(II) cylinder is very easy to synthesise, purify and characterise. Its characteristics and its DNA binding properties are considered representative for all the "parent cylinders" in general.

Spectroscopic methodologies, such us UV-vis, Circular Dichroism (CD), Linear Dichroism (LD) and 1D and 2D NMR were the first techniques to study DNA binding activities of Fe(II) cylinder at molecular level. All the results demonstrated that this agent binds B-DNA (both long DNA from calf thymus and smaller oligonucleotides) in a single binding mode up to DNA:complex ratio of 5:1. At this concentration, the binding occurs via the major groove although at higher loading of complex other kinds of interactions cannot be excluded.[13,15,28]

LD experiments confirm that the binding starts at very low concentration of Fe(II) cylinder (100:1=DNA:complex), with the consequent effect of loss of initial orientation of B-DNA. Atomic Force Microscopy (AFM) experiments[13] provided a molecular-level picture of the binding and showed that by increasing the concentration of Fe(II) cylinder in the presence of linear plasmid DNA, there is

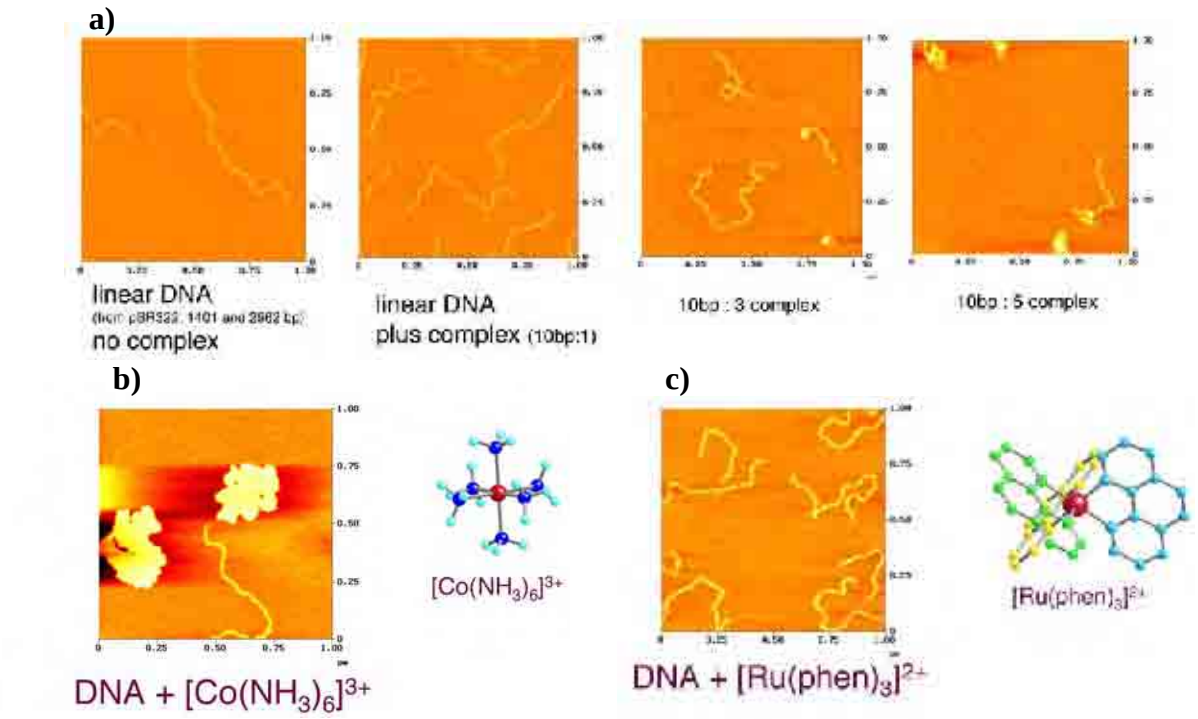

Figure 2.4 AFM images of linear plasmide DNA pBR322 in presence of **a)** several concentrations of $[Fe_2L_3]^{4+}$ **b)** $[Co(NH_3)_6]^{3+}$ and **c)** $[Ru(phen)_3]^{2+}$ (Figure adapted from ref. [13]).

bending followed by cooperative coiling of DNA around the complex (Figure 2.4-a)). This behaviour was interesting as it is unusual if compared with other known related mononuclear metal complexes: condensation agents such as $[Co(NH_3)_6]^{3+}$ and spermines cause aggregation of multiple DNA strands (Figure 2.4.b), and di-cationic $[Ru(phen)_3]^{2+}$ complex, whose structure can be seen as "half cylinder" produce simply bending of the DNA (Figure 4.c)).

The synthesis of the Ru(II) cylinder is not as straightforward as for Fe(II) and the yield not completely satisfactory (~33% at the moment). However the study of this complex is particularly important: the presence of Ru(II) centres provides the cylinder with a considerably better stability compared with other triple stranded cylinders, especially at higher temperatures; this allows the use of some techniques (such as PCR) whose experimental conditions are not always suitable for other cylinders. Moreover, the properties of luminescence and photo cleavage of this Ru(II) system add useful functionalities to the cylinders. Indeed ruthenium based

Figure 2.5: X-ray structure of Ru (II) cylinder (figure taken from ref.[21]).

drugs are among the most studied systems in the field of metallo-drugs in the last decade.[33-36] The X-ray structure of the Ru(II) cylinder is very similar to its Fe(II) analogue (Figure 2.5) and, as expected, the binding activity of the two complexes is comparable. There is no reason to suppose a different type of activity since shapes and dimensions play a decisive role for this type of DNA recognition. The photoresponse of the Ru(II) cylinder to DNA is very interesting: successive additions of ct-DNA to this complex induce both an enhancement in the intensity of the emission from the complex and a blue shift (8 nm) in the emission maximum. This increase in the luminescence occurs very rapidly and at DNA bases:complex ratio of 4:1 the intensity of the emission has almost doubled. At the moment different experiments are ongoing to convert this important property into useful applications, such as artificial DNA cleavage activity by photoactivation of ruthenium centres and the option of probing cylinder activity inside cells.

Although the cylinders were initially designed to target at the major groove of DNA, it was later discovered that the Fe(II) cylinder binds at the heart of DNA three way junctions (Figure 2.6), formed either with palindromic[18] or non palindromic[37] sequences of oligonucleotides. NMR and gel electrophoresis studies confirmed that this is not only a construct at the crystalline state, but a type of recognition that also occurs in solution and was also seen in other Y-shaped junction structures.[22,37] This is an unprecedented mode of interaction between a synthetic agent and nucleic acids and it could open an alternative way to achieve specific recognition of DNA. Most recently the ability of Fe(II) cylinder of stabilising G-quadruplex DNA has also been observed[38] and is currently under investigation in our lab.

Once the DNA recognition of parent cylinders had been described at molecular level, the study of their action in biological systems was also investigated.[30] IC_{50} values (half maximal inhibitory concentration) of the Fe(II) parent cylinder against

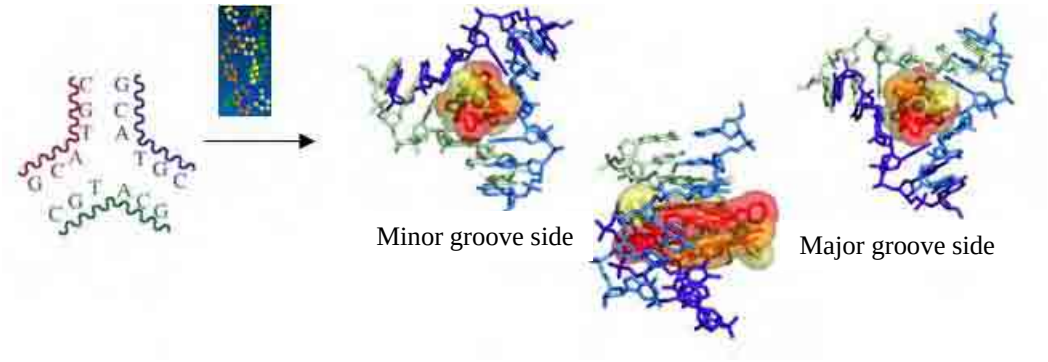

Figure 2.6: X-ray structure of Fe(II) cylinder binding at the heart of a three way junction formed by palindromic esanucleotides (Figure adapted from ref. [18]).

several cancer cell lines were evaluated using an MTT assay: a range of concentration of complex from 18 to 57 μM is needed to inhibit the mitochondrial activity (by 50%) in the cell cultures that have been tested and the Ru(II) cylinder exhibits a comparable cytotoxic activity. Such activity is approximately 5 times less than cisplatin activity, which is not surprising since a different molecular lever action is expected for these two agents. However, the cytotoxicity of parent cylinders is comparable with that exhibited by carboplatin, which is a cisplatin derivative that is alternatively employed in clinical treatments where there is resistance to cisplatin or drugs with lower toxicity are required.

Further experiments indicate that that Fe(II) parent cylinder is not mutagenic, as proved by Ames bacterial mutagenicity test, and is not genotoxic, as it does not generate DNA strands breaks in comet assay in mammalian cell lines. This aspect is particularly significant in drug design if we consider that the high mutagenicity and genotoxicity of cisplatin causes very serious side effects in chemotherapy.

Treatment of cultures of cancer cells with Fe(II) cylinder resulted in inhibitions of cellular proliferation and subsequent cell death by apoptosis, which is a further important requisite in drug action design: although cellular senescence and cell death by necrosis are also important, the ability of a drug to induce apoptosis is always preferred because it avoids nonselective necrotic mechanisms that produce adverse inflammatory responses.[39]

2.2.2 Other "cylinders".

The design of different variations on the "parent" triple-helicate-based "cylinders" has been possible using supramolecular chemistry as synthetic tool. Thus, many different cylinders have been synthesised, in order to investigate the effect of changes in the type of ligand and/or in the nature of the metal centres and/or in dimensions and shape of the complex, both for chemical and physical studies of the complexes and to observe the influence on DNA binding activity.

In Figure 2.7 there are three examples of ligands that have been employed to synthesise bulky Fe(II) cylinders.[16,20,29] Although these larger complexes bind the DNA, the binding properties are less remarkable than those of the parent Fe cylinder, and in some cases the mode of binding appears random without an apparent orientation of the cylinders as result of the interaction with DNA. This suggests that both the bending/coiling efficiency and the major groove targeting modality are related to size and dimensions of cylinders.

When reacted with tetrahedral metal ions such as silver(I) or copper(I), ligand L1 (Figure 2.3) forms a dinuclear species of composition $[M_2L1_2]^{2+}$. The flexibility of this ligand, coupled to the lability of these metal ions, leads to the presence in solution of two species in equilibrium[40]: a helicate (*rac*-isomer) in which each ligand strand wraps over and under the plane of metals ions, and a metallo-cyclophane (*meso*-isomer or box), in which one ligand lies above the plane of metal ions and the other lies below (Figure 2.8). To overcome the problem of the presence of two architectures in double stranded cylinders, ligand L5 (Figure 2.9) has been employed:

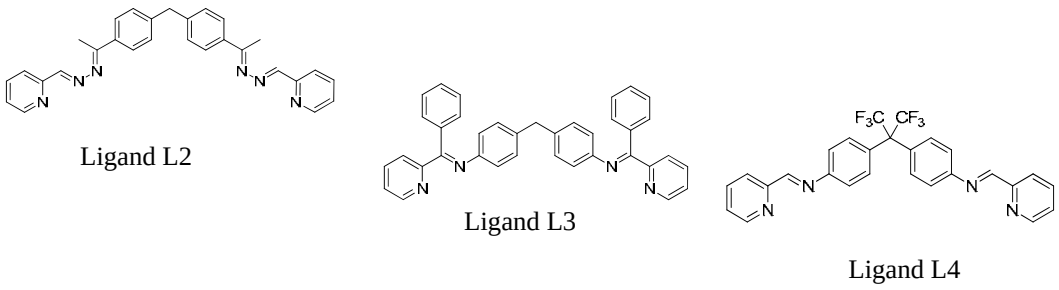

Figure 2.7: Three examples of ligands (L2[16], L3 and L4[29]) employed for the synthesis of bulky triple stranded Fe (II) cylinders.

Box (*meso* isomer) **Helix (*rac* isomer)**

Figure 2.8 Representation of cyclophane (box) and helix structures that are possible when ligand L1 is coordinated to tetrahedral metal ions.[40]

it contains bulky substituents in the central spacer and its reaction with tetrahedral metal ions results in the exclusive formation of the double stranded helical isomer. The larger steric bulk of the spacer twists the ligand, making the formation of the box isomer energetically unfavourable; the helix conformation is also stabilised by CH···π interactions between the end of the ethyl chains of one ligand and the aromatic ring of the spacer of the second molecule. The result is a very stable di-cationic Cu(I) double helicate complex, $[Cu_2L5_2]^{2+}$ which also binds ct-DNA but does not induce the same dramatic coiling and bending effect seen for the tetra-cationic triple helicates.[17] Since the copper(I) cylinder has very similar dimensions to the iron(II) cylinder and is only slightly different in shape (it appears a bit more like a "square" tube), the consistent difference in binding activity could in part depend on the lower positive charge of the copper system. These synthetic copper compounds

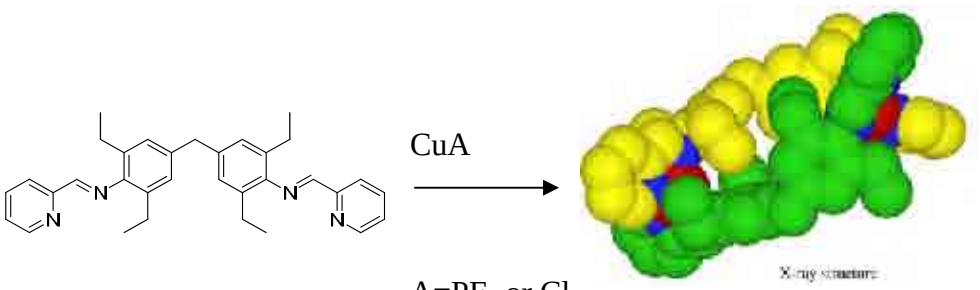

Ligand L5 Cu (I) double stranded cylinder

Figure 2.9 Bispyridylimine Ligand L5 with ethyl groups in the spacer to induce the formation of di- Cu(I) double stranded cylinder with helicate architecture (structure taken from ref. [17]).

can catalytically cleave DNA in presence of an oxidising agent,[41-44] acting as artificial nuclease; in fact, gel electrophoresis experiments confirm that the Cu(I) cylinder chops up plasmid DNA in the presence of hydrogen peroxide and shows some tendency to perform a double strand cleavage at the same site, which may reflect its di-nuclear nature.

A very important alternative to the di-Ru(II) "parent" cylinder described above is a set of double-stranded di-Ru(II) complexes which are based on the dinucleating bisazopyridine ligand (Ligand L6 in Figure 2.10).[19] In contrast to the "saturated" triple stranded helicate based on the bispyridylimine ligand system L1, the metals in the double stranded systems based on the azo analogue ligand L6 are "unsaturated" and two chlorides are required to complete the coordination of each Ru(II) centre. According to the configuration of each metal centre, several isomers are expected, five of which were isolated and characterised by X-ray crystallography. These complexes exhibit very exciting cytotoxic activities in both breast and ovarian cancer cell lines which is comparable with and in some case higher than cis-platin cytotoxicity. The different isomers show different levels of cytoxicity which would suggest that the activity of the drug depends on its architecture. In general all the cytotoxic azo ligand based Ru cylinders have lower IC_{50} values than the saturated imine ligand based triple helicates (i.e. are more active); this could suggest that the unsaturated Ru centres in the double stranded complexes could be directly involved in the binding with the DNA (Ru-DNA covalent bonds are frequent in Ru- based

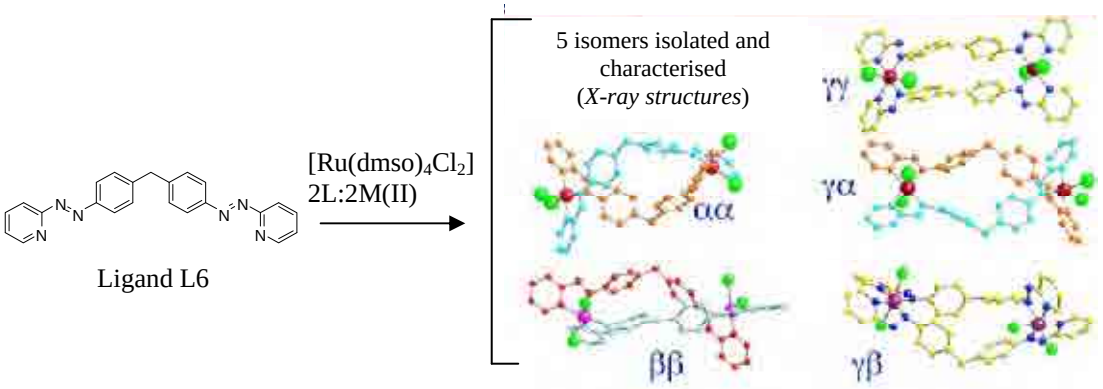

Figure 2.10. Bispyridil azo Ligand L6 and X-ray structures of 5 isomers of di Ru (II) double stranded cylinders (figure adapted from ref [19]).

drugs), whilst saturated triple helicate systems recognise the DNA by non-covalent interactions only involving the ligand surface of the cylinder.

2.3 Understanding dynamics in the Fe(II) cylinder.

2.3.1 Circular Dichroism.

In the following sections, as well as in Chapter 3 and 4, the chiralty of both helicates alone and helicate-DNA complexes will be object of analysis and discussion. Circular Dichroism (CD) is the most common spectroscopic technique for the study of chiral systems and is also widely employed to probe the interaction between DNA and other molecules, either biomolecules or synthetic agents.[45,46] This technique is based on the interaction between matter and circularly polarized light, whose electric field vector has a constant length, but rotates about its propagation direction, such to form a helix in the space while propagating (Figure 2.11). The light is referred as left or right circularly polarized when the helix is left or right handed respectively. The electronic rearrangement of chiral molecules, which are molecules that cannot be superimposed to their own mirror image, have no reflection plane so that the electrons move in some kind of helix as well. These kinds of systems absorb differently the left and the right circularly polarized light, and this difference in absorbance (A) is detected as CD signal (CD = A_l - A_r, where A_l and A_r are the

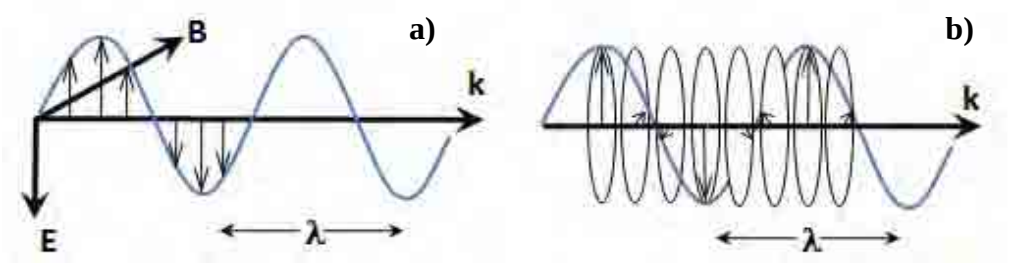

Figure 2.11. Representation of **a)** linearly and **b)** right circularly polarized electromagnetic radiation. In both cases **k** indicates the propagation direction of the radiation and arrows indicate the direction of electric field vector **E** which oscillates in the same plane of **k** in the linearly polarized light, whereas retains constant magnitude in time but traces out a helix about **k** if the light is circularly polarized.

absorbance of left and right circularly polarized light respectively, with a corresponding $\Delta\varepsilon=\varepsilon_l-\varepsilon_r$, where ε_l and ε_r are the molar extinction coefficients for left and right circularly polarized light). Chiral systems could be either small organic molecules or coordination complexes (in fact the chirality of helicates will be analysed by CD in the following sections and in Chapter 3), but also large secondary or tertiary structures such as proteins, membranes or DNA (CD is one of the methods employed for DNA binding studies by helicates in Chapter 4).

2.3.2 Structure and chirality of Fe(II) cylinder.

To date the tetra cationic Fe(II) triple helicate, described in section 2.2.1, is considered as one of the most representative cylinders: it is easy and very inexpensive to synthesise; each Fe(II) centre, is low spin and the system is diamagnetic so that both characterisation and experiments via NMR are possible. By changing the counter anion it is possible to dissolve the complex in different solvents (the chloride salt is soluble in water and alcoholic solvents, hexafluorophosphate and hexafluoroborate salts are soluble in other organic solvents such as acetonitrile, acetone and nitomethane). This allows both the study of chemical and physical characteristics of the system in different conditions and the investigation of its suitability for biological applications in water soluble conditions.

The molecular structure of Fe(II) parent cylinder has been determined by X-ray analysis (Figure 2.12. a)[24]: each Fe(II) centre is coordinated by three N imine-N pyridine bidentate units from three different strands of ligand L1 and the pseudo-octahedral geometry of each Fe(II) centre causes an intermolecular twisting at the level of the phenylene spacer units, with consequent formation of a triple helicate. In addition to metal ion-ligand interactions, there are six edge-face π-stacking interactions between the aryl rings of the spacer which contribute to stabilise the structure (Figure 2.12.b) and c)).

As in any other helical structure, the triple helicate-based cylinder has a right or left handedness: when it is viewed down its helical axis, it is right-handed or P (plus) helicate if it rotates clockwise and left-handed or M (minus) if it rotates anticlockwise. Furthermore, the two octahedral metal centres in any ligand L1 based cylinders are homo configurational, since they present the same optical configuration

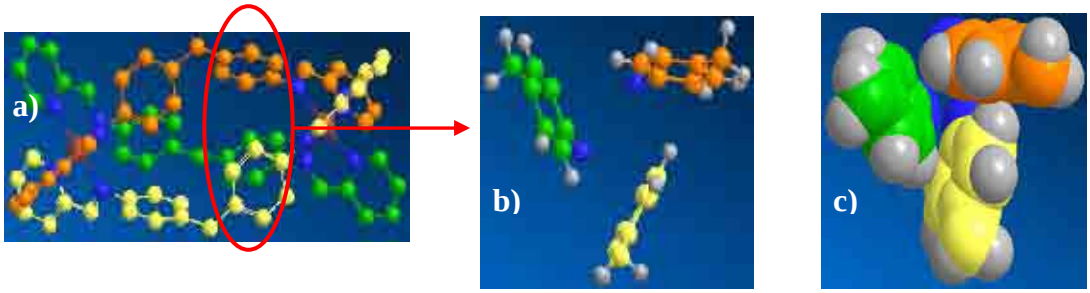

Figure 2.12. **a)** X-ray structure of Fe(II) parent cylinder. Highlighting the edge-face interactions: **b)** balls and sticks and **c)** space filling between aryl rings.

(ΔΔ or ΛΛ) in each enantiomer. Because of the geometry of theoctahedral metal ions and the symmetry of the ligand L1, the synthesis affords a racemic mixture of the two enantiomers of the triple stranded parent cylinders. However, the two enantiomers of Fe(II) cylinder can be separated on a cellulose column (or paper sheets, Figure 2.13.a)) eluted with 20 mM NaCl solution, and, as expected, they are perfectly equivalent by NMR and UV-Vis, but they present two distinct and opposite CD signals (Figure 2.13.b)). The first enantiomer eluted from the column is the M

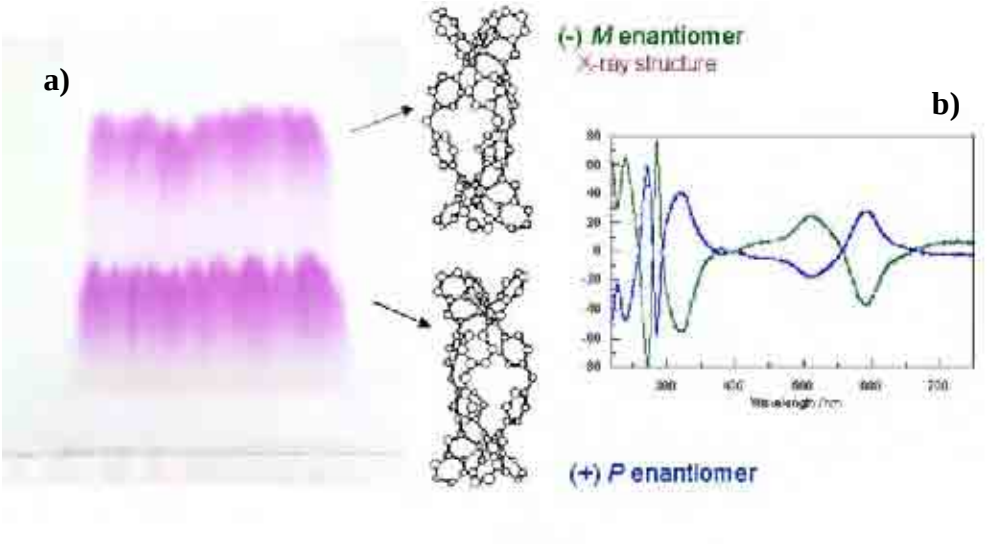

Figure 2.13. a) separation of M and P enantiomer of Fe(II) parent cylinder on cellulose and **b)** the corresponding CD signals (Figure adapted from ref. [47]).

enantiomer (confirmed by X-ray). The configuration of the Fe(II) centres of the M enantiomer is ΛΛ although its CD signal (green line in figure) presents a Cotton effect whose sign is typical for tris-chelate mono nuclear complexes with Δ configuration.[46,48] This confirms that the absolute configurations of metal centres in a polynuclear complex may be incorrectly assigned on the basis of CD data. In fact the CD sign and magnitude of these complexes not only depend on intranuclear exciton coupling between chromophores located on the same metal centre, but there is also the contribution of internuclear exciton coupling between chromophores located on two different metal centres, which is not present in mononuclear complexes. The CD signal is the result of which of these two contributions prevails in each specific polynuclear complex.[49]

The chirality of these systems is a very significant issue for applications in new drug design. The chirality of biomelocules (DNA, RNA, proteins) is the proof that systems with a specific orientation have been selected in nature. In some cases, the chirality of the DNA itself can influence its interaction with different structural or stereo isomers of the same agent. Indeed, it has been demonstrated that the M enantiomer of the Fe(II) cylinder has higher affinity in binding the DNA than the P enantiomer, whilst the binding activity of the racemic mix is an average between the activities of the two enatiomers separately.[27]

2.3.3 Characterisation and dynamic studies by ^{1}H NMR spectroscopy.

Part of the work presented in this thesis and described in this section and in the next section, concerns the study of the behaviour of the Fe(II) cylinder at different temperatures and in two different solvents (water and acetonitrile). This aims to achieve a better "chemical" knowledge of this system and understand whether there are remarkable changes of the molecule in certain conditions. The information obtained from these studies could also facilitate the understanding of DNA recognition studies and help the planning of the most appropriate biological tests. Some initial variable temperature (vt) NMR experiments of $[Fe_2L1_3](PF_6)_4$ in acetonitrile and estimation of free energies activation were already described in C.L. Painting PhD thesis,[50] but they are shown again in this section for the completeness of the discussion. Herein, the aim was to complete those vt-NMR studies with some

additional NMR experiments (also presented in this section) and perform a set of UV-Vis and CD thermal experiments (section 2.3.4) that combined with the NMR experiments would allow a better understanding of the dynamic behaviour of Fe(II) cylinder.

The bispyridylimine ligand L1 was synthesised by mixing 4,4'-methylenedianiline (1 eq) and 2-pyridine carboxaldehyde (2 eq) at room temperature in ethanol to obtain Schiff base formation[24]. A deep purple solution was obtained by mixing 3 eq of L1 with 2 eq of Fe(II) chloride, as cylinder $[Fe_2L1_3]Cl_4$ is formed. The counter anion can be exchanged from Cl^- to PF_6^- by addition of saturated methanolic solution of ammonium hexafluorophosphate which causes the precipitation of purple $[Fe_2L1_3](PF_6)_4$. In Figure 2.14 the ^1H NMR spectrum of the complex in CD_3CN at 298 K is compared with the spectra of its building block components (spacer + carboxaldehyde=Ligand L1). The pyridyl and imine protons of the complex are

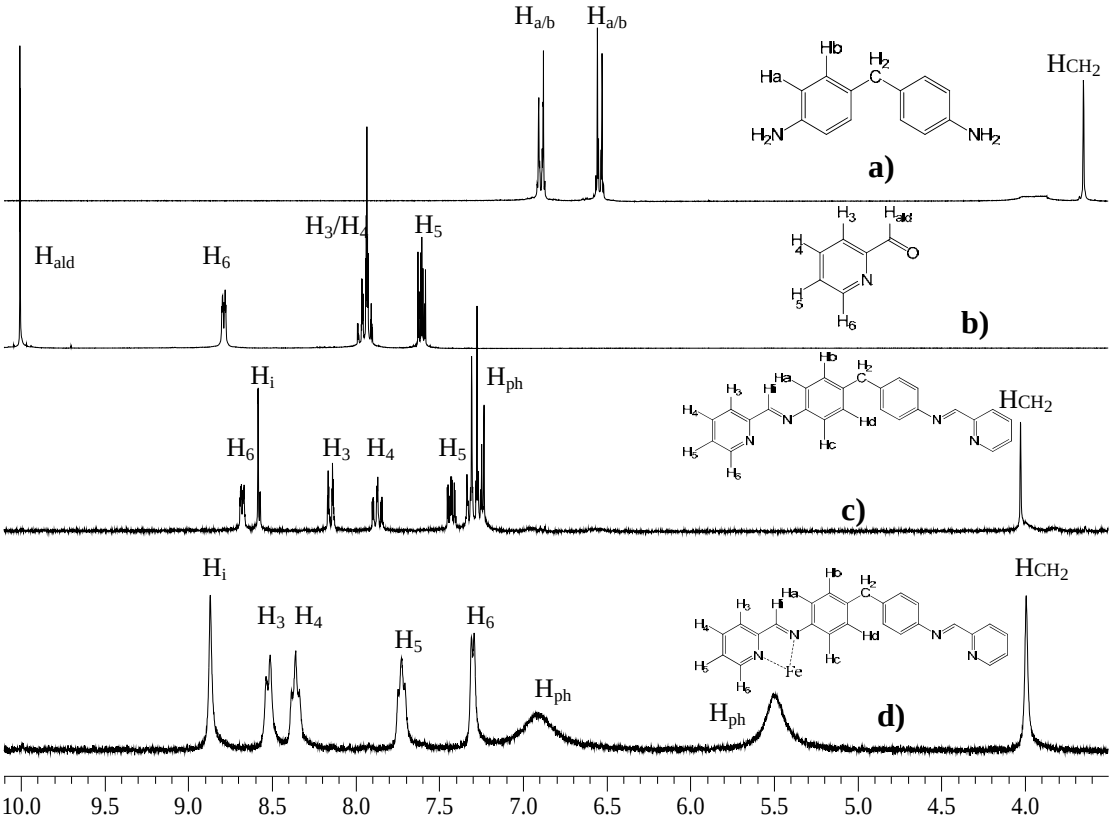

Figure 2.14. ^1H NMR (300 MHz, CD_3CN, 298K) of **a)** 4,4'-methylenedianiline, **b)** 2-pyridine carboxaldehyde, **c)** Ligand L1 and **d)** $[Fe_2L1_3](PF_6)_4$.

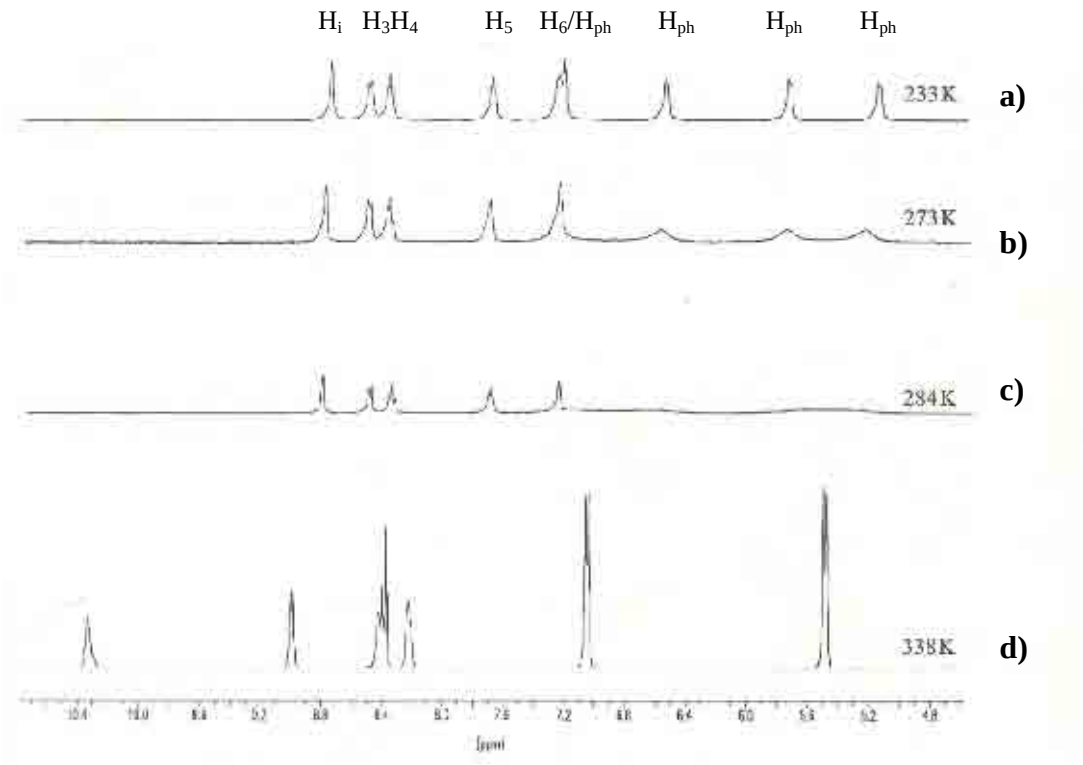

Figure 2.15. ^{1}H NMR (400 MHz) of $[Fe_2L1_3](PF_6)_4$ in CD_3CN at different temperatures (Figure taken from ref. [50])

shifted (compared to the ligand L1 protons) and H_6 and Hi present the most significant shifts as expected consequence of the coordination of N pyridine and N imine to Fe(II) ion. In the spacer and the ligand L1, protons Ha and c are equivalent, because of the symmetry of the phenylene group. In the same way Hb and d are equivalent. Consequently the phenylene protons appear as a set of 2 peaks, whose chemical shift and multiplicity depend on the substituent groups of the aryl ring (Figure 2.14 c)). However, when the complex is formed, the same protons appear as two broad signals at room temperature (Figure 2.14 d)).

^{1}H NMR variable temperature studies of the Fe(II) cylinder in acetonitrile, presented in C.L. Painting PhD thesis,[50] showed that at low temperature, up to 253 K, there are 4 separate resonances corresponding to the 4 phenyl protons, Ha, b, c and d (Figure 2.15 a)). By increasing the temperature, two main features are observed: i) the signals corresponding to phenylene protons Ha and c (and Hb and d) initially start to broaden (at 273 K, Figure 2.15 b)), then they flatten out (Figure 2.15 c)) and they coalesce in one broad band at room temperature until they become one single sharp doublet at 338 K (Figure 2.15 d)); ii) starting from ~300 K all the pyridine and

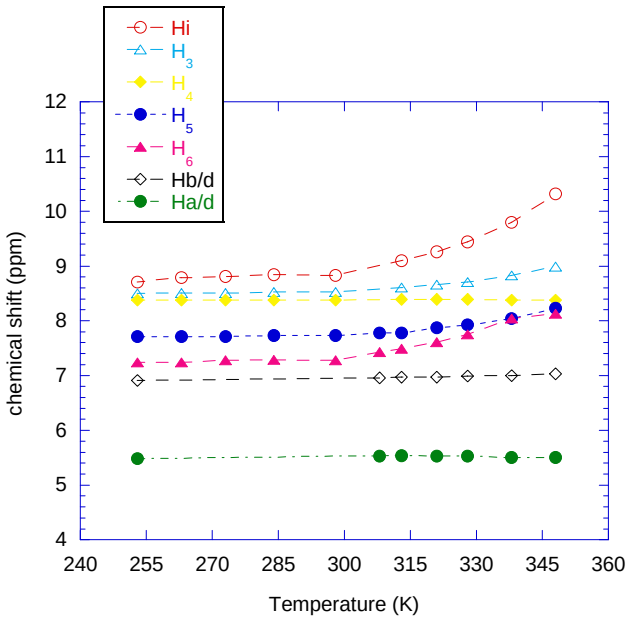

Figure 2.16. Chemical shifts (ppm) in function of the temperature (K) for each aromatic proton of $[Fe_2L1_3](PF_6)_4$ in CD_3CN. Hi and H_6 (red and pink curves respectively) exhibits the higher shift effect starting from 300 K.

imine proton peaks shift, but this effect is particularly significant for the H_i and H_6 protons, which are the closest protons to the two nitrogen responsible for the coordination. This is more evident in the graph in Figure 2.16 where chemical shifts versus temperature are reported for all the aromatic protons. In C.L. Painting PhD thesis, it was already suggested that these effects (the behaviour of the phenyl rings and the shift of H_i and H_6) might have two distinct causes, although both temperature depending, and herein this is further confirmed with additional experiments.

The behaviour of the phenylene protons is the result of a typical environmental exchange. Due to the involvement in face-edge π interactions (see X-ray structure Figure 2.12 b and c)), the two edges of the aryl rings are in two different environments (only one of two opposite edges point at the face of another ring). Consequently Ha and c and (Hb and d) are not each other equivalent as they are in the free ligand L1 or in the spacer. At low temperature the phenylene rings rotate very slowly and the rate constant for the exchange Ha-Hc from one environment to the other is lower than the frequency difference of the proton resonances in the separate environments and the two protons appear with two single signals. When the temperature increases, the phenylene rings start to rotate more freely and the two

protons Ha-Hc (and Hb-Hd) start to exchange with a higher rate constant comparable with their frequency difference; the two signals coalesce in one broadened signal at a coalescence temperature (*Tc*) of ~284 K. On further warming the speed of the phenylene rings increases and at a certain temperature Ha and c (and Hb and d) exchange so fast that their resonance appear as one sharp signal.

In this system the barriers to the phenylene rings spinning freely are (i) the π-stacking interactions must be broken and (ii) steric effects that probably force the rings to spin concertedly (if the phenylenes spin randomly within the triple helix the protons would clash). Free energy of activation and rate of spinning at the coalescence temperature where estimated in different solvents:[50,51] in CD_3CN $\Delta G^{\ddagger}_{288}$= 55.0±0.4 kJ/mol and $\Delta G^{\ddagger}_{285}$=55.2±0.4 kJ/mol, k_{288}=630±20 s^{-1} and k_{285}=450±20 s^{-1}; in CD_3NO_2 the value of *Tc* is the same for both peaks and $\Delta G^{\ddagger}_{294}$= 56.6±0.4 kJ/mol and k_{294}=540±20 s^{-1}; in CD_3OD $\Delta G^{\ddagger}_{294}$= 55.4±0.4 and k_{294}=450±20 s^{-1} (peaks overlap with solvent peak, thus only one set of value could be calculate). These values would be on the very high side if they just represent breaking of a single π-stacking interaction within the system[52] and this would seem to confirm that steric effects are also involved leading to concerted spinning.

Herein, it was possible to assign the two doublets at 338 K to the correspondent Ha/c or Hb/d protons by a combination of HSQC and HMBC experiments at 340 K . In the HSQC spectrum (Figure 2.17 a)) the cross peak correspondent to the CH_2 proton, confirms that the carbon at 40.1 (i) is the CH_2 carbon C1. The same spectrum (enlargement in Figure 2.17 b)) shows that the two carbon at 123.9 (ii) and 131.2 (iii) can be either C3 or C4 of the phenylene ring because each of them is correlated to one of the two phenylene protons. In the HMBC spectrum there are only two cross peaks relative to CH_2 protons (Figure 2.17 c), although this technique reveals long range heteronuclear couplings with proton observation up to 5 bonds. Consequently the carbon at δ 143.8 (iv), which is not correlated to any phenylene protons in the HSQC spectrum, is C2 and the signal at δ 131.2 (iii) necessary correspond to C3. Returning to the HSQC spectrum (Figure 2.17 b)), since the carbon at 131.2 (iii) corresponds to C3, then the carbon at 123.9 (ii) is C4 and from the correlations in the same spectrum we can confirm that the proton at 7.03 is Hb/d and the proton at 5.50 is the Ha/c at 340 K.

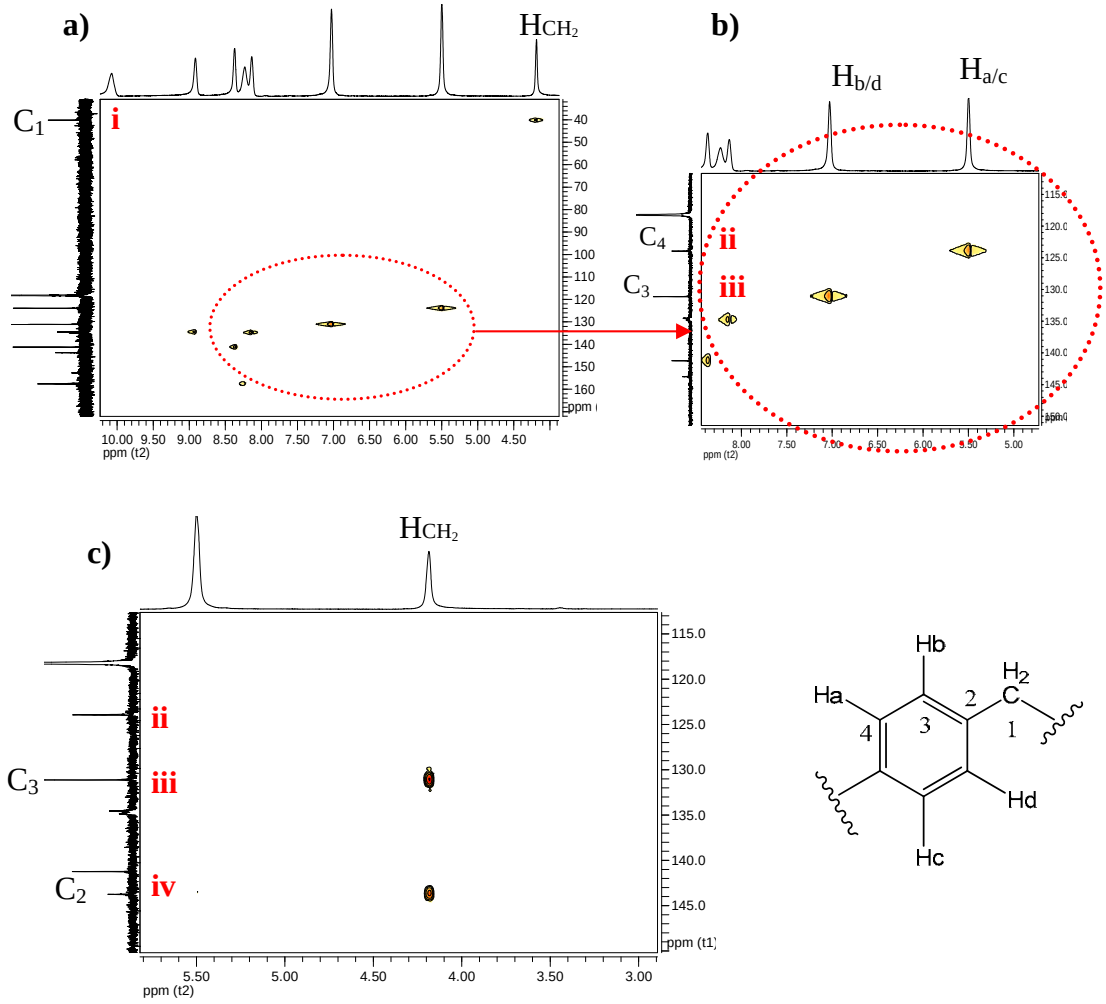

Figure 2.17. 2D NMR (500 MHz, 343 K) of $[Fe_2L1_3](PF_6)_4$ in CD_3CN: **a)** HSQC, **b)** enlargement from the HSQC in **a)** and **c)** HMBC. Carbon resonances significant for the discussion are: δ 40.1 (i), 123.5 (ii), 131.2 (iii), 143.8 (iv).

In order to exclude any effect of complex degradation in acetonitrile at temperature close to acetonitrile boiling point, the ^{1}H NMR spectrum of the complex was compared with the ^{1}H NMR spectra of the starting components (ligand L1, spacer and carboxaldehyde) at 340 K (Figure 2.18). It was observed that at this temperature there is no proton of the complex (Figure 2.18 d)) whose chemical shift coincides with any chemical shift of the protons from the starting materials (Figure 2.18 a), b) and c)).

In Table 2.1 all the chemical shifts of the complex and starting materials at 298 and 340 K are compared. The data were extracted from the NMR spectra shown in Figure 2.14 and 2.18 and are consistent with the results presented by C.L. Painting

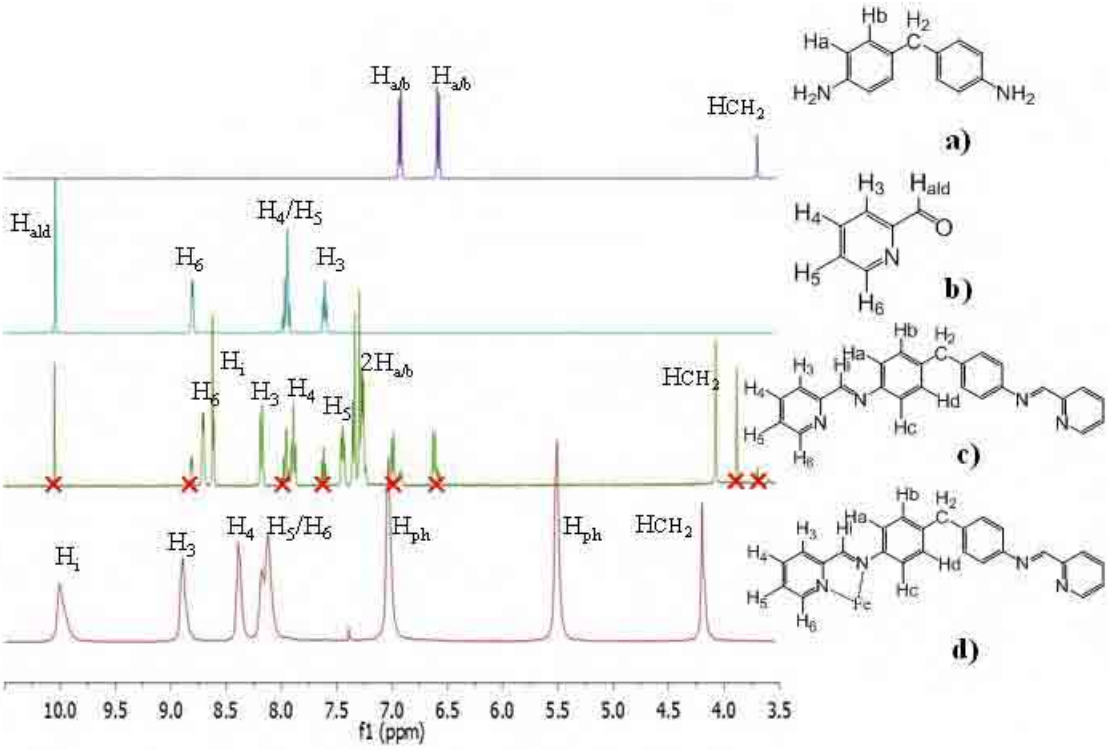

Figure 2.18. ^{1}H NMR (300 MHz, CD_3CN, 340K) of **a)** 4,4'-methylenedianiline, **b)** 2-pyridine carboxaldehyde, **c)** Ligand L1 and **d)** $[Fe_2L1_3](PF_6)_4$. In spectrum **c)**, peaks marked with a red cross correspond to protons of the compounds deriving from ligand degradation at high temperature (4,4'-methylenedianiline and 2-pyridine carboxaldehyde).

in her PhD thesis. The table highlights that the effect of protons shifting, as a consequence of the variation of temperature, concerns only the protons of the complex, whilst temperature does not affect the chemical shift of the protons of the starting compounds. ^{1}H NMR spectrum of ligand L1 (Figure 2.18 c)) presents, besides the protons of the ligand itself, also other peaks that correspond to both 4,4'-methylenedianiline and 2-pyridine carboxaldehyde protons (marked with red crosses) as consequence of imine bonds of the ligand L1 breaking at high temperature. Also the presence of half ligand (where only one of the two imine bond is broken) cannot be excluded. The instability of ligand L1 at high temperature is expected, as well as the fact that it is significantly more stable when it is involved in the formation of the complex.

These results (together with further UV-Vis thermal experiments described below

Compound (Temp. K)	H_{ald} (δ)	Hi (δ)	H_3 (δ)	H_4 (δ)	H_5 (δ)	H_6 (δ)	$H_{b/d}$ (δ)	$H_{a/d}$ (δ)	HCH_2 (δ)
a) (298 K)							6.93	6.56	3.69
a) (340 K)							6.92	6.57	3.70
b) (298 K)	10.03		8.80	7.95 (overlapped)		7.63			
b) (340 K)	10.05		8.80	7.95 (overlapped)		7.61			
c) (298 K)		8.62	8.17	7.90	7.46	8.81	7.31 (multiplet)		4.06
c) (340 K)		8.62	8.17	7.89	7.45	8.70	7.27 (multiplet)		4.07
d) (298 K)		8.94	8.58	8.41	7.79	7.37	6.99 (br)	5.55 (br)	4.05
d) (340 K)		9.90	8.83	8.38	8.04	7.96	7.00	5.50	4.18

Table 2.1. Comparing chemical shifts of ^1H NMR spectra (400 MHz, CD_3CN) of a) 4,4'-methylenedianiline, b) 2-pyridine carboxaldehyde, c) Ligand L1 and d) $[Fe_2L1_3](PF_6)_4$ at 298 K (blue) and 340 K (red).

in section 2.3.4) suggest that in vt-NMR experiments (Figure 2.16) complex degradation is not involved and the behaviour of the phenylene protons is due to a typical environmental exchange, whose energetic barrier has been quantified. However, UV-Vis and CD experiments described below suggest that the temperature-depending shift of Hi and H_6 is due to a distinct dynamic process that involves the two coordinating units of the helicate.

2.3.4 UV-Vis and CD studies of $[Fe_2L1_3](PF_6)_4$ in acetonitrile.

The UV-vis spectrum of $[Fe_2L1_3](PF_6)_4$ in acetonitrile (Figure 2.19) shows a band at 572 nm due to MLCT transition and 3 more bands at 324, 277, 237 nm, due to electronic transitions in the ligand L1. Since the NMR thermal experiments evidence

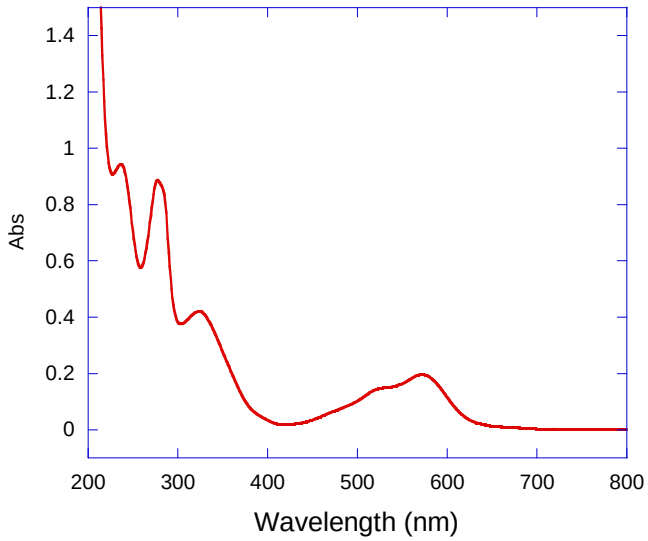

Figure 2.19. UV-Vis spectrum $[Fe_2L1_3](PF_6)_4$ in acetonitrile.

that the increasing of the temperature affects the protons that are closest to the two coordinating sites, suggesting that alterations related to the metal centres and their coordination occur, we were particularly interested to observe the behaviour of the MLCT band in different temperatures.

The thermal experiment in Figure 2.20 a) shows a linear decreasing of the absorbance at 572 nm of a 900 μM solution of the complex in acetonitrile, in 1 mm path length, when the temperature was raised from 5 to 78 °C in 1 °C/min rate (red circle). In the same experiment the temperature was then successively decreased from 78 to 5 °C with the same rate. The absorbance at 572 nm increases again, with exactly the same linearity, to reach exactly the same initial value at 5 °C.

The concentration used in the experiment in Figure 2.20 a) is comparable with NMR experiment concentrations (around 1000 μM), but this behaviour is not concentration dependent, as showed in Figure 2.20 b)**,** where the same experiment was carried out by using 50 μM complex solution in 1 cm path length and an analogous result was obtained. Individual scans of the complex in the whole UV-Vis region at different temperatures (Figure 2.21) confirm that upon increasing the temperature there are no new bands or other global spectral changes but only a linear decrease in magnitude of the absorbance at each maximum, and this process is reversible. This variation of the molar extinction coefficient ε at different

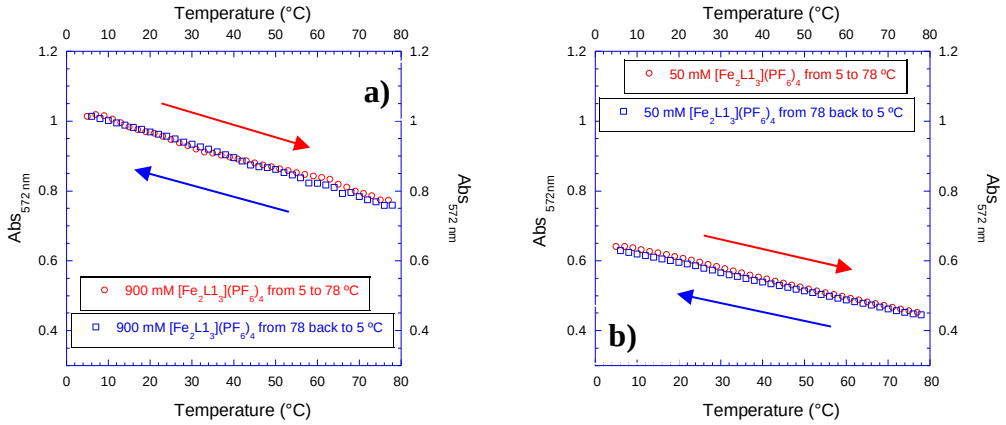

Figure 2.20. UV-Vis thermal experiment of **a)** 900 μM (1 mm path length) and **b)** 50 μM (1 cm path length) $[Fe_2L1_3](PF_6)_4$ in acetonitrile. In both experiments the absorbance at 572 nm is monitored when temperature is raised from 5 to 78 °C at 1 °C/min rate (red circle) and then decreased back to 5 °C at the same rate (blue square).

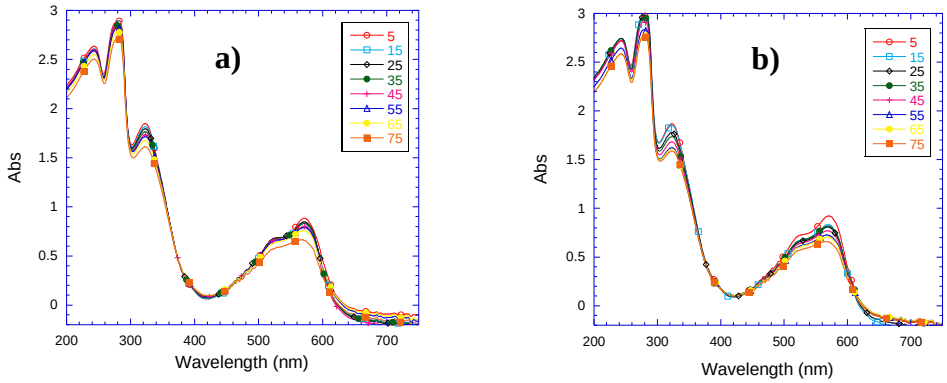

Figure 2.21. UV-Vis scans at 10 °C intervals of 75 μM $[Fe_2L1_3](PF_6)_4$ in acetonitrile (1 cm path length) **a)** when temperature was increased from 5 to 75 °C at 1 °C/min rate and **b)** decreased back to 5 °C at the same rate.

temperatures seems more likely to be due to small dynamic variations inside the structure of the complex rather than destruction of the compound (because the variation is reversible) or changes of the spin state of the Fe (II) centres (since the NMR does not broaden as might be expected if high spin iron centres were resent). However, the process observed by UV-Vis spectroscopy is not necessary that leading

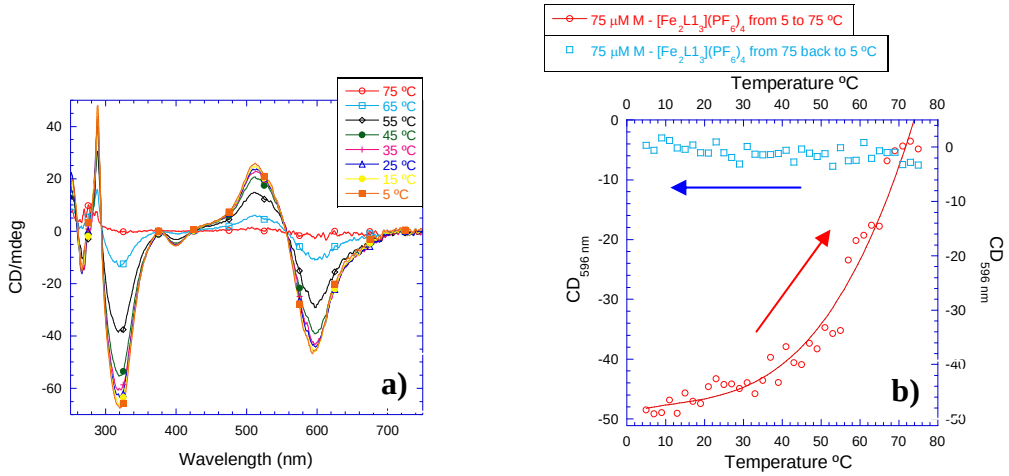

Figure 2.22. CD thermal experiments with 75 μM of M enantiomer of $[Fe_2L1_3](PF_6)_4$ in acetonitrile (1 cm path length): **a)** temperature was increased from 5 to 75 °C at 1 °C/min rate and CD scans were recorded with intervals of 10 °C; **b)** during the same experiment CD absorbance at 596 nm was monitored when temperature was increasing (red circle) and decreased back to 5 °C at the same rate (blue square).

to the chemical shifts in the NMR spectrum, since the linear variation in ε occurs between 5 at 70 °C, while the chemical shift effect only assets above 20 °C.

One process that we thought possible and wished to investigate was an interchange between P and M configurations. To explore this circular dichroism (CD) spectroscopy has been employed. CD scans of a 75 μM solution of the M enantiomer of $[Fe_2L1_3](PF_6)_4$ in acetonitrile at different temperatures (Figure 2.22 a)) show a loss of CD signal on increasing the temperature. The graph in Figure 2.22 b) (CD at 596 nm vs temperature) indicates an exponential type loss of signal and complete racemisation isobserved at 70 °C. The fact that the complex in acetonitrile racemises (as is evident from CD data) but it does not break apart (see UV-Vis and NMR experiments) suggests that it is thermodynamically stable but kinetically labile. To verify whether racemisation occurs only at highest temperatures, the CD signals of the M enantiomer of both PF_6^- and Cl^- Fe(II) cylinders (in acetonitrile and water respectively) were monitored at room temperature over a 14 days period (Figure 2.23). For each solution of complex in acetonitrile and water, both CD and UV-Vis spectra were recorded every 24-48 hours and the magnitude of CD absorbance at 596 nm (which is the minimum of the band at higher wavelengths of the CD spectrum)

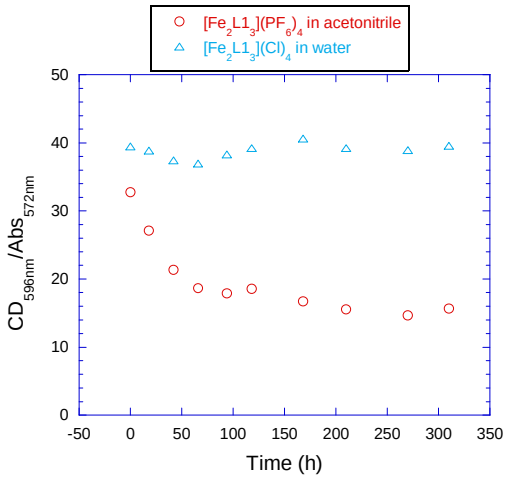

Figure 2.23. CD absorbance at 596 nm (normalized from the corresponding UV-Vis absorbance at 572 nm) of $[Fe_2L1_3](PF_6)_4$ (red circle) and $[Fe_2L1_3](Cl)_4$ (blue triangle) in acetonitrile and water respectively as a function of the time.

was divided by the magnitude of the corresponding UV-Vis absorbance at 572 nm (which is the maximum of the MLCT band) to normalise from any degradation effects. The graph in Figure 2.23 shows that the complex is enantiomerically stable in water at room temperature but in acetonitrile there is loss of ~50% of enantiomeric purity during the first 50 hours and then the CD signal remains approximately stable for the rest of the period over which it was observed. However, the thermal experiment described in Figure 2.22 is carried out over 2 hours (to go from 10 to 70 °C), consequently contribution of kinetic instability in that experiment can be considered irrelevant.

Interestingly, the loss of CD signal in Figure 2.22 becomes significant starting from ~40 °C and approximately at this temperature, in NMR experiments, the signals of Hi and H_6 start significantly to shift to low fields (Figures 2.15 and 2.16). This might therefore be the same process observed in the NMR studies.

Obviously, the racemisation of the triple helicate is a consequence of the inversion of the configuration of the two tris(chelate) Fe centres at higher temperatures. Several possible mechanisms that cause racemisation in mono nuclear tris(chelate) complexes have been described.[53,54] One mechanism involves temporary but complete dissociation of one or more ligands, with formation of intermediate complexes where, in some case, the solvent is also involved. This type of mechanism occurs when the rate of dissociation of the complex is higher than the rate of

racemisation. Both NMR and UV-Vis thermal studies described above suggest that this is not occurring: if there is ligand exchange we would expect the chemical shifts of the phenyl protons at high temperature to be an average between their chemical shifts in the complex and the free ligand. Also there are no changes in the UV-Vis profile at high temperature (no new bands) and this does not support the possibility of ligand dissociation and/or formation of intermediates.

Other mechanisms for mononuclear compounds are based on intramolecular pathways in which ligands interchange each other without bond rupture. At least four of these mechanisms, where the symmetry of the intermediates is allowed, have been identified (Figure 2.24).[54] The "push through" and the "crossover" pathways are based on six coplanar ligands and four coplanar ligands transition states respectively. They both require large metal ligand bond stretches to relieve steric barriers and are energetically unfavourable. The other two mechanisms are known as Bailar twist[55] and Rây-Dutt[56] twist and, since they require more modest bond stretches, they are believed to be the most frequent in intramolecular racemisation. The Rây-Dutt, also

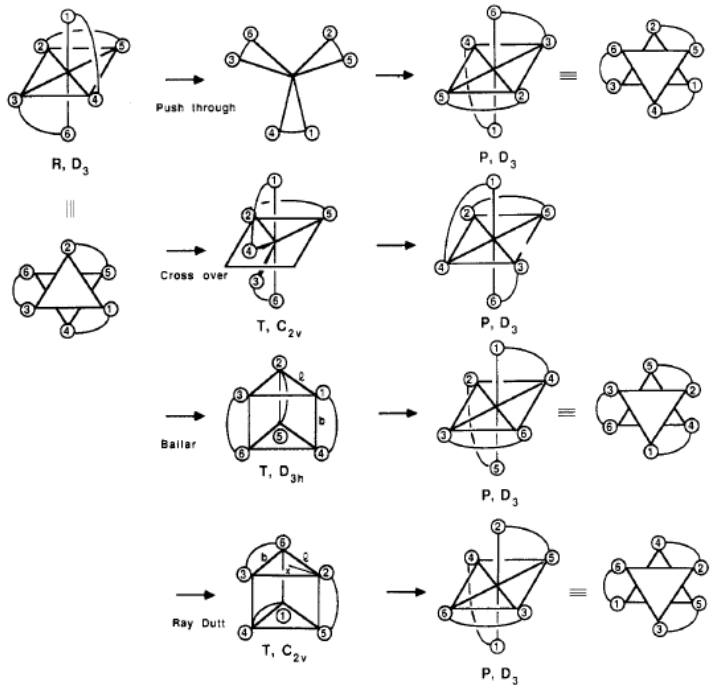

Figure 2.24. Four intramolecular mechanism for racemization of a tris(chelate) octahedral compplex (R = reactant, T = transition state, P = product, figure taken from ref. [54]).

known as the rhombic twist, involves rotating a trigonal face that is not associated with a threefold axis of the complex through a C_{2v} transition state into its mirror image. With the Bailar twist pathway the complex twist about a threefold axis via the formation of a trigonal prismatic intermediate with D_{3h} symmetry. Defining the bite *b* as the distance between donor atoms in the same chelating ligand and *l* as the distance between donor atoms on neighbouring chelate ligands, usually a rhombic twist is favoured when *b* is much greater the *l*; Bailar twist mostly occurs when *b* is smaller than *l*.

The Fe(II) cylinder is a di-nuclear complex in which the metal centres of each enantiomer have specific configurations and reciprocal orientations defined by the rigidity and the orientation of each poly chelating ligand L1, and for this reason not all the intramolecular mechanisms are possible. Figure 2.25 a) shows the detail of the two tris(chelate) complex units (A and B) extracted from the X-ray structure of the M enatiomer. They both have Λ configuration and are in pseudo-parallel reciprocal orientation. Figure 2.25 b) shows the configuration of the two metal centres from the M enantiomer, and chelating units with their corresponding spacers are indicated with plain and dash lines respectively. Dash lines indicate how each spacer connects the imine nitrogens of two different chelating units that belong to the same ligand (for example dash green line represents the spacer that connect nitrogen 5 of complex A to nitrogen 2' of complex B). In the same way the P enantiomer is represented in Figure 2.25 d) (obviously the 2 metal centres have Δ configuration after racemisation). Because of the structure of the two enantiomer-helicates, the coordinating imine nitrogen 4, 5 and 6 of the metal centre A and the 1', 2' and 3' of metal centres B, must remain on the side of the metal centre that looks at the other metal centre. Only by Bailar twist mechanism this is possible in each phase of the racemisation event. Any other intramolecular mechanisms (among those described above) or a combination of them (supposing that the two complex units racemise with two different mechanisms) would require that one or more of the coordinating imine nitrogen ends pointing at the external edge of the cylinder, and this would be possible only with helicate rupture.

Furthermore, comparing the Bailar twist and Rây-Dutt pathway for a single tris(chelate) units (Figure 2.26), only the former involves a rotation that is simultaneously equivalent for all the chelating units so that the racemisation process

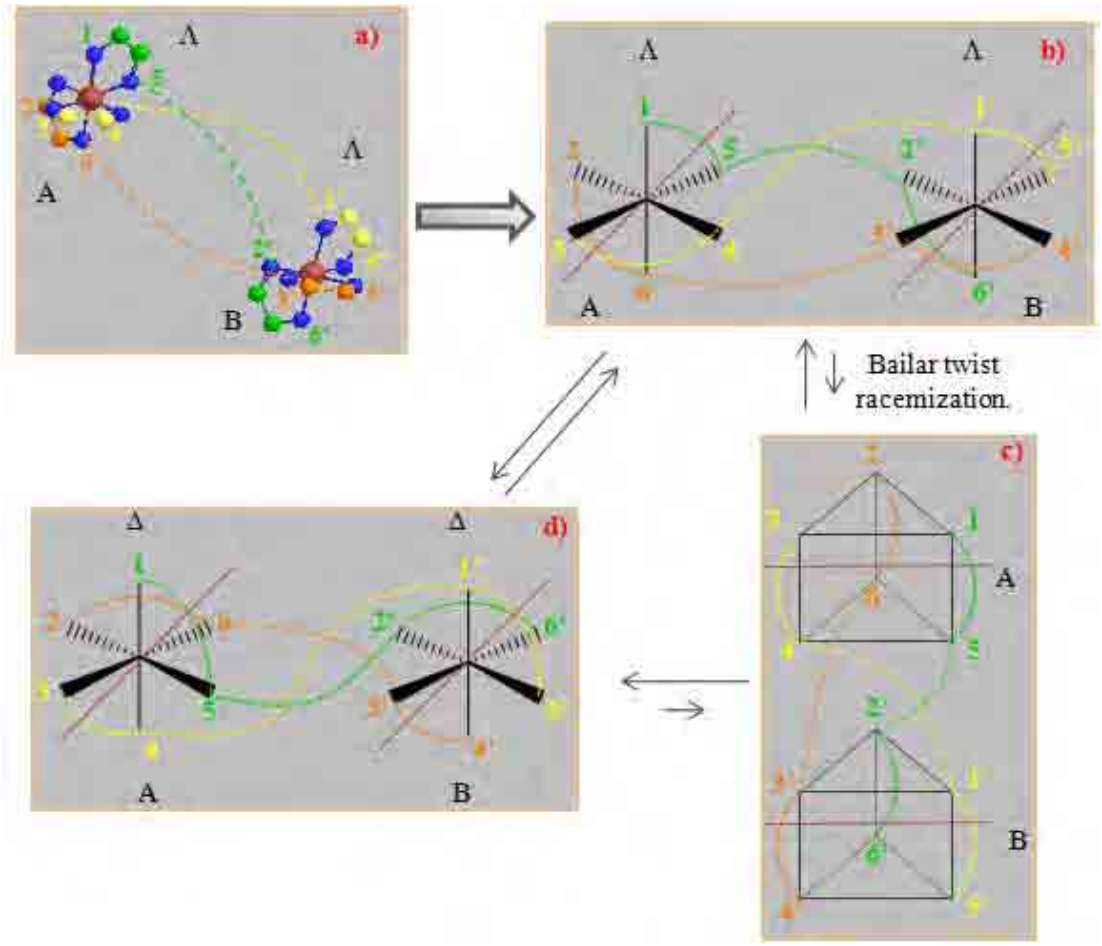

Figure 2.25. a) two tris(chelate) Fe (II) centres (ΛΛ configuration) from the X-ray structure of the M enantiomer of the Fe(II) cylinder; in **a)**, **b)**, **c)** and **d)** the dash lines represent how each spacer connect each couple of chelating units (from the same ligand) between the two centres; **b)** representation of the configurations of the two metal centres of M enantiomer; **c)** possible transition state of the two metal centres in case of Bailar twist; **d)** representation of the configurations (ΔΔ) of the two metal centres of P enantiomer after Bailar twist racemization.

influences equally all the protons neighbouring the coordinating nitrogens. This would be consistent with the mode in which Hi and H_6 (next to N imine and N pyridine respectively) shift in vt NMR experiment. Thus an intramolecular racemisation of the helicate must likely proceed by a Bailar twist mechanism.

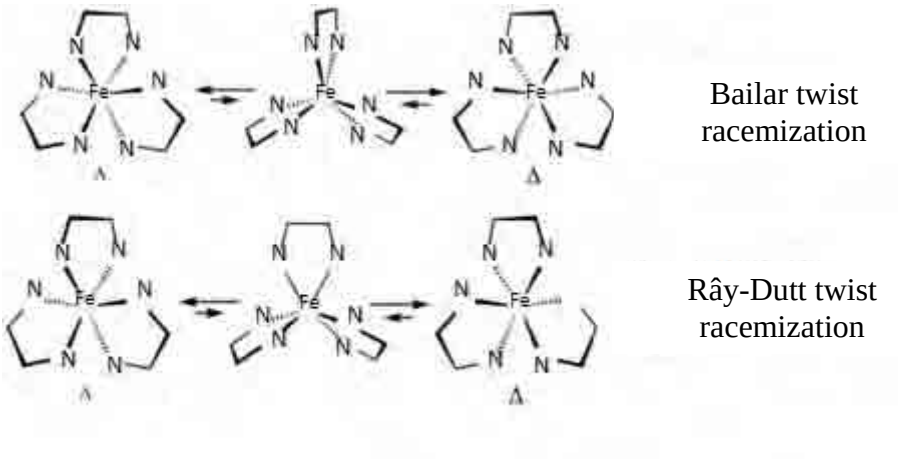

Figure 2.26 Possible rcemisation of one tris(chelate) Fe centre by Bailar twist or Rây-Dutt twist are compared.

2.3.5 UV-Vis and CD studies of $[Fe_2L1_3](Cl)_4$ in water.

The previously described experiments investigated the stability of the compound in the coordinating solvent acetonitrile where temperatures below as well as above ambient can be explored. However, since the parent cylinders are designed for biological application we were interested to explore the perhaps more relevant stability and lability of the chloride salt of the Fe(II) cylinder, $[Fe_2L1_3](Cl)_4$, in water.

An analogous thermal experiment is shown in Figure 2.27 a), carried out with 900 μM $[Fe_2L1_3](Cl)_4$ in water with a 1 mm path length. As in acetonitrile, in this case the absorbance at 573 nm (this is the λ_{max} of the complex in water for the MLCT band) decreases when the temperature is increased from 6 to 76 °C at 1°C/min rate (red circle) and returns to the same initial value when the temperature is decreased back to 6 °C (blue square), although this does not occur with the same linearity observed in the experiments in acetonitrile. In a different experiment (Figure 2.27 b)) if the temperature is raised up to 96 °C, then a dramatic decrease of the absorbance starts from ca 70 °C and, although the absorbance increases again when the sample is cooled down, it never reaches the same initial value. This suggests that, in these analogous concentration conditions, dynamic effects occur in water as in acetonitrile, but that degradation of the complex, most probably due to hydrolysis of imine bond

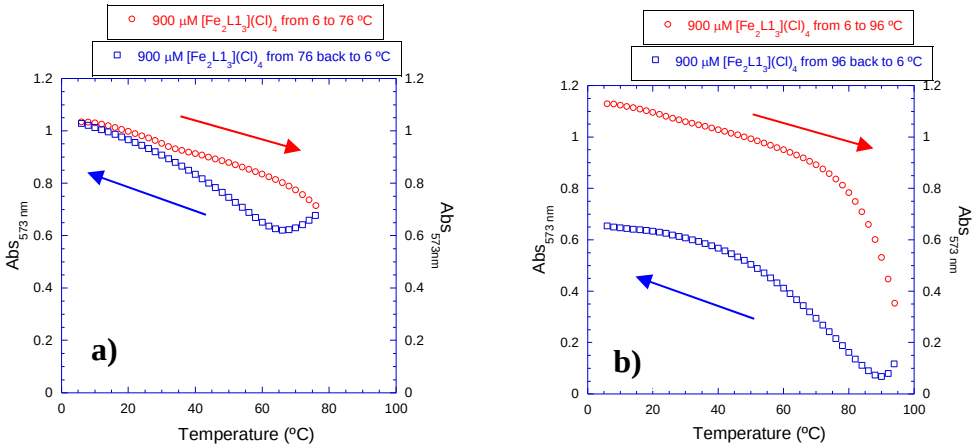

Figure 2.27. UV-Vis thermal experiments with 900 μM (1 mm path length) $[Fe_2L1_3](Cl)_4$ in water. In both experiments the absorbance at 573 nm is monitored when temperature is **a)** increased from 6 to 76 °C and decreased from 76 back to 6 °C at 1 °C/min rate and **b)** increased from 6 to 96 °C and decreased from 96 back to 6 °C at the same rate.

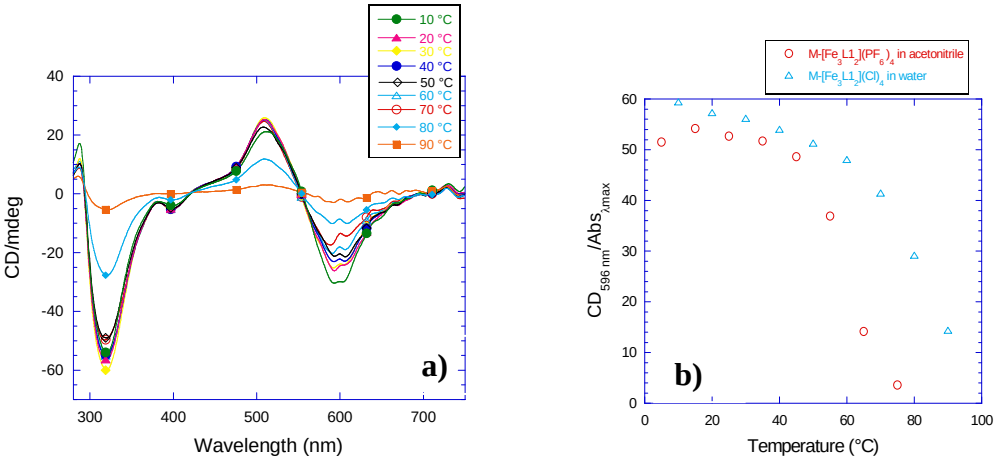

Figure 2.28. a) CD thermal experiments with 50 μM of M enatiomer $[Fe_2L1_3](Cl)_4$ in water (1 cm path length) temperature was increased from 10 to 90 °C at 1 °C/min rate and CD scans were recorded with intervals of 10 °C. **b)** Plotting of CD magnitude at 596 nm (divided by the corresponding value of absorbance at λ_{max} in MLCT band) as a function of temperature of M-$[Fe_2L1_3](Cl)_4$ in water (from thermal experiment in Figure 2.28 a)) and M-$[Fe_2L1_3](PF_6)_4$ in acetonitrile (from thermal experiment in Figure 2.22 a)).

of the ligand, also occurs in water at high temperatures.

CD scans of the M enantiomer of $[Fe_2L1_3](Cl)_4$ at different temperatures (Figure 2.28.a)) confirm that the complex racemises in water when the temperature increases, whilst this does not occur if the complex is kept at room temperature (Figure 2.23). In Figure 2.28.b) the decrease magnitude of the CD signal at 596 nm as a function of the temperature for M-$[Fe_2L1_3](Cl)_4$ in water and M-$[Fe_2L1_3](PF_6)_4$ in acetonitrile (from experiment shown in Figure 2.22 a)) are compared (CD values were normalised dividing by the corresponding values of absorbance at λ_{max} in the MLCT band, to eliminate the effect of concentration and complex degradation). It seems that the complex racemises faster in acetonitrile than in water when temperature is increased, but also at room temperature, the complex in acetonitrile shows higher lability (Figure 2.23). This could be related to the solvent itself or to the counter anion or a combination of the two factors. At lower concentrations of complex in water, the effect of degradation increases; at 50 μM concentration all the complex is destroyed at high temperature (Figure 2.29 a).

DNA binding properties of racemic (rac) $[Fe_2L1_3](Cl)_4$ (described above) have been already reported in several publications, and the better binding ability of M enantiomer over P enantiomer has been demonstrated, suggesting a role of the chirality of the triple helicates in their DNA binding properties. The ability of the complex to stabilise DNA by increasing DNA melting temperature (Tm) beyond 100 °C has also been reported.[57] It was interesting to verify whether (vice versa) ct-DNA also stabilises the complex in water from racemisation/degradation. Figure 2.29.b) shows the variation of UV-vis absorbance at λ_{max} of the MLCT band as a function of the temperature for M, P and rac-$[Fe_2L1_3](Cl)_4$ (50 μM in 1 mM sodium cacodylate and 20 mM sodium chloride) in the presence of ct-DNA. A concentration of 5 bp of DNA per cylinder was selected as the cylinder can fit across ~5 base pairs. For all the DNA-complex adducts, the absorbance decreased when the temperature was raised from 6 to 96 °C (red empty circles) at 1 °C/min rate. But starting from 70 °C there is a dramatic drop in absorbance for the P-$[Fe_2L1_3](Cl)_4$-DNA adduct only. This effect is not so remarkable for the M-$[Fe_2L1_3](Cl)_4$-DNA adduct whose absorbance decreases the least at the end of the experiment. The rac-$[Fe_2L1_3](Cl)_4$-DNA adduct is half way in between the P and M values, indicating that is a sum of its P and M component effects. When the samples were cooled down at the same rate (blue plain

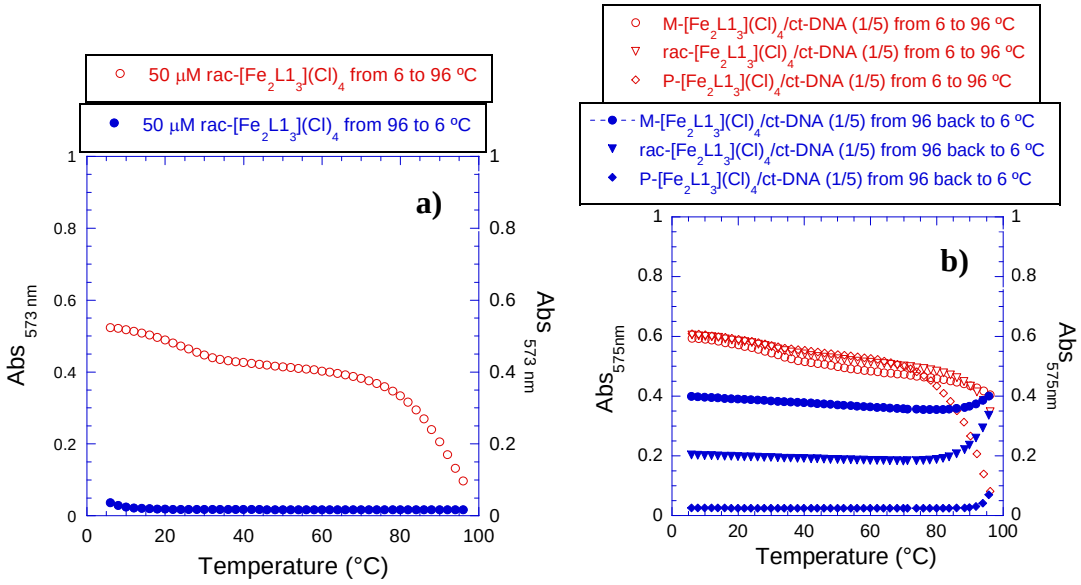

Figure 2.29. Uv-vis thermal experiments in 1 mM sodium cacodylate and 20 mM sodium chloride in which absorbance at λ_{max} of MLCT band (573 nm if only complex and 575 nm for complex-ct-DNA adduct) is monitored during increase of temperature from 6 to 96 °C (red markers) and decreasing from 96 back to 6 °C (blue markers) at 1 °C/min rate. **a)** 50 μM rac-$[Fe_2L1_3](Cl)_4$ only; **b)** ct-DNA (5 times excess in bp) in the presence of M (circles), rac (triangles) and P (turbots) -$[Fe_2L1_3](Cl)_4$.

markers), the absorbance of both rac and M-$[Fe_2L1_3](Cl)_4$-DNA adducts slightly re-increased, although not reaching the initial values. The experiment suggests that the degradation is ~34% for M-$[Fe_2L1_3](Cl)_4$ and ~67% for the rac, whilst the absorbance of the P-$[Fe_2L1_3](Cl)_4$-DNA adduct is completely lost. These results, compared with the graph in Figure 2.29.a) suggest that the DNA can in part "protect" the M-Fe cylinder from degradation at high temperature, but not the P enantiomer, whilst for rac-cylinder there is an average result between M and P. This is consistent with the known higher DNA binding affinity of M enantiomer but may also point to different binding modes.

The ability of ct-DNA to "protect" each enantiomer from racemisation has also been investigated. Figure 2.30.a) shows CD scans of M-$[Fe_2L1_3](Cl)_4$/ct-DNA (1/5) adducts at 10 °C intervals when temperature was raised from 10 to 90 °C in 1 °C/min rate (the graphs focus on the cylinder CD spectroscopy). The CD signal slightly decreases on increasing the temperature, but it is not completely lost as observed in

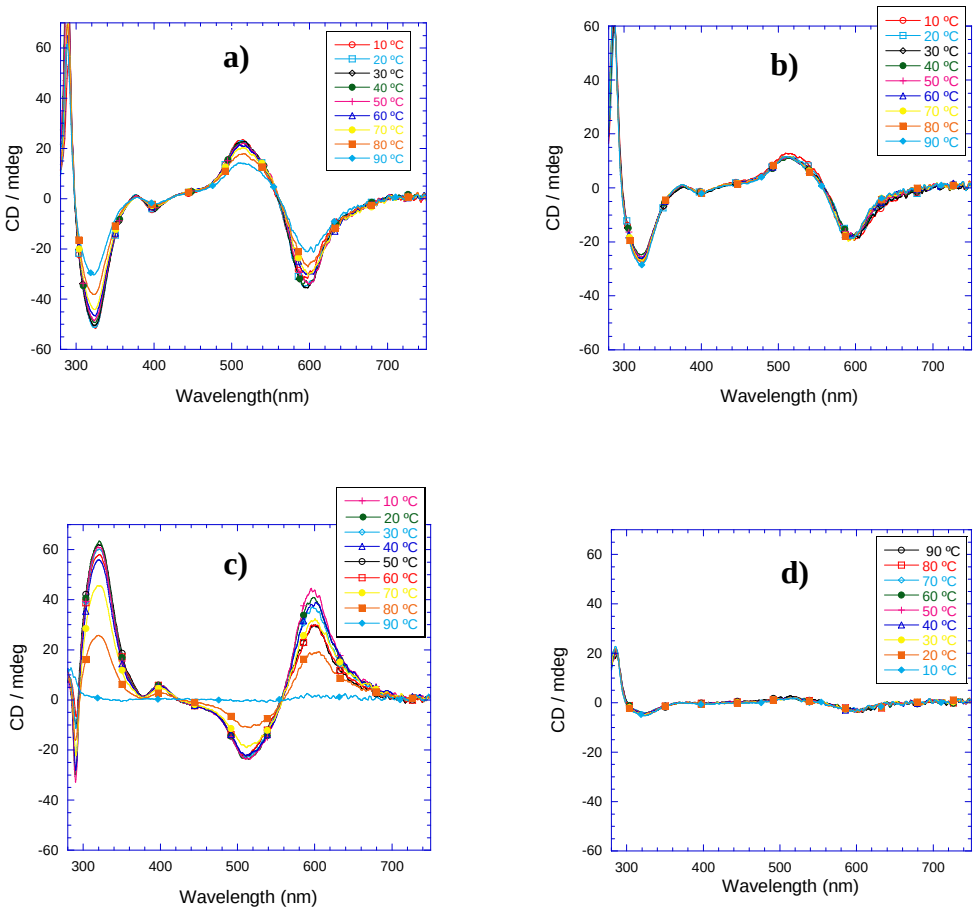

Figure 2.30. CD thermal experiments with 250 mM ct-DNA in 1 mM sodium cacodylate and 20 mM sodium chloride of a) and b) 50 μM M enantiomer of $[Fe_2L1_3](Cl)_4$ in and c) and d) 50 μM M enantiomer of $[Fe_2L1_3](Cl)_4$. In **a)** and **c)** temperature was increased from 10 to 90 °C at 1 °C/min rate and CD scans were recorded at 10 °C intervals; **b)** and **d)** are referred to the same experiments when temperature was decreased back to 10 °C.

the absence of DNA both in water and acetonitrile. At 90 °C the CD absorbance at 598 nm decreased of ~35% and the CD signal remains constant when the temperature is decreased back to 10 °C (Figure 2.30.b)). In the same experiment UV-Vis scans for each corresponding CD scan were recorded confirming a loss of ~34% of absorbance at 575 nm as in Figure 2.29.b) (data not shown). This indicates that the loss of CD signal in Figure 2.30.a) is due to complex decomposition rather than any configurational change into the M complex, suggesting that the binding to the DNA is such that the cylinder cannot freely racemise. As expected, the same experiment

with P-[Fe_2L1_3]$(Cl)_4$/ct-DNA (1/5) adducts lead to complete loss of CD signal (Figure 2.30.c) and d), mainly due to the complete degradation of the complex, whose configuration is responsible of inferior binding affinity with DNA.

2.4 Conclusions.

The dynamic behaviour of Fe(II) parent cylinder has been investigated by NMR, CD and UV-Vis thermal experiments. The ^1H NMR spectra at different temperatures of the PF_6 complex in acetonitrile indicate that dynamic processes occur and these cause the coalescence of phenyl protons and the shifts of the protons (H_i and H_6) that are adjacent to the two coordinating nitrogen atoms. Both the effects occur at ~35-40 °C. The coalescence of phenyl protons is due to their reciprocal environmental exchange whilst the shift of H_i and H_6 might be related to racemisation of the two tris(chelate) Fe(II) centres, as CD thermal experiments of the M enantiomer of the complex show that racemisation increases exponentially starting from ~40 °C. UV-Vis and CD thermal experiments in acetonitrile, of the racemic complex and the M enantiomer, suggest that the complex is thermodynamically stable but kinetically labile, as there is not degradation (variations of temperature do not affect the UV-vis profile of the complex) but there is racemisation (the CD signal of the M enantiomer is lost as the temperature is increased). The complex is labile in acetonitrile also at room temperature. There is no evidence that the racemisation occurs with ligand dissociation or with the involvement of the solvent. An intramolecular mechanism of racemisation is implicit and the Bailar twist mechanism, involving both the metal centres, seems the only possible way in which the complex rearrangement can occur.

UV-Vis and CD thermal experiments were performed also with the chloride complex in water. Similar dynamic behaviour, related to racemisation, was observed in water too, although the complex appears less labile in this solvent. However, a direct comparison concerning the influence of the two solvents is not possible since the complex is rather unstable in water at high temperatures. The CD and UV-Vis thermal experiments in water and in presence of ct-DNA show that DNA “protects” the complex from its degradation at high temperature and the M enantiomer from its racemisation. This protection effect is not as efficient for the P enantiomer,

confirming the different binding affinity and/or mode of the two enantiomers to the DNA.

2.5 Experimental.

2.5.1 Materials.

All chemicals and solvents were purchased from Sigma-Aldrich, Fisher, Alfa Aesar, or Fluorochem and used as received. Deuterated solvents for NMR were supplied by Goss Scientific. Different solutions of rac, M and P- $[Fe_2L1_3](PF_6)_4$ and $[Fe_2L1_3](Cl)_4$, in acetonitrile and water respectively, were prepared in the day of the experiment and the concentrations were measured spectroscopically by using the molar extinction coefficient of the complex at longer wavelength ε_{572}=16900 $mol^{-1}dm^3cm^{-1}$. The ct-DNA (highly polymerised) was purchased from Sigma-Aldrich and it was dissolved in water (ultrapure 18.2 MΩ, Fisher) without any further purification. Stock solutions of ct-DNA were kept frozen until the day of use. The DNA concentrations of those stocks were determined by UV-Vis measurements using the known molar extinction coefficient of ε_{259}=6600 $mol^{-1}dm^3cm^{-1}$ per DNA base pairs. Stock solutions of 1M NaCl and 100 mM sodium cacodylate buffer (pH 6.8) were prepared and, together with ct-DNA and rac, M or P-$[Fe_2L1_3](Cl)_4$ stock solutions, were used to obtain final solutions of ct-DNA/complex at the required ratios, NaCl 10 mM and sodium cacodylate 1 mM.

2.5.2 Synthesis of racemic Fe(II) cylinder.

Ligand L1 and racemic $[Fe_2L1_3](Cl)_4$ and $[Fe_2L1_3](PF_6)_4$ were synthesised according with the procedure previously described in literature[24]. Ligand L1 (3 eq) and iron (II) chloride (2 eq) were heated under reflux in methanol under dinitrogen for 2 hours. The resulting purple coloured solution was cooled and treated with saturated methanolic ammonium hexafluorophosphate. The purple precipitate of $[Fe_2L1_3](PF_6)_4$ was isolated by filtration and abundantly washed with methanol.
^{1}NMR (CD_3CN, 300 MHz, 298 K) δ 8.87 (1H, s, H_i), 8.51 (1H d, J=7.7 H_3), 8.36 (1H, t, J=7.7 Hz, H_4), 7.72 (1H, t, J=7.7 Hz, H_5) 7.31 (1H, d, J=4.8 Hz, H_6), 6.90

(2H, br, $H_{b/d}$), 5.48 (2H, br, $H_{a/c}$), 3.99 (1H, s, H_{CH2}). Mass spectrum (ESI): m/z 311 $[Fe_2L1_3]^{4+}$ 100%, 421 $[Fe_2L_3F]^{3+}$ 1%, $[Fe_2L_3(PF_6)]^{3+}$ 5%.

Exchange of counter anion from PF_6^- to Cl^- was obtained by treating $[Fe_2L1_3](PF_6)_4$ with ion exchange resin (Dowex® 1X8 chloride form, 100-200 mesh, supplied by Sigma-Aldrich) in water. The resulting purple solution was freeze dried.
^{1}NMR (D_2O, 300 MHz, 298 K) δ 8.89 (1H, s, H_i), 8.44 (1H d, J=7.7 H_3), 8.27 (1H, t, J=7.72 Hz, H_4), 7.58 (1H, t, J=6.66 Hz, H_5) 7.27 (1H, d, J=5.5 Hz, H_6), 7.1 (2H, br, $H_{b/d}$), 6.6 (2H, br, $H_{a/c}$), 3.89 (1H, s, H_{CH2}).
^{1}NMR (CD_3OH, 300 MHz, 298 K) δ 9.13 (1H, s, H_i), 8.67 (1H d, J=7.3 H_3), 8.49 (1H, td, J=1.1, 7.7 Hz, H_4), 7.85 (1H, t, J=1.1, 7.3 Hz, H_5) 7.43 (1H, d, J=5.2 Hz, H_6), 7.03 (2H, br, $H_{b/d}$), 5.58 (2H, br, $H_{a/c}$), 3.4.05 (1H, s, H_{CH2}).

2.5.3 Separation of enantiomers.

Separation of M and P enantiomers of $[Fe_2L1_3](Cl)_4$ was obtained by using cellulose (20 mM from Aldrich) column eluted with 20 mM NaCl, as previously reported.[47] After the first purple band (corresponding to M enantiomer) was collected, pressure was applied to the column to improve the elution of the second band. Both enantiomers were freeze dried and successively desalted by re-dissolving the complex in methanol and filtering off most of NaCl, followed by desalting with Sephadex G-10 (Aldrich) in water and further freeze drying. The UV-Vis and CD of each band were collected and since the CD_{max}/Abs_{max} ratios (where CD_{max} and Abs_{max} are the magnitudes of CD and UV-Vis absorbance respectively for each maximum in the spectra) corresponding to the two enantiomers are equal and opposites, the compounds were considered enantiomerically pure. M and P $[Fe_2L1_3](Cl)_4$ were dissolved in methanol and treated with saturated methanolic ammonium hexafluorophosphate, to exchange the counter anion, The precipitates were collected by filtration and, also in this case CD an UV-vis spectra in acetonitrile confirmed the presence of enantiomerically pure M and P- $[Fe_2L1_3](PF_6)_4$.

2.5.4 Spectroscopy.

NMR spectroscopy.

300 and 500 MHz ^{1}H NMR spectra were performed on Bruker AC 300 and DRX500 spectrometers respectively. Coupling constants are given in Hz and multiplicities of the spectroscopic data are recorded as follows: s = singlet, d = doublet, dd = double doublet, t = triplet, q = quartet, dt= double triplet, br = broaden.

UV-Vis spectroscopy.

UV-Vis thermal experiments were run in a Varian Cary 5000 spectrophotometer with Cary temperature controller. 1 or 10 mm cuvettes were used depending on the concentration of the complex in each experiment. Variations of temperatures were always performed at 1 rate °C/min and adsorbance at the maximum wavelength (λ_{max}) of the MLCT band (572 nm in acetonitrile, 573 and 575 nm in water, without and with ct-DNA respectively) of the complex was monitored. Before starting each thermal experiment, the samples were left 20 min in the machine at the starting temperature to allow the absorbance to stabilize. Cuvettes were always carefully sealed to avoid solvents evaporation at higher temperatures.

Circular dichroism.

CD thermal experiments were carried out in 10 mm pathlength cuvettes using a Jasco J-715 spectropolarimeter supported with Jasco PTC-423S temperature controller and RTE 111 bath circulator from Neslab. Variations of temperature were applied at 1 °C/min rate and for each thermal experiment i) CD absorbance at 576 nm was read at 2 °C intervals and ii) CD and UV-vis scans were collected simultaneously at 10 °C intervals. Holding time of 1 min was set up before each CD/UV-Vis scan. Final CD/UV-Vis scans were the results of 8 accumulation scans. Before starting each thermal experiment, the samples were left 20 min at the starting temperature to allow the absorbance to stabilize. Cuvettes were always carefully sealed to avoid solvents evaporation at higher temperatures.

2.6 References.

(1) *Introduction to Protein Structure*; Branden, C., Tooze, J., Ed; Garland Publishing, Inc., 1991.
(2) *Nucleic acid structure and recognition*; Neidle, S., Ed; Oxford University Press. Oxford, 2002.
(3) Lehn, J. M. *Science* **1993**, *260*, 1762-1763.
(4) *Supramolecular Chemistry. Concepts and Perspectives*; Lehn, M.J., Ed; VHC, Weinheim, 1995
(5) Lehn, J. M. *Angew. Chem. Int. Ed. Engl.* **1990**, 29, 1304-1319.
(6) Balzani, V.; Gomez-Lopez, M.; Stoddart, J. F. *Accounts of Chemical Research* **1998**, *31*, 405-414.
(7) Dickert, F. L.; Hayden, O. *Trac-Trends in Analytical Chemistry* **1999**, *18*, 192-199.
(8) Zhang, S. G. *Nature Biotechnology* **2003**, *21*, 1171-1178.
(9) Kramer, R.; Lehn, J. M.; Marquisrigault, A. *Proceedings of the National Academy of Sciences of the United States of America* **1993**, *90*, 5394-5398.
(10) Elrod-Erickson, M.; Benson, T. E.; Pabo, C. O. *Structure with Folding & Design* **1998**, *6*, 451-464.
(11) Ramji, D. P.; Foka, P. *Biochemical Journal* **2002**, *365*, 561-575.
(12) Jones, S.; Barker, J. A.; Nobeli, I.; Thornton, J. M. *Nucleic Acids Research* **2003**, *31*, 2811-2823.
(13) Hannon, M. J.; Moreno, V.; Prieto, M. J.; Moldrheim, E.; Sletten, E.; Meistermann, I.; Isaac, C. J.; Sanders, K. J.; Rodger, A. *Angewandte Chemie-International Edition* **2001**, *40*, 880-884.
(14) Meistermann, I.; Rodger, A.; Hannon, M. J.; Moreno, V.; Prieto, M. J.; Sletten, E.; Moldrheim, E. *Journal of Inorganic Biochemistry* **2001**, *86*, 335-335.
(15) Moldrheim, E.; Hannon, M. J.; Meistermann, I.; Rodger, A.; Sletten, E. *Journal of Biological Inorganic Chemistry* **2002**, *7*, 770-780.
(16) Uerpmann, C.; Malina, J.; Pascu, M.; Clarkson, G. J.; Moreno, V.; Rodger, A.; Grandas, A.; Hannon, M. J. *Chemistry-a European Journal* **2005**, *11*, 1750-1756.
(17) Childs, L. J.; Malina, J.; Rolfsnes, B. E.; Pascu, M.; Prieto, M. L.; Broome, M. L.; Rodger, P. M.; Sletten, E.; Moreno, V.; Rodger, A.; Hannon, M. J. *Chemistry-a European Journal* **2006**, *12*, 4919-4927.
(18) Oleksi, A.; Blanco, A. G.; Boer, R.; Uson, I.; Aymami, J.; Rodger, A.; Hannon, M. J.; Coll, M. *Angewandte Chemie-International Edition* **2006**, *45*, 1227-1231.
(19) Hotze, A. C. G.; Kariuki, B. M.; Hannon, M. J. *Angewandte Chemie-International Edition* **2006**, *45*, 4839-4842.
(20) Peberdy, J. C.; Malina, J.; Khalid, S.; Hannon, M. J.; Rodger, A. *Journal of Inorganic Biochemistry* **2007**, *101*, 1937-1945.
(21) Pascu, G. I.; Hotze, A. C. G.; Sanchez-Cano, C.; Kariuki, B. M.; Hannon, M. J. *Angewandte Chemie-International Edition* **2007**, *46*, 4374-4378.
(22) Cerasino, L.; Hannon, M. J.; Sletten, E. *Inorganic Chemistry* **2007**, *46*, 6245-6251.

(23) *Bioinorganic Chemistry*; Bertini, I., Gray, H.B., Lippard, S.J., Valentine, J.S., Ed.; University Science Books, Mill Valley, California, 1994.
(24) Hannon, M. J.; Painting, C. L.; Jackson, A.; Hamblin, J.; Errington, W. *Chemical Communications* **1997**, 1807-1808.
(25) Hannon, M.; Meistermann, I.; Isaac, C. J.; Rodger, A.; Moreno, V.; Prieto, M. J.; Sletten, E.; Moldrheim, E. *Journal of Inorganic Biochemistry* **2001**, *86*, 56-56.
(26) Hannon, M. J.; Childs, L. J. *Supramolecular Chemistry* **2004**, *16*, 7-22.
(27) Meistermann, I.; Moreno, V.; Prieto, M. J.; Moldrheim, E.; Sletten, E.; Khalid, S.; Rodger, P. M.; Peberdy, J. C.; Isaac, C. J.; Rodger, A.; Hannon, M. J. *Proceedings of the National Academy of Sciences of the United States of America* **2002**, *99*, 5069-5074.
(28) Khalid, S.; Hannon, M. J.; Rodger, A.; Rodger, P. M. *Chemistry-a European Journal* **2006**, *12*, 3493-3506.
(29) Malina, J.; Hannon, M. J.; Brabec, V. *Nucleic Acids Research* **2008**, *36*, 3630-3638.
(30) Hotze, A. C. G.; Hodges, N. J.; Hayden, R. E.; Sanchez-Cano, C.; Paines, C.; Male, N.; Tse, M. K.; Bunce, C. M.; Chipman, J. K.; Hannon, M. J. *Chemistry & Biology* **2008**, *15*, 1258-1267.
(31) Pascu, M.; Clarkson, G. J.; Kariuki, B. M.; Hannon, M. J. *Dalton Transactions* **2006**, 2635-2642.
(32) Malina, J.; Hannon, M. J.; Brabec, V. *Chemistry-a European Journal* **2008**, *14*, 10408-10414.
(33) Bergamo, A.; Stocco, G.; Casarsa, C.; Cocchietto, M.; Alessio, E.; Serli, B.; Zorzet, S.; Sava, G. *International Journal of Oncology* **2004**, *24*, 373-379.
(34) Alessio, E.; Mestroni, G.; Bergamo, A.; Sava, G. *Current Topics in Medicinal Chemistry* **2004**, *4*, 1525-1535.
(35) Alessio, E.; Mestroni, G.; Bergamo, A.; Sava, G. In *Metal Ions in Biolgical Systems, Vol 42: Metal Complexes in Tumor Diagnosis and as Anticancer Agents* 2004; Vol. 42, p 323-351.
(36) Hotze, A. C. G.; Caspers, S. E.; de Vos, D.; Kooijman, H.; Spek, A. L.; Flamigni, A.; Bacac, M.; Sava, G.; Haasnoot, J. G.; Reedijk, J. *Journal of Biological Inorganic Chemistry* **2004**, *9*, 354-364.
(37) Malina, J.; Hannon, M. J.; Brabec, V. *Chemistry-a European Journal* **2007**, *13*, 3871-3877.
(38) Yu, H. J.; Wang, X. H.; Fu, M. L.; Ren, J. S.; Qu, X. G. *Nucleic Acids Research* **2008**, *36*, 5695-5703.
(39) Fadeel, B.; Orrenius, S. *Journal of Internal Medicine* **2005**, *258*, 479-517.
(40) Childs, L. J.; Pascu, M.; Clarke, A. J.; Alcock, N. W.; Hannon, M. L. *Chemistry-a European Journal* **2004**, *10*, 4291-4300.
(41) Sigman, D. S.; Bruice, T. W.; Mazumder, A.; Sutton, C. L. *Accounts of Chemical Research* **1993**, *26*, 98-104.
(42) Pitie, M.; Donnadieu, B.; Meunier, B. *Inorganic Chemistry* **1998**, *37*, 3486-3489.

(43) Zhao, Y. M.; Zhu, J. H.; He, W. J.; Yang, Z.; Zhu, Y. G.; Li, Y. Z.; Zhang, J. F.; Guo, Z. J. *Chemistry-a European Journal* **2006**, *12*, 6621-6629.
(44) Chen, C. H. B.; Milne, L.; Landgraf, R.; Perrin, D. M.; Sigman, D. S. *ChemBioChem* **2001**, *2*, 735-740.
(45) *Circular Dichroism and the Conformational Analysis of Biomolecules* Fasman, G. D., Ed.; Plenum Press, New York, 1996.
(46) *Circular Dichroism and Linear Dichroism*; Rodger, A., Norden, B. , Ed.; Oxford University Press, 1997.
(47) Hannon, M. J.; Meistermann, I.; Isaac, C. J.; Blomme, C.; Aldrich-Wright, J. R.; Rodger, A. *Chemical Communications* **2001**, 1078-1079.
(48) *Inorganic Chemistry, Principles of Structure and Reactivity* 4ed.; Huheey, J. E., Keiter, E. A., Keiter, R.L., Ed.; HarperCollins College Publishers., 1993
(49) Telfer, S. G.; Tajima, N.; Kuroda, R. *Journal of the American Chemical Society* **2004**, *126*, 1408-1418.
(50) *PhD Thesis, University of Warwick*; Painting, C. L., Ed., 1998.
(51) *Spectroscopic methods in organic chemistry*; 4 ed.; Williams, D. H., Fleming, I., Ed.; McGRAW-HILL Book Company (UK) Limted.
(52) *Supramolecular Chemistry*; Steed, J. W., Atwood, J.L., Ed.; Wiley, 2000.
(53) J.E. Huheey, E. A. Keiter, R.L. Keiter Inorganic Chemistry, Principles of Structure and Reactivity, Fourth Edition, 1993, HarperCollins College Publishers.
(54) Rodger, A.; Johnson, B. F. G. *Inorganic Chemistry* **1988**, *27*, 3061-3062.
(55) Bailar, J. C. *Journal of Inorganic & Nuclear Chemistry* **1958**, *8*, 165-175.
(56) Rây, P.C. and Dutt, N. K. *Journal of Indian Chemical Society* **1943**, 20, 81.
(57) Rodger, A.; Sanders, K. J.; Hannon, M. J.; Meistermann, I.; Parkinson, A.; Vidler, D. S.; Haworth, I. S. *Chirality* **2000**, *12*, 221-236.

CHAPTER 3

END-FUNCTIONALISATION OF CYLINDERS: CONJUGATION WITH SHORT PEPTIDES AND AMINO ACIDS.

3.1 Planning a second generation of metallo-supramolecular cylinders using bioconjugate chemistry technology.

The technology of bioconjugate chemistry concerns the joining of two or more molecular entities with different functional and/or structural features, usually by linkages of covalent nature, to assembly hybrid systems for biological applications. In the last decades this has been a key approach in many fields of modern biotechnology and drug discovery because it allows the design and construction of systems with a combination of useful characteristics, to selectively interfere in biological events or to work as probes in organisms.

Synthetic agents that exhibit the ability to interact with biomolecules and can potentially be employed as drugs, are not always able to circulate in biological systems and/or recognise specific targets. The diffusion and the delivery of drugs to specific targets is often achieved by conjugating the drug to appropriate carriers such as biomolecules (proteins[1-3], glycoproteins, liposomes[4]), synthetic polymers (PNA[5,6], dendrimers[7,8]) or biocompatible nano-materials (nanoparticles[9,10], carbon nanotubes[11,12]). Dendrimers, well known highly branched synthetic polymers, are often used as scaffolds for the conjugation of a high number of molecules with a specific function. In the resulting system the function of the conjugated molecule is significantly amplified. For example, in the field of new vaccine design, the conjugation of antigenic peptides on the surface of dendritic structures allows a considerable increasing of the antigenic activity compared to that exhibited by systems in which the antigenic peptide is carried by proteins.[13]

The technology of prodrugs is also widely investigated in medicinal chemistry and is based on the synthesis of substances that are administered in an inactive form. This inactive prodrug is delivered to the target and then metabolised *in vivo* (for example by selective enzymatic action) to release the active drug. The design and

synthesis of such systems is often achieved by conjugation methodologies. Beside drugs design, many other significant area of biotechnology, such as construction of biosensors[14] and design of biomarkers for molecular imaging[15], often depend on bioconjugate chemistry as strategy of assembling of the desired system. From a synthetic point of view, the conjugation is such to not compromise any of the chemical and/or biological and/or physical properties of the single elements that are intended to be joined.

In the last decade this approach has also been employed in the field of DNA binding agents. In Chapter 1 the different modalities in which synthetic molecules interact with DNA have been described. Although many of these agents are particularly effective in interfering with the activity of DNA and in fact many drugs are based on this kind of action, there are not many examples of molecules that can recognise specific DNA sequences or genes. This is still a major issue in this field because many undesired side effects related to these drugs depend on their inability to target only those genes that are responsible for a certain disease, compromising the general functionality of the organism. Furthermore, the delivery of the drug-molecules through the organism and the ability to penetrate cell membrane are also two aspects that, in some cases, limit the development of a DNA binder to an effective drug. The option of combining the action of known DNA binding agents with elements that can potentially discriminate different sequences of nucleic acids is very often investigated. Peptide sequences, oligonuclotides and most recently peptide nucleic acids are the synthetic motifs that are more frequently employed for this purpose, as it has been reviewed in Chapter 1.

The remarkable results concerning metallo-supramolecular cylinders as potential anti-cancer drugs (widely described in Chapter 2), encouraged the idea of designing a second generation of cylinders based on their conjugation with elements that could somehow improve their characteristics and/or add new functions. Importantly, cylinders specifically recognise the DNA major groove and distinctive DNA structures such as three way junctions, but they do not present any significant binding affinity toward specific DNA base sequences as most of DNA binding agents. The conjugation of cylinders with DNA recognition motifs is one possible approach to improve their selectivity, as this method was successful for other DNA binding agents for different applications.

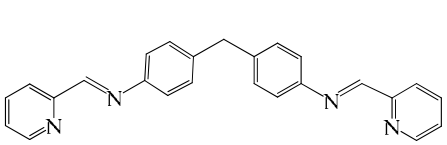

L**1**

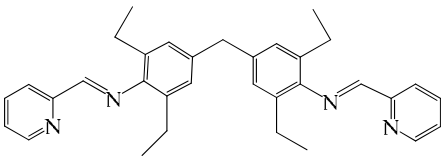

L**5**

Figure 3.1. Parent bis-pyridylimine ligand L1 and L5.

The work presented in this chapter and in Chapter 4, aimed to establish a versatile synthetic procedure, based on bioconjugate chemistry technology, to functionalise cylinders with amino acids and short peptides (as chosen DNA recognition motifs), investigate about the structural characteristics of the achieved compounds and verify whether the new hybrids retain the DNA binding properties and the cytotoxic activity of the unconjugated parent cylinders. In particular, the triple stranded Fe(II) cylinder $[Fe_2L1_3]^{4+}$ is the most exciting and well explained cylinder, for its unprecedented DNA binding properties and important biological activity,[16-21] whilst the Cu(I) double stranded cylinder $[Cu_2L5_2]^{2+}$ exhibits interesting DNA cleavage activity[22] (ligands L1 and L5 in Figure 3.1) and this project focused on the end-functionalisation of these two important types of bis-pyridylimine ligands based cylinders.

3.2 First conjugated cylinders: design criteria and selection of amino acids.

Two main aspects were considered for the design of the first conjugated cylinders: the choice of an appropriate site where the conjugating units could be attached to the cylinder with the most suitable synthetic procedure, and the selection of the amino acids to include in the conjugating units.

Key features in the efficiency of cylinders as DNA binders are their specific shape and dimensions (which allow them to selectively target to DNA major groove and Y-shaped junctions), the presence of aromatic rings on their surface (which form π–staking interactions with DNA bases) and the presence of positive charge (from the metals) that further promotes the binding with the negatively charged DNA. In addition, the Cu(I) centres are responsible of the artificial nuclease activity of double

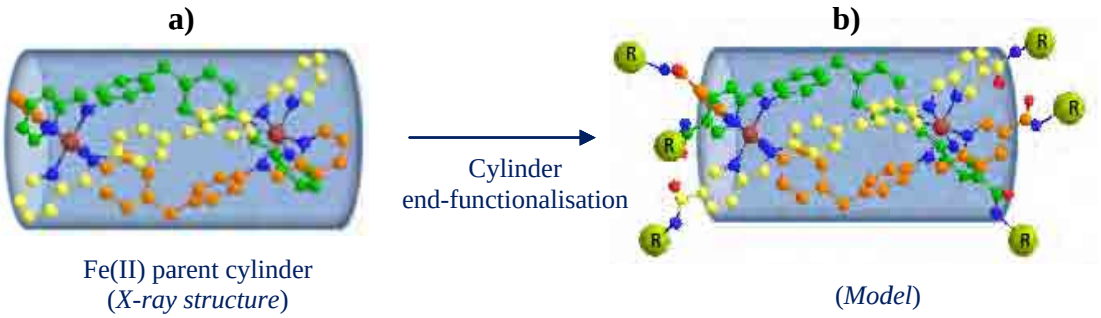

Figure 3.2. Schematic representation of designed end-functionalised cylinder. Attachment at the 5 positions of pyridine rings should not affect the cylinder central core.

stranded cylinders. Aiming to keep intact all these features and planning the attachment of 6 conjugating groups, the conjugated functionalities should be positioned at the ends of the cylinder and far away from the central cylindrical core. Considering the structure of the Fe(II) parent cylinder (Figure 3.2.a)), the 5-position of the pyridine rings emerged as the most appropriate attachment site to avoid any interference with the metal-coordinating units or with the central core of the cylinder.

Regarding the selection of the amino acids to be included in the conjugating units, in many examples of DNA binders-peptide conjugates reported in literature, the selected conjugating peptide is usually within those sequences that in natural proteins are responsible of "reading" specific DNA base sequences or can guarantee the formation of secondary structural motifs that recognise DNA.[23,24] In other examples, the peptide sequence is chosen from those that recognise specific receptors on the cell membrane, to improve cell uptake or to target at receptors of specific kind of cells.[25,26] This is indeed a very reasonable and often successful approach, but since this was the first attempt of end-functionalisation of cylinders with bio-molecular units there was a need to explore the effect of conjugation on cylinders' structure and activity or whether the conjugation was synthetically achievable. For this reason the attachment of short peptides or single amino acids was herein decided.

Nevertheless, the choice of the amino acids to attach was based on the observation that in DNA recognition by proteins in natural system, there are few amino acids that are involved most recurrently than others in the *direct* DNA-protein contact (Chapter

1, table 1.2).[27] Arginine is the amino acid involved most often in contacts both with DNA and RNA, because of the wide range of hydrogen bond patterns that it can form with nucleic acids. Moreover, the guanidinium group, the protonated form of guanidine side chain of arginine, is an excellent anion binding site because it remains protonated over an extremely wide pH range (pK_a=13.5 for the parent CN_3H_6) and can participate in double hydrogen bonds with carboxylates, phosphate, sulphate etc.[28] In fact, interactions between the ariginine guanidinium group and the phosphate backbone of nucleic acids are also very frequent; Frankel et al proposed a very interesting example known as "arginine fork", to describe the mode in which the arginine-rich Tat protein from immune-deficiency virus (HIV) protein binds specifically to an RNA stem-loop structure named TAR (Figure 3.3).[29,30] The proposed model suggested that the η and ε nitrogens from the same arginine residue of the Tat protein can form specific network of hydrogen bonds with different adjacent pairs of phosphates of the Tar region and that these arrangements are likely to occur near RNA loops and bulges and not within double-stranded A-form RNA. Thus, arginine side chains may be commonly used to recognise specific RNA structures. Arginine is also a very important amino acid in cellular uptake, since cell penetrating peptides (short peptides that facilitate the penetration of various molecular cargos inside cells) usually contain high abundance of positively charged

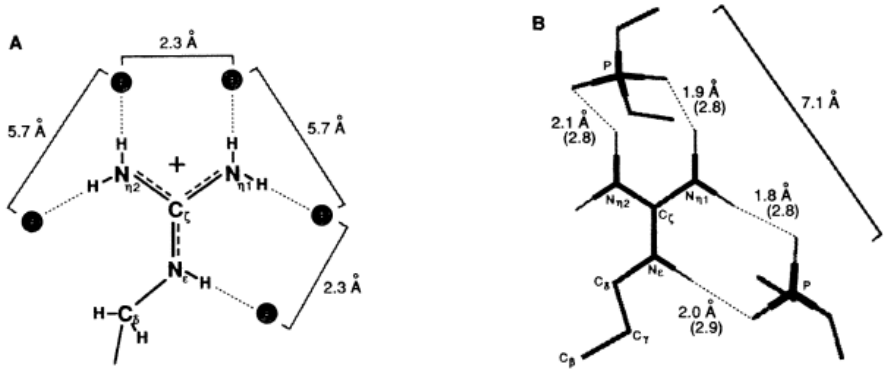

Figure 3.3. Model of "arginine fork" proposed by Frankel et al (A) possible hydrogen bonding configurations for arginines. There are five hydrogen bond donors on arginine and distances between possible acceptors positions are indicated. (B) One possible configuration of an "arginine fork" based on energy minimization calculation (Figure adapted from ref. [29]).

lysine and arginine residues.[31-35] This inspired the design of several drug molecules conjugated to arginine rich peptides to improve both cell uptake and water solubility. For example, Vásquez et al. demonstrated that distamycine tripyrrole analogues (which are well known AT reach minor groove binders) conjugated to an octa-arginine peptide not only improve cell penetrating and nuclear localization but target A-rich DNA sites with high affinity in living HeLa cells.[36] Serine is also one of the amino acids that are known to form interactions with DNA in natural system. It has a relative inert side chain that is desirable when designing the synthetic procedure to employ.

On the basis of these observations three type of conjugating units to attach at the edges of the cylinder were chosen. The short tripeptide of sequence Gly-Gly-Ser was the first selected. The plan was to anchor the peptide via amide bond formation using its N-terminus, with the two glycine residues could provide a linker which would have minimal steric bulk between the cylinder core and the serine residue. Eventually, formation of hydrogen bonds between glycine residues, anchored to different ligands, could help to stabilise the final hybrid. The conjugation with single amino acids was also planned. The target was conjugating with serine residues, because studies comparing Gly-Gly-Ser-cylinder with Ser-cylinder conjugates could help to understand if the length of the conjugating unit had any influence on the stability and/or DNA binding activity of the hybrids. A further target was the conjugation with arginine residues, due to the importance of this amino acid both in natural DNA-protein contacts and in the design of synthetic drugs.

3.3 Will the conjugation affect the chirality of cylinders?

A further aspect in the designs of conjugated cylinders concerns the effect of the attachment of amino acids on the chirality of the hybrids. Achiral ligands that are employed for the assembly of helicates, usually yield a racemic mixture of complexes under equilibrium conditions. For example the symmetric pyridylimine based ligands L1 and L5 yield the mixture of left and right handed cylinder-helicates (Chapter 2 section 2.3.1). However, properly designed chiral polynucleating ligands, can stereospecifically form a single homochiral isomer complex. For example the incorporation of carbon stereocentres at the extremities of bis-bidentate ligands leads

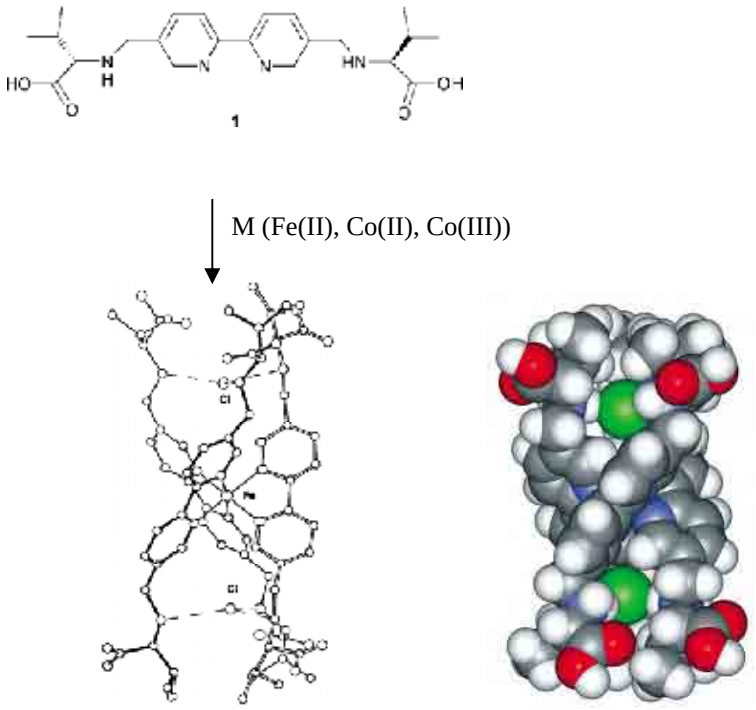

Figure 3.4. L-valine substituted 5,5'-bipyridyl ligand **1** designed by Telfer et al. lead to diastereospecific formation of Δ-$[M(\mathbf{1})_3]^{n+}$ mono nuclear helicates with octahedral metals (Fe(II), Co(II), Co(III)). In the space filling structure representation chloride ions are shown in green and carboxylate oxigens in red (figure adapted from ref [37]).

to the exclusive (or partial) formation of one of the possible diastereoisomers of di-nuclear double and triple stranded helicates, whose helicate handedness and metal configurations are enantiomerically pure.

Telfer[37] et al synthesised a valine 5,5'-substituted bipyridine ligand (Figure 3.4) that forms only Δ-M complexes diastereospecifically, with the L-valinate arms forming a chiral anion-binding pocket for chloride ions in the solid state. Tsang et al.[38] demonstrated that the chiral pyridyl-thiazole ligand L (Figure 3.5) forms di-cationic double stranded helicates with prevalence of P configuration.

The interest in achieving enantiomerically pure helicates, avoiding complicated and not always successful procedures of enantiomers purification (mainly based on chromatographic or crystallographic methodologies), has led to the investigation of alternative strategies. Cozzi and Siegel developed a method in which achiral ligand strands can be anchored to a chiral template during the helicate assembly so that the enantiomericity of the helicate can be dictated by the configuration of the

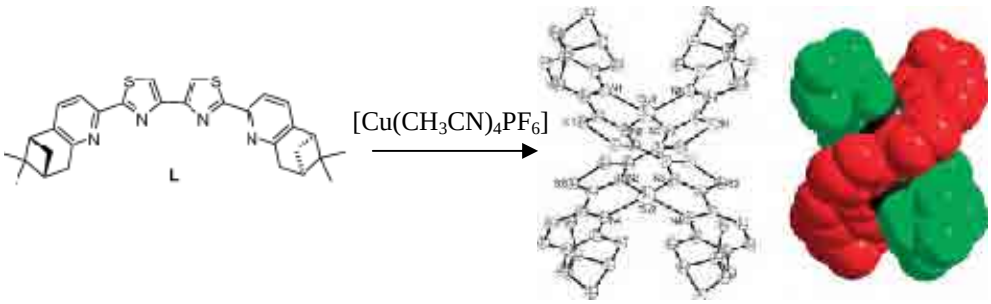

Figure 3.5. The chiral pyridyl thiazole ligand L by Tsang et al. yield diastereoselective formation of the P enantiomer of di copper(I) helicate figure taken from ref [38]).

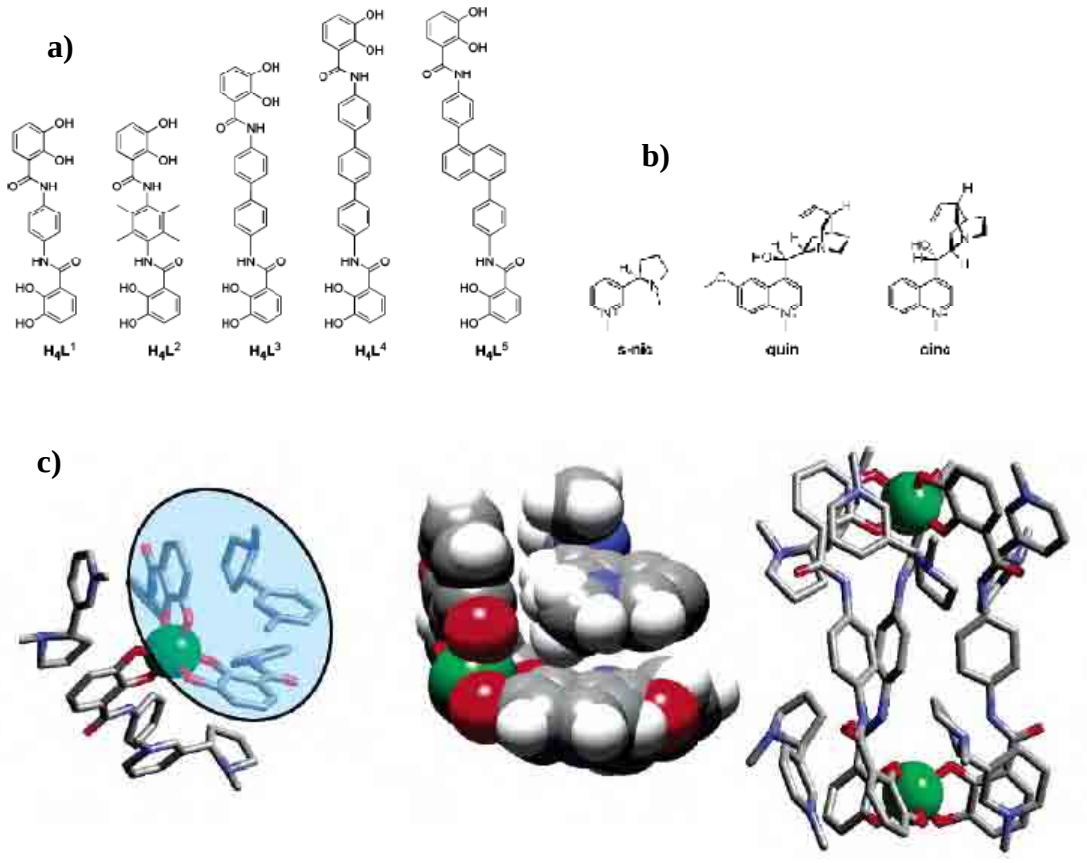

Figure 3.6. Raymond strategy: **a)** set of achiral bis-bidentate catecholate ligands and **b)** chiral cations (N-methyl-s-nicotinium (**s-nic**), N-methyl cinchoninium (**cinc**) and N-methyl quininium (**quin**)) investigated; **c)** crystal structure of the $K(s\text{-}nic)_5[Ga_2L1_3]$ helicate (right) with the detail of the interaction between two catecholate rings and one s-nic ion (left and middle). Figure adapted from ref [39]).

template.[40,41] Raymond et al.[39] studied how the chirality of negatively charged di-gallium(III) triple helicates, based on achiral bis-bidentate catecholate ligands, is influenced by the presence of chiral cations (Figure 3.6). This influence depends on van der Waals and cation-π interactions between the helicate and the chiral cations. Chiral induction via interaction with asymmetric ion pairing has been reviewed by Lacour et al.[42,43] Despite alternative methods, the covalent integration of chiral auxiliary on the ligand, to influence the chirality of the supramolecular assembly, is the most explored approach to achieve diasteroisomerically pure (completely or partially pure) assemblies.[44-48]

In the same way the attachment of amino acids at the extremities of the parent bis pyridylimine ligands could not only influence the DNA binding activity of the cylinders, but also affect their chirality. The conjugation of serine and arginine in both their configurations (D and L) would allow this to be probed.

3.4 Synthesis and characterisation of conjugated cylinders.

The strategy applied for the synthesis of end-conjugated cylinders is showed in Figures 3.7 and 3.8. Compound (**4**) in Figure 3.7 represents a growing peptide chain on the resin of a standard solid phase peptide synthesis with Fmoc chemistry,[49-51] where R is any of the conjugating units designed (the tripeptide Gly-Gly-L-Ser or one of the amino acids D or L-Ser and D or L-Arg). 6-Dimethoxymethyl-nicotinic acid (**3**), synthesised according to previously reported procedures,[52] presents a carboxylic group at the 5 position of the pyridine ring that can form an amide bond with the terminal amino group of the tripeptide (or amino acid) directly on the resin. In this way the desired conjugating unit was attached to the 5 position of the pyridine ring with high yield (a Kaiser Test[53] was performed to verify the completeness of the coupling reaction) and avoiding complicated purification steps for the coupling reaction in solution. Following cleavage from the resin, deprotection and purification by RP-HPLC, 2-formyl-5-R-pyridine (**7-a, b, c, d, e**) proved a good precursor for the synthesis of end-functionalised pyridylimine based ligands as they can form Schiff bases with different diamine spacers. The carboxylic groups of the conjugating units were ‘protected’ by carboxy amidation both to avoid the eventual competition of carboxylic oxygen in metal coordination and because the presence of negative

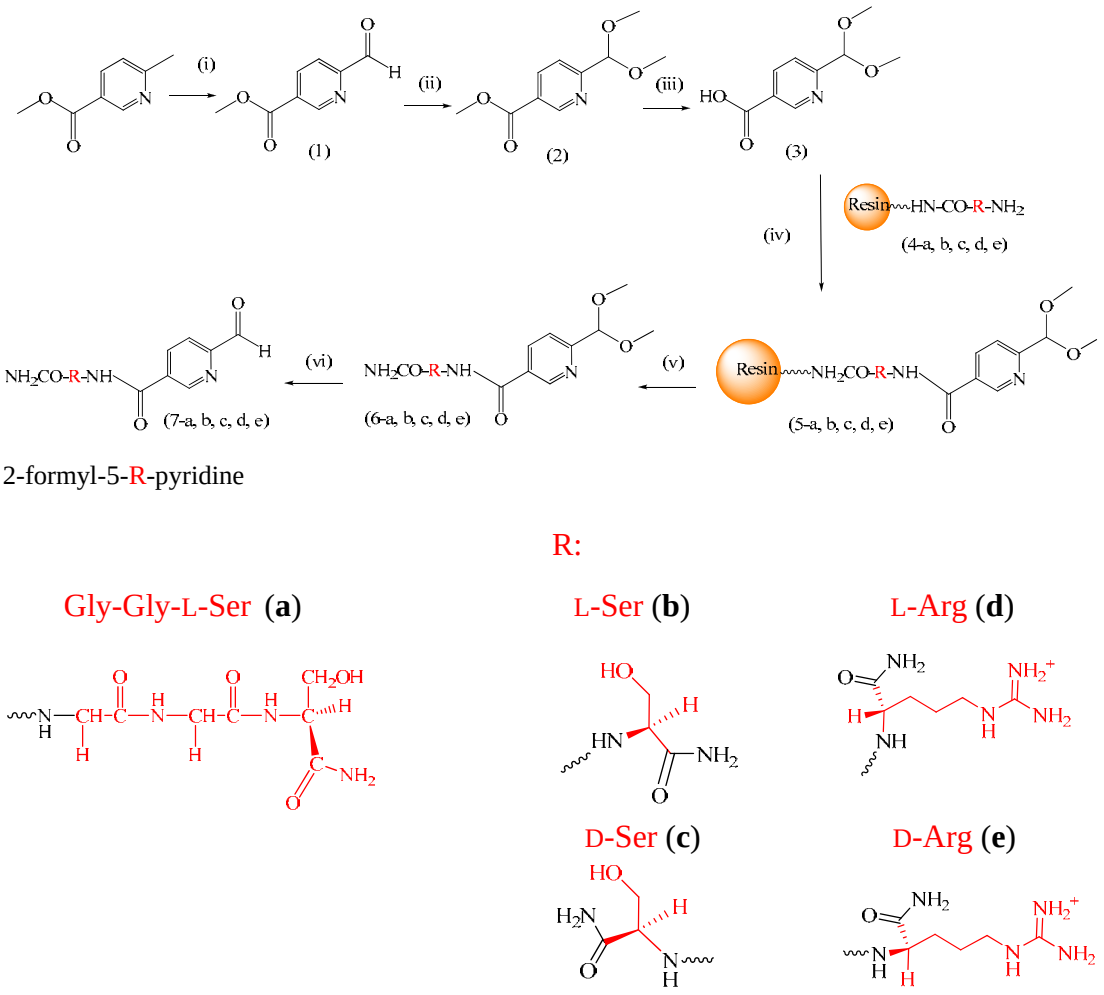

Figure 3.7. Scheme of synthesis of precursor 2-formyl-5-R-pyridine; (i) I_2 /DMSO, (ii) $CH(OCH_3)_3$, HCOOH, H_2SO_4, (iii) 1M NaOH in MeOH, (iv) HBTU, DIEA, (v) 95% TFA, 2.5% Water, 2.5% TIS, (vi) 1M HCl in THF, 6 days.

charges on the final hybrids would not have favourable influence on DNA binding. For the synthesis of the conjugated complexes two routes were possible (Figure 3.8). One way consisted in the synthesis of the end-conjugated ligands LR1 and LR2 by reaction of (**7**) with 4,4'-methylenedianiline (**8**) or 4,4'-methylenbis (2,6-diethylaniline) (**9**) respectively (routes (vii) and (viii) plain black arrows), followed by reaction with the appropriate metal salt. Although the formation of ligands was always possible, only the Gly-Gly-Ser conjugated ligands La1 and La2 were achieved pure. This happened because pyridylimine based ligands, both parents and conjugates, are relatively unstable. It is not possible to purify them by standard

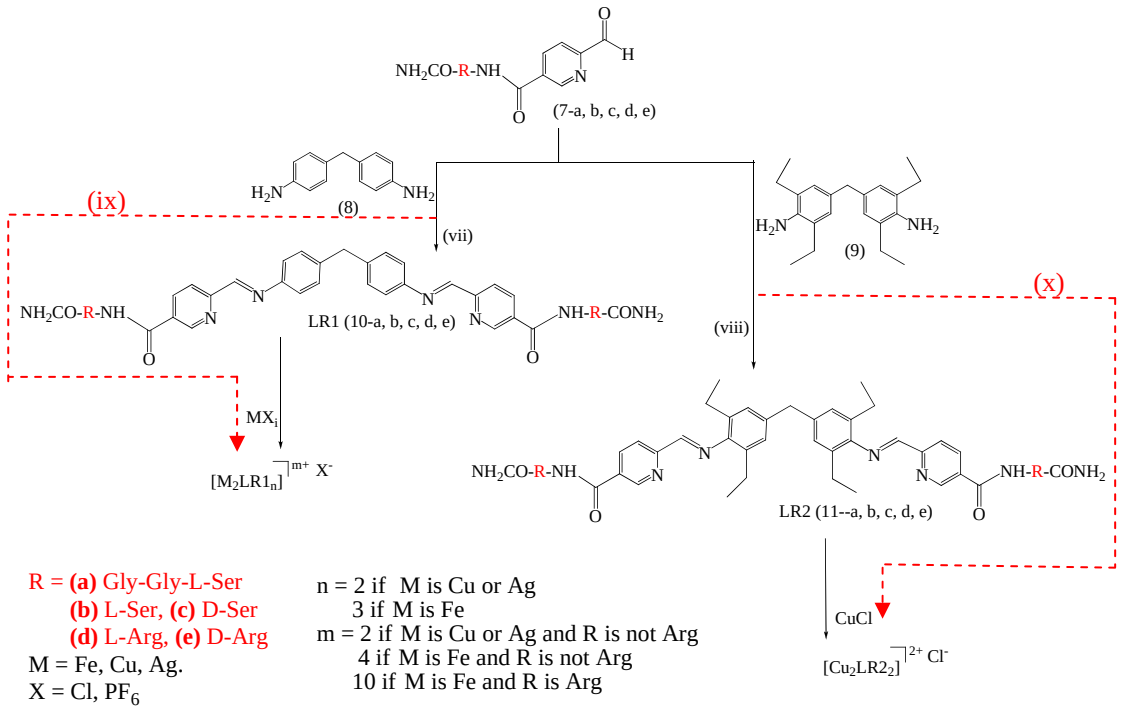

Figure 3.8. Scheme of synthesis of conjugated cylinders. Starting from precursor (**7**) two routes were designed: synthesis of the Ligands LR1 and LR2 ((vii) and (viii), black plain arrows) from which the complexes are obtained by reaction with appropriate metal salts, and the 'one pot' synthesis ((ix) and (x), dashed red arrows) where the complexes are achieved directly by reaction of (**7**), the spacers ((**8**) or (**9**)) and the desired metal salt in the same mix. (vii) and (vii) reflux MeOH. (ix) and (x) nitrogen atmosphere and different solvents and temperature conditions depending on the metal ion.

chromatographic techniques and the best way to obtain them pure is by precipitation and washing. Ligands La1 and La2 are soluble only in DMSO, thus they were purified by combining washings with methanol and water (in which the starting materials were soluble). This was not possible with the other conjugated ligands for which a combination of solvents able to wash off only the starting materials or either a procedure of re-crystallisation was not found. However, the synthesis of the ligands is important but not essential, and all the complexes could be achieved using the 'one pot synthesis' ((ix) and (x), red dashed lines in Figure 3.8) in which the precursor (**7-a, b, c, d, e**), the chosen spacer ((**8**) or (**9**)) and the appropriate metal salt reacted in one mix to afford the desired complexes, skipping the ligand synthesis and purification step. It is known that sometimes, in metallo-supramolecular assembly,

the presence of the metal "assists" the synthesis of the ligand *in situ* because it drives the equilibrium toward the formation of the final architecture. The complexes obtained were purified by washing and/or re-crystallisation.

Figure 3.9 shows the list of conjugated cylinders that have been purified and characterised: 5 Fe(II) triple stranded cylinders conjugated with Gly-Gly-L-Ser, L-Ser, D-Ser, L-Arg and D-Arg ($[Fe_2(L\mathbf{a}1)_3]^{4+}$, $[Fe_2(L\mathbf{b}1)_3]^{4+}$, $[Fe_2(L\mathbf{c}1)_3]^{4+}$, $[Fe_2(L\mathbf{d}1)_3]^{10+}$ and $[Fe_2(L\mathbf{e}1)_3]^{10+}$), 4 Cu(I) double stranded cylinders conjugated with Gly-Gly-L-Ser, L-Ser, D-Ser ($[Cu_2(L\mathbf{a}1)_2]^{2+}$, $[Cu_2(L\mathbf{a}2)_2]^{2+}$, $[Cu_2(L\mathbf{b}2)_2]^{2+}$ and $[Cu_2(L\mathbf{c}2)_2]^{2+}$) and 1 Ag(I) double stranded cylinder conjugated with Gly-Gly-L-Ser ($Ag_2(L\mathbf{a}1)_2]^{2+}$). Several attempts of synthesis of the double stranded Cu(I) cylinder conjugated to arginine residues were unsuccessful most probably because other chelating units of the ligand competed with the bispyridylimine units in the coordination of the Cu(I) ions. Furthermore, the Ag(I) cylinder ($Ag_2(L\mathbf{a}1)_2]^{2+}$) was

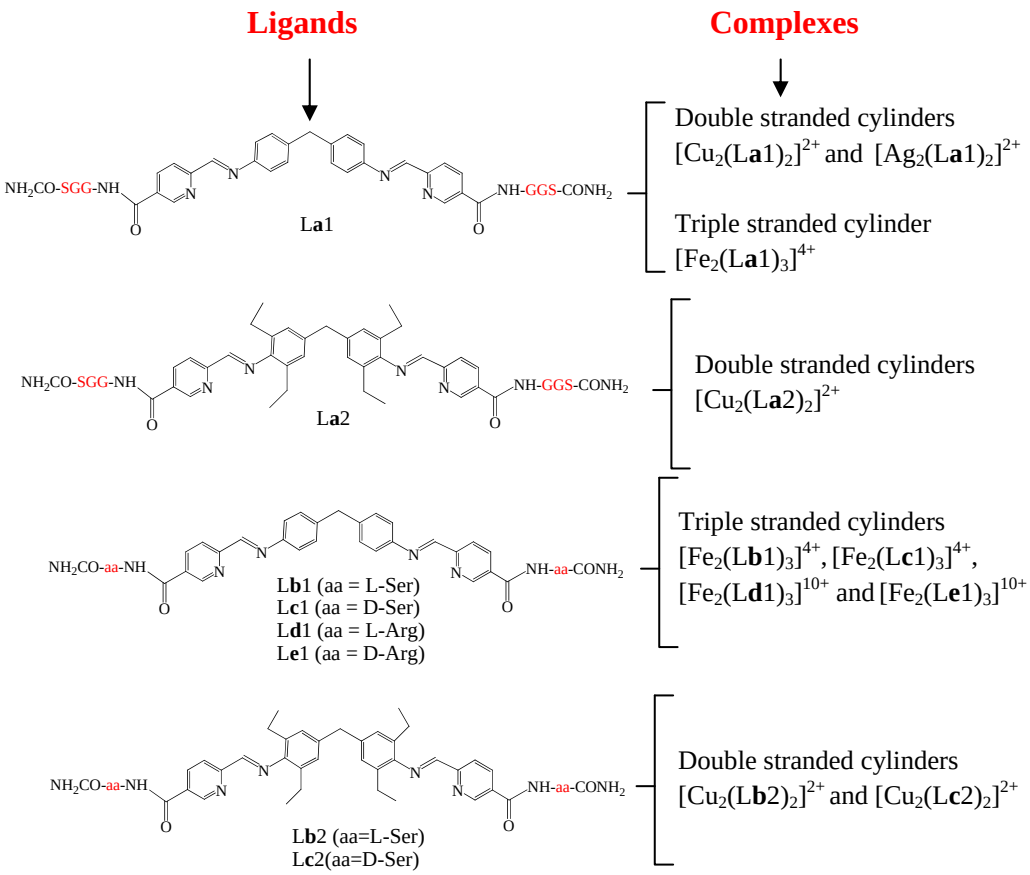

Figure 3.9. List of synthesised complexes (right) and the corresponding ligands (left).

isolated only as PF_6 salt which is not soluble in water so this complex was not employed in subsequent DNA binding studies. All the compounds were characterised by mass spectrometry and ^1H NMR spectroscopy with the support of COSY experiments for the assignment of the resonances (see Appendix A). Despite many attempts of crystallisation no crystals big enough for X-ray characterisation were obtained. It was not possible to obtain accurate elemental analysis data because the compounds are very hygroscopic and molecules of water interfered with the interpretation of the results. In general the compounds are not very stable in water (see Chapter 4, section 4.1). Ser-conjugates are the more stable complexes, but by NMR in water there is always a very small amount of hydrolysis products observed. For this reason controls with starting materials were always carried out for all DNA binding studies and cytotoxicity tests, to ensure that the activity observed was not due to hydrolysis products. Mass spectrometry (both ESI-MS and MALDI) was unsuccessful for arginine conjugates because of their charge and instability, although NMR and UV-Vis spectroscopy were perfectly consistent with the expected compound.

All the triple stranded Fe(II) conjugated cylinders in water present the same UV-Vis profile both in the MLCT region and in the ligand region of the spectrum (Figure 3.10). The MLCT band of the conjugates present a λ_{max} at 599 nm in water whilst the λ_{max} of the parent Fe(II) cylinder in the MLCT region is at 572 nm. Analogously all the Cu(I) conjugates have the same profile in the visible region the MLCT band present a shift of 25 nm at higher wavelength compared to the uncojugated Cu(I) complex. This suggests that all the conjugated cylinders present the same central di-metallic core (the helicate) and, compared to the corresponding parent cylinders, the presence of the amide group at the 5 position of the pyridine rings causes a shift at higher wavelengths of the λ_{max} of both the MLCT band and the bands where the bispyridylimine ligands absorb.

Further useful information was obtained from ^1H NMR data. All the spectra of the conjugated cylinders exhibit one single set of signals, indicating that the conjugation did not disturb the symmetry that is typical for these metallo-supramolecular architectures. Table 3.1 reports the chemical shifts of the protons of the central cylinder core (the pyridine H_{6py}, H_{3py} and H_{4py}, the imine H_7 and the spacer methyl H_{11} protons) for the Fe(II) and Cu(I) conjugated cylinders in water and acetonitrile

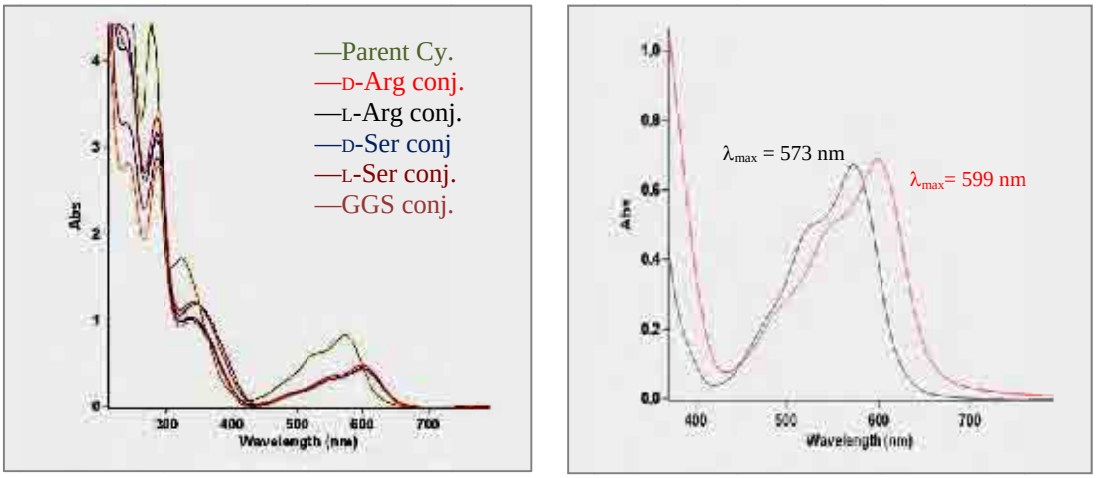

Figure 3.10. UV-Vis in water of the five Fe(II) conjugated cylinders compared with the Fe(II) parent cylinder (left). On the right the MLCT bands of the L-Ser conjugate (red trace) and the unconjugated Fe(II) parent cylinder (black trace).

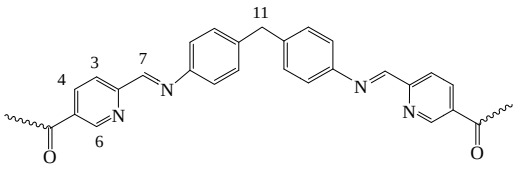

	H_7 (δ)	H_{4py} (δ)	H_{3py} (δ)	H_{6py} (δ)	H_{11} (δ)
Parent $[Fe_2(L1)_3]^{4+}$	8.62	8.27	8.44	7.27	3.90
Ligand La1	8.64	8.32	8.19	9.11	3.99
$[Fe_2(La1)_3]^{4+}$	9.03	8.65	8.64	7.55	3.99
$[Fe_2(Lb1)_3]^{4+}$	9.05	8.68	8.63	7.50	3.98
$[Fe_2(Lc1)_3]^{4+}$	9.04	8.69	8.64	7.54	3.93
$[Fe_2(Ld1)_3]^{10+}$	9.04	8.66	8.61	7.57	4.02
$[Fe_2(Le1)_3]^{10+}$	9.08	8.69	8.67	7.60	3.97
Parent $[Cu_2(L5)_2]^{2+}$	8.56	8.00	8.22	8.53	3.89
Ligand La2	8.32	8.41	8.23	9.13	3.86
$[Cu_2(La2)_2]^{2+}$	8.74	8.60	8.19	8.98	3.85
$[Cu_2(Lb2)_2]^{2+}$	8.68	8.56	8.15	9.02	3.84
$[Cu_2(Lc2)_2]^{2+}$	8.68	8.55	8.16	9.02	3.88

Table 3.1. Comparing chemical shifts of ^1H NMR spectra of conjugated and parent Fe(II) cylinders (in D_2O, 298 K) and Cu(I) cylinders (in CD_3CN, 298 K). Chemical shifts of ligands La1 and La2 (in dmso-d6) are also shown.

respectively. The corresponding resonances of the parent unconjugated cylinders and the ligand La1 are reported too. All the conjugated Fe(II) cylinders present the same values of chemical shifts for the protons indicated: the imine proton H_7 at low fields (at 9.0 ppm), the two pyridine protons H_{4py} and H_{3py} almost overlapping each other, the pyridine proton H_{6py} at 7.5 ppm and the proton of the spacer H_{11} at 4.0 ppm. This would indicate that all the conjugated Fe(II) cylinders keep the same architecture for the central helicate core, independently of the type or the length of the attached peptide. Comparing the chemical shifts of the protons of Fe(II) conjugates and Fe(II) parent cylinder, we cannot expect exactly the same set of signals for the pyridine regions, because of the presence of the amide groups in 5 position of the conjugated ligands. However, imine H_7 and pyridine H_{6py} protons, neighbouring the two coordinating nitrogens, have similar chemical shifts in conjugated and unconjugated complexes. Most importantly, comparing the NMR spectra of the free parent ligand L1 with the Fe(II) parent cylinder, a typical high field shift of the H_{6py} proton occurred as consequence of the neighbour pyridine nitrogen coordination (see Chapter 2, section 2.3.2). An analogous effect occurs for the H_{6py} proton of any Fe(II) conjugated cylinder. Finally, the signals corresponding to the phenyl protons of any Fe(II) conjugate are broad bands exactly as it has been described for the parent cylinder in Chapter 2. These results confirm that the conjugated complexes present a central helicate core with the same symmetry observed for the unconjugated helicates and imine and pyridine nitrogens are again responsible for the coordination of the Fe(II) centres. UV-Vis and NMR spectroscopy indicate that all the Fe(II) conjugated cylinders have a central cylinder core with the same architecture. Moreover, the presence of amino acids of opposite configuration (D or L) does not influence the ^{1}H NMR spectrum, as $[Fe_2(L\mathbf{b}1)_3]^{4+}$ and $[Fe_2(L\mathbf{c}1)_3]^{4+}$ exhibit exactly the same set of signals, both for the protons of the cylinder core and the protons from the conjugated amino acids. Equally, $[Fe_2(L\mathbf{d}1)_3]^{10+}$ and $[Fe_2(L\mathbf{e}1)_3]^{10+}$ have precisely the same ^{1}H NMR spectra. Analogous results were obtained for the Cu(I) complexes: they all present the same set of signals by ^{1}H NMR for the central cylinder core and D and L-Ser conjugates exhibits identical spectra.

3.5 Chirality of conjugated cylinders. CD studies.

CD scans of the conjugated cylinder were undertaken to explore whether the presence of the stereocenter Cα of the amino acids at the edges of the cylinder influenced the handedness of the central helicate, by promoting partial or total formation of one of the two possible diasteroisomers.

The two opposite CD spectra of M and P enantiomer of parent Fe(II) cylinder ($[Fe_2(L1)_3]^{4+}$), whose characteristics are widely discussed in Chapter 2, are shown again in Figure 3.11.a) to be compared with the CD spectra of D and L-Arg conjugated Fe(II) cylinders ($[Fe_2(L\mathbf{d}1)_3]^{10+}$ and $[Fe_2(L\mathbf{e}1)_3]^{10+}$ respectively) in Figure 3.11.b). The CD signals of two solutions of the arginine-conjugates in water (Cl^- as counter anion) are precisely the opposite of each other, and their shape correspond strictly to the signals of the enantiomers of the Fe(II) unconjugated cylinder, both in the MLCT and in the ligand region of the spectra. These CD signals in the visible region can only be due to the cylinder core of the conjugates and this suggests that the cylinder core of $[Fe_2(L\mathbf{d}1)_3]^{10+}$ is a P triple helicate whilst the centre of

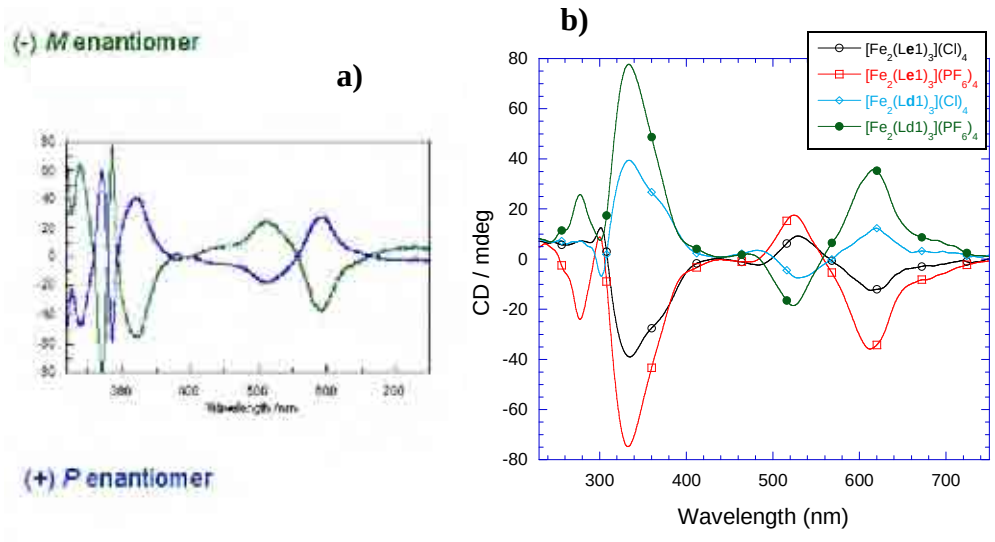

Figure 3.11. CD spectra of **a)** M and P enatiomers of parent Fe(II) cylinder in water ($[Fe_2(L1)_3]^{4+}$) and **b)** L and D-Arg conjugated Fe(II) cylinders ($[Fe_2(L\mathbf{d}1)_3]^{10+}$ and $[Fe_2(L\mathbf{e}1)_3]^{10+}$ respectively) both PF_6^- salt in acetonitrile and Cl^- salt in water. All the solutions of conjugated complexes have the same UV-Vis absorbance magnitude at the MLCT band.

($[Fe_2(L\mathbf{e}1)_3]^{10+}$ is the opposite enantiomer, an M triple helicate. This result indicates that the conjugation of two arginine residues at the 5 positions of the pyridine rings of the bis-pyridylimine ligands, promotes the formation of one specific diasteroisomer of the resulting hybrid cylinder which depend on the configuration of the Cα of the arginine. Consequently the handedness of the central helicate core is also influenced and the CD spectra indicate that the conjugation with D-arginine induces formation of M helicate and the L-arginine promotes the P helicate.

The CD signals of the PF_6^- complexes in acetonitrile (at the same concentrations) are also equal and opposite, as shown in Figure 3.11 b). The four solutions shown in CD graph had the same concentrations and they all presented the same value of absorbance at 599 nm (λ_{max} of MLCT band) by UV-vis analysis, but the CD magnitude of each band is higher for the PF_6^- complexes in acetonitrile than the chloride complexes in water. This effect was not observed for the Fe(II) parent cylinder where CD bands of the separated enantiomers always keep the same magnitude, independent of the counter anion or the solvent that was used. This could suggest a possible role of the counter anion, rather than the solvent, in the induction of one specific helicate. The interactions that the PF_6^- anions form with the complex might stabilise the formation of one specific helicate better than the interactions of Cl^-, so that the diasteroisomeric purity of PF_6^- complexes is superior. Since this effect depends on the configuration of the arginine residues conjugated at the extremities of the helicate, it is possible that these interactions involve either the amino acid backbones or the positively charged side chains of the arginine residues, as in the helicate reported by Telfer (Figure 3.4).

The CD analysis of the Fe(II) serine conjugates was more ambiguous. The CD profile in acetonitrile of $[Fe_2(L\mathbf{b}1)_3](PF_6)_4$ and $[Fe_2(L\mathbf{c}1)_3]\ (PF_6)_4$ is comparable with the CD signal of the two arginine conjugates (Figure 3.12) although the connection with the Cα configuration of the linked amino acid is inverted: it seems that the L-Ser induces M enantiomericity to the central helicate core whilst D-Ser promotes P. However, when the counter anion is exchanged to chloride and the analysis carried out in water, this typical profile is lost and CD signals are present but difficult to interpret. No CD signal was observed for the tripeptide Fe(II) cylinder conjugate ($[Fe_2(L\mathbf{a}1)_3]^{4+}$), possibly because the L-Serine residues are too distant from the helicate core to affect its handedness.

The tripeptide Cu(I) conjugate, $[Cu_2(L\mathbf{a}1)_2]^{2+}$ did not exhibit any CD signal whilst the CD spectrum of $[Cu_2(L\mathbf{a}2)_2]^{2+}$ presented very distinctive bands (Figure 3.13), both in the MLCT and in the ligand region. It is unclear why the later complex should be more sensitive to the presence of the serine groups. It is known that the

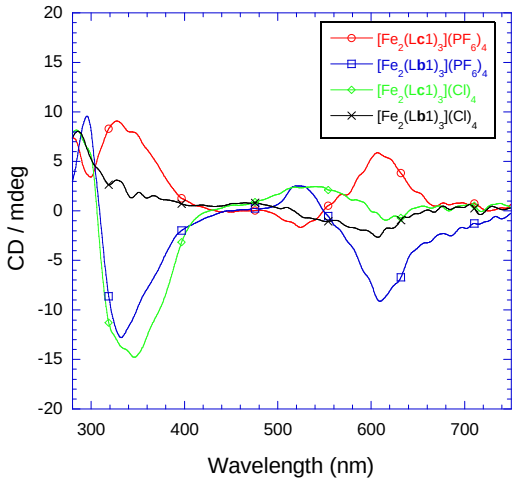

Figure 3.12. L and D-Ser conjugated Fe(II) cylinders ($[Fe_2(L\mathbf{b}1)_3]^{4+}$ and $[Fe_2(L\mathbf{c}1)_3]^{4+}$ respectively) both PF_6^- salt in acetonitrile and Cl^- salt in water. All the solutions of conjugated complexes have the same UV-Vis absorbance magnitude at the MLCT band.

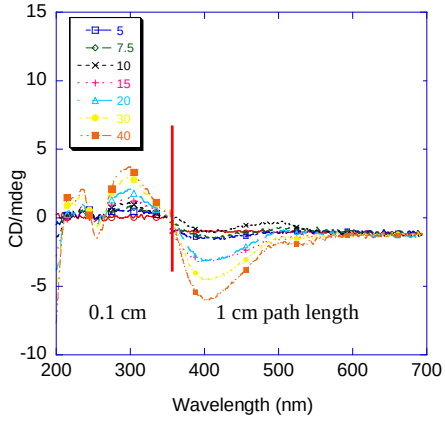

Figure 3.13. CD spectra of different concentrations (in μM in the legend) of Gly-Gly-Ser Cu(I) double stranded conjugate $[Cu_2(L\mathbf{a}2)_2]^{2+}$ in water. The MLCT region (750-350 nm) was analysed in 1 cm cuvette and the UV region (350-200 nm) in 0.1 cm cuvette.

unconjugated ligand L1 with Cu(I) forms a mix of helicate and box isomers (Chapter 2, section 2.2.2), and this was proved by ^{1}H NMR spectroscopy in which two types of signals corresponding to the methyl proton of the central spacer were present (a singlet for the helicate and a doublet for the box isomer). The analogous proton of the conjugate complexes could not be properly observed because the corresponding signal is usually overlapped with the signals of the peptide protons. Consequently it was not possible to establish whether the two isomers are present and eventually if this is related to the absence of CD signal for this complex. Furthermore, the two D and L-serine Cu(I) conjugates $[Cu_2(L\mathbf{b}2)_2]^{2+}$ and $[Cu_2(L\mathbf{c}2)_2]^{2+}$ do not have CD signal either, which made more complicated an interpretation about the role that the type of spacer or the length of the conjugating unit had in affecting the handedness of the central helicate of Cu(I) conjugates.

3.6 NMR studies with Δ-TRISPHAT. Comparing D and L-Arg conjugated Fe(II) cylinders with the parent Fe(II) cylinder.

3.6.1 Fe(II) parent cylinder and Δ-TRISPHAT.

CD studies revealed that only the conjugation with arginine residues produced an unambiguous effect on the chirality of the Fe(II) triple helicate. NMR studies of $([Fe_2(L\mathbf{d}1)_3]^{10+}$ and $[Fe_2(L\mathbf{e}1)_3]^{10+}$ in the presence of a chiral NMR shift reagent for cationic coordination complexes could provide further information about the diasteroisomeric purity of the two complexes and the chirality of the helicate core. Lacour and co-workers proposed the use of the now popular chiral anion *tris*(tetrachlorobenzenediolato) phosphate(V) (TRISPHAT,) Figure 3.14) as a chiral NMR shift reagent after they were able to separate the Λ and Δ-TRISPHAT isomers.[54-56] Now the tetrabutylammonium salt of Δ-TRISPHAT is commercially available and it has been demonstrated that one specific isomer of TRISPHAT can preferentially bind to specific isomers of mono and di-nuclear coordination complexes causing distinctive NMR chemical shifts of the protons involved in the interaction.[57-59] Moreover, TRISPHAT can be used to resolve racemic mixture of complexes by selective extraction and crystallisation[60,61] or as chiral component of eluents for chromatographic resolution.[62]

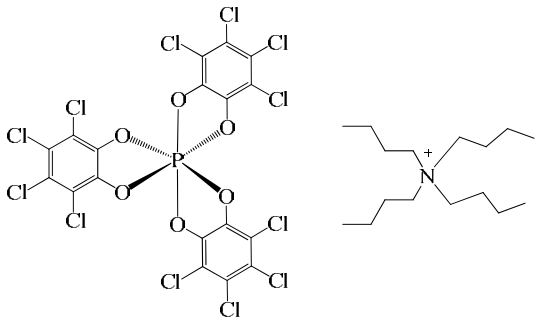

Figure 3.14. Δ-TRISPHAT, [Tetrabutylammonium][Δ-tris(tetrachloro-1,2-benzenediolato) phosphate(V)]

TRISPHAT showed to be particularly effective in interacting differently with opposite enantiomers of metallo-supramolecular helicates.[60] For this reason NMR studies of Fe(II) parent cylinder in the presence of TRISPHAT were previously carried out in Hannon group by C.R. Pearmund as part of his PhD thesis project.[63] He demonstrated that the addition of Λ-TRISPHAT anion to an acetonitrile solution of racemic Fe(II) triple helicate cylinder ($[Fe_2(L1)_3]^{4+}$) resulted in the splitting of some of the resonances to give two identical set of signals, suggesting that the anion interacts differently with each enantiomer. The splitting mainly involved the protons nearest the pyridyl and the imine coordinating nitrogens and the methyl proton of the central spacer, suggesting that these were the preferred area of interaction with the chiral anion.

A similar experiment was herein repeated by using 2 equivalents of Δ-TRISPHAT added to a solution of racemic $[Fe_2(L1)_3](PF_6)_4$ in CD_3CN (Figure 3.15). To understand which of the two enantiomers interact with Δ-TRISPHAT, the same experiment was performed using an enantiomerically "impure" solution of the M enantiomer of $[Fe_2(L1)_3](PF_6)_4$; this solution contained mostly the M enantiomer, as revealed by its CD profile, but also a ~10% of P enantiomer as known impurity, so that the signals of each enantiomer could be identified in the NMR spectrum. The experiment (Figure 3.16) shows that the addition of Δ-TRISPHAT causes a shift of the methyl proton of the central spacer (H_{11}) for the M enatiomer, whilst shifts of the imine and 6-pyridyl protons (H_7 and H_6 respectively) concern only the P enantiomer. This would suggest that both enantiomers interact with Δ-TRISPHAT, but while the contact with the P enantiomer concerns the coordination units of the helicate,

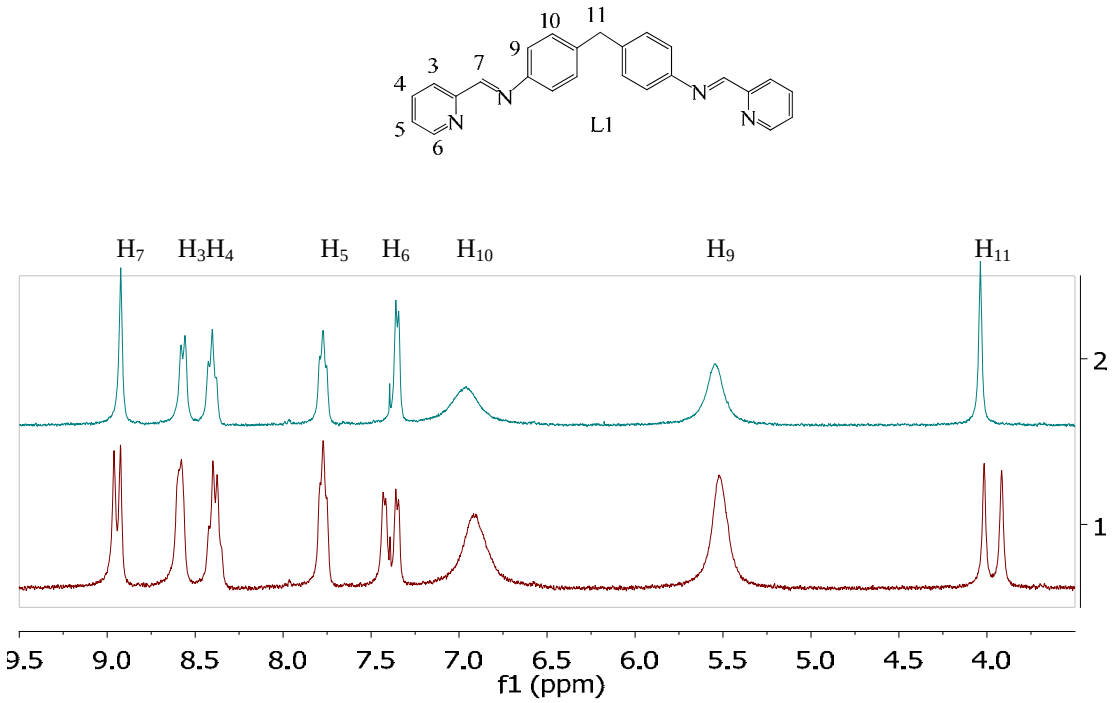

Figure 3.15. ^{1}H NMR (300 MHz, CD_3CN, 298K) of (**2**) a racemic mixture of $[Fe_2(L1)_3](PF_6)_4$ and (**1**) the same complex solution to which 2 equivalents of Δ-TRISPHAT were added.

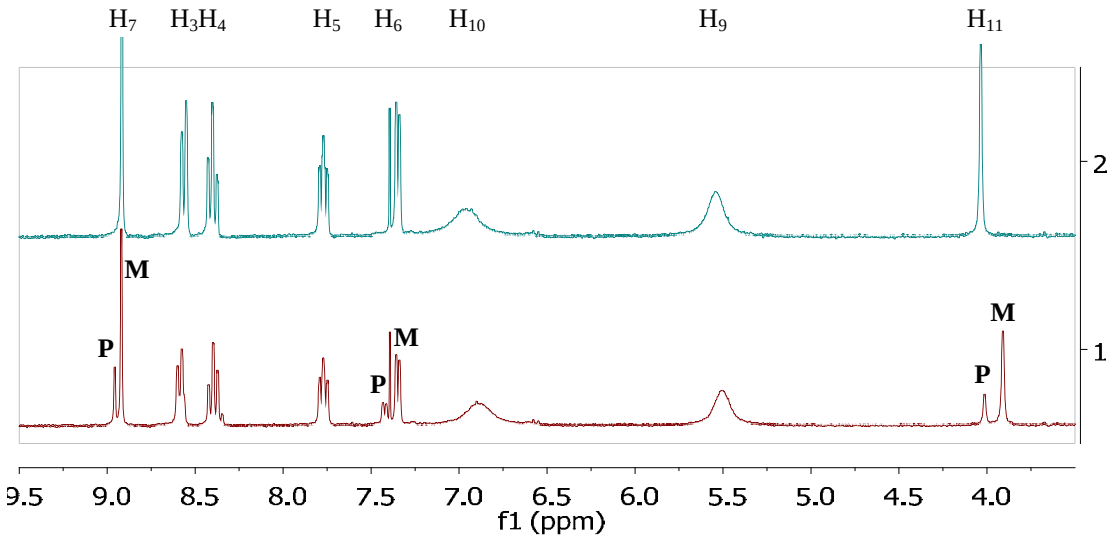

Figure 3.16. ^{1}H NMR (300 MHz, CD_3CN, 298K) of (**2**) a solution of the M enantiomer of $[Fe_2(L1)_3](PF_6)_4$ containing ~ 10% of the P enantiomer and (**1**) the same complex solution to which 2 equivalents of Δ-TRISPHAT were added.

the M enantiomer is affected only in the area of the central spacer. These experiments could not be performed with the chloride salt of Fe(II) parent cylinder in water or methanol, since TRISPHAT is not soluble in these solvents. However this feature allowed further but different studies of the Fe(II) cylinder-Δ-TRISPHAT adducts: five solutions of 6 mg of $[Fe_2(L1)_3](Cl)_4$ in 3 ml of water were prepared in test tubes and 3 ml of acetonitrile solutions containing Δ-TRISPHAT at different concentrations were added to each complex solution. Each test tube finally contained 725 μM of $[Fe_2(L1)_3](Cl)_4$ in 6 ml of water/acetonitrile (1/1), and increasing Δ-TRISPHAT/$[Fe_2(L1)_3](Cl)_4$ ratio (0.5, 0.75, 1, 1.5 and 2). A light purple precipitate was formed in each tube (Figure 3.17) and the amount of solid was visibly proportional to the amount of Δ-TRISPHAT present in the mixture. All the mixtures were filtered and the precipitates and filtrates were separately collected and analysed by CD in acetonitrile/methanol=8:2 (Figure 3.18.a)). The CD signals of each precipitate corresponded to the profile of the M enantiomer of the parent cylinder and the magnitudes of the CD bands decreased when more Δ-TRISPHAT was added. In contrast, the filtrates contained P enantiomer, whose concentration increased by increasing the amount of Δ-TRISPHAT. UV-Vis scans of each solution were collected (both precipitate and filtrate), CD magnitudes at 596 nm were divided by the corresponding values of UV-vis absorbance at 572 nm and plotted as a function of Δ-TRISPHAT/$[Fe_2(L1)_3](Cl)_4$ ratio (chart in Figure 3.18.b)). These experiments demonstrate that Δ-TRISPHAT forms an adduct with M enantiomer that causes the precipitation of $[Fe_2(L1)_3](Cl)_4$ in these solvent conditions (water/acetonitrile=1/1)

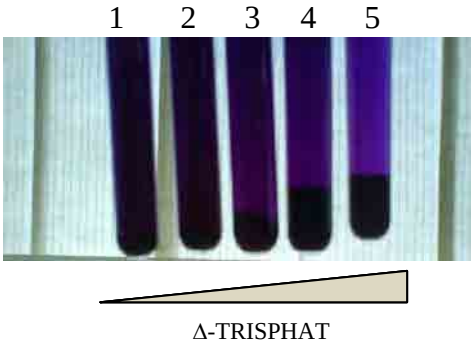

Figure 3.17. Five solutions of 725 μM of $[Fe_2(L1)_3](Cl)_4$ in water/acetonitrile (1/1 ratio, 6 ml) with increasing Δ-TRISPHAT/$Fe_2(L1)_3](Cl)_4$ ratio (0.5 (1), 0.75 (2), 1 (3), 1.5 (4) and 2 (5)).

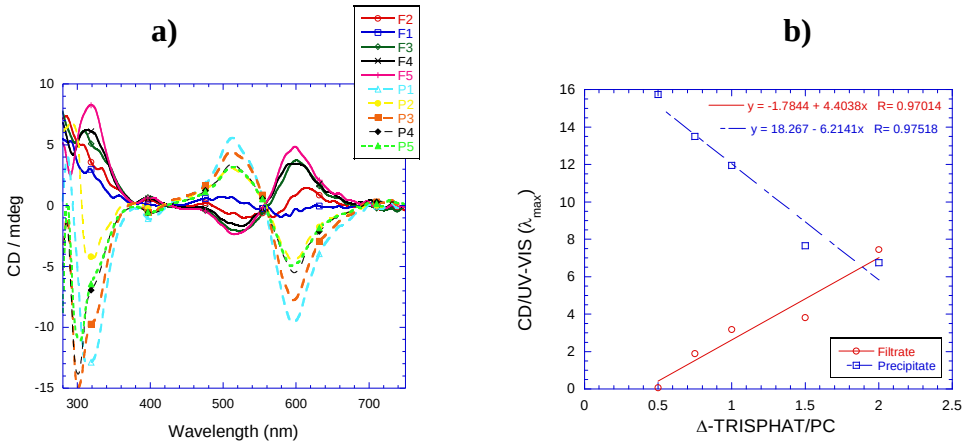

Figure 3.18. a) CD scans in acetonitrile/methanol (8/1) of each precipitate and filtrate (P and F in the legend) collected and separated from each tube of the experiment in Figure 3.17. **b)** CD magnitudes (both filtrate and precipitate) at 596 nm was divided by the corresponding value of UV-vis absorbance at 572 nm and plotted in function of Δ-TRISPHAT/$Fe_2(L1)_3](Cl)_4$ ratio

whilst most of the P enantiomer stays in solution. However, adding more Δ-TRISPHAT, the enantiomeric purity of the precipitate decreases, indicating that at some point also the P enantiomer-Δ-TRISPHAT adduct precipitates. The filtrate contains larger excess of P enantiomer when the addition of more Δ-TRISPHAT has promoted the precipitation of the M enantiomer. This study further confirms that the Δ-TRISPHAT binds differently to the two enantiomers in a way that the two adducts have different solubility in the solvent conditions investigated, and might form the basis for an alternative strategy to separate the two enantiomers (although the precipitation is not exclusively of one enantiomer and different conditions should be investigated). An initial experiment with a small amount of Λ-TRISPHAT that was available showed exactly the opposite result.

3.6.2 Arginine conjugated Fe(II) cylinders and Δ-TRISPHAT.

As the M and P enantiomer of the Fe(II) parent cylinder could be identified by NMR after their interaction with Δ-TRISPHAT, the same experiment was performed to study L and D-arginine Fe(II) conjugated cylinders $[Fe_2(L\mathbf{d}1)_3](PF_6)_{10}$ and $[Fe_2(L\mathbf{e}1)_3](PF_6)_{10}$. ^{1}H NMR spectra of the two complexes in CD_3CN are identical as

shown in spectra (**4**) and (**3**) in Figure 3.19, where the signals corresponding to the protons of the arginine conjugating units are marked with red crosses. The addition of Δ-TRISPHAT (2 equivalents) causes shifts of the imine and 6-pyridyl protons (H_7 and H_6) in the L-arginine conjugate $[Fe_2(L\mathbf{d}1)_3](PF_6)_{10}$ (Figure 3.19 (**2**)) and only the shift of the methyl proton of the central spacer H_{11} in the D-arginine conjugate $[Fe_2(L\mathbf{e}1)_3](PF_6)_{10}$ (Figure 3.19 (**1**)). This is exactly the same effect observed for the two enantiomers of Fe(II) parent cylinder and confirms that the helicate centres of L and D arginine conjugates are respectively in P and M configuration, as suggested by

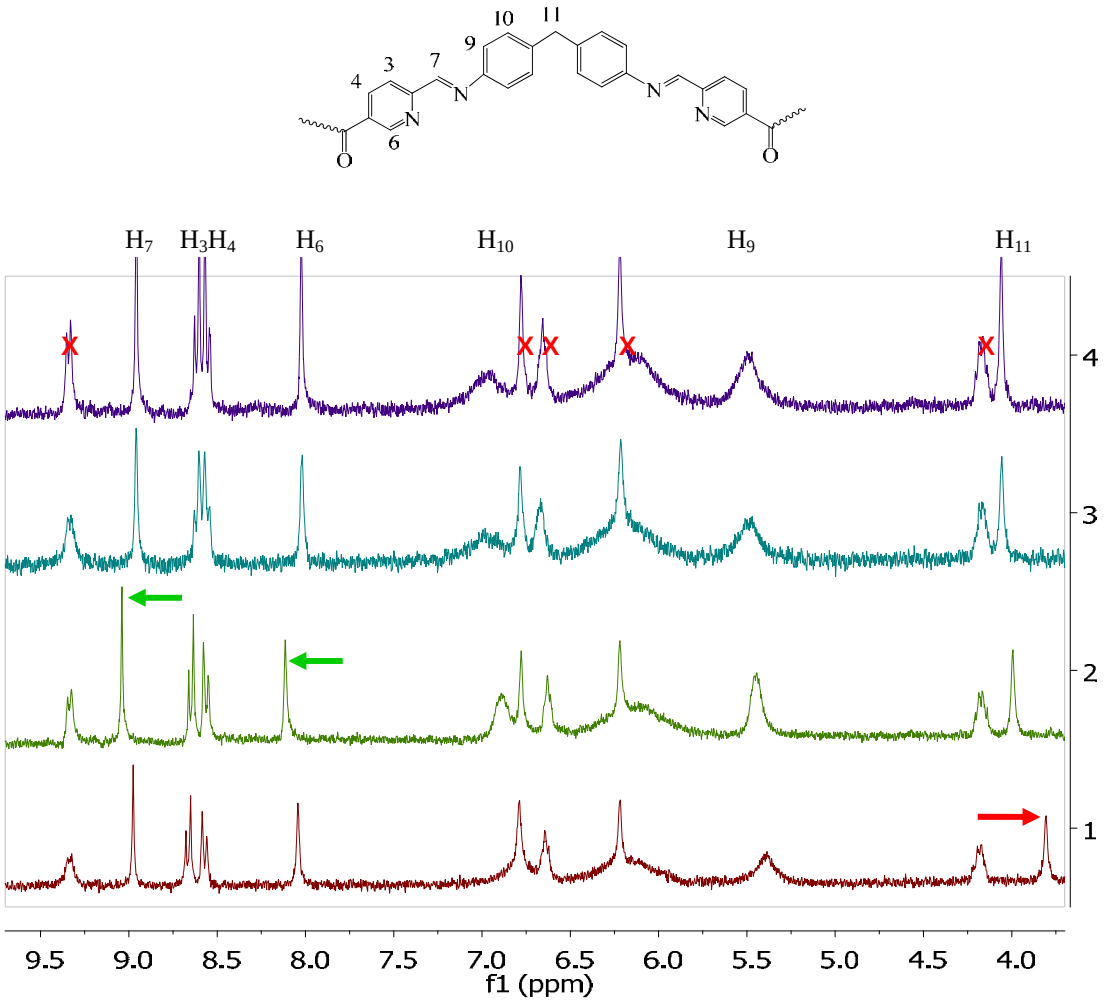

Figure 3.19. ^{1}H NMR (300 MHz, CD_3CN, 298K) of (**4**) $[Fe_2(L\mathbf{d}1)_3](PF_6)_{10}$ (L-Arg conjugate), (**3**) $[Fe_2(L\mathbf{e}1)_3](PF_6)_{10}$ (D-Arg conjugate), (**2**) the same solution of $[Fe_2(L\mathbf{d}1)_3](PF_6)_{10}$ with 2 equivalents of Δ-TRISPHAT and (**1**) the same solution of $[Fe_2(L\mathbf{e}1)_3](PF_6)_{10}$ with 2 equivalents of Δ-TRISPHAT. The signals marked with a red cross correspond to protons from the arginine conjugating units.

CD spectroscopy. The protons of the side conjugating units are not affected by the presence of Δ-TRISPHAT, despite the presence of the positive charged side chains of the arginine residues. This could be because these protons are too distant to be affected in the NMR spectrum by the eventual interaction between the guanidinium group and the TRISPHAT, or this interaction simply does not occur, possibly because prevented by the presence of PF_6^- anions. But it is evident that the central helicate cores of the conjugates are free to interact with the Δ-TRISPHAT as the unconjugate enantiomers do. Interestingly, for each NMR spectrum of conjugate-Δ-TRISPHAT there is only one set of signals which prove that the two conjugates in acetonitrile are diastereoisomerically pure.

3.7 Conclusions.

Synthetic routes to allow amino acids and short peptides to be conjugated onto the cylinder structure were established herein. The approach is flexible and based on amide bond formation between the conjugating unit and the 5 position of the pyridine rings of the parent bis-pyridylimine ligands (L1 or L5), so that the final complex hybrid of general formula M_2L_n holds 2n conjugating units. The synthesised and characterised conjugates were: five Fe(II) triple stranded, one Cu(I) double stranded and one Ag(I) double stranded based on the ligand L1 and three Cu(I) double stranded based on the ligand L5. ^{1}H NMR and UV-Vis studies suggested that the anchored amino acid residues at the edge of the cylinder do not prevent the formation of the central cylinder core, in which imine and pyridine nitrogen are responsible for the coordination of the metal centres as in the unconjugated complexes. The chirality of the central helicate is, in some cases, influenced by the presence of the attached amino acids. This effect is uncertain in serine (both D and L) Fe(II) triple stranded conjugates and is absent in Gly-Gly-Ser Fe(II) triple stranded and serine (both D and L) Cu(I) L5-based conjugates. Only three hybrids exhibited very distinctive CD signals: the Gly-Gly-Ser Cu(I) double stranded L5-based and D and L-Arg Fe(II) triple stranded. CD analysis and ^{1}H NMR experiments in the presence of Δ-TRISPHAT as NMR shift reagent indicate that the conjugation of D-Arg induces the central helicate core to preserve the M configuration whilst the L-arginine promotes P helicate formation. The two PF_6^- arginine conjugates are diastereoisomerically pure

in acetonitrile whilst diastereoisomeric impurity of the corresponding Cl^- complexes in water cannot be excluded.

3.8 Experimental.

3.8.1 Materials.

All chemicals and solvents were purchased from Sigma–Aldrich, Fisher, Alfa Aesar, or Fluorochem and used as received. Deuterated solvents for NMR were supplied by Goss Scientific. Resins, amino acids and reagents for the peptide synthesis were Novabiochem products supplied by Merck Biosciences Ltd. Thin layer chromatography (TLC) was carried out on silica gel pre-coated aluminium sheets (Silica Gel 60 F254), supplied by MERCK KGaA. Visualisation used UV light (254/365). Column chromatography was performed using laboratory grade solvents on Silica Gel 60 (0.043–0.063 mm, supplied by Fluorochem, Glossop, UK) under gravity or with gentle pressure applied using nitrogen flow. All reverse phase high performance liquid chromatography (HPLC) analyses and purifications were performed on Dionex Summit HPLC systems with Chromoleon software, using HPLC grade solvents, supplied by Fisher. Analytical HPLC were acquired with the aid of a Summit P580 quaternary low pressure gradient pump with built in vacuum degasser while, for the preparative HPLC, a high pressure gradient pump was employed on the same machine. Phenomenex Luna 10l C18 (2) columns were used for analytical (250 x 4.6 mm, 1 ml/min flow) and preparative (250 x 21.2 mm, 21 ml/min flow) RP-HPLC.

NMR, UV-Vis and Circular Dichroism analyses were performed using the instruments described in section 2.5.4. Electrospray Ionisation (ESI) analyses, including accurate mass calculation (High Resolution Mass Spectrometry, HRMS) where possible, were carried out on a Micromass LCT Time of Flight Mass Spectrometer in positive ionisation mode and processed by MassLynx software. Infrared spectra were recorded on a Perkin Elmer Spectrum 100 FTIR spectrometer as neat films and wavelengths (ν) are quoted in cm^{-1}.

3.8.2 Synthesis of 6-formyl-nicotinic acid methyl ester (1).

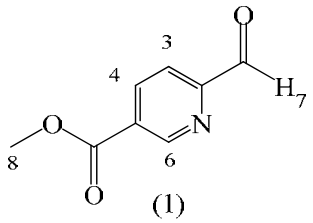

(1)

This compound was prepared by slight modifications of a reported procedure.[52] Methyl 6-methylnicotinate (5.54 g, 36.7 mmol) was mixed with iodine (9.31 g, 36.7 mmol), and a small amount of DMSO was added to promote mixing. After 5 min of mixing, DMSO (20 ml) was added and this solution was added to a heated solution of DMSO (35 ml) at 130 °C. The temperature was slowly raised to 160 °C and the mixture was stirred at this temperature for 15 min. After cooling down the solution, a small amount of a saturated aqueous solution of Na_2CO_3 was added. The product was extracted with diethyl ether. Evaporation of the solvent gave the crude product, which was purified by column chromatography (CH_2Cl_2/EtOAc = 4:1). The product was obtained as an off-white solid in 2.06 g yield (33%). TLC with CH_2Cl_2/EtOAc = 4:1 as eluent (Rf = 0.69). ^{1}H NMR (400 MHz, $CDCl_3$, 298 K) δ 10.14 (1H, s, H_7), 9.30 (1H, d, ^4J = 1.8 Hz, H_{6py}), 8.38 (1H, dd, ^3J and ^4J = 8.0, 1.8 Hz, H_{4py}), 8.02 (1H, d, ^3J = 8.0 Hz, H_{3py}), 4.19 (3H, s, H_8). EI mass analysis: m/z = 165.2 $[M+H]^+$.

3.8.3 Synthesis of 6-dimethoxymethyl-nicotinic acid methyl ester (2).

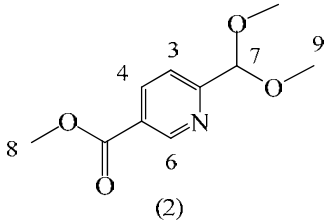

(2)

6-Formyl-nicotinic acid methyl ester (**1**) (0.83 g, 5.03 mmol) was dissolved in trimethylorthoformate (20 ml), formic acid (2 ml) and sulphuric acid (2 drops). The mixture was heated to 50 °C and stirred at this temperature for 30 min, followed by stirring overnight at room temperature. Water (30 ml) and diethyl ether (30 ml) were added, the layers were separated and the aqueous layer extracted with diethyl ether (2x). The combined diethyl ether layers were washed with aqueous saturated Na_2CO_3

and dried with $MgSO_4$. Evaporation of the solvent gave a light yellow solid in 0.75 g yield (71%). ^{1}H NMR (400 MHz, $CDCl_3$, 298 K) δ 9.28 (1H, d, ^{4}J = 2.2 Hz, H_{6py}), 8.52 (1H, dd, ^{3}J and ^{4}J = 8.0, 2.2 Hz, H_{4py}), 7.64 (1H, d, ^{3}J = 8.0 Hz, H_{3py}), 5.23 (1H, s, H_7), 4.00 (3H, s, H_8) 3.49 (6H, s, H_9). EI mass analysis: m/z = 210.0 $[M+H]^+$.

3.8.4 Synthesis of 6-dimethoxymethyl-nicotinic acid (3).

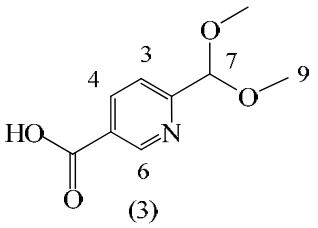

(3)

6-Dimethoxymethyl-nicotinic acid methyl ester (2) (0.95 g, 4.5 mmol) was dissolved in MeOH (6 ml) and 1 M NaOH (6 ml) was added. The resulting mixture was stirred overnight at room temperature. The methanol was evaporated and HCl (1 M) was added until pH ~2-3. The compound was extracted with ethyl acetate (3x) and evaporation of the collected organic layers yielded 90% of pure yellow compound. ^{1}H NMR (400 MHz, $CDCl_3$, 298 K) δ 8.71 (1H, d, ^{4}J = 2.0 Hz, H_{6py}), 8.12 (1H, dd, ^{3}J and ^{4}J = 8.0, 2.0 Hz, H_{4py}), 7.53 (1H, d, J = 8.0 Hz, H_{3py}), 5.38 (1H, s, H_7), 3.44 (6H, s, H_9). EI mass analysis: m/z = 196.0 $[M+H]^+$.

3.8.5 2-Dimethoxymethyl-5-(a)-pyridine (4-a to 6-a).

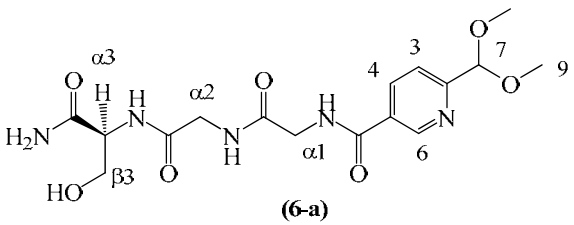

(6-a)

Standard manual solid phase synthesis with fluorenylmethoxcarbonil (Fmoc) chemistry was applied.[49-51] Rink Amide MHBA resin (loading grade 0.525 mmol/g) was used to obtain carboxamide peptide and a 2.8 mmol synthesis scale was applied. For the chain assembly, Fmoc-Gly-OH and Fmoc-Ser(t-Bu)-OH were used as Fmoc protected amino acids, and 6-dimethoxymethyl-nicotinic acid (**3**) was the last compound to be coupled at the N-terminal of the growing chain by amide bond

formation. For each Fmoc deprotection the resin was treated with a solution of 20% piperidine in dimethylformamide (DMF, 60 ml) and each coupling reaction was carried out by using amino acid/HBTU/ DIEA = 3:3:6 in relation to the synthesis scale, in DMF. A standard Kaiser test[53] was used to verify that each coupling reaction was complete. After the solid phase synthesis was complete, the resin was treated with 50 ml of cleavage solution (trifluoroacetic acid (TFA)/H_2O/triisopropylsilane = 9.5:0.25:0.25) for 3 h at room temperature. Then the mixture was filtrated, and the volume of the collected solution was reduced to few milliliters by evaporation. The crude compound was obtained by cold precipitation with diethyl ether and then analysed and purified by RP-HPLC. From 0 to 100% of acetonitrile 0.05% TFA in H_2O 0.05% TFA in 40 min was the gradient used for this analysis. Pure (**6**) was achieved with 68% of yield (0.755 g). ^{1}H NMR (400 MHz, D_2O, 298 K) δ 8.97 (1H, d, ^4J = 2.1 Hz, H_{6py}), 8.49 (1H, dd, ^3J and ^4J = 8.1, 2.1 Hz, H_{4py}), 7.84 (1H, d, ^3J = 8.1 Hz, H_{3py}), 5.60 (1H, s, H_7), 4.38 (1H, t, ^3J = 5.1 Hz, $H_{\alpha 3}$), 4.14 (2H, s, $H_{\alpha 1}$), 3.98 (2H, s, $H_{\alpha 2}$), 3.82 (2H, t, ^3J = 5.1 Hz, $H_{\beta 3}$), 3.43 (6H, s, H_9). HRMS (ESI) analysis calcd. for $C_{16}H_{23}N_5O_7Na$ 420.1495 $[M+Na]^+$; found 420.1499. IR (ν) = 3232 (br m), 2982 (w), 1652 (vs), 1532 (s), 1489 (w), 1410 (w), 1333 (w), 1255 (w), 1199 (m), 1180 (m), 1150 (w), 1070 (br m), 1021 (m), 973 (m), 799 (s), 720 (s) cm^{-1}.

3.8.6 2-Dimethoxymethyl-5-(b, c, d, e)-pyridine (4-b, c, d,e to 6-b,c,d,e).

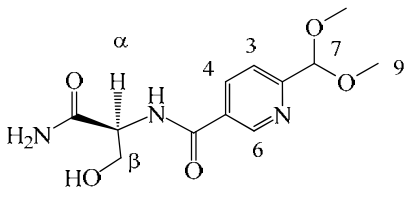

(6-b)

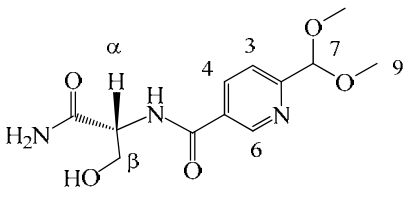

(6-c)

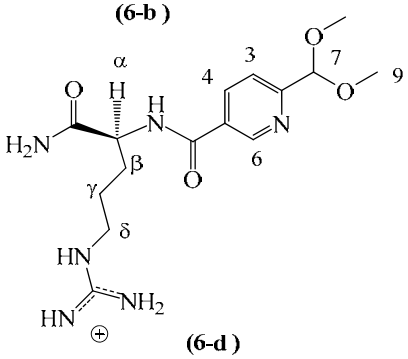

(6-d)

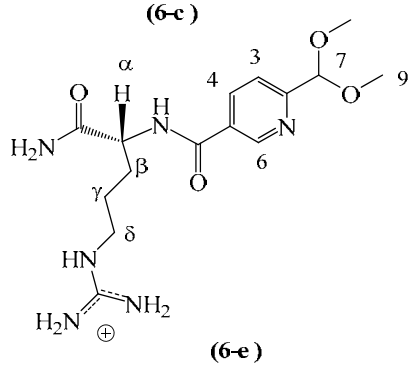

(6-e)

The same procedure described above for the synthesis of 2-dimethoxymethyl-5-(**a**)-pyridine was applied to obtain the other four compounds 2-dimethoxymethyl-5-(R)-pyridine where R is L-Ser (**6-b**), D-Ser (**6-c**), L-Arg (**6-d**) and D-Arg (**6-e**), using Fmoc-L-Ser(t-Bu)-OH, Fmoc-D-Ser(t-Bu)-OH, Fmoc-L-Arg(Pbf)-OH or , Fmoc-D-Arg(Pbf)-OH respectively as protected amino acids for the attachment on the resin. Purifications by RP-HPLC (From 0 to 100% of acetonitrile 0.05% TFA in H_2O 0.05% TFA in 40 min) gave pure yellow compounds (Yields: 73% **6-b,** 68% **6-c,** 38% **6-d,** 69% **6-e**).

2-dimethoxymethyl-5-(b)-pyridine (6-b): ^{1}H NMR (400 MHz, MeOD, 298 K) δ 9.09 (1H, d, ^{4}J = 2.2 H_{6py}), 8.51 (1H, dd, ^{3}J and ^{4}J = 8.1, 2.2 Hz, H_{4py}), 7.84 (1H, d, ^{3}J = 8.1 Hz, H_{3py}), 5.50 (1H, s, H_7), 4.68 (1H, t, ^{3}J = 5.1, Hz, H_α), 3.94 (2H, d, ^{3}J = 5.1 Hz, H_β) 3.30 (6H, s, H_9). HRMS (ESI) analysis calcd. for $C_{12}H_{17}N_3O_5Na$, 306.1066 $[M+Na]^+$; found 306.1068. IR (ν) = 318 (br m), 2885 (w), 1649 (vs), 1531 (s), 1420 (w), 1339 (m) 1102 (m), 1073 (br s) 909 (w), 836 (br m), 798 (w), 719 (m) cm^{-1}.

2-dimethoxymethyl-5-(c)-pyridine (6-c): ^{1}H NMR (400 MHz, MeOD, 298 K) δ 9.07 (1H, d, ^{4}J = 2.2 H_{6py}), 8.51 (1H, dd, ^{3}J and ^{4}J = 8.1, 2.2 Hz, H_{4py}), 7.85 (1H, d, ^{3}J = 8.1 Hz, H_{3py}), 5.55 (1H, s, H_7), 4.61 (1H, t, ^{3}J = 5.1, Hz, H_α), 3.94 (2H, d, ^{3}J = 5.1 Hz, H_β) 3.35 (6H, s, H_9). HRMS (ESI) analysis calcd. for $C_{12}H_{17}N_3O_5Na$, 306.1066 $[M+Na]^+$; found 306.1069. IR (ν) = 3181 (br m), 2892 (w), 1649 (vs), 1530 (s), 1420 (w), 1292 (m) 1178 (m), 1073 (br s) 910 (w), 836 (br m) 719 (m) cm^{-1}.

2-dimethoxymethyl-5-(d)-pyridine (6-d): ^{1}H NMR (400 MHz, MeOD, 298 K) δ 9.01 (1H, d, ^{4}J = 2.0 H_{6py}), 8.37 (1H, dd, ^{3}J and ^{4}J = 8.2, 2.0 Hz, H_{4py}), 7.75 (1H, d, ^{3}J = 8.2 Hz, H_{3py}), 5.45 (1H, s, H_7), 4.59 (1H, dd, ^{3}J = 5.3, 8.8 Hz, H_α), 3.32 (6H, s, H_9) 3.24 (2H, td, ^{3}J = 2.9, 7.0, Hz, H_δ), 1.99 (1H, m H_β), 1.83 (1H, m H_β), 1.72 (2H, m, H_γ). HRMS (ESI) analysis calcd. for $C_{15}H_{25}N_6O_4$, 353.1937 $[M]^+$; found 353.1931. IR (ν) = 3187 (br m), 2892 (w), 1648 (vs), 1533 (s), 1422 (w), 1293 (w), 1198 (s), 1130 (vs), 914 (w), 839 (m), 799 (w), 722 (m) cm^{-1}.

2-dimethoxymethyl-5-(e)-pyridine (6-e): ^{1}H NMR (400 MHz, MeOD, 298 K) δ 9.03 (1H, d, ^{4}J = 2.0 H_{6py}), 8.36 (1H, dd, ^{3}J and ^{4}J = 8.2, 2.0 Hz, H_{4py}), 7.75 (1H, d, ^{3}J = 8.2 Hz, H_{3py}), 5.41 (1H, s, H_7), 4.62 (1H, dd, ^{3}J = 5.3, 8.8 Hz, H_α), 3.32 (6H, s, H_9) 3.26 (2H, td, ^{3}J = 2.9, 7.0, Hz, H_δ), 1.99 (1H, m H_β), 1.83 (1H, m H_β), 1.72 (2H,

m, H_γ). HRMS (ESI) analysis calcd. for $C_{15}H_{25}N_6O_4$, 353.1937 $[M]^+$; found 353.1933. IR (ν) = 3194 (br m), 2892 (w), 1651 (vs), 1532 (s), 1424 (w), 1321 (br w), 1179 (s), 1126 (vs), 914 (w), 836 (m), 799 (w), 720 (m) cm^{-1}.

3.8.7 2-formyl-5-(R)-pyridine (7-a, b, c, d, e).

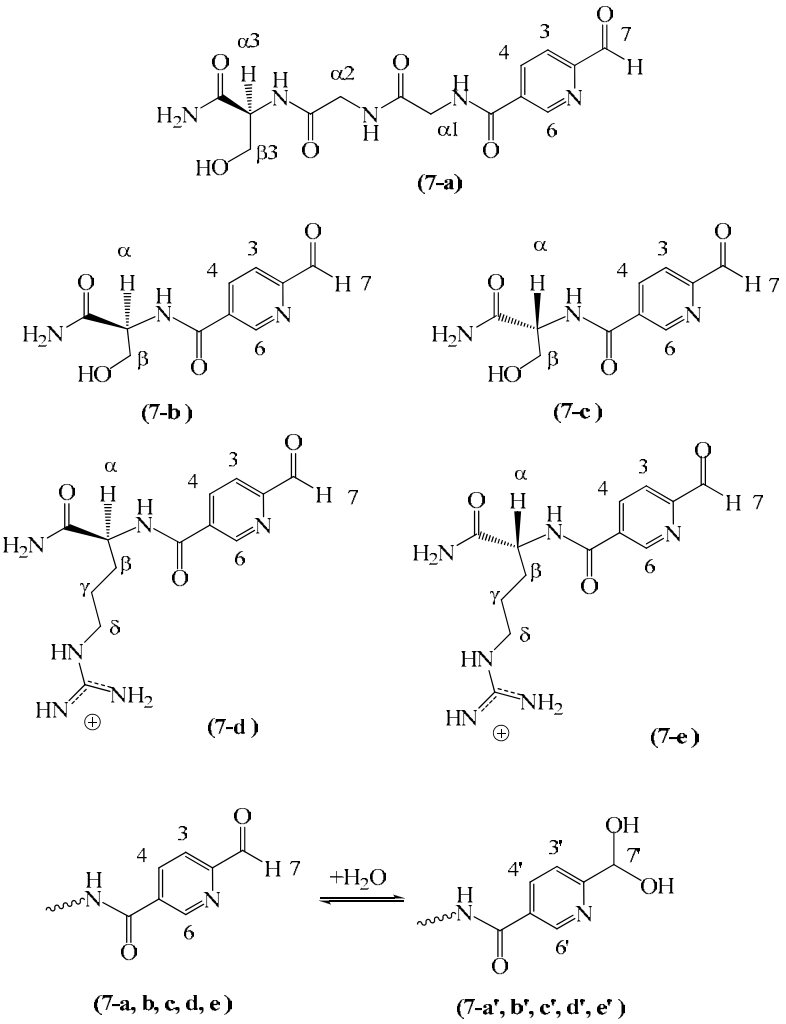

Deprotection of aldehyde group was achieved using the same procedure for all 2-dimethoxymethyl-R-pyridine compounds where R is Gly-Gly-L-Ser (**6-a**), L-Ser (**6-b**), D-Ser (**6-c**), L-Arg (**6-d**) and D-Arg (**6-e**). 2-Dimethoxymethyl-R-pyridine (1 mmol) was partially dissolved in 18 ml of THF and 3 ml of 1M HCl were added in 1 hour time at 0 °C. The mixture was stirred at room temperature and the reaction was monitored by analytical RP-HPLC every day (from 0 to 100% of methanol in water in 40 min for **7-a, b, c**; from 0 to 100% of acetonitrile in water in 40 min for **7-d, e**). The peak corresponding to the unprotected aldehyde (~ 3 min earlier than starting protected compound) was present in the chromatogram after 24 hours, but the

reaction was promoted by adding small quantities (~ 1 ml) of 1M HCl until the chromatogram showed the unprotected aldehyde as the main compound. 3-4 days were sufficient to have a complete reaction. The crude was purified by preparative RP-HPLC (from 0 to 100% of methanol in water in 70 min, 22 ml/min flow, acetonitrile instead of methanol was used only for **7-d, e**) and freeze dried, obtaining pure compound (Yields: 59% **7-a**, 54% 7-**b,** 57% **7-c,** 38% **7-d,** 31% **7-e**).

All the ^{1}H NMR spectra, both in D_2O and in MeOD, of 2-formyl-R-pyridine (7-a, b, c, d, e), shows two set of signals, because in solution the aldehyde group is in equilibrium with the hydrate form (as showed in the scheme above). Consequently the spectra present the resonances of the protons of the pyridine rings of both the species, the resonance of the aldehyde proton and that from the hydrate species. In the region of the signals due to the protons in the peptide chain, there is the contribution of both the species.

2-formyl-5-(a)-pyridine (7-a): ^{1}H NMR (400 MHz, D_2O, 298 K) δ 9.98 (1H, s, H_7), 9.06 (1H, d, ^{4}J = 2.0, H_{6py}), 8.90 (3.2H, d, ^{4}J = 2.0, $H_{6'py}$), 8.41 (1H, dd, ^{3}J and ^{4}J = 8.1, 2.0 Hz, H_{4py}), 8.32 (3.2H, dd, ^{3}J and ^{4}J = 8.1, 2.0 Hz, $H_{4'py}$), 8.08 (1H, d, ^{3}J = 8.1 Hz, H_{3py}), 7.76 (3.2H, d, ^{3}J = 8.1 Hz, $H_{3'py}$), 6.04 (3H, s, $H_{7'}$), 4.39 (4.7H, t, ^{3}J = 4.8 Hz, $H_{\alpha 3}$), 4.13 (9.2H, s, $H_{\alpha 1}$), 3.98 (9.2H, m, $H_{\alpha 2}$), 3.83 (9.2H, m, $H_{\beta 3}$). HRMS (ESI) analysis calcd. for $C_{14}H_{17}N_5O_6Na$, 374.1077 $[M+Na]^+$; found 374.1074. IR (ν) = 3258 (br m), 2968 (w), 1643 (vs), 1529 (s), 1489 (w), 1411 (w), 1332 (w), 1250 (w), 1199 (m), 1179 (m), 1150 (w), 1073 (br m), 1021 (m), 971 (m), 799 (s), 720 (s) cm^{-1}.

2-formyl-5-(b)-pyridine (7-b): ^{1}H NMR (400 MHz, D_2O, 298 K) δ 9.97 (1H, s, H_7), 9.05 (1H, d, ^{4}J = 2.2 Hz, H_{6py}), 8.86 (2.3H, d, ^{4}J = 2.2, $H_{6'py}$), 8.37 (1H, dd, ^{3}J and ^{4}J = 2.2, 8.1 Hz, H_{4py}), 8.27 (2.3H, dd, ^{3}J and ^{4}J = 2.2, 8.1 Hz, $H_{4'py}$), 8.07 (1H, d, ^{3}J = 8.1 Hz, H_{3py}), 7.31(2.3 H, d, ^{3}J = 8.1 Hz, $H_{3'py}$), 6.01 (2.3H, s, $H_{7'}$), 4.59 (3.3H, t, ^{3}J = 5.5 Hz, H_{α}), 3.92 (3.3 H, d, ^{3}J = 5.5 Hz, H_{β}). HRMS (ESI) analysis calcd. for $C_{10}H_{11}N_3O_4Na$, 260.0647 $[M+Na]^+$; found 260.0649. IR (ν) = 3211 (br m), 2870 (w), 1643 (vs), 1534 (s), 1415 (w), 1294 (m), 1190 (m), 1040 (br s) 908 (w), 852 (br m), 799 (w), 720 (m) cm^{-1}.

2-formyl-5-(c)-pyridine (7-c): ^{1}H NMR (400 MHz, D_2O, 298 K) δ 10.0 (1H, s, H_7), 9.09 (1H, d, ^{4}J = 2.2 Hz, H_{6py}), 8.86 (4.8H, d, ^{4}J = 2.2, $H_{6'py}$), 8.31 (1H, dd, ^{3}J and ^{4}J = 2.2, 8.1 Hz, H_{4py}), 8.27 (4.8 H, dd, ^{3}J and ^{4}J = 2.2, 8.1 Hz, $H_{4'py}$), 8.00 (1H, d, ^{3}J =

8.1 Hz, H_{3py}), 7.31(4.8 H, d, ^3J = 8.1 Hz, $H_{3'py}$), 6.01 (4.8H, s, $H_{7'}$), 4.58 (5.8H, t, ^3J = 5.5 Hz, H_α), 3.90 (5.8 H, d, ^3J = 5.5 Hz, H_β). HRMS (ESI) analysis calcd. for $C_{10}H_{11}N_3O_4Na$, 260.0647 $[M+Na]^+$; found 260.0648. IR (ν) = 3198 (br m), 2892 (w), 1643 (vs), 1532 (s), 1418 (w), 1290 (m), 1170 (m), 1042 (br s), 910 (w), 832 (br m), 799 (w), 719 (m) cm^{-1}.

2-formyl-5-(d)-pyridine (7-d): ^1H NMR (400 MHz, MeOD, 298 K) δ 9.00 (1H, d, ^4J=2.4 $H_{6'py}$), 8.32 (1H, dd, ^3J and ^4J = 2.4, 8.3, Hz, $H_{4'py}$), 7.75 (1H, d, ^3J = 8.3 Hz, $H_{3'py}$), 5.59 (1H, s, $H_{7'}$), 4.62 (1H, dd, ^3J = 5.3, 8.8 Hz, H_α), 3.27 (2H, dt, ^3J = 2.3, 6.8, Hz, H_δ), 1.99 (1H, m H_β), 1.83 (1H, m H_β), 1.70 (2H, m H_γ). Only less than 10% of aldeyde form was present in the spectrum δ 10.07 (s, H_7), 9.20 (d, ^4J=2.4 $H_{6'py}$), 8.42 (dd, ^3J and ^4J = 2.4, 8.3, Hz, H_{4py}), 8.06 (d, ^3J = 8.3 Hz, $H_{3'py}$). HRMS (ESI) analysis calcd. for $C_{13}H_{19}N_6O_3$, 307.1519 $[M]^+$; found 307.1511. IR (ν) = 3163 (br m), 2952 (w), 1643 (vs), 1530 (s), 1417 (w), 1291 (w), 1175 (m), 1040 (br s), 910 (m), 865 (br m) cm^{-1}.

2-formyl-5-(e)-pyridine (7-e): ^1H NMR (400 MHz, MeOD, 298 K) δ 8.98 (1H, d, ^4J=2.4 $H_{6'py}$), 8.33 (1H, dd, ^3J and ^4J = 2.4, 8.3, Hz, $H_{4'py}$), 7.77 (1H, d, ^3J = 8.3 Hz, $H_{3'py}$), 5.57 (1H, s, $H_{7'}$), 4.62 (1H, dd, ^3J = 5.3, 8.8 Hz, H_α), 3.27 (2H, dt, ^3J = 2.3, 6.8, Hz, H_δ), 1.99 (1H, m H_β), 1.83 (1H, m H_β), 1.70 (2H, m H_γ). Only less than 10% of aldeyde form was present in the spectrum δ 10.08 (s, H_7), 9.20 (d, ^4J=2.4 $H_{6'py}$), 8.43 (dd, ^3J and ^4J = 2.4, 8.3, Hz, H_{4py}), 8.07 (d, ^3J = 8.3 Hz, $H_{3'py}$). HRMS (ESI) analysis calcd. for $C_{13}H_{19}N_6O_3$, 307.1519 $[M]^+$; found 307.1511. IR (ν) = 3186 (br m), 2892 (w), 1640 (vs), 1536 (s), 1422 (w), 1292 (w) 1198 (s), 1127 (br s), 915 (m), 836 (br m) cm^{-1}.

3.8.8 Ligand La1.

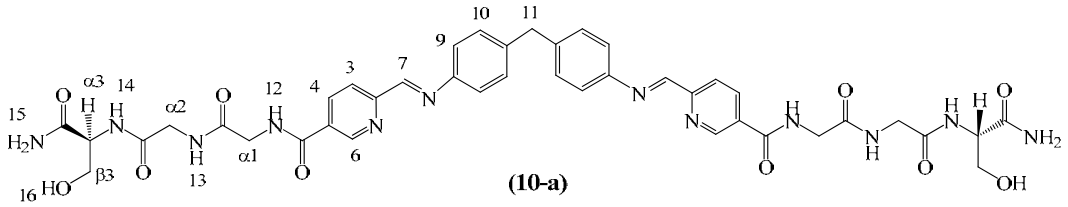

(10-a)

To 84.7 mg of 2-formyl-5-(a)-pyridine (**7-a**) (0.242 mmol), 6 ml of methanol were added and the suspension was sonicated and heated at 50–60 °C for 5 min. A

solution of 4,4'-methylenedianiline (**8**) (23.9 mg, 0.121 mmol) in 3 ml of methanol was added drop wise (over 10 min) to the mixture, the temperature raised to reflux and the mixture stirred at reflux for 6 h. The yellow precipitate that formed was isolated by filtration and abundantly washed with methanol and diethyl ether, dried under vacuum, washed again with water and finally washed with diethyl ether and dried to afford 85 mg of compound (**10-a**) (yield: 81%). Since the ligand La1 (**10-a**) is not soluble in methanol or in water, but it is partially soluble in a water/methanol mix, the drying between the two washing is very important to avoid a partial dissolution of the compound. ^{1}H NMR (400 MHz, DMSO-d_6, 298 K) δ 9.16 (1H, t, ^{3}J = 5.8 Hz, H_{12}), 9.11 (1H, d, ^{4}J = 1.9 Hz, H_{6py}), 8.64 (1H, s, H_7), 8.32 (1H, dd, ^{3}J and ^{4}J = 8.3, 1.9 Hz, H_{4py}), 8.25 (1H, t, ^{3}J = 5.8 Hz, H_{13}), 8.19 (1H, d, ^{3}J = 8.3, H_{3py}), 7.81 (1H, d, ^{3}J = 7.8 Hz, H_{14}), 7.31 (4H, s, $H_{9/10}$), 7.17 (1H, s, H_{15}), 7.07 (1H, s, H_{15}), 4.81 (1H, t, ^{3}J = 5.3 Hz, H_{16}), 4.15 (1H, dt, ^{3}J = 7.8, 5.3 Hz, $H_{\alpha 3}$) 3.99 (1H, s, H_{11}), 3.91 (2H, d, ^{3}J = 5.8 Hz, $H_{\alpha 1}$), 3.74 (2H, dd, ^{4}J and ^{3}J = 13.6, 5.8 Hz, $H_{\alpha 2}$), 3.56 (2H, m, J = 16.1, 10.7, 5.8 Hz, $H_{\beta 3}$). HRMS (ESI) analysis calcd. for $C_{41}H_{44}N_{12}O_{10}Na$, 887.3201 $[M+Na]^{+}$; found 887.321. IR (ν) = 3286 (br m), 2893 (w), 1637 (vs), 1537 (s), 1503 (w shoulder), 1412 (w), 1372 (w), 1326 (w), 1235 (m), 1199 (m), 1025 (w), 993 (w), 916 (w), 8.54 (m), 784 (w) cm^{-1}.

3.8.9 Ligand La2.

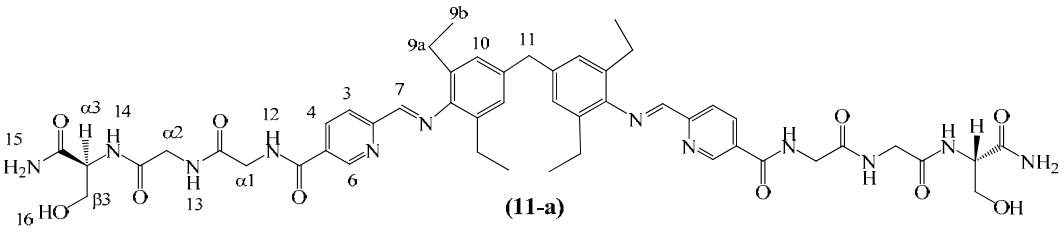

The procedure used for La1 was applied for the synthesis of ligand La2, but 4,4'-methylenbis(2,6-diethylaniline) (**9**) was used instead of 4,4'-methylenedianiline. A yellow compound was achieved yielding 72 mg (61%). ^{1}H NMR (400 MHz, DMSO-d_6, 298 K) δ 9.22 (1H, t, ^{3}J = 5.5 Hz, H_{12}), 9.13 (1H, d, ^{4}J = 1.9 Hz, H_{6py}), 8.41 (1H, dd, ^{3}J and ^{4}J = 8.3, 1.9 Hz, H_{4py}), 8.32 (1H, s, H_7), 8.25 and 8.23 (overlapped 1H, t, ^{3}J = 5.3 Hz, H_{13} + 1H, d, ^{3}J = 8.3, H_{3py}), 7.81 (1H, d, J = 7.8 Hz, H_{14}), 7.18 (1H, s, H_{15}), 7.07 (1H, s, H_{15}), 6.99 (2H, s, H_{10}), 4.81 (1H, t, ^{3}J = 5.8 Hz, H_{16}), 4.16 (1H, dt, ^{3}J =

7.8, 5.3 Hz, $H_{\alpha 3}$) 3.97 (2H, d, ^3J = 5.5 Hz, $H_{\alpha 1}$), 3.86 (1H, s, H_{11}), 3.77 (2H, dd, ^3J and J^4 = 13.6, 5.3 Hz, $H_{\alpha 2}$), 3.56 (2H, m, J = 10.7, 5.3 Hz, $H_{\beta 3}$), 2.39 (4H, q, ^3J = 7.8, 7.3 Hz, H_{9a}), 1.01 (6H, t, ^3J = 7.3 Hz, H_{9b}). HRMS (ESI) analysis calcd. for $C_{49}H_{60}N_{12}O_{10}Na$ 999.4453 $[M+Na]^+$; found 999.4465. IR (ν) = 3280 (br m), 2892 (w), 1650 (vs), 1601 (m shoulder), 1532 (s), 1410 (w), 1290 (br m), 1202 (w), 1168 (w), 1047 (m), 1020 (m), 911 (w), 852 (w), 760 (w) cm^{-1}.

3.8.10 $[Cu_2(La1)_2](Cl)_2$

To a stirred nitrogen purged suspension of Ligand La1 (**10-a**) (26.0 mg, 0.030 mmol) in 3 ml of methanol, solid $[Cu(CH_3CN)_4][PF_6]$ (16.7 mg, 0.045 mmol) was added to give a red-brown mixture. The mixture was stirred overnight under nitrogen atmosphere and a red-brown precipitate was collected by filtration, abundantly washed with methanol, and dried with diethyl ether (yield: 54.1%). ^1H NMR (500 MHz, D_2O/CD_3CN = 1:2, 298 K) δ 9.42 (1H, br, H_{6py}), 9.13 (1H, br, H_7), 8.71 (1H, br, $H_{3/4py}$), 8.36 (1H, br, $H_{3/4py}$), 7.57 (2H, br, $H_{9/10}$), 7.37 (2H, br, $H_{9/10}$), 7.24 (1H, s, H_{15}), 6.83 (1H, s, H_{15}), 4.56 (1H, br, $H_{\alpha 3}$), 4.37 (1H, s, H_{11}), 4.29 (2H, br/m, $H_{\alpha 1}$), 4.15 (2H, br/m, $H_{\alpha 2}$), 4.01 (2H, m, $H_{\beta 1}$). ESI mass analysis m/z = 928.2 $[Cu_2(La1)_2]^{2+}$. IR (ν) = 3286 (br m), 2893 (w), 1650 (vs), 1537 (s), 1412 (w), 1328 (w), 1079 (m), 1048 (m), 993 (w), 918 (w), 8.54 (m), 784 (w) cm^{-1}.

The complex was passed through ion-exchange resin (Dowex 1x8–100 mesh (Cl)), to exchange the counter anion to Cl^-. ESI mass analysis confirmed that the ion exchange did not affect the complex. UV–Vis (water) λ_{max} (nm) = 515, 344, 240, 205.

3.8.11 $[Ag_2(La1)_2](PF_6)_2$

To a stirred nitrogen purged suspension of Ligand La1 (**10-a**) (30.0 mg, 0.034 mmol) in 3 ml of methanol was added solid $AgPF_6$ (12.8 mg, 0.051 mmol) to give a dark yellow mixture. The mixture was stirred overnight at room temperature under nitrogen atmosphere and the yellow precipitate was collected by filtration, abundantly washed with methanol and dried with diethyl ether (26.4 mg, yield: 66%). ^1H NMR (400 MHz, DMSO-d_6, 298 K) δ 9.22 (1H, t, ^3J = 5.8 Hz, H_{12}), 9.18

(1H, d, ^4J = 1.9 Hz, H_{6py}), 8.97 (1H, s, H_7), 8.47 (1H, dd, ^3J and ^4J = 8.3, 1.9 Hz, H_{4py}), 8.28 (1H, t, ^3J = 5.8 Hz, H_{13}), 8,17 (1H, d, ^3J = 8.3, H_{3py}), 7.81 (1H, d, ^3J = 8.3 Hz, H_{14}), 7.42 (2H, d, ^3J = 8.3 Hz, $H_{9/10}$), 7.32 (2H, d, ^3J = 8.3 Hz, $H_{9/10}$), 7.18 (1H, s, H_{15}), 7.06 (1H, s, H_{15}), 4.80 (1H, br, H_{16}), 4.19 (1H, dt, ^3J = 8.3, 5.3 Hz, $H_{\alpha 3}$) 4.0 (1H, s, H_{11}), 3.95 (2H, d, ^3J = 5.8 Hz, $H_{\alpha 1}$), 3.76 (2H, m, ^3J and ^4J = 12.2, 5.8 Hz, $H_{\alpha 2}$), 3.55 (2H, m, ^3J = 16.1, 8.3, 5.8 Hz, $H_{\beta 3}$). ESI mass analysis m/z = 973.21 $[Ag_2La1_2]^{2+}$.

3.8.12 $[Fe_2(La1)_3](Cl)_4$

To solid 2-formyl-5-(a)-pyridine (**7-a**) (25 mg, 0.071 mmol) and $FeCl_2$ x $4H_2O$ (4.7 mg, 0.023 mmol), 4,4'-methylenedianiline (**8**) (7.1 mg, 0.035 mmol) pre-dissolved in methanol (3 ml) have added. The mixture was stirred overnight to give a blue-dark precipitate that was collected by filtration, abundantly washed with methanol and dried with diethyl ether (16.3 mg, yield: 50%). ^{1}H NMR (500 MHz, D_2O, 298 K) δ 9.03 (1H, s, H_7), 8.65 (2H, overlapped d, ^3J = 8.1 Hz, H_{3py} + d, ^3J = 8.1 Hz, H_{4py}), 7.55 (1H, s, H_{6py}), 7.00 (2H, br, $H_{9/10}$), 5.95 (2H, br, $H_{9/10}$), 4.56 (1H, br tr, $H_{\alpha 3}$), 4.32 (2H, br d, $H_{\alpha 1}$), 4.11 (2H, m, $H_{\alpha 2}$), 3.99 (1H, s, H_{11}), 3.96 (2H, m, $H_{\beta 3}$). ESI mass analysis m/z = 677.29 $[Fe_2(La1)_3]^{4+}$, 460.61 $[Fe(La1)]^{2+}$. IR (ν) = 3254 (br m), 2892 (w), 1645 (vs), 1532 (s), 1410 (w), 1372 (w), 1324 (w) 1260 (w), 1076 (w), 1018 (w), 993 (w), 918 (w), 8.58 (m), 784 (w) cm^{-1}. UV–Vis (water) λ_{max} (nm) = 599 (with a shoulder at 546), 338, 205. ε_{599} = 12,900 M^{-1} cm^{-1}.

3.8.13 $[Cu_2(La2)_2](PF_6)_2$

To a stirred nitrogen purged suspension of ligand La2 (**11-a**) (55.0 mg, 0.056 mmol) in 4 ml of methanol was added solid $[Cu(CH_3CN)_4]$ $[PF_6]$ (31.6 mg, 0.084 mmol) to give a red-brown mixture. The mixture was stirred overnight under nitrogen atmosphere and a red-brown precipitate was collected by filtration, washed with methanol and dried with diethyl ether (39.2 mg, yield: 62%). 1H NMR (500 MHz, D_2O/CD_3CN = 1:3, 298 K) δ 8.98 (1H, s, H_{6py}), 8.74 (1H, s, H_7), 8.60 (1H, br d, ^3J = 7.7 Hz, H_{4py}), 8.19 (1H, d, ^3J = 7.7 Hz, H_{3py}), 7.08 (1H, br, H_{10}), 6.53 (1H, br, H_{10}), 4.39 (1H, t, ^3J = 5.0 Hz, $H_{\alpha 3}$), 4.14 (2H, s, $H_{\alpha 1}$), 3.97 (2H, d, ^4J = 3.3 Hz, $H_{\alpha 2}$), 3.87

(1H, s, H_{11}), 3.80 (2H, m, $H_{\beta 3}$), 0.98 (6H, br, H_{9b}), 0.48 (4H, br, H_{9a}). ESI mass analysis m/z = 1040.88 $[Cu_2(La2)_2]^{2+}$. IR (ν) = 3278 (br m), 2892 (w), 1644 (vs), 1601 (m shoulder), 1534 (s), 1414 (w), 1292 (m), 1202 (w), 1168 (w), 1047 (m), 1026 (m), 909 (w), 852 (w), 760 (w) cm^{-1}.

3.8.14 $[Cu_2(La2)_2](Cl)_2$

The same procedure used for the synthesis of $[Cu_2(La2)_2](PF_6)_2$ was applied, but $[Cu(CH_3CN)_4]$ $[PF_6]$ was replaced with CuCl. The red-brown precipitate, collected by filtration, was dissolved in water, the impurity in suspension eliminated by filtration, and the resulting dark red solution was freeze dried to afford 25.3 mg (yield: 42%) of dark red compound. ^{1}H NMR (500 MHz, D_2O, 298 K) δ 9.52 (1H, br, H_7), 9.27 (1H, br, H_{6py}), 9.15 (1H, br, H_{4py}), 8.70 (1H, br, H_{3py}), 7.61 (1H, br, H_{10}), 7.06 (1H, br, H_{10}), 4.91 (1H, br, $H_{\alpha 3}$), 4.66 (2H, br, $H_{\alpha 1}$), 4.49 (2H, br, $H_{\alpha 2}$), 4.33 (3H, br, overlapped H_{11}+ $H_{\beta 1}$), 3.145–2.910 (4H, br, H_{9a}), 1.507 (3H, br, H_{9b}), 1.043 (3H, br, H_{9b}). ESI mass analysis m/z = 1040.92 $[Cu_2(La2)_2]^{2+}$. UV–Vis (water) λ_{max} (nm) = 500, 255 (with shoulders at 328 and 286), 206.

3.8.15 $[Fe_2(Lb1)_3](Cl)_4$

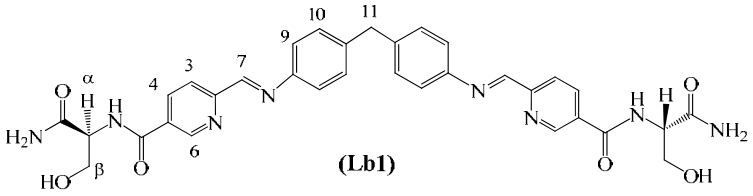

(Lb1)

1 ml of 4,4'-methylenedianiline (**8**) (18.7 mg, 0.09 mmol) in methanol was added dropwise to a stirring solution of 2-formyl-5-(b)-pyridine (**7-b**) (45 mg, 0.189 mmol) in 2 ml of methanol at 50°C in nitrogen atmosphere. In few minute an intense yellow mixture is formed. Temperature was raised to reflux and solid $FeCl_2$ x $4H_2O$ (12.5 mg, 0.063 mmol) was added to the mixture, causing immediate formation of dark blue mixture. The mixture was stirred in nitrogen atmosphere in reflux for 1 hour and at room temperature overnight. Water was added to the mixture until all the crude was in solution and saturated methanolic solution of NH_4PF_6 was added drop

wise to obtain dark-blue precipitate $[Fe_2(Lb1)_3](PF_6)_4$, which was filtrated and washed with diethyl ether, cold methanol/ethanol (1/1) and diethyl ether (50 mg, 61% yield). Counter anion was exchanged from PF_6^- to Cl^- using ion exchange resin (Dowex 1x8–100 mesh (Cl), Sigma-Aldrich). ^{1}H NMR (400 MHz, D_2O, 298 K) δ 9.05 (1H, s, H_7), 8.68 (1H, d, ^3J = 8.1 Hz, H_{4py}), 8.63 (1H, d, ^3J = 8.1 Hz, H_{3py}), 7.50 (1H, d, ^4J = 1.9 Hz, H_{6py}), 6.70 (2H, br, H_{10}), 5.50 (2H, br, H_9), 4.51(1H, br t, H_α), 3.98 (1H, s, H_{11}), 3.87 (2H, m, H_β). ESI mass analysis m/z = 506.41 $[Fe_2(Lb1)_3]^{4+}$, 665.22 $[Fe(Lb1)_2]^{2+}$, 693.10 $[Fe(Lb1)]^+$, 637.48 $[(Lc1)+H]^+$, 660.48 $[(Lc1)+Na]^+$. IR (ν) = 3288 (br m), 2892 (w), 1648 (vs), 1612 (m shoulder) 1541 (s), 1500 (m shoulder), 1411 (w), 1318 (w), 1292 (br, m) 1205 (w), 1168 (w), 1074 (m), 1018 (m), 993 (w shoulder), 916 (w), 862 (w) cm^{-1}. UV–Vis (water) λ_{max} (nm) = 599 (with a shoulder at 546), 338, 286, 240. ε_{599} = 12,900 M^{-1} cm^{-1}.

3.8.16 $[Fe_2(Lc1)_3](Cl)_4$

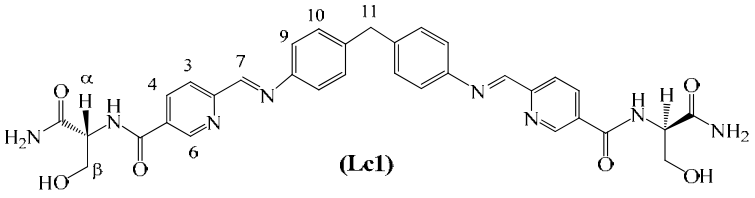

(Lc1)

The same procedure used for the synthesis of $[Fe_2(Lb1)_3](Cl)_4$ was herein applied, but using 2-formyl-5-(c)-pyridine (**7-c**) (54mg, 66% yield). ^{1}H NMR (400 MHz, D_2O, 298 K) δ 9.04 (1H, s, H_7), 8.69 (1H, d, ^3J = 8.1 Hz, H_{4py}), 8.64 (1H, d ^3J = 8.1 Hz, H_{3py}), 7.54 (1H, d, ^4J = 1.9 Hz, H_{6py}), 6.85 (2H, br, H_{10}), 5.68 (2H, br, H_9), 4.51 (1H, br t, H_α), 3.95 (1H, s, H_{11}), 3.87 (2H, m, H_β). ESI mass analysis m/z = 506.41 $[Fe_2(Lc1)_3]^{4+}$, 665.22 $[Fe(Lc1)_2]^{2+}$, 710.97 $[Fe_2(Lc1)_2](Cl)^{2+}$, 637.48 $[(Lc1)+H]^+$, 660.42 $[(Lc1)+Na]^+$. IR (ν) = 3250 (br m), 2893 (w), 1654 (vs), 1591 (m shoulder) 1536 (s), 1500 (m shoulder), 1413 (w), 1317 (w), 1293 (br m), 1205 (w), 1168 (w), 1050 (m), 1016 (m), 993 (w shoulder), 917 (w), 862 (w) cm^{-1}. UV–Vis (water) λ_{max} (nm) = 599 (with a shoulder at 546), 338, 286, 240. ε_{599} = 12,900 M^{-1} cm^{-1}.

3.8.17 $[Fe_2(Ld1)_3](Cl)_{10}$

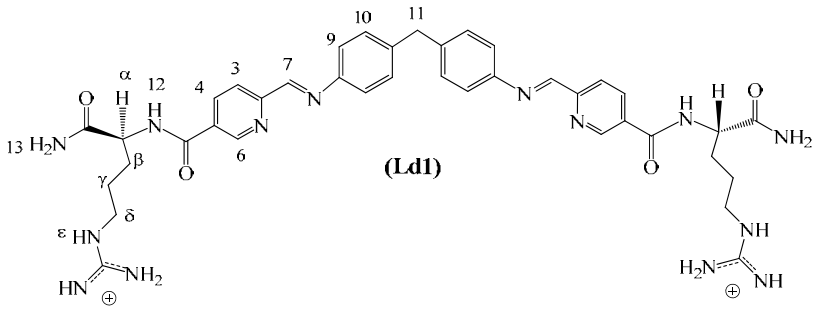

1 ml of 4,4'-methylenedianiline (**8**) (12.9 mg, 0.065 mmol) in methanol was added dropwise to a stirring solution of 2-formyl-5-(d)-pyridine (**7-d**) (40mg, 0.130 mmol) in 2 ml of methanol at 50°C in nitrogen atmosphere. In few minute an intense yellow mixture is formed. Temperature was raised to reflux and solid $FeCl_2$ x $4H_2O$ (8.5 mg, 0.0043 mmol) was added to the mixture, causing immediate formation of dark blue solution. The solution was stirred in nitrogen atmosphere in reflux for 1 hour and at room temperature overnight. Diethyl ether was added to the solution to afford the precipitation of a blue solid which was collected by filtration and washed with ethanol and diethyl ether, dried overnight on P_2O_5 to achieve 30.7 mg of chloride complex (51% yield) ^{1}H NMR (400 MHz, D_2O, 298 K) δ 9.04 (1H, s, H_7), 8.66-8.61 (overlapped 1H, dd ^3J = 8.1 Hz, H_{4py}+ 1H, d, ^3J = 8.1 Hz, H_{3py}), 7.57 (1H, s, H_{6py}), 7.03 (2H, br, H_{10}), 5.50 (2H, br, H_9), 4.31 (1H, dd, ^3J and ^4J = 5.8, 8.0, H_α), 3.93 (1H, s, H_{11}), 3.14 (2H, t, ^3J = 7.2 Hz, H_δ) 1.80 (2H, br m, H_β), 1.58 (2H, br m, H_γ). UV–Vis (water) λ_{max} (nm) = 599 (with a shoulder at 546), 340, 282 (shoulder), 238. ε_{599} = 12,900 M^{-1} cm^{-1}.

Saturated methanolic solution of NH_4PF_6 was added drop wise to 20 mg of chloride complex dissolved in the minimum volume of methanol to obtain dark-blue precipitate $[Fe_2(Ld1)_3](PF_6)_{10}$, which was filtrated and washed with diethyl ether, cold methanol/ethanol (1/1) and diethyl ether (16 mg, 57% yield). ^{1}H NMR (500 MHz, CD_3CN, 298 K) δ 9.33 (1H, d, ^3J = 6.7 Hz, H_{12}) 8.98 (1H, s, H_7), 8.57 (1H, d ^3J = 8.0 Hz, H_{4py}), 8.54 (1H, d ^3J = 8.0 Hz, H_{3py}), 8.01 (1H, s, H_{6py}), 6.73 (1H, s, H_{13}) 6.61 (1H, br, H_ε) 6.21(1H, s, H_{13}) 6.07 (2H, br, $H_{9/10}$), 5.44 (2H, br, $H_{9/10}$), 4.13 (1H, br dt, H_α), 4.02 (1H, s, H_{11}), 3.14 (2H, m, H_δ), 1.72 (2H, br, H_β), 1.47 (2H, br H_γ). IR (ν) = 3160 (br m), 2912 (w), 1643 (vs), 1536 (m), 1500 (w shoulder), 1415 (w), 1318

(w), 1290 (w), 1200 (m), 1172 (m) 1129 (m), 1017 (w), 916 (w), 861 (w), 719 (w) cm^{-1}.

3.8.18 $[Fe_2(Le1)_3](Cl)_{10}$

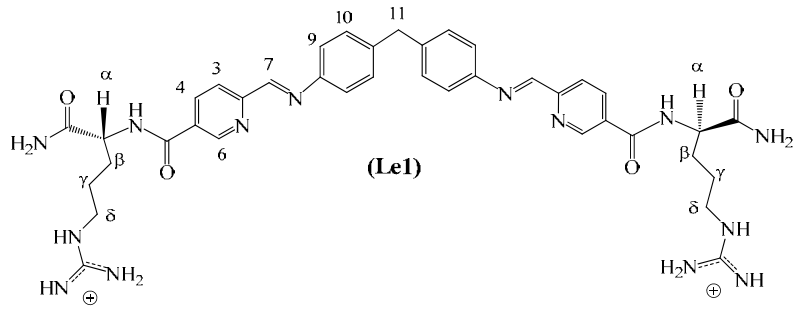

The same procedure used for the synthesis of $[Fe_2(Ld1)_3](Cl)_4$ was herein applied, but using 2-formyl-5-(e)-pyridine (**7-e**) (28.3 mg, 47% yield). ^{1}H NMR (400 MHz, D_2O, 298 K) δ 9.08 (1H, s, H_7), 8.69-8.67 (overlapped 1H, dd, ^3J = 8.1 Hz, H_{4py}+ 1H, d, ^3J = 8.1 Hz, H_{3py}), 7.60 (1H, s, H_{6py}), 7.03 (2H, br, H_{10}), 5.50 (2H, br, H_9), 4.36 (1H, dd, ^3J and ^4J = 5.8, 8.0, H_α), 3.97 (1H, s, H_{11}), 3.18 (2H, t, ^3J = 7.2 Hz, H_δ) 1.85 (2H, br m, H_β), 1.61 (2H, br m, H_γ). UV–Vis (water) λ_{max} (nm) = 599 (with a shoulder at 546), 340, 282 (shoulder), 238. ε_{599} = 12,900 M^{-1} cm^{-1}.

^{1}H NMR (500 MHz, CD_3CN, 298 K) δ 9.33 (1H, d, ^3J = 6.7 Hz, H_{12}) 8.95 (1H, s, H_7), 8.60 (1H, d ^3J = 8.0 Hz, H_{4py}), 8.57 (1H, d, ^3J = 8.0 Hz, H_{3py}), 8.01 (1H, s, H_{6py}), 6.78 (1H, s, H_{13}) 6.66 (1H, br, H_ε) 6.20 (1H, s, H_{13}) 6.19 (2H, br, H_{10}), 5.44 (2H, br, $H_{9/10}$), 4.17 (1H, br dt, H_α), 4.05 (1H, s, H_{11}), 3.18 (2H, m, H_δ), 1.72 (2H, br, H_β), 1.47 (2H, br H_γ). IR (ν) = 3167 (br m), 2912 (w), 1646 (vs), 1536 (m), 1500 (w shoulder), 1478 (w), 1412 (w), 1319 (w), 1290 (w), 1203 (m), 1166 (m) 1112 (w), 1017 (w), 918 (w), 862 (w), 719 (w) cm^{-1}.

3.8.19 $[Cu_2(Lb2)_2](Cl)_2$

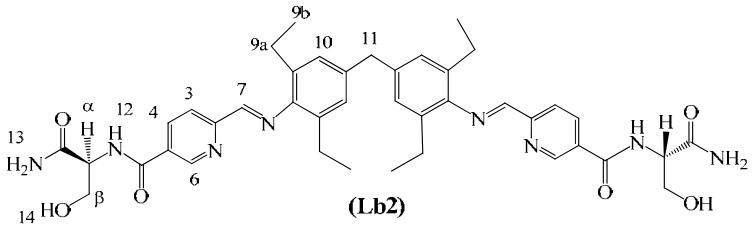

4 ml of dried methanol where added to 29 mg (0.12 mmol) of 2-formyl-5-(b)-pyridine (**7-b**), 23 mg (0.06 mmol) of 4,4'-methylenbis(2,6-diethylaniline) (**9**) and 19 mg (0.061mmol) of $[Cu(CH_3\,CN)_4]\,[PF_6]$ in nitrogen atmosphere. The mixture was stirred at 60 °C for one hour and it turned to dark red-brown after 10 min, followed by overnight stirring at room temperature, in nitrogen atmosphere and protected in aluminium foil. Few drops of water were added to the mixture to dissolve it completely and precipitation with diethyl ether gave a red-brown compound that was washed with diethyl ether, ethanol, water, ethanol and dried with diethyl ether. 28 mg (47%) of pure compound were obtained. ^{1}H NMR (500 MHz, CD_3CN, 298 K) δ 9.02 (1H, s, H_{6py}), 8.68 (1H, br, H_7), 8.56 (1H, br d, ^3J = 8.0 Hz, H_{4py}), 8.15 (1H, d, ^3J = 8.0 Hz, H_{3py}), 7.57 (1H, br d, ^3J = 6.9 Hz, H_{12}), 6.60 (2H, br, H_{10}), 6.57 (1H, s, H_{13}), 6.00 (1H, s, H_{13}), 4.57 (1H, br m, H_α), 3.84 (3H, br d, overlapped H_{11}+H_β), 2.40 (4H, br, H_{9a}), 0.80 (6H, br, H_{9b}). ESI mass analysis m/z =812.2 $[Cu_2(Lb_2)_2]^{2+}$. IR (ν) = 3200 (br m), 2892 (w), 1648 (vs), 1601 (m shoulder), 1532 (s), 1417 (w), 1292 (br m), 1202 (w), 1168 (w), 1047 (m), 1020 (s), 911 (w), 852 (w), 760 (w) cm^{-1}. Counter anion was exchanged from PF_6^- to Cl^- using ion exchange resin (Dowex 1x8–100 mesh (Cl), Sigma-Aldrich). ^{1}H NMR signals were broadened because of the presence of paramagnetic impurities. ESI mass analysis confirmed m/z =812.2 $[Cu_2(Lb_2)_2]^{2+}$. UV–Vis (water) λ_{max} (nm) = 500, 337, 254

3.8.20 $[Cu_2(Lc2)_2](Cl)_2$

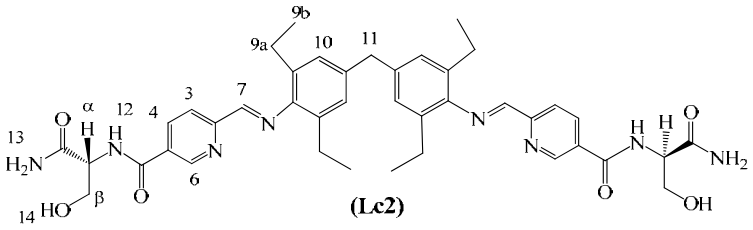

(Lc2)

The same procedure described for $[Cu_2(Lb2)_2](Cl)_2$ was used, but using 2-formyl-5-(c)-pyridine (**7-c**) to obtain 22 mg (37% yield) of pure compound. ^{1}H NMR (500 MHz, CD_3CN, 298 K) δ 9.02 (1H, s, H_{6py}), 8.68 (1H, s, H_7), 8.55 (1H, br d, H_{4py}), 8.16 (1H, d, ^3J = 8.0 Hz, H_{3py}), 7.57 (1H, br d, ^3J = 6.9 Hz, H_{12}), 6.83 (2H, br, H_{10}), 6.53 (1H, s, H_{13}), 6.01 (1H, s, H_{13}), 4.56 (1H, br m, H_α), 3.88 (3H, m, overlapped H_{11}+H_β), 2.41 (4H, br, H_{9a}), 1.00 (6H, br, H_{9b}). ESI mass analysis m/z =812.2 $[Cu_2(Lc2)_2]^{2+}$. IR (ν) = 3198 (br m), 2892 (w), 1643 (vs), 1601 (m shoulder), 1532 (s), 1415 (w), 1294 (br m), 1202 (w), 1168 (w), 1047 (m), 1021 (s), 908 (w), 852 (w), 760 (w) cm^{-1}. Counter anion was exchanged from PF_6^- to Cl^- using ion exchange resin (Dowex 1x8–100 mesh (Cl), Sigma-Aldrich). ^{1}H NMR signals were broadened because of the presence of paramagnetic impurities. ESI mass analysis confirmed m/z =812.2 $[Cu_2(Lc_2)_2]^{2+}$. UV–Vis (water) λ_{max} (nm) = 500, 337, 254.

3.8.21 Circular dichroism, UV-Vis and NMR experiments with Δ-TRISPHAT.

CD scans of the conjugates were carried out in 10 or 1 mm path length cuvettes (depending on the concentration of the complex in each experiment) using a Jasco J-715 spectropolarimeter. Each CD scan was always supported by a corresponding UV-Vis scan, carried out with a Varian Cary 5000 spectrophotometer. The chirality of the complexes was analysed by CD in acetonitrile for hexafluorophospate complexes and in water for chloride complexes. When CD signals of different complexes had to be compared, previous UV-vis analysis in the MLCT region was carried out to ensure that the complexes had the same concentrations.

^{1}H NMR experiments with Δ-TRISPHAT (purchased from Sigma-Aldrich) were carried out as follows: NMR spectra of the complexes alone in CD_3CN were run, then 2 equivalent of Δ-TRISPHAT were added directly to the complex solution in the NMR tube. NMR spectra were run 15 min after that Δ-TRISPHAT was completely dissolved.

The experiment of precipitation of the chloride Fe(II) parent cylinder with Δ-TRISPHAT was carried out dissolving 30 mg of complex in 15 ml of water. The solution was divided in five aliquots of 3 ml each in five test tubes, with 1.45 mM concentration of complex in each tube. Separately, five solutions with different concentrations of Δ-TRISPHAT in 3 ml of acetonitrile were prepared (0.725, 1.087, 1.45, 2.175 and 2.9 mM) and each solution was added drop wise one complex solution. At the end each tube contained 0.725 mM of complex and Δ-TRISPHAT/complex ratio of 0.5, 0.75, 1 and 2. The mixtures were left in the fridge overnight and the then filtered. The collected filtrates were freeze dried and the precipitates were accurately washed with water and then dried over P_2O_5. The filtrates and the precipitates were re-dissolved in acetonitrile/methanol (8/1) for the UV-vis and CD analysis.

3.9 References

(1) De Wolf, F. A.; Brett, G. M. *Pharmacological Reviews* **2000**, *52*, 207-236.
(2) Malafaya, P. B.; Silva, G. A.; Reis, R. L. *Advanced Drug Delivery Reviews* **2007**, *59*, 207-233.
(3) Uherek, C.; Wels, W. *Advanced Drug Delivery Reviews* **2000**, *44*, 153-166.
(4) Lambert, D. M. *European Journal of Pharmaceutical Sciences* **2000**, *11*, S15-S27.
(5) Pooga, M.; Land, T.; Bartfai, T.; Langel, U. *Biomolecular Engineering* **2001**, *17*, 183-192.
(6) Miyajima, Y.; Ishizuka, T.; Yamamoto, Y.; Sumaoka, J.; Komiyama, M. *Journal of the American Chemical Society* **2009**, *131*, 2657-2662.
(7) Esfand, R.; Tomalia, D. A. *Drug Discovery Today* **2001**, *6*, 427-436.
(8) Medina, S. H.; El-Sayed, M. E. H. *Chemical Reviews* **2009**, *109*, 3141-3157.
(9) Peer, D.; Karp, J. M.; Hong, S.; FaroKhzad, O. C.; Margalit, R.; Langer, R. *Nature Nanotechnology* **2007**, *2*, 751-760.
(10) Brigger, I.; Dubernet, C.; Couvreur, P. *Advanced Drug Delivery Reviews* **2002**, *54*, 631-651.

(11) Liu, Z.; Cai, W. B.; He, L. N.; Nakayama, N.; Chen, K.; Sun, X. M.; Chen, X. Y.; Dai, H. J. *Nature Nanotechnology* **2007**, *2*, 47-52.
(12) Kam, N. W. S.; Jessop, T. C.; Wender, P. A.; Dai, H. J. *Journal of the American Chemical Society* **2004**, *126*, 6850-6851.
(13) Sadler, K.; Tam, J. P. *J Biotechnol* **2002**, *90*, 195-229.
(14) Vo-Dinh, T.; Cullum, B. *Fresenius Journal of Analytical Chemistry* **2000**, *366*, 540-551.
(15) Kovar, J. L.; Simpson, M. A.; Schutz-Geschwender, A.; Olive, D. M. *Analytical Biochemistry* **2007**, *367*, 1-12.
(16) Hannon, M. J.; Moreno, V.; Prieto, M. J.; Moldrheim, E.; Sletten, E.; Meistermann, I.; Isaac, C. J.; Sanders, K. J.; Rodger, A. *Angewandte Chemie-International Edition* **2001**, *40*, 880-884.
(17) Meistermann, I.; Moreno, V.; Prieto, M. J.; Moldrheim, E.; Sletten, E.; Khalid, S.; Rodger, P. M.; Peberdy, J. C.; Isaac, C. J.; Rodger, A.; Hannon, M. J. *Proceedings of the National Academy of Sciences of the United States of America* **2002**, *99*, 5069-5074.
(18) Oleksi, A.; Blanco, A. G.; Boer, R.; Uson, I.; Aymami, J.; Rodger, A.; Hannon, M. J.; Coll, M. *Angewandte Chemie-International Edition* **2006**, *45*, 1227-1231.
(19) Cerasino, L.; Hannon, M. J.; Sletten, E. *Inorganic Chemistry* **2007**, *46*, 6245-6251.
(20) Hotze, A. C. G.; Hodges, N. J.; Hayden, R. E.; Sanchez-Cano, C.; Paines, C.; Male, N.; Tse, M. K.; Bunce, C. M.; Chipman, J. K.; Hannon, M. J. *Chemistry & Biology* **2008**, *15*, 1258-1267.
(21) Malina, J.; Hannon, M. J.; Brabec, V. *Nucleic Acids Research* **2008**, *36*, 3630-3638.
(22) Childs, L. J.; Malina, J.; Rolfsnes, B. E.; Pascu, M.; Prieto, M. L.; Broome, M. L.; Rodger, P. M.; Sletten, E.; Moreno, V.; Rodger, A.; Hannon, M. J. *Chemistry-a European Journal* **2006**, *12*, 4919-4927.
(23) Vazquez, O.; Vazquez, M. E.; Blanco, J. B.; Castedo, L.; Mascarenas, J. L. *Angewandte Chemie-International Edition* **2007**, *46*, 6886-6890.
(24) Fitzsimons, M. P.; Barton, J. K. *Journal of the American Chemical Society* **1997**, *119*, 3379-3380.
(25) Mukhopadhyay, S.; Barnes, C. M.; Haskel, A.; Short, S. M.; Barnes, K. R.; Lippard, S. J. *Bioconjugate Chemistry* **2008**, *19*, 39-49.
(26) Brunner, J.; Barton, J. K. *Biochemistry* **2006**, *45*, 12295-12302.
(27) *Nucleic Acid Structure and Recognition*; Neidle, S., Ed.; Oxford University Press. Oxford 2002.
(28) *Supramolecular Chemistry*; Steed, J. W., Atwood, J.L., Ed.; Wiley, 2000.
(29) Calnan, B. J.; Tidor, B.; Biancalana, S.; Hudson, D.; Frankel, A. D. *Science* **1991**, *252*, 1167-1171.
(30) Tao, J. S.; Frankel, A. D. *Proceedings of the National Academy of Sciences of the United States of America* **1992**, *89*, 2723-2726.
(31) Goun, E. A.; Pillow, T. H.; Jones, L. R.; Rothbard, J. B.; Wender, P. A. *Chembiochem* **2006**, *7*, 1497-1515.
(32) Futaki, S. *Advanced Drug Delivery Reviews* **2005**, *57*, 547-558.
(33) Rothbard, J. B.; Kreider, E.; Vandeusen, C. L.; Wright, L.; Wylie, B. L.; Wender, P. A. *Journal of Medicinal Chemistry* **2002**, *45*, 3612-3618.

(34) Wender, P. A.; Rothbard, J. B.; Jessop, T. C.; Kreider, E. L.; Wylie, B. L. *Journal of the American Chemical Society* **2002**, *124*, 13382-13383.
(35) Wright, L. R.; Rothbard, J. B.; Wender, P. A. *Current Protein & Peptide Science* **2003**, *4*, 105-124.
(36) Vazquez, O.; Blanco-Canosa, J. B.; Vazquez, M. E.; Martinez-Costas, J.; Castedo, L.; Mascarenas, J. L. *Chembiochem* **2008**, *9*, 2822-2829.
(37) Telfer, S. G.; Bernardinelli, G.; Williams, A. F. *Chemical Communications* **2001**, 1498-1499.
(38) Tsang, C. S.; Yeung, H. L.; Wong, W. T.; Kwong, H. L. *Chemical Communications* **2009**, 1999-2001.
(39) Yeh, R. M.; Raymond, K. N. *Inorganic Chemistry* **2006**, *45*, 1130-1139.
(40) Woods, C. R.; Benaglia, M.; Cozzi, F.; Siegel, J. S. *Angewandte Chemie-International Edition* **1996**, *35*, 1830-1833.
(41) Annunziata, R.; Benaglia, M.; Cinquini, M.; Cozzi, F.; Woods, C. R.; Siegel, J. S. *European Journal of Organic Chemistry* **2001**, 173-180.
(42) Lacour, J.; Hebbe-Viton, V. *Chemical Society Reviews* **2003**, *32*, 373-382.
(43) Lacour, J.; Frantz, R. *Organic & Biomolecular Chemistry* **2005**, *3*, 15-19.
(44) Baret, P.; Gaude, D.; Gellon, G.; Pierre, J. L. *New Journal of Chemistry* **1997**, *21*, 1255-1257.
(45) Baum, G.; Constable, E. C.; Fenske, D.; Housecroft, C. E.; Kulke, T. *Chemistry-a European Journal* **1999**, *5*, 1862-1873.
(46) Reid, S. D.; Wilson, C.; De Matteis, C. I.; Love, J. B. *European Journal of Inorganic Chemistry* **2007**, 5286-5293.
(47) Prabaharan, R.; Fletcher, N. C.; Nieuwenhuyzen, M. *Journal of the Chemical Society-Dalton Transactions* **2002**, 602-608.
(48) Meyer, M.; Kersting, B.; Powers, R. E.; Raymond, K. N. *Inorganic Chemistry* **1997**, *36*, 5179-5191.
(49) Merrifield, B. *Science* **1986**, *232*, 341-347.
(50) *Solid Phase Peptide Synthesis a Pratical Approach*; Atherton, E., Sheppard, R.C., Ed.; Oxford University Press, 1989.
(51) *An Introduction to Peptide Synthesis*; Bailey, P. D., Ed.; Wiley, 1990.
(52) Markovac, A.; Stevens, C. L.; Ash, A. B.; Hackley, B. E. *Journal of Organic Chemistry* **1970**, *35*, 841-&.
(53) Kaiser, E. T.; Mihara, H.; Laforet, G. A.; Kelly, J. W.; Walters, L.; Findeis, M. A.; Sasaki, T. *Science* **1989**, *243*, 187-192.
(54) Lacour, J.; Ginglinger, C.; Favarger, F.; TorcheHaldimann, S. *Chemical Communications* **1997**, 2285-2286.
(55) Lacour, J.; Ginglinger, C.; Grivet, C.; Bernardinelli, G. *Angewandte Chemie-International Edition in English* **1997**, *36*, 608-610.
(56) Ginglinger, C.; Jeannerat, D.; Lacour, J.; Juge, S.; Uziel, J. *Tetrahedron Letters* **1998**, *39*, 7495-7498.
(57) Monchaud, D.; Lacour, J.; Coudret, C.; Fraysse, S. *Journal of Organometallic Chemistry* **2001**, *624*, 388-391.
(58) Ratni, H.; Jodry, J. J.; Lacour, J.; Kundig, E. P. *Organometallics* **2000**, *19*, 3997-3999.

(59) Planas, J. G.; Prim, D.; Rose, E.; Rose-Munch, F.; Monchaud, D.; Lacour, J. *Organometallics* **2001**, *20*, 4107-4110.
(60) Jodry, J. J.; Lacour, J. *Chemistry-a European Journal* **2000**, *6*, 4297-4304.
(61) Lacour, J.; Goujon-Ginglinger, C.; Torche-Haldimann, S.; Jodry, J. J. *Angewandte Chemie-International Edition* **2000**, *39*, 3695-3697.
(62) Lacour, J.; Torche-Haldimann, S.; Jodry, J. J.; Ginglinger, C.; Favarger, F. *Chemical Communications* **1998**, 1733-1734.
(63) *PhD Thesis, University of Warwick*; Pearmund, C. R., Ed., 2006.

CHAPTER 4

DNA RECOGNITION AND CYTOTOXIC ACTIVITY OF CONJUGATED CYLINDERS

4.1 Preliminary considerations about the stability of the complexes.

In this chapter the DNA binding properties of the conjugated cylinders, prepared in Chapter 3, are explored using different spectroscopic and electrophoresis methodologies. In some cases it is possible to compare their properties with those exhibited by the corresponding unconjugated cylinders. Also investigated is whether the DNA nuclease activity of the conjugated Cu(I) complexes is preserved, if the conjugated Fe(II) cylinders are able to target DNA three way junctions and if they exhibit cytotoxicity against cancer cell lines.

Before describing these studies some general consideration of the stability of the conjugates is relevant. The Fe(II) conjugates in water are not as stable as the parent Fe(II) cylinder. Uv-Vis absorption scans of the chloride complexes in water were collected every half hour at room temperature for 30 hours and the chart in Figure 3.1.a) shows that, for all the complexes, the absorbance at the λ_{max} of the MLCT band decreases with time, indicating their degradation. The two arginine conjugates are the least stable (with half life of ~ 2.5 hours), followed by the tripeptide conjugate (4 hours half life). The two serine conjugates are more stable, since they do not completely degrade in the time scale of the experiment and 15 hours are needed to observe their decomposition by half, however the parent Fe(II) cylinder does not show significant degradation for the entire time of UV-vis detection. This suggests that the length and charge of the conjugated units influences the stability of the chloride Fe(II) cylinder in water. The stability of the complexes was also monitored in presence of calf thymus (ct) DNA. The chart in figure 4.1.b) shows the variation of absorbance at the same wavelengths of solutions of complexes containing ct-DNA at DNA:complex ratio of 6:1. The same complex concentrations of the experiment in absence of DNA were used, except for the two arginine conjugates, where more diluted solutions had to be used to avoid the precipitation of the DNA caused by the complex itself (see below). For all the complexes a

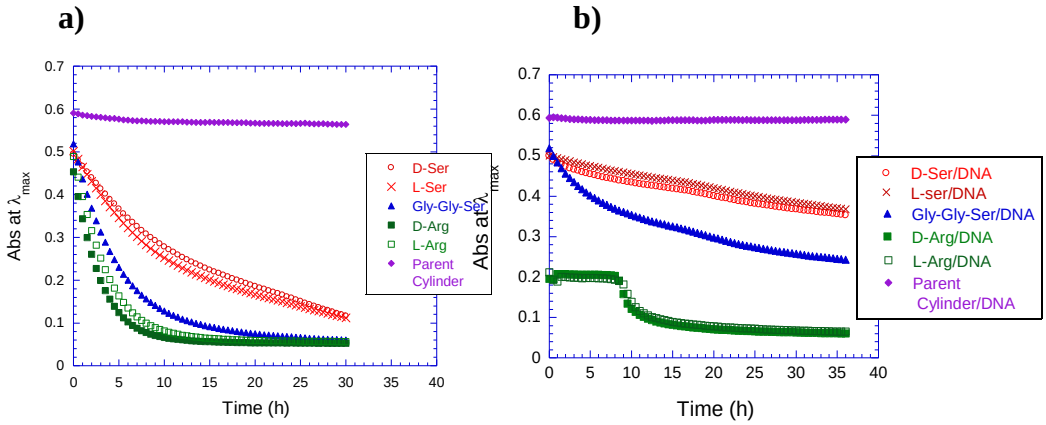

Figure 4.1. Absorbance at λ_{max} of the MLCT band versus time (h) at room temperature of **a)** Fe(II) complexes, conjugates and parent cylinder in water (35 μM complexes concentration) and **b)** Fe(II) complexes in water in presence of ct-DNA; in **b)** concentrations of 35 μM and 200 μM were used for the complexes and the DNA respectively, except for the two arginine conjugates where the same ratio DNA/complex was used but 2.5 times diluted solutions were used (see Figure 4.2). λ_{max} was 599 nm for the conjugates and 573 nm for the parent cylinder. The conjugating units are used to indicate the corresponding conjugate in the legends.

significant improvement of the stability in presence of DNA was observed. In 36 hours the absorbance at λ_{max} of the MLCT band decreases by 28% and 52% for the serine and the tripeptide conjugates respectively. The arginine conjugate/DNA adducts appear stable for the first 9 hours, but then their degradation begins and 10.5 h are needed to observe degradation by half. However, a direct comparison between the arginine conjugates and the other complexes is not accurate in this case, since the different concentration conditions that had to be used may affect the percent of complex degradation in a certain time. In general, the enhanced stability of the complexes is evidence that they all bind to DNA in a way that the DNA "protects" the complexes from being decomposed. All the Cu(I) conjugated cylinders are as stable as the parent Cu(I) cylinders, as their UV-vis profile was completely unaltered during the time in which they were monitored (36 hours at room temperature).

Because of the instability of the conjugates, all the experiments described in this chapter were carried out preparing fresh stock solutions of the complexes. The concentrations of the prepared stock solutions were always checked by UV-Vis

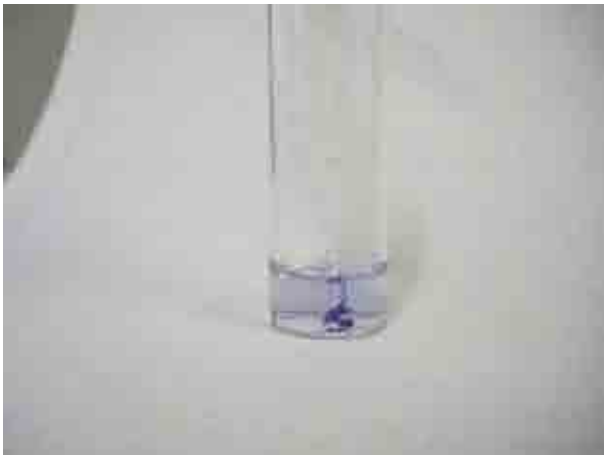

Figure 4.2. 300 μM of ct-DNA with arginine conjugated cylinder. DNA:complex ratio is 20:1 but precipitation of blue strands is visible already at 60:1 ratio.

using the calculated molar extinction coefficient ε at 599 nm of 12,900 M^{-1} cm^{-1}. The stock solutions were kept on ice for the time in which they were used, and their UV-vis profiles were monitored at the end of the each experiment to check that degradation did not occur. Furthermore, control experiments were carried out separately using the compounds that can arise from the degradation of the complexes, such as the spacer, the peptide/amino acid-pyridine fragment and iron ions. In each experiment, none of these compounds exhibited any DNA binding activity, even at concentrations three times higher than those used for the complexes. Only the spacer showed a minor DNA intercalating effect detectable only by Linear Dichroism (LD, section 4.3), at DNA:spacer ratio of 3:1 which was considered irrelevant when compared to the major effect caused by the complexes. In this way, it could be assumed that any result observed was due to the action of the conjugates only.

A further important feature of the two arginine conjugates was observed: they are able to form aggregates with the DNA with consequent precipitation of the DNA as blue strands (Figure 4.2), most probably because of the high positive charge of these complexes.[1-5] Different conditions of concentration were investigated, to find those in which precipitation of DNA-complex aggregates did not occur, since this would have affected the DNA recognition experiments in solutions. It was found that the

maximum concentration of DNA to use is 100 μM (with 10 mM NaCl and 1mM of sodium cacodylate buffer, with a pH of 6.8). Above this concentration, even small additions of arginine conjugate caused precipitation of DNA (formation of aggregates is visible already at 60:1=DNA:complex).

4.2 DNA binding studies by circular dichroism (CD).

In Chapter 2 and 3, CD has been used to observe the chirality of helicates, but this is also one of the most common techniques to study the interaction of biomolecules (such as nucleic acids and protein) with other agents (either synthetic agents or other biomolecules). The chiral centres of the primary structure of DNA are the carbons of the ribose-phospate backbone, which do not produce any transitions in the UV-vis region that are easily detectable. But the single nucleotides have distinctive CD signals that are induced by the chiral ribose into the transitions of the neighbouring bases. The CD bands of any secondary structure of DNA originate from the transitions of the bases in the UV region, but depend also on the reciprocal orientation and distances of the bases and consequently the signal is strictly connected to the asymmetric orientation and conformation of the structure itself. Indeed, different forms of DNA exhibit different CD signals depending on their geometric parameters rather than their bases composition, so that the most common structures such as B-, A- or Z-DNA can be identified by their characteristic CD spectra.[6] The CD spectrum of B-DNA extracted from calf thymus (ct) (shown in Figure 4.3) presents the characteristic B-DNA pattern below 300 nm, with a shortwave negative and a longwave positive band of nearly equal intensity, with an intersection point at the UV absorption maximum (260 nm). When DNA is analysed in presence of another molecule, such as a synthetic agent, if such molecule does not have a CD signal because it is not chiral or it is in the form of a racemic mixture, modifications in the CD spectrum of the DNA can arise from DNA-synthetic agent interactions and provide information about the type of binding.

CD studies of B-DNA with racemic Fe(II) parent cylinder $[Fe_2(L1)_3](Cl)_4$ have already been reported[7,8] and a typical CD titration with this complex is shown in Figure 4.4. The racemic mixture of $[Fe_2(L1)_3](Cl)_4$ does not have a CD signal, but, when it binds to the asymmetric DNA, CD is induced by the DNA into complex

transitions and an induced CD signal (ICD) is formed with bands in the visible region, where the complex absorbs. The ICD signal of $[Fe_2(L1)_3](Cl)_4$ in the presence of ct-DNA presents characteristic bands at 315 and 375 nm (transitions from the ligand) and at 541 and 615 nm (MLCT bands), whose magnitude increases on increasing the concentration of the complex up to a DNA(bp):complex=8:1 ratio.

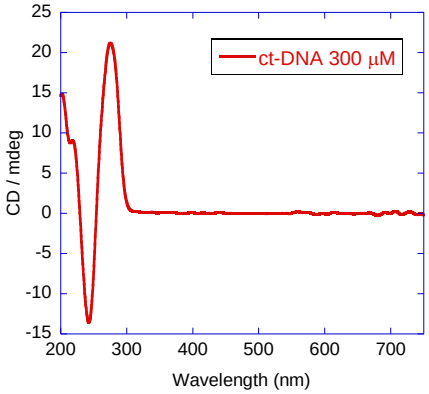

Figure 4.3 CD signal of 300 μM (in base pairs) B-DNA from calf thymus (ct).

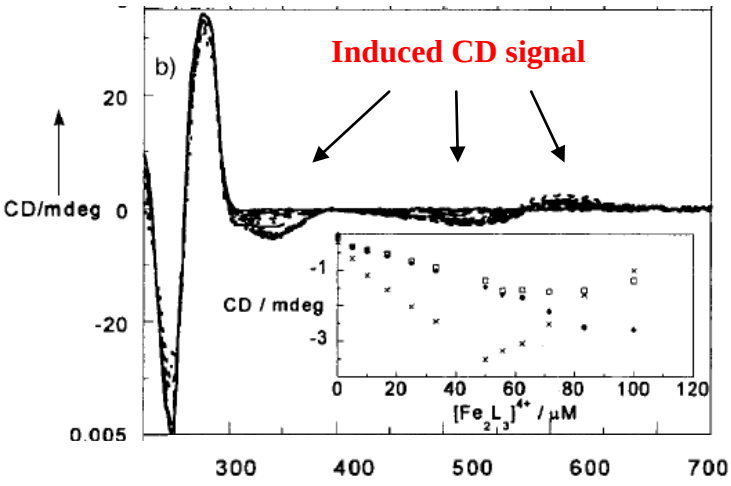

Figure 4.4 Example of titration of 500 μM (in bases) ct-DNA in 20 mM NaCl and 1 mM $Na(CH_2)_2AsO_2 \cdot 3H_2O$ buffer (pH 6.8) with increasing concentrations of parent $[Fe_2(L1)_3]^{4+}$. The DNA base:$[Fe_2(L1)_3]^{4+}$ ratios are for smallest magnitude spectra to largest: 2.5:1, 3:1, 3.5:1, 4:1, 4.5:1, 5:1, 7.5:1, 10:1, 15:1, 25:1, and 50:1. Insert shows CD at key wavelengths as a function of complex concentration. Insert wavelengths are: x CD at 315 nm, □ CD at 375 nm ♦ CD at 541 nm (Figure taken from reference 7).

This behaviour indicates that, up to these concentrations, the complex binds to DNA in one single mode (consistently with the binding in the major groove explained in Chapter 2). Different binding modalities cannot be excluded at higher complex concentrations. Further information that can be obtained from CD studies concerns the effect of the cylinder binding on the structure of the DNA: although the CD signal of the DNA in the UV region is slightly perturbed, it still retains the same profile of the B-DNA in absence of the complex, suggesting that the binding of the complex to the DNA does not affect its secondary structure.

Analogous CD titrations were performed with the Fe(II) conjugates cylinders. Figure 4.5 shows the CD of 300 μM of ct-DNA with increasing concentrations of the tripeptide conjugate $[Fe_2(L\mathbf{a}1)_3]Cl_4$. Using the same stock solution of complex, two equal titrations were performed, one analysed with a 0.1 cm cuvette (to avoid saturation of the signal in the UV region that occurs at these concentrations of DNA and complex, Figure 4.5.a)) and the other was analysed in 1 cm cuvette, to better visualise the less intense signal in the MLCT region (Figure 4.5.b)). In the UV region, the CD signal of the B-DNA is perturbed by the addition of the complex, with small decreases in the magnitudes of all the bands and at higher complex loading the λ_{max} of the positive band of the DNA (275 nm) shifts 5 nm to higher wavelengths. An induced CD shows as a shoulder at 300 nm. In the ligand and

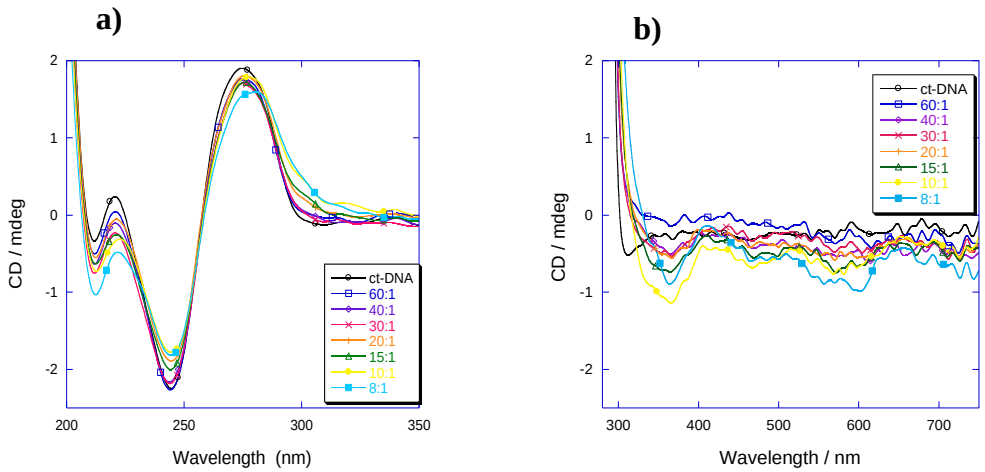

Figure 4.5. CD of 300 μM of ct-DNA in 20 mM NaCl and 1 mM $Na(CH_2)_2AsO_2 \cdot 3H_2O$ (pH 6.8) with increasing concentration of the Gly-Gly-Ser conjugate ($[Fe_2(L\mathbf{a}1)_3]Cl_4$). The legends show ct-DNA/complex ratios. **a)** Uv region (200-350 nm) was analysed in 0.1 cm cuvette and **b)** the visible region (750-280 m) in 1 cm cuvette.

MLCT regions of the complex spectroscopy (Figure 4.5.b)), ICD bands are evident at high complex loading only. These ICD signals prove that the Fe(II) tripeptide conjugate binds to the DNA and it does not cause modification of the B-DNA conformation. The produced ICD signal in the visible region appears weaker than that seen with the parent cylinders; however a direct comparison would be difficult as the two complexes have different value of ε.

Similar titrations were performed using the Fe(II) D-Ser conjugate $[Fe_2(L\mathbf{c}1)_3]Cl_4$ (Figure 4.6.a) and b)) and the L-Ser conjugate $[Fe_2(L\mathbf{b}1)_3]Cl_4$ (Figure 4.6.c) and d)).

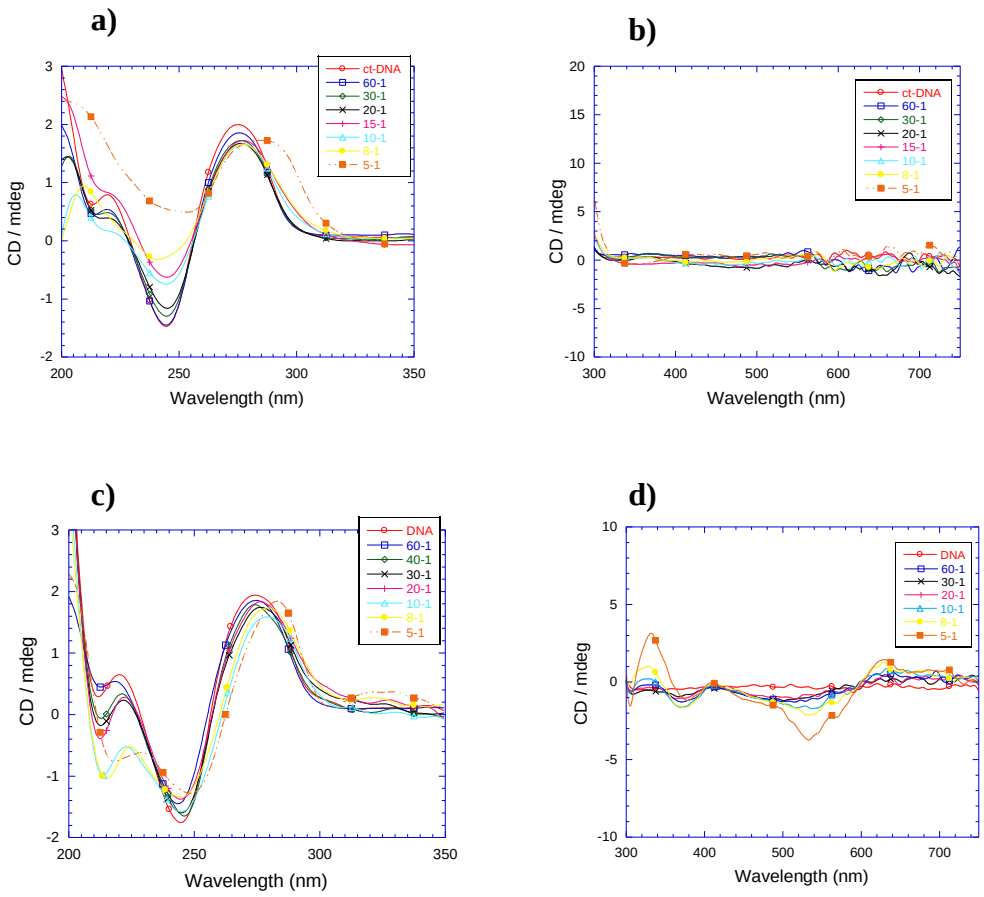

Figure 4.6. CD of 300 μM of ct-DNA in 20 mM NaCl and 1 mM $Na(CH_2)_2AsO_2 \cdot 3H_2O$ (pH 6.8) with increasing concentration of D-Ser conjugate $[Fe_2(L\mathbf{c}1)_3]Cl_4$ **a)** Uv region (200-350 nm) in 0.1 cm cuvette and **b)** visible region (750-280 m) in 1 cm cuvette). Same titration with the L-Ser conjugate $[Fe_2(L\mathbf{b}1)_3]Cl_4$. **(c)** Uv region (200-350 nm) in 0.1 cm cuvette and **d)** visible region (750-280 m) in 1 cm cuvette). The signals of the complex alone were subtracted from the signals of the complex/DNA adducts at the corresponding complex concentrations.

These two complexes have their own CD signals (Chapter 3) and for this reason the signal of the complex alone was subtracted from each signal of complex-DNA adduct at the corresponding concentration, to eliminate contribution of the CD absorbance of the complex. As observed for the tripeptide conjugate, these two complexes also produce a very little perturbation of the DNA signal suggesting that binding occurs without modification of the B-DNA conformation and only at 5:1 ratio (DNA:complex) the shifts of the bands at 275 nm become relevant. Observing the two MLCT regions only the L-Ser conjugate exhibits ICD bands that are visible from 10:1. This could initially suggest a different affinity and/or different binding mode for the two complexes toDNA, but all the successive analysis of these two complexes with different techniques, did not reveal important difference in their activity. Rather, this difference might originate from a different level of chirality of the two complexes that produce DNA-complex adducts with different ICD signals in the visible region.

CD titrations were also performed with the two arginine conjugates, but using 100 μM of starting ct-DNA solution (Figure 4.7 a) to d)). Also in this case, the CD signals of the complexes alone were subtracted from the signals of the DNA-complex adducts. In both titrations, ICD signals are observed with relatively intense induced bands at 300, 335, 534 and 614 nm and the two complexes present opposite profiles. This confirms that the two arginine conjugates also bind the DNA, although a direct comparison with the other Fe(II) conjugates it is not possible because all the complexes have different intrinsic CD profiles in water. In Figure 4.7. e) the two ICD signals of the DNA/complex adducts at 8:1 are compared and in this case the signal of the DNA alone was also subtracted from the adducts. It seems that the bands of the ICD signal of the D-Arg conjugate/DNA adduct have higher intensity, both the bands in the visible region and, more evidently, the band at 300 nm. This might indicate a different DNA binding affinity and/or mode between the two complexes.

A difference in DNA binding between L and D-Arg conjugates is indeed expected, since the central helicates of these two complexes are in P and M conformation respectively and it was demonstrate that the unsubstituted P and M isomers bind the DNA differently.[8] However, this needs to be confirmed by other techniques, because a small difference in the CD profile of the complex alone could affect the accuracy of the analysis of DNA-complex adducts.

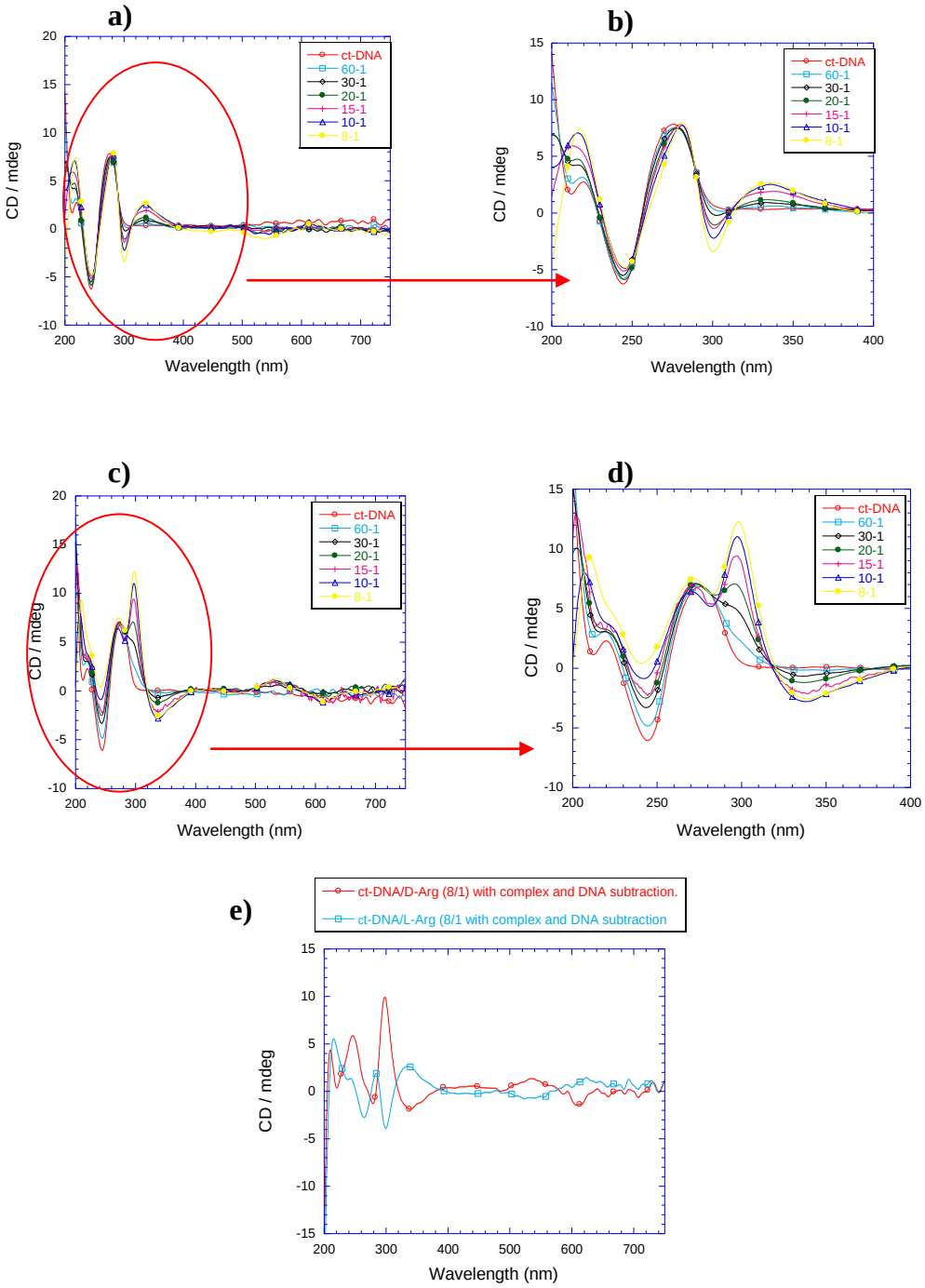

Figure 4.7. CD of 100 μM of ct-DNA in 20 mM NaCl and 1 mM $Na(CH_2)_2AsO_2 \cdot 3H_2O$ (pH 6.8) with increasing concentration of **a)** and **b)** L-Arg conjugate $[Fe_2(L\mathbf{d}1)_3]Cl_4$ and **c)** and **d)** D-Arg conjugate $[Fe_2(L\mathbf{e}1)_3]Cl_4$ (in **b)** and **d)** the enlargement of the UV regions). The legends show decreasing ratio of DNA:complex. The signals of the complex alone were subtracted from the signals of the complex/DNA adducts at the corresponding complex concentrations. **e)** ICD signals of ct-DNA/L-Arg and ct-DNA/D-Arg both at 8:1 ratio where the signals of both complexes alone and ct-DNA alone were subtracted from the DNA-complex adducts.

D and L-Arg conjugated cylinders in presence of poly[G-C] and poly[A-T] DNA were also analysed by CD, to verify whether the complexes exhibits any binding preference between these polymers. Figure 4.8.a) shows how the CD signals of these two types of DNAs are slightly different (as a consequence of their different ε at 260 nm) and the CD of poly[G-C] and poly[A-T] mixed at 1:1 ratio is also shown. The ICD signals of the D-Arg conjugate with poly[G-C], poly[A-T] and the mix poly[G-C]/poly[A-T](1/1) at DNA:complex concentration of 10:1 are shown in Figure 4.8.b). The signals of the complex alone and the corresponding DNAs alone were

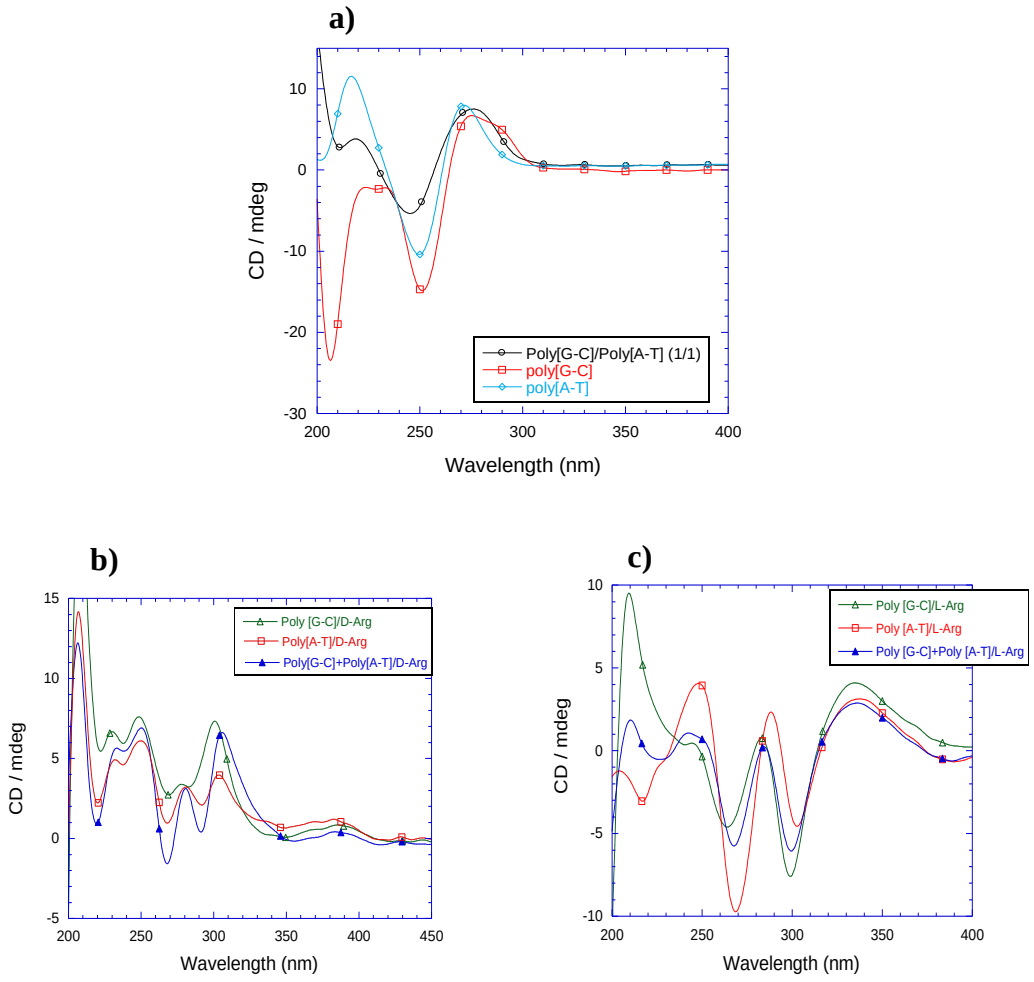

Figure 4.8. CD of 100 μM of poly[G-C], poly[A-T] and a mix (1/1) of poly[G-C] and poly[A-T] in 10 mM NaCl and 1 mM $Na(CH_2)_2AsO_2 \cdot 3H_2O$ (pH 6.8) **a)** only DNAs **b)** with D-Arg conjugate $[Fe_2(L\mathbf{e}1)_3]Cl_4$ at ratio 10:1 of D-Arg/DNAs and **c)** with L-Arg conjugate $[Fe_2(L\mathbf{d}1)_3]Cl_4$ at ratio 10:1 of L-Arg/DNAs. The signals of the complex alone and DNAs alone were subtracted from the signals of the complex/DNA adducts.

subtracted to the signal of the DNA-complex adducts. The resulting ICD signals between 200 and 300 nm are different for the poly[G-C]-complex and poly[A-T]-complex adducts. The intensity of the ICD band at 300 nm (where the ligand absorbs) of the D-Arg complex/poly[G-C] is higher than the intensity of the same band of D-Arg complex/poly[A-T]. The intensity of the band relative to the complex with the mix of the two DNAs is an average between the other two. The same experiment was carried out with the L-Arg conjugate (Figure 4.8.c)) and an analogous behaviour was observed at 300 nm. It is difficult to extract any unambiguous information at lower wavelength, as too many CD signals are overlapped in the UV region. In the visible region the complexes exhibit the same behaviour in the presence of different DNA sequences. Thus, these experiments suggest that the two complexes might bind differently the two different DNA polymers analysed, but this has to be further proved with the use of methodologies that are more appropriate to study the DNA binding selectivity of chiral complexes. This will object of future work (see Chapter 5).

4.3 Linear dichroism studies.

The Linear Dichroism (LD) technique is based on the principle that electronic transitions in molecules are fixed in a specific orientation and that if the molecules themselves are aligned in a specific orientation then the polarization of the transition may be probed by the differential absorption of oriented linearly polarized light. In practice two linearly polarized light beams that are parallel or perpendicular to the direction of the orientation of the molecules are used and the difference in absorbance can be recorded as LD signal.[9-11]

There are several methods to provide orientation to long and small molecules. The technique used herein is known as *flow orientation* and is based on the use of the Couette flow cell that is represented in Figure 4.9.a). The cell is made of two coaxial cylinders, one internal to the other, and the solution to analyse is placed into the narrow gap between the two cylinders. The rotation of the internal cylinder causes the orientation of the molecules by viscous drag and this orientation can be probed with linearly polarised light. With the flow orientation method, only long molecules,

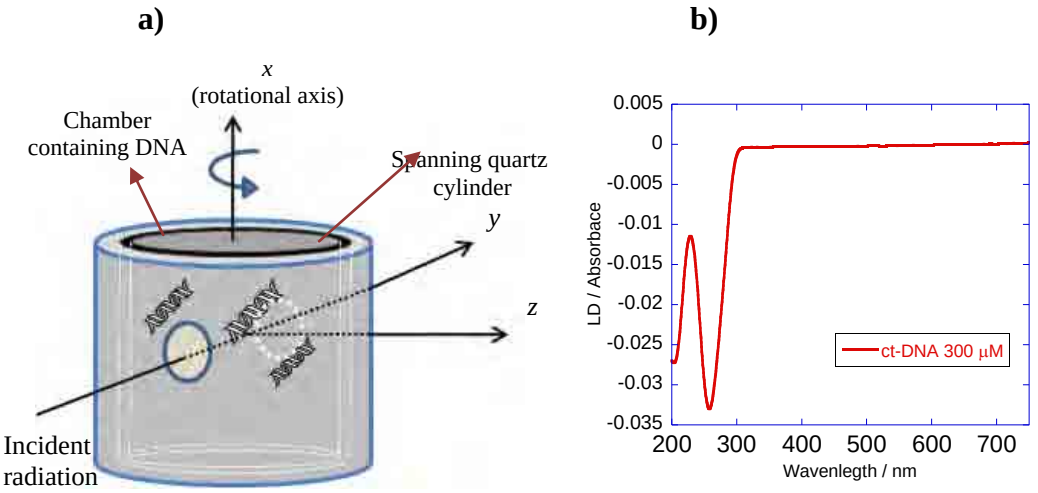

Figure 4.9. a) Representation of a Couette flow cell. The incident radiation is perpendicular to the rotation axis of the internal cylinder. Strands of long DNA (more than 1000 base pairs) are oriented upon the rotation of the internal cylinder. **b)** LD spectrum of B-DNA from calf thymus.

such as DNA with more than 1000 base pairs, present significant and detectable orientation and in Figure 4.9.b) the typical LD spectrum of B-DNA from calf thymus is showed. With this method, small molecules do not orient and do not show any LD signal. However, if a small molecule, such as a synthetic agent, binds to the oriented DNA (or in general to a long molecule with LD signal), then the resulting LD spectrum changes in relation to both the contribution of newly oriented electronic transitions from the small molecule attached and to possible variations of the DNA orientation occurring upon its interaction with the agent.

LD titration of 100 μM of ct-DNA with all the Fe(II) conjugated cylinders were performed and compared with the parent unconjugated cylinder. In Figure 4.10 a) to f) all the titrations with the Fe(II) complexes are shown: in a) the parent $[Fe_2(L1)_3]Cl_4$, in b) the tripeptide conjugated $[Fe_2(L\mathbf{a}1)_3]Cl_4$, in c) and d) the L and D-Ser conjugated $[Fe_2(L\mathbf{b}1)_3]Cl_4$ and $[Fe_2(L\mathbf{c}1)_3]Cl_4$, in e) and f) the L and D-Arg conjugated $[Fe_2(L\mathbf{d}1)_3]Cl_{10}$ and $[Fe_2(L\mathbf{e}1)_3]Cl_{10}$). For the parent Fe(II) cylinder, the gradual loss of signal at 260 nm, as increasing concentrations of complex are added, is a consequence of the loss of the initial orientation of the DNA strands resulting from either an increase in DNA flexibility or a shortening of the DNA by kinking,

bending, compaction, or aggregation of DNA. Moreover the complex itself acquires an induced orientation as a consequence of its binding to the DNA, and, since the binding is not random, a systematic increasing of induced LD signal occurred in the MLCT region of the complex.[7] Analogous results are obtained with the conjugated Fe(II) complexes. In all the titrations carried out, there is a significant loss of signal at 260 nm as a consequence of changes in the orientation of the DNA caused by the binding of the complexes. The three conjugates $[Fe_2(L\mathbf{a}1)_3]Cl_4$, $[Fe_2(L\mathbf{b}1)_3]Cl_4$ and $[Fe_2(L\mathbf{c}1)_3]Cl_4$ also exhibit induced LD signals in the MLCT region which confirms that their binding to the DNA is not random but in an oriented fashion. However, no induced LD signal in the visible region is observed when the DNA is titrated with the two arginine conjugates $[Fe_2(L\mathbf{d}1)_3]Cl_{10}$ and $[Fe_2(L\mathbf{e}1)_3]Cl_{10}$. In some cases the absence of induced LD bands in the visible region is due to the ability of the agent to cause condensation/aggregation of the DNA with consequent precipitation of strands of DNA-agent adducts. As explained in section 4.1, the arginine conjugate are indeed able to precipitate the DNA but this does not occur at the concentration conditions selected for these titrations. The absence of bands in the MLCT region of the complexes is a little surprising given the response of the parent cylinder and the other three conjugates but it does not per se mean that the complexes do not bind in a specific manner. Nature and shape of the induced LD in complex spectroscopy is the same for parent as for L and D-Ser and tripeptide conjugates, implying a similar mode of binding. However, the presence of six guanidinium groups at the edges of the arginine conjugate cylinders could offer different possibilities of interaction with the DNA, including contacts with the phosphate groups, in addition to the binding at the major groove through the helicate core.

The analysis of the decrease of the LD adsorbance at 260 nm is useful to compare the behaviour of different complexes on the DNA orientation. In this case, the behaviour of the two arginine conjugated has to be discussed separately from all the other complexes, because of the absence of induced LD signal. In fact, all the other complexes present induced LD bands not only in the MLCT region, but also in the UV region and these bands overlap with that originating from the DNA, contributing to the value of absorbance at 260 nm especially at low DNA:complex ratio. In contrast, when the DNA is titrated with the two arginine conjugates, the absorbance at 260 nm originates from the DNA only.

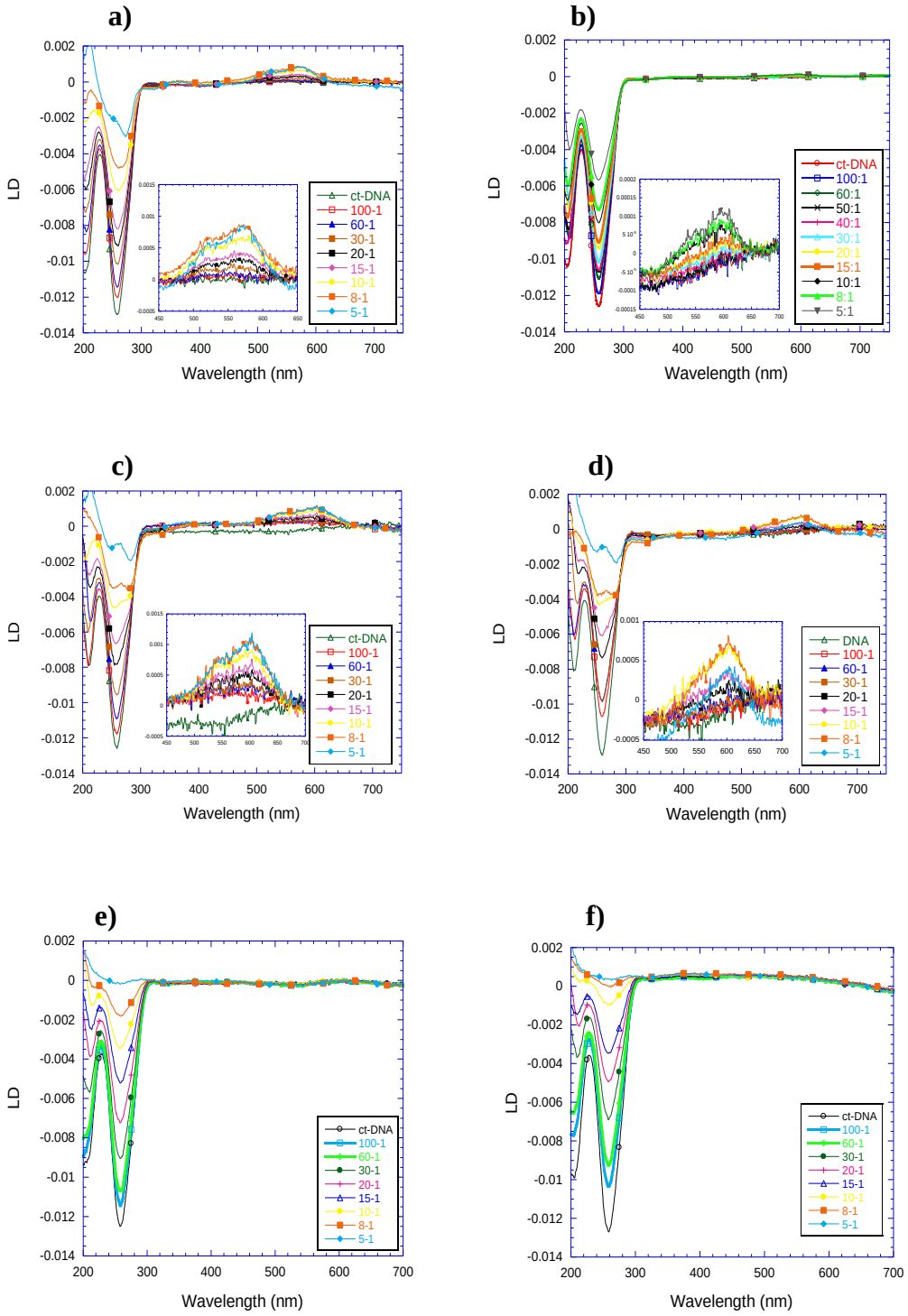

Figure 4.10. LD of 100 μM of ct-DNA in 10 mM NaCl and 1 mM $Na(CH_2)_2AsO_2 \cdot 3H_2O$ (pH 6.8) with increasing concentration of **a)** $[Fe_2(L1)_3]Cl_4$, **b)** $[Fe_2(L\mathbf{a}1)_3]Cl_4$, **c)** $[Fe_2(L\mathbf{b}1)_3]Cl_4$, **d)** $[Fe_2(L\mathbf{c}1)_3]Cl_4$, **e)** $[Fe_2(L\mathbf{d}1)_3]Cl_{10}$ and **f)** $[Fe_2(L\mathbf{e}1)_3]Cl_{10}$. The legends show decreasing ratios of DNA:complex and, where necessary, inserts show the enlargement of the corresponding MLCT regions.

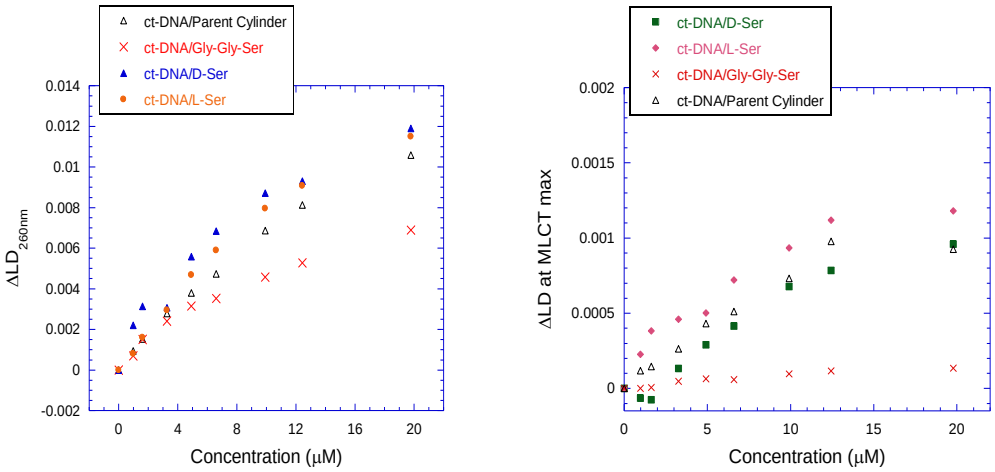

Figure 4.11. a) Plotting of ΔLD absorbance at 260 nm vs complex concentration extracted from the titrations with $[Fe_2(L1)_3]Cl_4$, $[Fe_2(L\mathbf{a}1)_3]Cl_4$, $[Fe_2(L\mathbf{b}1)_3]Cl_4$ and $Fe_2(L\mathbf{c}1)_3]Cl_4$. **b)** From the same titrations, plotting of ΔLD absorbance at the λ_{max} of the MLCT band vs complex concentration (λ_{max} is 574 nm for parent $[Fe_2(L1)_3]Cl_4$ and 600 nm for $[Fe_2(L\mathbf{a}1)_3]Cl_4$, $[Fe_2(L\mathbf{b}1)_3]Cl_4$ and $[Fe_2(L\mathbf{c}1)_3]Cl_4$). $\Delta LD=LD-LD_{DNA}$ where LD is the value of LD absorbance at λ_{max} and LD_{DNA} is the LD absorbance of the DNA at the same wavelength. In the legends the complexes are indicated with their conjugating units.

The chart in Figure 4.11 a) shows the variation of the ΔLD absorbance at 260 nm as a function of the complex concentrations, extracted from the titrations with the parent $[Fe_2(L1)_3]Cl_4$, the tripeptide conjugate $[Fe_2(L\mathbf{a}1)_3]Cl_4$, the L and the D-Ser conjugates $[Fe_2(L\mathbf{b}1)_3]Cl_4$ and $Fe_2(L\mathbf{c}1)_3]Cl_4$ shown in Figure 4.10 a), b), c) and d). ΔLD is the difference between the absorbance at 260 nm after each addition of complex and the absorbance of DNA alone (100 μM) at the same wavelength. The chart in figure 4.11.b) shows the analogous plotting, but using ΔLD values at the λ_{max} of the induced bands in the MLCT region (λ_{max} is 574 nm for parent $[Fe_2(L1)_3]Cl_4$ and 600 nm for $[Fe_2(L\mathbf{a}1)_3]Cl_4$, $[Fe_2(L\mathbf{b}1)_3]Cl_4$ and $[Fe_2(L\mathbf{c}1)_3]Cl_4$). From these data, the parent Fe(II) cylinder and the two serine conjugated Fe(II) cylinders exhibit similar activity in affecting the orientation of the DNA, whilst the tripeptide conjugated Fe(II) cylinder is the least effective complex.

Separately, the chart in Figure 4.12 shows the variation of ΔLD at 260 nm versus complex concentration corresponding to the titration with the two arginine conjugates (from Figure 4.10 e) and f)). The D-Arg conjugate emerges as the more

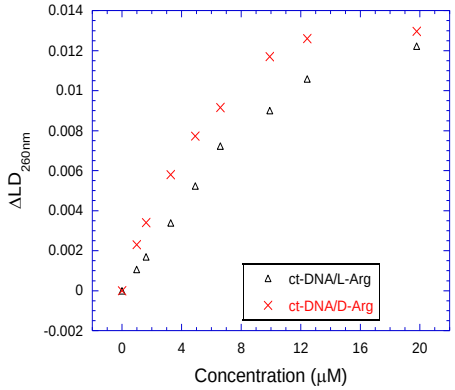

Figure 4.12. Plotting of ΔLD absorbance at 260 nm vs complex concentration extracted from the titrations with $[Fe_2(L\mathbf{d}1)_3]Cl_{10}$ and $[Fe_2(L\mathbf{e}1)_3]Cl_{10}$. In the legend the complexes are indicated with their conjugating units.

DNA/complex ratio	% of loss of LD signal at 260 nm upon interaction with increasing concentrations of cylinders					
	L-Arg conjugate	D-Arg conjugate	Parent Cylinder	GGS conjugate	D-Ser conjugate	L-Ser conjugate
100.0	8.6	18.3	7.3	5.6	17.1	6.4
60.0	13.7	27.1	11.8	12	24.3	12.8
30.0	27.4	46.1	21.5	19.2	23.7	23.6
20.0	42.4	61.4	29.4	25.2	43.3	37.4
15.0	58.5	72.8	36.7	28.2	53	47.1
10.0	72.9	92.9	53.1	36.6	67.5	63.6
8.0	85.6	100	62.9	42.2	72.1	72.6
5.0	98.9	100	81.8	55.1	92.3	92

Table 4.1. The percent of loss of LD signal at 260 nm caused by addition of increasing concentrations of different complexes was calculated using the titrations shown in Figure 4.10.

active in causing modification to the DNA and this supports the CD results and is consistent with the fact that the D-Arg conjugation induces the central helicate core in M configuration (see Chapter 3) and with the demonstrated[8] higher ability of this enantiomer in coiling the DNA.

Table 4.1 offers a complementary vision of the effect of these conjugated cylinders from LD titration, by comparing the % of loss of LD signal at 260 nm upon adding increasing concentrations of complexes. At low concentration of D-Arg

conjugate already 18.3% of the initial LD signal at 260 nm is lost, against the only 8.6% caused by the L-Arg conjugate. The LD signal decreases by half at 30:1 (DNA:complex ratio) and a complete loss of the signal occurs at 8:1 ratio. Slightly higher concentrations of L-Arg conjugate are needed to produce the same effect. By contrast, the tripeptide conjugate causes only 55% of the DNA LD signal lost at 260 nm even at high complex concentrations (5:1 ratio), whilst the two serine conjugate and the parent cylinder present similar behaviour with the parent cylinder slightly less effective. However, at very low complex concentration (100:1 and 60:1 ratios) the D-Ser conjugate provokes a remarkable higher loss of LD signal, compared to L-Ser and parent cylinder. The reason for this is unclear, since it was not possible to establish the actual conformation of the helicate core of the serine conjugates (Chapter 3) and whether this, eventually, influences the DNA binding.

Analogous titrations were performed with the Cu(I) complexes, the parent $[Cu_2(L5)_2]Cl_2$, the two tripeptide conjugates $[Cu_2(L\mathbf{a}1)_2]Cl_2$ and $[Cu_2(L\mathbf{a}2)_2]Cl_2$, and the two L and D-Ser conjugates $[Cu_2(L\mathbf{b}2)_2]Cl_2$ and $[Cu_2(L\mathbf{c}2)_2]Cl_2$ (Figure 4.13 a) to e)). All the complexes exhibit DNA binding and coiling, but they are less effective than the Fe(II) cylinders. This is the expected consequence of the smaller positive charge of the complexes, and also the absence of one ligand strand offer less possibility of hydrophobic interactions with the DNA. The magnitude of induced LD bands in the MLCT region increases in all the titrations, except that with $[Cu_2(L\mathbf{a}1)_2]Cl_2$. This is not surprising since the nature of the ligand of this Cu(I) complex does not ensure the exclusive formation of the helicate conformation (box conformation cannot be excluded),[12] so that more binding mode are possible for this complex.

The chart in Figure 4.13.f) reports the variation of ΔLD at 260 nm in function of complex concentration. All the conjugates exhibits comparable activity by LD. The L-Ser conjugate seems slightly more effective than the D-Ser conjugate, but all the conjugated complexes are unequivocally less active than their unconjugated equivalent.

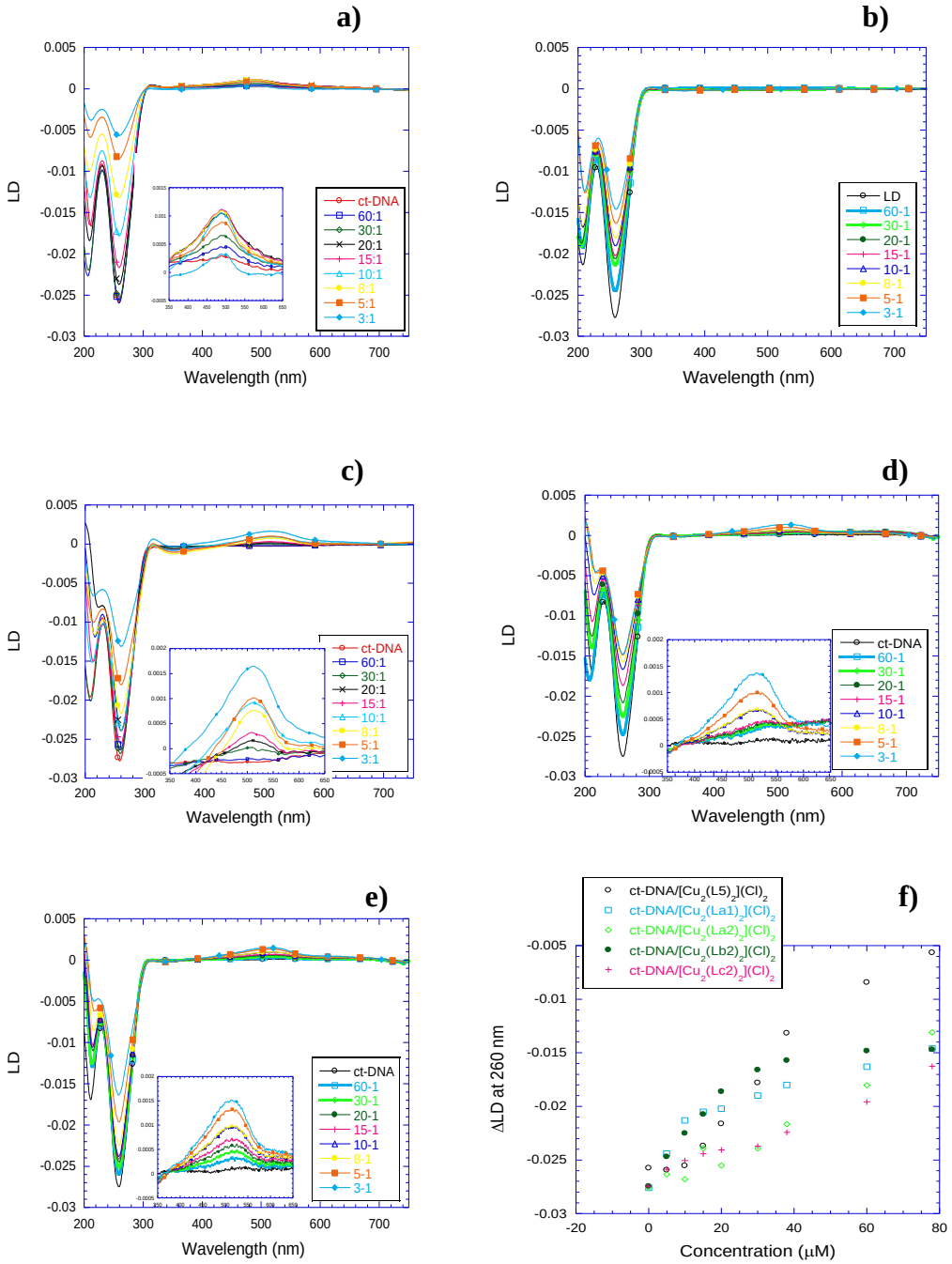

Figure 4.13. LD of 300 μM of ct-DNA in 20 mM NaCl and 1 mM $Na(CH_2)_2AsO_2 \cdot 3H_2O$ (pH 6.8) with increasing concentration of **a)** parent $[Cu_2(L5)_2]Cl_2$, **b)** Gly-Gly-Ser conjugate $[Cu_2(L\mathbf{a}1)_2]Cl_2$, **c)** Gly-Gly-Ser conjugate $[Cu_2(L\mathbf{a}2)_2]Cl_2$, **d)** L-Ser conjugate $[Cu_2(L\mathbf{b}2)_2]Cl_2$ and **e)** D-Ser conjugate $[Cu_2(L\mathbf{c}2)_2]Cl_2$. The legends show decreasing ratios of DNA:complex and, where necessary, inserts show zoom of the corresponding MLCT region. In **f)** the plotting of the ΔLD at 260 nm in function of complex concentration.

4.4 Gel Electrophoresis studies.

Gel electrophoresis is one of the most common techniques used for the separation of bio-molecules such as DNA, RNA and proteins. It is based on the principle that these molecules have a specific net charge that can be used to cause their migration along an appropriate gel matrix under the effect of an electric field applied to the gel. The electric field drives the molecules toward the electrode with the opposite charge and the velocity of the migration (v) depends on the strength of the electric field (E) applied, the net charge of the molecule (z) and the frictional coefficient (f):

$$v = Ez/f$$

The frictional coefficient f depends on the shape and mass of the migrating molecule and on the viscosity of the medium that contrast the mobility of the molecules throughout the pores of the matrix. Usually, the matrix is a cross linked polymer, that assumes the consistence of a gel, whose composition and porosity is chosen according with the molecule to analyse. Generally, polyacrylamide gels are used to analyse short sequences of nucleic acids (DNA or RNA) and proteins (this method is also known as PAGE electrophoresis), whilst agarose gels are used for bigger molecules such as plasmid DNA. The scheme in Figure 4.14 represents a typical agarose gel used to analyse a big molecule of DNA such as plasmid DNA. This is a type of double stranded circular DNA that occurs naturally in bacteria. The main

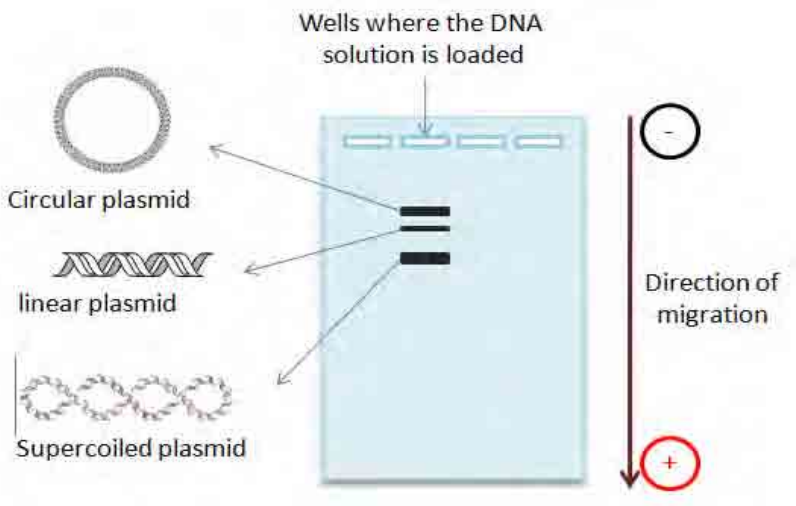

Figure 4.14. Representation of three different conformations of plasmid DNA that migrate with different rate on an agarose gel.

conformations that plasmid DNA can assume are: the supercoiled conformation, where the DNA is compact with a twist built up; the circular conformation, which can be obtained upon enzymatic or artificial cut of one of the strands of the supercoiled plasmid causing the opening of the supercoiling to a relaxed circular structure; the linear conformation, deriving from a double cut of both strands of supercoiled or circular DNA. Solutions containing a mix of these three conformations of plasmid can be loaded in wells on the surface of the gel and, when the electric current is applied at the two sides of the gel, the DNA migrates toward the positive electrode, but the different conformations of DNA migrate with a different rate according with their shapes. In this case the supercoiled plasmid runs faster than circular plasmid and the linear conformation has an intermediate rate.

There are different methods to visualise the bands on the gel after the electrophoresis run is complete. For DNA run on agarose gel, the gel can be stained by luminescent compounds that interact with the DNA. For example the gel can be treated with ethidium bromide which intercalates between the DNA bases and can be detected upon exposing of the gel to light. When shorter sequences of DNA are analysed on polyacrylamide gel (and at lower concentrations), then a more sensitive technique of visualisation is necessary and in this case the DNA is labelled with radioactive isotopes and an autoradiogram of the gel can be recorded.

Herein, both agarose and polyacrylamide gel techniques were employed. The first to explore the nuclease activity of the conjugated Cu(I) cylinders in presence of an oxidising agent, and the second to verify whether the conjugated Fe(II) cylinders bind into the DNA three way junction as the unconjugated cylinder does.

4.4.1 Agarose gel to test nuclease activity of Cu(I) complexes.

The copper complexes of some di-imine ligands, (for example copper(I/II) bis-phenanthroline) are known to exhibit oxidative DNA cleavage properties.[13-15] The unsubstituted cylinder $[Cu_2(L5)_2]Cl_2$ has been shown to cleave DNA in presence of hydrogen peroxide. Interestingly it displays some double strand cleavage activity which may reflect its di-nuclear nature with two linked sites capable of cleaving two strands[16]. To verify that the conjugated Cu(I) cylinders ($[Cu_2(L\mathbf{a}1)_2]Cl_2$, $[Cu_2(L\mathbf{a}2)_2]Cl_2$, $[Cu_2(L\mathbf{b}2)_2]Cl_2$ and $[Cu_2(L\mathbf{c}2)_2]Cl_2$) retain the same DNA cleavage

capacity, gel electrophoresis (1% agarose) experiments using supercoiled plasmid pBR322 DNA were performed. Solutions of 90 μM of plasmid were incubated with each Cu(I) complex at different concentrations (different DNA:complex ratios) in presence of hydrogen peroxide (HP) as oxidising agent. Solutions containing only DNA-complex adducts without HP were also analysed and all the resulting gels are shown in Figure 4.15. Although the nuclease activity of parent $[Cu_2(L5)_2]Cl_2$ has already been reported, the experiment was performed also with this complex (gel **a**)) to provide a standard for comparison. In each gel lanes 1 and 2 are DNA (plasmid pBR322, 90 μM) and DNA with 25 mM of HP respectively, to confirm that HP alone does not affect the DNA. The DNA is mainly present in the supercoiled conformation (band C in gel a)), but the circular conformation is also visible (band A in gel a)). Gel **a**) shows that using parent $[Cu_2(L5)_2]Cl_2$, the supercoiled conformation disappears already at 30:1(DNA:complex ratio).[16] The circular and the linear (band B) conformations are both visible at 30:1 and they gradually disappear as the concentration of complex is increased, whilst formation of a broad smear (band D) becomes visible to indicate that the DNA is chopped in fragments of different length that run in the gel with different rates. Nuclease activity was observed for all the conjugates, although the complete absence of the supercoiled conformation occurs at higher concentrations of complex. The tripeptide conjugate ($[Cu_2(L\mathbf{a}2)_2]Cl_2$, gel **b**)[17]) and the L-Ser conjugate ($[Cu_2(L\mathbf{b}2)_2]Cl_2$, gel **c**)) cause rupture of the supercoiled DNA at 10:1 and 15:1 respectively, with successive formation of ladder at higher complex concentrations, so that the L-Ser conjugates seems slightly more effective. The D-Ser conjugate (gel d)) provokes the break of the supercoiled conformation at 15:1 but for unclear reasons, the chopping is not complete at higher complex concentrations as it occurs for the other two conjugates. The artificial nuclease activity of the tripeptide conjugated $[Cu_2(L\mathbf{a}1)_2]Cl_2$ (gel **e**)), is not so efficient as the former complexes (supercoiled DNA is still present at high complex loading, although visibly less abundant). In all the gels, the concurrent presence of supercoiled, circular and linear DNA is consistent with the possibility of the simultaneous double strand cleavage due the action of both metal centres, that was already hypothesised for the parent $[Cu_2(L\mathbf{5})_2]Cl_2$. Lanes 10 to 13 of gels b), d) and e) are relative to the complexes incubated with the DNA without HP and it is evident that they do not affect the DNA in these conditions, as it was already

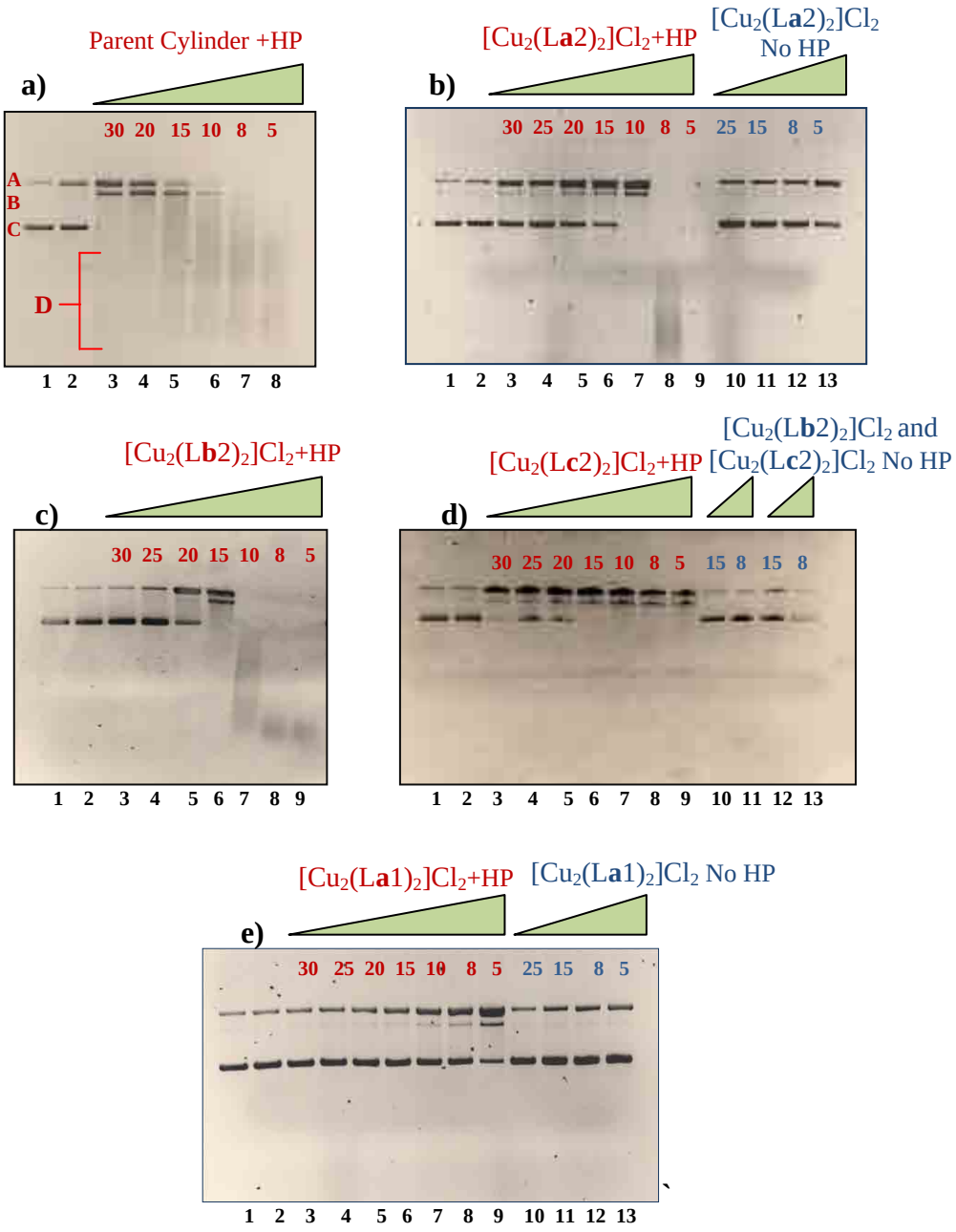

Figure 4.15. The ethidium bromide stained gels of pBR322 plasmid and **a)** parent $[Cu_2(L5)_2]Cl_2$, **b)** $[Cu_2(L\mathbf{a}2)_2]Cl_2$, **c)** $[Cu_2(L\mathbf{b}2)_2]Cl_2$ **d)** ($[Cu_2(L\mathbf{c}2)_2]Cl_2$and **e)** $[Cu_2(L\mathbf{a}1)_2]Cl_2$. The lanes are numbered in black at the bottom of each gel. For each gel: Lane 1: DNA of reference (90 μM); Lane 2: DNA with HP (25 mM, after 1 hour of incubation). The red values on the top of the gels are referred to the DNA/complex ratios of samples that were incubated with 25 mM of HP. The blue values correspond to DNA/complex ratios of samples incubated without HP. For gel **d)** only, lane 10 to 13 are: DNA:$[Cu_2(L\mathbf{b}2)_2]Cl_2$=15:1 (10), DNA:$[Cu_2(L\mathbf{b}2)_2]Cl_2$=8:1 (11), DNA:$[Cu_2(L\mathbf{c}2)_2]Cl_2$=15:1 (12) and DNA:$[Cu_2(L\mathbf{b}2)_2]Cl_2$=8:1 (13), without HP.

observed for the parent $[Cu_2(L\mathbf{5})_2]Cl_2$.

In conclusion, all the conjugates exhibit the ability of chopping plasmid DNA in the presence of HP, but with different efficiency. However they are all less effective than the parent Cu(I) complex and this is consistent with the better DNA binding that the parent complex showed by LD experiments.

4.4.2 PAGE electrophoresis to test the DNA three way junction binding of Fe(II) complexes.

In Chapter 2 it has been explained that one of the most exciting qualities of parent Fe(II) cylinders is their ability to bind at the heart of a DNA three way junctions (3WJ). This was observed for the first time when the crystal structure of the complex in presence of the palidromic hexanucleotide 5'-d(CGTACG)-3' was obtained.[18] Successively, it was of interest to verify that this was not an artefact of crystallisation, but a type of action that could also occur in solution. J. Malina et al.[19] carried out PAGE electrophoresis experiments using three different strands of 14-mer non palindromic oligonucleotide that can potentially form a three way junction of seven base pairs per arm.[20] Those experiments demonstrated that the Fe(II) parent cylinder promotes the formation of the three way junction between the three strands and, moreover, stabilises such structure even when temperature conditions are not favourable for the formation of the junction in absence of the complex. Those results also highlighted the importance of the shape of the cylinder in stabilising the three way junction (bulky cylinders were not successful), and that the M enantiomer of the parent cylinder is slightly more effective than the P enantiomer. An analogous PAGE electrophoresis experiment was carried out by Siriporn Phongtongpasuk, from the Hannon group, using the facilities of the Functional Genomics and Proteomics Unit of the school of Bioscience at the University of Birmingham. In this experiment all the conjugated Fe(II) cylinders were incubated with the same three strands of oligonucleotide used by Malina (Figure 4.16.a)) and analysed by polyacrylamide gel. Figure 4.16. b) shows the autoradiogram of the gel run at room temperature in which Lanes 1, 2 and 3 contain strands S3*, S3*+S2 and S3*+S2+S1 respectively where S3* is the strands labelled with ^{32}P at the 5' extremity. These strands are relatively short and in these conditions of buffer and temperature they do not interact to form

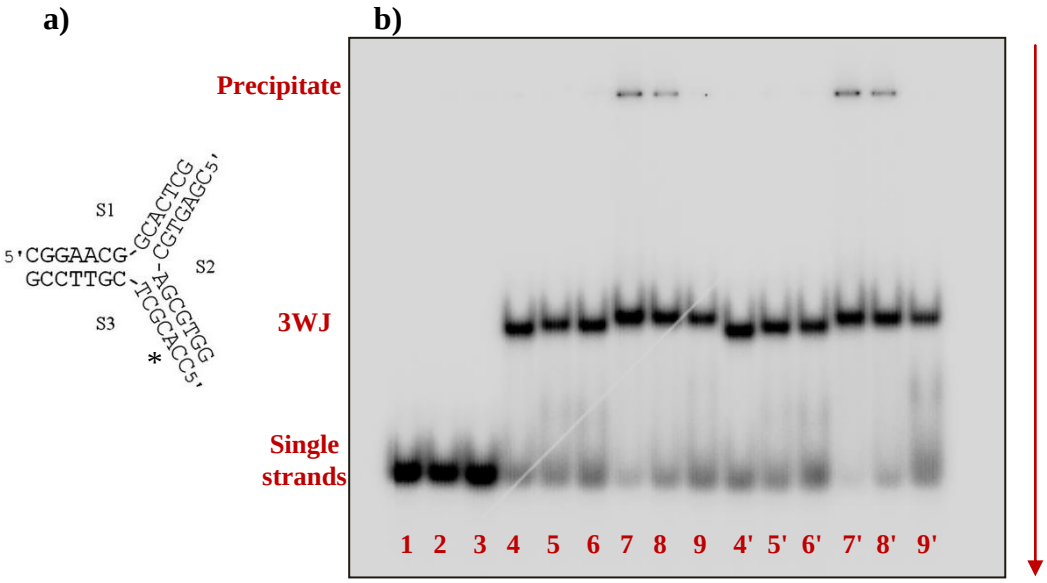

Figure 4.16. a) The three sequences of oligonuctleotide used to assembly the three way junction are indicated as S1, S2 and S3* where S3* is the ^{32}P labelled strand. **b)** Polyacrylamide gel (autoradiogram) at room temperature of the three strands incubated with the conjugated Fe(II) cylinders. Lane 1 to 3 are the controls S3*, S3*+S2, S3*+S2+S1 respectively; Lane 4 to 9: S3*+S2+S1 (0.4 μM for each strand, 1.2 μM total concentration of DNA) in presence of parent $[Fe_2(L1)_3]Cl_4$ (4), $[Fe_2(L\mathbf{c}1)_3]Cl_4$ (5), $[Fe_2(L\mathbf{b}1)_3]Cl_4$ (6), $[Fe_2(L\mathbf{e}1)_3]Cl_{10}$ (7), $[Fe_2(L\mathbf{d}1)_3]Cl_{10}$ (8) and $[Fe_2(L\mathbf{a}1)_3]Cl_4$ (9). Lane 4' to 9': the same solutions, separately prepared, were loaded in the same order for a more accurate analysis. All the loaded samples contained 0.4 μM of complex to have a theoretical 3WJ:complex ratio of 1:1.

either the three way junction or a double strand (only at ~5 °C a partial formation of 3WJ could occur[19,20]) and for this reason they run as single bands with the same rate in the gel. However, incubation of the three strands with any conjugated Fe(II) cylinder leads to the formation of a three way junction. Lanes 4 to 9 contain S3*+S2+S1 in the presence of the parent cylinder $[Fe_2(L1)_3]Cl_4$ as control (Lane 4), the D and L-Ser conjugated $[Fe_2(L\mathbf{c}1)_3]Cl_4$ and $[Fe_2(L\mathbf{b}1)_3]Cl_4$ (Lane 5 and 6), the D and L-Arg conjugated $[Fe_2(L\mathbf{e}1)_3]Cl_{10}$ and $[Fe_2(L\mathbf{d}1)_3]Cl_{10}$ (Lane 7 and 8) and the tripeptide conjugated $[Fe_2(L\mathbf{a}1)_3]Cl_4$ (Lane 9). Lanes 4' to 9' contain the same samples in the same order, loaded a second time for a better accurateness of the analysis. All the complexes exhibit a similar ability to promoting the formation of the three way junction. As expected, the rate of migration of the 3WJ-complex adduct is slightly different depending on the charge and the dimension of the complexes: the

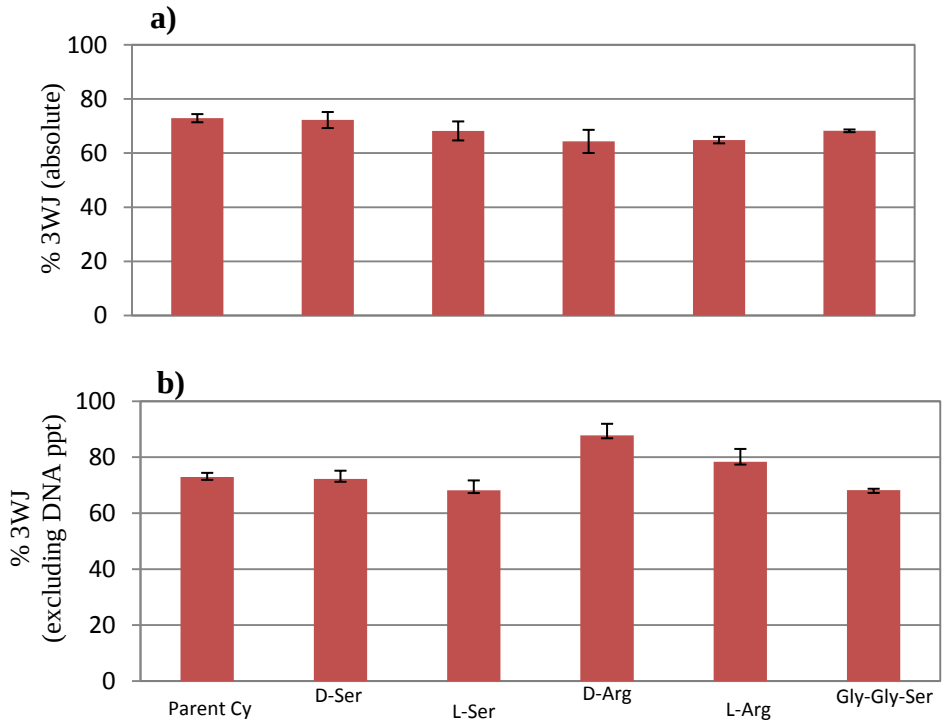

Figure 4.17. Quantification of the intensity of the bands (by Quantity one) from the gel in Figure 4.16. % of three way junction formed in presence of each complex **a)** absolute considering the precipitation of the DNA in the wells and **b)** only relative to the bands of single strand. The labels indicate the complexes according with their conjugating units.

arginine conjugates have a higher positive charge so that they form adducts with the DNA that run more slowly toward the positive electrode. The tripeptide conjugate-3WJ is slower than any serine conjugate-3WJ, most probably because the first complex is more extended. The 3WJ-serine conjugates have nearly the same ratethan the 3WJ-parent cylinder adduct. From the gel, it is visible that the lanes relative to the 3WJ-arginine conjugates adducts are those with fewer amounts of single strands, although formation of precipitate DNA-complex is also evident in the corresponding wells. The bands of the gel have been quantified to calculate the percent of three way junction that was formed for each complex. In the chart in Figure 4.17.a) the effective % of 3WJ has been calculated as follows:

$$\% \text{ 3WJ} = [I_{3WJ}/(I_{ss}+I_{3WJ}+I_{ppt})]*100$$

where $I_{3WJ,}$ I_{ss}, and I_{ppt} are the measured intensities of the bands relative to the three way junctions, the single strands and the precipitates in the wells for each lane. This is the reasonable method to quantify the real percent of 3WJ that is formed for each complex, but in this case the I_{ppt} is zero for all the complexes except the arginine conjugates. However, it is not possible to estimate how that precipitate would have contribute if it was free to run in the gel, and all the DNA that run in those lanes is entirely involved in the formation of the 3WJ. For this reason the percent of 3WJ relatively to the single strands only was calculated as follows:

$$\% \text{ 3WJ} = [I_{3WJ}/(I_{ss}+I_{3WJ})]*100$$

and the values reported in the chart of Figure 4.17.b). This shows that the arginine conjugates promote a relative higher formation of 3WJ with the D-Arg the most effective. The parent cylinder and the serine conjugates exhibit comparable activity and the tripeptide conjugate is, also in this experiment, the less effective.

4.5 Cytotoxic activity by MTT assay.

Triple stranded parent cylinders, both Fe(II) and Ru(II) exhibited a significant toxicity in cancer cell lines[21] and herein it was investigated whether the conjugated Fe(II) cylinders preserve this characteristic. One common method to verify the toxicity of candidate drugs is to calculate their *half maximal inhibitory concentration* (IC_{50}) values, which indicate the concentration of drug that is needed to inhibit a given biological process by half. In this case the IC_{50} is the concentration of complex that is needed to inhibit by 50% the viability of cancer cells thus that the lower is this value, the higher is the cytotoxic activity of the complex. IC_{50} values of the Fe(II) conjugated cylinders were measured in collaboration with Victoria Sadovnikova, from the Hannon group, and using the facilities kindly made available by Prof. Kevin Chipman, Dr. Chris Bunce and Dr. Nicholas Hodges from the School of Bioscience of the University of Birmingham.

Two human cancer cell lines (ovarian A2780 and breast MDA-MB-231) were treated with all the conjugated Fe(II) cylinders (the tripeptide conjugated $[Fe_2(L\mathbf{a}1)_3]Cl_4$, the L and D-Ser conjugated $[Fe_2(L\mathbf{b}1)_3]Cl_4$ and $[Fe_2(L\mathbf{c}1)_3]Cl_4$, L and

D-Arg conjugated $[Fe_2(L\mathbf{d}1)_3]Cl_{10}$ and $[Fe_2(L\mathbf{e}1)_3]Cl_{10}$) and the same cell lines were also treated with the parent $[Fe_2(L1)_3]Cl_4$ and with the known anticancer agent cisplatin as a control and standard for comparison. Each cell line was incubated in medium with six different concentrations of each compound (200, 100, 50, 25, 12.5 and 6 μM) for 72 hours and IC_{50} values were calculated by performing the colorimetric test known as MTT assays. Yellow MTT (3-(4,5-dimethylthiazol-2-yl)-2,5-diphenyltetrazolium bromide, a tetrazole) is reduced to purple formazan by the mitochondrial reductase in living cells (Figure 4.18), thus the amount of living cells after the incubation with the synthetic complexes can be estimated by treating them with MTT, incubating for two hours, and measuring (by UV-Vis spectroscopy) the amount of formazan that is formed, which is proportional to the amount of living cells after the treatment. The table and the chart shown in Figure 4.19 report the calculated IC_{50} values in μM. The first important result is that all the conjugated compounds present a remarkable cytotoxic activity in the tested cell lines. The cytotoxicity of the conjugated cylinders in A2780 varies between 5 and 9 μM, which is comparable with the cytotoxicity of the cisplatin and they appear more active than the parent cylinder. In MDA-MB-231 all the compounds present a comparable cytotoxicity. $[Fe_2(L\mathbf{a}1)_3]Cl_4$ and $[Fe_2(L\mathbf{d}1)_3]Cl_{10}$ tend to be slightly less active among the conjugates. The lower activity of the first complex is expected, since it showed slightly less affinity in binding the DNA in the spectroscopic experiments. The result concerning the L-Arg conjugates $[Fe_2(L\mathbf{d}1)_3]Cl_{10}$ is unclear, although the fact that

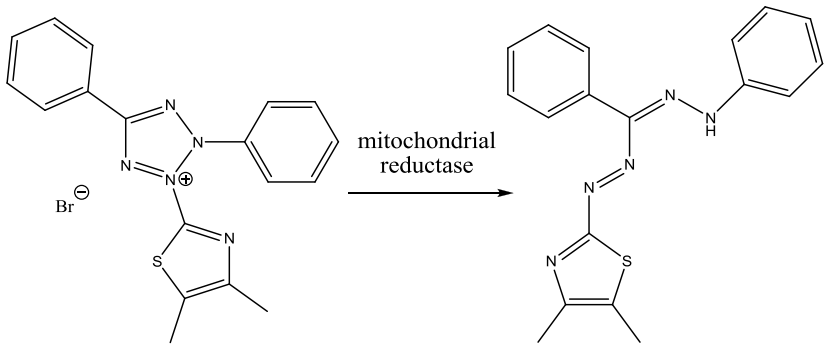

Figure 4.18. Reduction of MTT to formazan by mitochondrial reductase in living cells.

Table 4.2. IC_{50} values (μM)

Compound	A2780	MDA-MB-231
Gly-Gly-Ser conj.	**9±2**	**34±6**
L-Ser conj.	**7±3**	**23±1**
D-Ser conj.	**5±2**	**29±3**
L-Arg conj.	**9±2**	**35±7**
D-Arg conj.	**6±3**	**26±1**
Parent $[Fe_2(L1)_3]Cl_4$	**14±2**	**27±3**
cisplatin	**4±2**	**27±3**

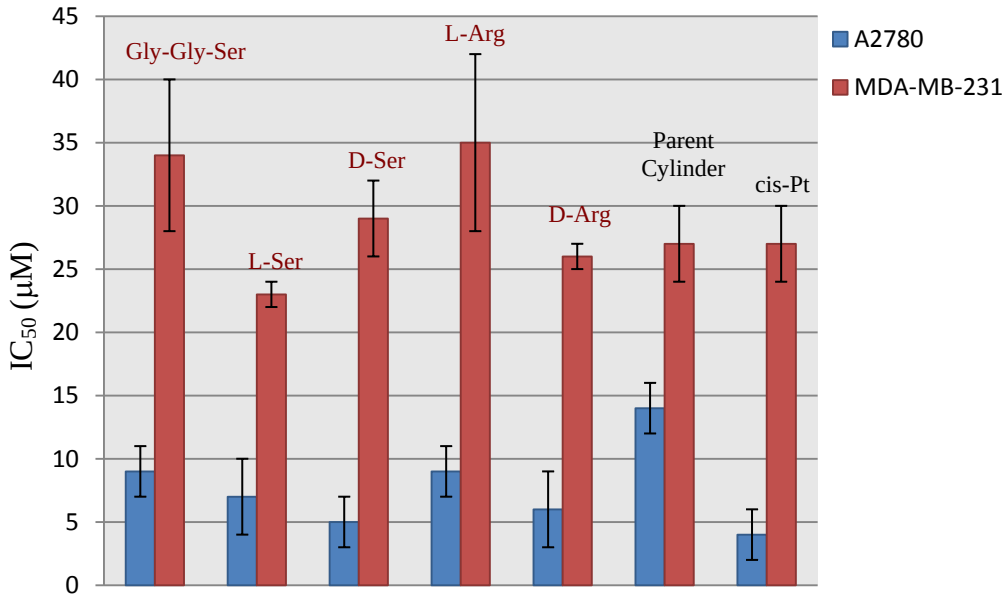

Figure 4.19. Table and chart indicating the IC_{50} values (μM) of the conjugated Fe(II) cylinders, parent Fe(II) cylinders and cisplatin for A7280 and MDA-MB-231 cell lines. The conjugates are labelled indicating their conjugating units.

this conjugation induces the helicate core in P conformation, which is the less active in binding the DNA, might also influence the cytoxicity of the complex. In section 4.1 it was explained that the conjugated complexes are less stable than the parent cylinder and, particularly, the two arginine conjugates are the complexes that degrade more rapidly. Although this could have negatively influenced the cytotoxicity of the conjugates, they exhibit significant IC_{50} values and in the future it will be interesting

to verify if the presence of the conjugating units, especially the arginine residues, improve the cell uptake of the cylinders. The same cell lines were treated with all the possible fragments that can be obtained by complex degradation (the spacer and the aldehyde components) and all the MTT assays revealed IC_{50} values higher than 100 μM, confirming that those cytotoxic activities are only due to the complexes.

4.6 Conclusions.

In this Chapter several techniques were used to study the DNA recognition and the cytotoxicity of the conjugated cylinders. The stability of the conjugates in water was monitored by UV-vis spectroscopy at room temperature for 36 hours and it was observed that none of the Fe(II) conjugates is as stable as the Fe(II) parent cylinder. D and L serine complexes are the most stable among the conjugates, followed by the tripeptide conjugate. The two arginine conjugates degrade faster. This would suggest that the anchoring of units at the edges of the triple stranded Fe(II) cylinders reduces the stability of the complexes in water, at least for the conjugating units explored herein. The effect is not so dramatic with the conjugation of a neutral and relatively small amino acid such as the serine, but the instability increases with the attachment of the larger tripeptide. For the arginine conjugates the higher instability might be due both to the size of the amino acid and the presence of the high positive charge at the sides of the cylinders. However, the stability of the complexes in water improves drastically in presence of DNA, to indicate that the complexes interact with the DNA and such interaction "protects" in part the complexes from their degradation. In contrast all the Cu(I) conjugates in water are as stable as the unconjugated Cu(I) complexes. CD titrations with ct-DNA and the Fe(II) conjugates were performed. Each conjugate exhibits ability in binding the DNA, possibly in one single mode and without affecting the B-DNA conformation. CD spectroscopy is not the most suitable technique for a comparison of the DNA binding affinity between the conjugates, since the different inherent chirality of the conjugates themselves may differently influence the ICD signals. However D and L-arginine have equal and opposite CD signals so that a comparison between these two complexes could be examined. The D-Arg conjugate/ct-DNA adduct exhibits more intense ICD bands than the L-Arg conjugate/ct-DNA at the same complex concentrations. This might indicate higher

binding affinity for the D-Arg conjugate. ICD signals of D and L-Arg in presence of poly[A-T] and poly[G-C] were also analysed. The resulting ICD profiles are different in the region where the ligand absorbs and this might signify that the complexes bind differently poly[A-T] and poly[G-C]. A deeper investigation of a possible DNA binding selectivity of these two complexes with more specific techniques could be object of future investigation (see Chapter 5).

LD titrations of the Fe(II) conjugates with the ct-DNA confirmed that these complexes are able to bend/coil the DNA. The DNA coiling ability of the two serine conjugates is comparable with that observed for the Fe(II) parent cylinder. At higher complex loading any remarkable difference was observed between D and L-serine whilst at lower complex concentrations (up to 60:1) the D-Ser induces twice higher change of DNA orientation than the L-Ser cylinder. The tripeptide conjugate seems slightly less effective in coiling the DNA than the serine conjugates and the parent cylinder, indicating that the presence of a longer conjugating chain may negatively affect the binding activity of the cylinder. An increase of the induced LD signal upon increasing the complex concentration was observed for the serine and the tripeptide conjugates and this confirms that these complexes bind the DNA in an oriented fashion. The two arginine conjugates also cause remarkable DNA coiling. At high loading complexes (DNA:complex=5:1) the LD signal of the oriented DNA is completely lost. The D-Arg is more effective than the L-Arg conjugate in coiling the DNA. This would confirm the CD result and, more interestingly, the fact that the M enantiomer conformation of the triple stranded helicate, here induced by the anchored D-arginine, is more effective in DNA recognition than the P enantiomer. Surprisingly, the two arginine conjugates do not exhibit induced LD signal in the complex spectroscopy. This does not exclude that the complexes bind in the major groove (through the helicate core) in an oriented fashion as the other cylinders do. But different kind of interactions between the guanidinum groups of the arginine residues and the DNA are theoretically possible and, given the response of the LD experiments, cannot be excluded. LD titrations were also performed with the Cu(I) conjugates. All the Cu(I) complexes present DNA coiling/bending activity, although less remarkable than that exhibited by the Fe(II) complexes. This might be due to their lower positive charge. No remarkable differences between the Cu(I) conjugates were observed and only the D-Ser complex appeared slightly less effective. However,

all the conjugates exhibit lower DNA coiling properties than their unconjugated analogous. Most importantly, agarose gel electrophoresis experiments confirm that the Cu(I) conjugates retain a remarkable artificial nuclease activity, which was the main feature of the parent Cu(I) cylinders.

Polyacrylamide gel electrophoresis experiments demonstrate that all the Fe(II) conjugated complexes recognise the DNA three way junctions, so that this important characteristic of the triple stranded cylinders was not affected by the end-conjugation. The conjugates and the parent cylinder show similar ability in binding the three way junction, although the D-Arg conjugate seems to be the complex that better stabilises this structure of DNA. This would be consistent with the M conformation of the helicate core (induced by the D-arginine residues), which is known to bind more efficiently to 3WJ.

Finally, all the Fe(II) conjugates present cytotoxicity against cancer cell lines that is comparable with and, for one cell line, even higher than that observed for the parent cylinder. Also in this study the D-Arg cylinder was the most effective. Since the conjugates did not show remarkable higher DNA binding than the parent cylinder at molecular level, an improved cell uptake could be the reason of the higher cytotoxicity of the conjugates and this will be object of future investigations.

4.7 Experimental.

4.7.1 Materials.

Ultrapure water (18.2 MΩ, by Fisher) was used in all Circular and Linear dichroism experiments and for the solutions to analyse by electrophoresis gel. The ct-DNA, (highly polymerised), poly[d(G-C)$_2$] and poly[d(A-T)$_2$] were purchased from Sigma-Aldrich and they were dissolved in water without any further purification. Stock solutions of DNAs were kept frozen until the day of use. The DNA concentrations of those stocks were determined by UV-Vis measurements using the known molar-extinction coefficient of ε_{258}=6600 mol^{-1}dm^{3}cm^{-1} per DNA base for ct-DNA and poly[d(A-T)$_2$] and ε_{256}=8400 mol^{-1}dm^{3}cm^{-1} per DNA base for poly[d(G-C)$_2$]. Also stock solutions of 1M NaCl and 100 mM sodium cacodylate buffer (pH 6.8) were prepared and, together with DNA stocks, were used to obtain the final solutions to

analyse. Commercially available tris-acetate-EDTA (TAE, from Fisher) working buffer was used for gel electrophoresis of pBR322 pllasmid DNA (New England Biolabs).

4.7.2 Circular Dichroism.

Spectra were collected in cuvettes of 1 cm pathlength or 2 mm pathlength (depending on the concentration to use in a specific region of the spectrum) using a Jasco J-715 spectropolarimeter. Spectroscopic titrations were performed from which CD absorption spectra were recorded. For each titration three solutions were prepared: solution A of DNA (300 or 100 μM for Cu(I) or Fe(II) complex respectively), NaCl (20 or 10 mM for Cu(I) or Fe(II) complex respectively) and sodium cacodylate buffer (10 mM); stock solution B of complex in water (500 or 165 μM for Cu(I) or Fe(II) complex respectively); Stock solution C of DNA (600 or 300 μM for Cu(I) or Fe(II) complex respectively), NaCl (40 or 20 mM for Cu(I) or Fe(II) complex respectively) and sodium cacodylate buffer (20 mM). First solution A was recorded to have the CD spectrum of DNA without complex. Then the titration was performed decreasing the DNA:complex ratio from 60:1 to 8:1 by adding aliquots of solution B. For each volume of solution B, the same volume of solution C was added to ensure that the concentration of ct-DNA, NaCl and sodium cacodylate remained unaltered.[9]

4.7.3 Linear Dichroism.

Flow LD spectra were collected by using a flow Couette cell (Krometek) in a Jasco J-715 spectropolarimeter adapted for LD measurements. Long molecules, such as DNA can be orientated in a flow Couette cell. The flow cell consists of a fixed outer cylinder and a rotating solid quartz inner cylinder, separated by a gap of 0.5 mm, giving a total pathlength of 1 mm. The titrations performed with ct-DNA were identical to those described for the CD experiments.

4.7.4 Agarose gel electrophoresis.

The electrophoresis experiments were carried out by using gel trays of 210x150 mm with an 11-toothed comb to produce the sample wells. A Electrophoresis Power Supply-EPS 301 system was used as a constant voltage supply set to 180 V and 125 mA. The gel was prepared warming up 2 gr of agarose (from USB corporation) in 1 x Tris acetate buffer (1 x TAE, which was obtained by dilution of 100 ml of 10 x TAE, supplied by SIGMA, in 1 L of water). The same 1 x TEA buffer was used as working buffer. The solutions to analyse were prepared in 16 μl of volume containing: 96.3 μM pBR322 plasmid DNA, 25 μM hydrogen peroxide (from a fresh 250 μM stock solution) where required and different concentrations of complexes (from 50 μM stock solution in water) to obtain solution with different plasmid/complex ratio. The solutions were incubated for 1 h at 37 °C and then 4 μl of loading buffer (30% glycerol and 0.25% bromophenol blue in ultra pure water) were added. 16 μl of each solution were loaded and the samples ran for 2 h. After electrophoresis the gel was stained in 100 ml of 1 x TEA buffer containing 1 ml of ethidium bromide solution (0.5 mg ml^{-1}) for 15-20 min followed by a washing with $MgCl_2$ 100 mM for 5 min. The gel was visualized using a UVtec-uvipro platinum system.

4.7.5 Polyacrylamide gel electrophoresis.

This procedure was kindly provided by Siriporn Phongtongpasuk (from M.J. Hannon group), who performed the PAGE experiments. The formations of DNA three way junction by the complexes were probed using 15% native polyacrylamide gel electrophoresis run in TB buffer pH 8.3 comprising of 89 mM tris(hydroxymethy) amino methane, 89 mM boric acid. The oligonucleotides were purchased from MWG Eurosin, which provided the three sequences purified by PAGE. One strand of DNA (S3) was labelled with ^{32}P at 5' terminus by using T4 polynucleotide kinase (by New England BioLab) and [γ-^{32}P] adenosine 5'-triphosphate (by Perkin Elmer). The labelled strand was purified by QIA quick nucleotide removal kit. Briefly, 10 volumes of Buffer PN were added to 1 volume of the reaction sample. Then the mixture was transferred onto spin column and

centrifuged column at 6000 rpm for 1 minute. The supernatant was discarded. The column was transferred into a new elution tube and buffer PE was added (500 μl). Then discard the flow-through and repeat wash with another 500 μl of Buffer PE. The column was centrifuged again at 13,000 rpm for 1 minute to get rid of the buffer residual. The column was transferred into 1.5 ml eppendorf. Then 30 μl of milliQ water was added to the column and allowed to stand for 5 minute before centrifuged at 13,000 rpm for 2 minutes to obtain 8 μM of stock radiolabeled DNA. Stechiometric amounts of oligonucleotide were mixed with complexes to have final concentrations to load on the gel of 0.4 μM of each single strand (1.2 μM total concentration of DNA) and 0.4 μM of complex (so that the theoretical 3 way junction: complex is 1:1) in the TBN buffer containing mM tris(hydroxymethy) amino methane, 89 mM boric acid and 100 μM NaCl. The solutions were incubated at room temperature for 1 hour and followed on ice for 15 minutes. The samples were analyzed by 15% polyacrylamide gel electrophoresis for 3.50 hours at 5 W at room temperature. Then the gel was exposed on phosphor plate for an hour. The image was obtained from Molecular imager FX (Bio-Rad). The images were quantified by Quantity one.

4.7.6 Cell culture and MTT assay.

This procedure has been written in collaboration with Victoria Sadovnikova (from the Hannon group) who carried out part of the assays. DMEM medium and FBS were obtained from Invitrogen. Antibiotic antimycotic solution, L-glutamine, trypsin-EDTA, HEPES buffer solution, sodium pyruvate, MTT (3-(4,5-Dimethylthiazol-2-yl)-2,5-diphenyltetrazolium bromide) and DMSO were purchased from Sigma, UK. Tissue culture flasks, 96 well microtiter plates were obtained from Appleton Woods, UK.

Two human cell lines were used (A2780-ovarian and MDA-MB-231 – breast cancer cell lines) in assessing the cytotoxicity of the synthesized compounds. All cell lines grew as monolayers in DMEM medium supplemented with 10% FBS, 1% L-glutamine, 1% HEPES buffer, 1% sodium piruvate and 1% antibiotic. Cells were maintained in the incubator at 37 C° and humidified atmosphere and regularly checked for absence of contamination. Cells were collected from the tissue culture

flaks using 10% trypsin-PBS solution. Single cell suspensions were prepared, cells counted using cell counting chamber and placed in 96 microtiter plates at the concentration of 10.000 cells/well MDA-MB-231 and 4000 cells/well A2780 to a total volume 100μL per well. Plates were maintained at 37C° and humidified atmosphere in the incubator for 24 hours to allow cells to attach to the surface.[22] Cells were treated with 6 different concentrations of the synthesized complexes dissolved in fresh medium (200, 100, 50, 25, 12.5, 6 μM), and incubated for 72 hours.

MTT solution was prepared by dissolving yellow 3-(4,5-Dimethylthiazol-2-yl)-2,5-diphenyltetrazolium bromide (MTT) 0.25g in 50 mL of phosphate-buffered saline. The solution was stored at 4 °C in a dark place. 20 μL of MTT solution was added in each well of the 96 well plates, except 3 wells of the control. Cells were further incubated for 2 hours. The medium was carefully removed and 200 μL of DMSO was added in each well to dissolve the formed purple crystals of formazan. Absorbance was measured in 15-20 minutes after the addition of DMSO using a 96-well plate reader (BioRad) set at 590 nm.[23] All experiments were repeated at least two or three times for more accurate results.

4.8 References.

(1) Kasyanenko, N.; Afanasieva, D. *Nanomaterials for Applications in Medicine and Biology* **2008**, 29-38.
(2) Pelta, J.; Livolant, F.; Sikorav, J. L. *Journal of Biological Chemistry* **1996**, *271*, 5656-5662.
(3) Gosule, L. C.; Schellman, J. A. *Journal of Molecular Biology* **1978**, *121*, 311-326.
(4) Wilson, R. W.; Bloomfield, V. A. *Biochemistry* **1979**, *18*, 2192-2196.
(5) Widom, J.; Baldwin, R. L. *Journal of Molecular Biology* **1980**, *144*, 431-453.
(6) Ivanov, V. I.; Minchenk.Le; Schyolki.Ak; Poletaye.Ai *Biopolymers* **1973**, *12*, 89-110.
(7) Hannon, M. J.; Moreno, V.; Prieto, M. J.; Moldrheim, E.; Sletten, E.; Meistermann, I.; Isaac, C. J.; Sanders, K. J.; Rodger, A. *Angewandte Chemie-International Edition* **2001**, *40*, 880-884.
(8) Meistermann, I.; Moreno, V.; Prieto, M. J.; Moldrheim, E.; Sletten, E.; Khalid, S.; Rodger, P. M.; Peberdy, J. C.; Isaac, C. J.; Rodger, A.; Hannon, M. J. *Proceedings of the National Academy of Sciences of the United States of America* **2002**, *99*, 5069-5074.
(9) *Circular Dichroism and Linear Dichroism*; Rodger, A., Norden, B. , Ed.; Oxford University Press, 1997.

(10) Simonson, T.; Kubista, M. *Biopolymers* **1993**, *33*, 1225-1235.
(11) Rodger, A.; Marrington, R.; Geeves, M. A.; Hicks, M.; de Alwis, L.; Halsall, D. J.; Dafforn, T. R. *Physical Chemistry Chemical Physics* **2006**, *8*, 3161-3171.
(12) Childs, L. J.; Pascu, M.; Clarke, A. J.; Alcock, N. W.; Hannon, M. L. *Chemistry-a European Journal* **2004**, *10*, 4291-4300.
(13) Sigman, D. S.; Bruice, T. W.; Mazumder, A.; Sutton, C. L. *Accounts of Chemical Research* **1993**, *26*, 98-104.
(14) Pitie, M.; Donnadieu, B.; Meunier, B. *Inorganic Chemistry* **1998**, *37*, 3486-3489.
(15) Pitie, M.; Boldron, C.; Gornitzka, H.; Hemmert, C.; Donnadieu, B.; Meunier, B. *European Journal of Inorganic Chemistry* **2003**, 528-540.
(16) Childs, L. J.; Malina, J.; Rolfsnes, B. E.; Pascu, M.; Prieto, M. L.; Broome, M. L.; Rodger, P. M.; Sletten, E.; Moreno, V.; Rodger, A.; Hannon, M. J. *Chemistry-a European Journal* **2006**, *12*, 4919-4927.
(17) Cardo, L.; Hannon, M. J. *Inorganica Chimica Acta* **2009**, *362*, 784-792.
(18) Oleksi, A.; Blanco, A. G.; Boer, R.; Uson, I.; Aymami, J.; Rodger, A.; Hannon, M. J.; Coll, M. *Angewandte Chemie-International Edition* **2006**, *45*, 1227-1231.
(19) Malina, J.; Hannon, M. J.; Brabec, V. *Chemistry-a European Journal* **2007**, *13*, 3871-3877.
(20) Kadrmas, J. L.; Ravin, A. J.; Leontis, N. B. *Nucleic Acids Research* **1995**, *23*, 2212-2222.
(21) Hotze, A. C. G.; Hodges, N. J.; Hayden, R. E.; Sanchez-Cano, C.; Paines, C.; Male, N.; Tse, M. K.; Bunce, C. M.; Chipman, J. K.; Hannon, M. J. *Chemistry & Biology* **2008**, *15*, 1258-1267.
(22) Price, P.; McMillan, T. J. *Cancer Research* **1990**, *50*, 1392-1396.
(23) Mosmann, T. *Journal of Immunological Methods* **1983**, *65*, 55-63.

CHAPTER 5

CONCLUSIONS AND FUTURE WORK.

5.1 Conclusions.

The work presented in this thesis has concerned two main themes: i) the study of the behaviour of the di-nuclear Fe(II) supramolecular cylinder at different temperature conditions and in two different solvents (water and acetonitrile), and ii) the synthesis, characterisation and biological activity of cylinders conjugated to short peptides and amino acids.

The NMR, CD and UV-vis thermal experiments described in Chapter 2 demonstrate that a fluxional process occurs in the di-nuclear Fe(II) triple helicate in acetonitrile when the temperature is increased. The complex in acetonitrile is stable at high temperatures and the fluxional process is possibly related to a mechanism of intramolecular racemisation that involves the two metal centres. In other words, the increase of the temperature causes racemisation of the two metal-complex units which lose their initial configuration. The racemisation occurs most probably by Bailar twist mechanism, and it seems that the process becomes significant from ~40 °C. Since the Fe(II) cylinder binds strongly DNA and has interesting cytotoxic activity against cancer cell lines, it is currently object of different biological studies to verify the potential of this complex as an effective drug. For this reason CD and UV-vis thermal experiments were carried out also in water showing that similar racemisation effect occurs, but the complex exhibits also a concentration dependent instability in water at higher temperatures (over 70 °C). However, the binding of the complex with the DNA prevents both racemisation and part of the degradation of the M enantiomer of the cylinder, whilst this “protection” by the DNA is not so effective for the P enatiomer, confirming that the two complexes bind the DNA with different affinity and/or modality. The information rising from these studies should be useful for the planning of biological experiments with the cylinder where temperature is involved (such as PCR or incubation of the cylinder with biomolecules or after cell treatment). It should always be taken into account that M and P enantiomers are unstable and labile in water when temperature is increased, but the presence of the

DNA has a different influence on their lability and stability depending on the enantiomer with which it is interacting.

In Chapter 3 a versatile protocol for the conjugation of amino acids and short peptides at the edges of bis-pyridylimine ligand based cylinders has been established. The method allows the anchoring of 2 conjugating units at the edges of the ligands, thus the final peptide-cylinder hybrids of general formula M_2L_n bear 2n conjugated peptides. 5 Fe(II) triple stranded, 4 Cu(I) double stranded and 1 Ag(I) double stranded conjugated cylinders were synthesised and characterised. The L1 based Fe(II) triple stranded cylinders were conjugated with the tripeptide GGS and with the amino acids D and L-Arg, D and L-Ser. Their characterisation suggests that all the conjugates present a central di-Fe(II) helicate core whose NMR and UV-Vis spectroscopy is independent from the conjugated unit. Similarly, the Cu(I) conjugates (ligand L5 and L1 based) and the Ag(I) conjugate (ligand L5 based) present a central di-metal cylinder core that is not affected by the conjugating units at the edges. Interestingly, the appended peptides influence the chirality of the central helicates. For most of the complexes this influence is not easily explicable, although it seems to depend on the counter anion and/or the solvent that is used. Less ambiguous is the effect of the arginine conjugation: both NMR and CD experiments indicates that the D-Arg induces the M conformation of the central helicate, whilst the L-Arg induces the P conformation.

In Chapter 4 the DNA binding properties of the conjugates with ct-DNA were investigated by CD and LD spectroscopy. A direct comparison between the different conjugates and the corresponding unconjugated cylinders was not always possible because of the different CD profiles and the different induced CD and LD signals relative to the complexes. However all the conjugates exhibits DNA binding features comparable to those previously observed for the parent cylinder:[1] the binding occurs but it does not affect the B-DNA conformation, most probably one single binding mode occurs and all the complexes cause bending/coiling of the DNA. For the two triple stranded arginine conjugates the possibility of more binding modes cannot be excluded. In addition, all the Cu(I) complexes retain the artificial DNA nuclease activity that was previously observed for the unconjugated Cu(I) cylinder,[2] although the activity seems slightly lower.

All the Fe(II) conjugates are cytotoxic against cancer cell lines and the calculated

values of IC_{50} are comparable with and in some cases lower than those relative to the parent cylinder. In addition, the Fe(II) conjugates retain the ability to bind and stabilise the DNA three way junctions as the parent Fe(II) cylinder does. In all these studies, especially LD, gel electrophoresis and cytotoxicity tests, D and L-arginine conjugates display a difference in activity that is equivalent to that showed by the M and P enantiomers of the parent cylinder.[3,4] This suggests that a rational design of the conjugated biomolecules could affect the biological activity of the resulting conjugated cylinder by influencing its chirality.

5.2 Future work.

In this work the conjugation of cylinders with biomolecules was achieved for the first time and several features concerning the effect of the conjugation on the stability, chirality and biological activity of the conjugates were established. One of the main aims of the conjugation strategy is to verify whether the presence of amino acids and peptides can provide the cylinders with sequence selectivity binding. Preliminary CD studies of the arginine conjugates in presence of poly(dA-dT) and poly(dG-dC) suggest that a binding preference toward poly(dG-dC) might occur but the intrinsic CD signal of the complexes prevents an unambiguous interpretation of the results. *DNA footprinting*[5] is one of the most common methods to investigate the sequence specificity of DNA-binding agents, thus both the DNA binding of the Fe(II) conjugates and the possible specificity of the artificial nuclease activity of the Cu(I) conjugates should be analysed with this technique in the future. Furthermore, despite the low stability of the Fe(II) conjugates in water, they exhibits a cytotoxicity against cancer cell lines that is comparable with and in same case more efficient than that exhibited by the parent cylinder. It is possible that a better cell uptake, caused by the presence of the amino acids (especially for the arginine conjugates), is involved and a comparison between the cell uptake of the parent cylinder and its conjugates should be a topic for future studies.

The design of different end-functionalised cylinders, with different type of conjugations is currently under investigation. Using the synthetic approach described herein, Fe(II) parent cylinders bear 6 conjugating units. These units have to be designed in a way that the stability of the final hybrids is not significantly affected.

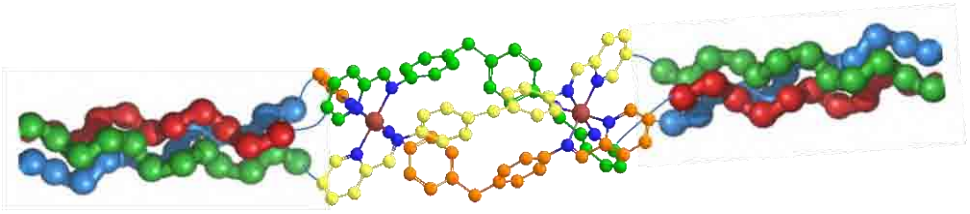

Figure 5.1 Representation of a hypothetical triple stranded cylinder conjugated to peptides triple helixes (collagen like).

A rather challenging strategy would consist in the attachment of longer peptide sequences that could interact each other at the edges of the cylinder, for example promoting the formation of peptide triple helixes or β-sheets motifs once that they are anchored (see model in Figure 5.1). This might contribute to the stabilisation of the entire hybrid and insertion of secondary structure motifs might promote the interaction with the DNA.

However, if the conjugating units do not present the right pattern of interactions, they can cause destabilisation of the structure of the final hybrids. This occurs in part with the conjugation of the arginine residues: although these complexes exhibit remarkable binding properties and cytotoxicity, they are not particularly stable, probably because the long positive charged side chains of the arginine residues are to close each other. A mono or di-conjugation (one conjugation per edge) of the cylinder, rather than the 6 conjugation achieved so far, could help to resolve issues related to the presence of inconvenient interactions between conjugating units that are anchored at the same edge of the helicate. This could be achieved by the assembly of "capping" units at the edges of the cylinder as in the model in Figure 5.2. Particularly suitable might be a tripodal structure, whose arms could be linked to the three strands of the ligands, and it should bear a further active group that allow the attachment of biomolecules or any other group with a desired function. The tripodal compound cyclotriveratrylene (CTV) showed in Figure 5.2 has already been used to promote the formation of Fe(II) based triple stranded complexes[6] and the induction of triple helixes formation of collagen peptides.[7] It presents amino groups suitable for the formation of amide bonds with the carboxylic groups at the 5 positions of the bis-pyridylimine ligands and a synthetic strategy to achieve

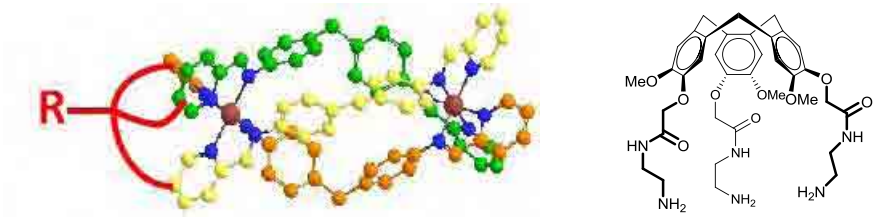

Figure 5.2 Representation of mono-capped Fe(II) cylinder (left) and the structure of cyclotriveratrylene (CTV, right)

cylinders capped with CTV units is currently under investigation.

5.2.1 Dansylcadaverine-Fe(II) cylinder conjuagate.

The studies carried out with amino acids conjugates indicated that the stability of the hybrids is not dramatically affected with the conjugation of short and neutral units anchored at the 5 position of the pyridine ring. Thus, the conjugation with other type of functionalities can be planned. Particularly, the labelling of the Fe(II) cylinder with fluorescent groups might offer the possibility of probing the agent inside cells. In this prospect, the conjugation of the Fe(II) cylinder with dansylcadaverine[8] groups has been designed and achieved via amide bond formation, using a similar synthetic approach that was used for the peptide-conjugates (Figure 5.3). All the intermediate compounds shown in Figure 5.3 and the final complex $[Fe_2(Ld)_3](BF_4)_4$ were characterised by mass spectrometry and ^1H NMR (see Appendix A). Preliminary NMR analysis of the complex in acetonitrile shows that the signals of the protons of the central helicate (the pyridine, the phenyl and the imine protons) have the same chemical shift values that were observed for the peptide-Fe(II) cylinder conjugates (see Chapter 3 and Figure 5.4.a)). In addition, the UV-Vis spectrum of $[Fe_2(Ld)_3](BF_4)_4$ in acetonitrile retains (in the visible region) the same profile of the other Fe(II) cylinder conjugates described in Chapter 3. These first data suggest that also in this case the conjugation at the position 5 of the pyridine rings of the bispyridylimine ligand does not affect the symmetry of the central helicate core, once that the dansylcadaverine-cylinder conjugate is formed. Further characterisation of the complex is currently ongoing and DNA binding studies and fluorescence experiments have to be planned in the nearest future.

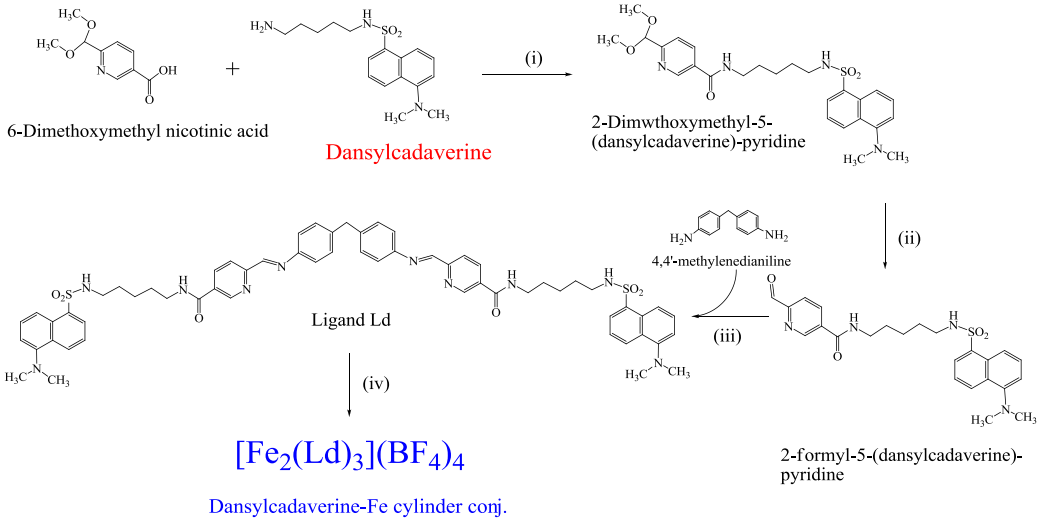

Figure 5.3 Scheme of synthesis of dansylcadaverine-Fe(II) cylinder conjugate; (i) EEDQ in MeOH, N_2 atmosphere for 3 days, (ii) 1 M HCl in THF for 3 days, (iii) overnight in EtOH, (iv) reflux in MeOH.

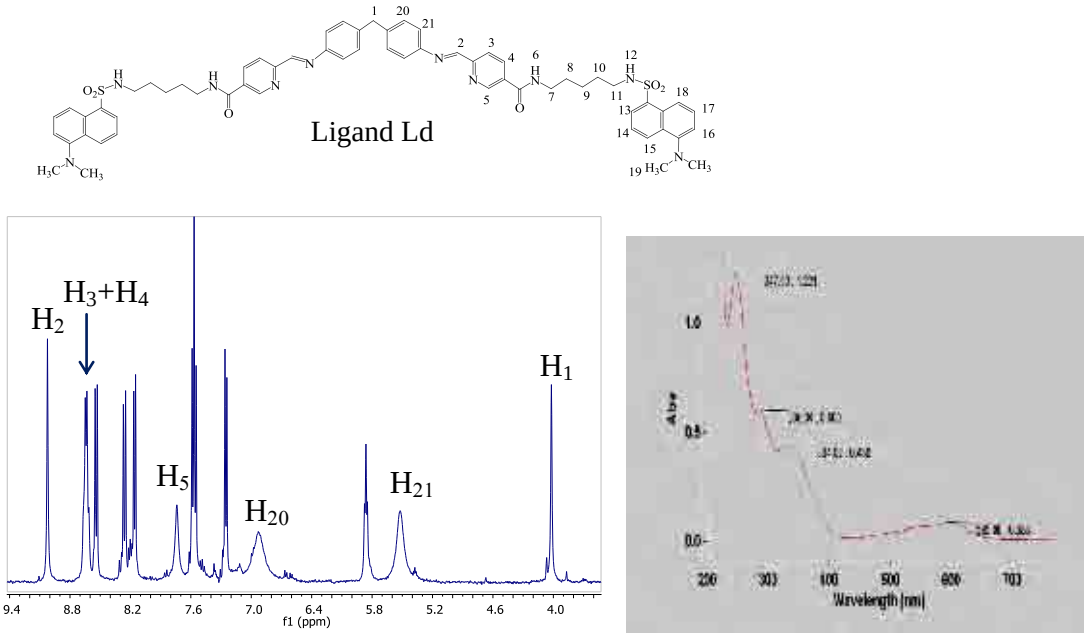

Figure 5.4.a) ^{1}H NMR of $[Fe_2(Ld)_3](BF_4)_4$ in CD_3CN (298 K). Only the signals of the central cylinder core are assigned (see section 5.3.4 and Appendix A for the complete characterisation). **b)** UV-Vis spectrum of $[Fe_2(Ld)_3](BF_4)_4$ in acetonitrile showing the characteristic MLCT and ligand bands of the central helicate core (see section 3.4 for a comparison).

5.3 Experimental

Materials and methods described in section 3.8.1 were employed also for the two syntheses below. Dansylcadaverine was purchased from Sigma-Aldrich.

5.3.1 Synthesis of 2-Dimethoxymethyl-5-(dansylcadaverine)-pyridine.

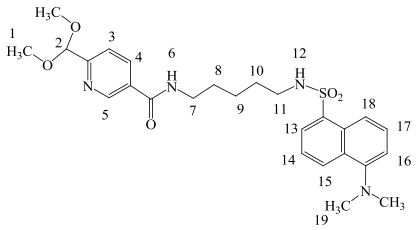

250 mg (1.2 mmol, 1) of 6-dimethoxymethyl-nicotinic acid (whose synthesis has been described in section 3.8.4 (3)) were dissolved in 15 ml of methanol together with 5 equivalents of EEDQ. 200 mg (0.6 mmol) of dansylcadaverine (previously dissolved in 3-5 ml of methanol) were added and the mixture was stirred for 3 days at room temperature and in N_2 atmosphere. The reaction was monitored by analytical RP-HPLC (from 0 to 100% of acetonitrile 0.05% TFA in H_2O 0.05% TFA in 40 min) to confirm that the dansylcadaverine was completely consumed and the crude was purified by preparative RP-HPLC (from 0 to 100% of acetonitrile 0.05% TFA in H_2O 0.05% TFA in 70 min, 22 ml/min flow) affording 108 mg of yellow pure (by analytical HPLC) compound (52% yield).

^{1}H NMR (400 MHz, MeOD, 298 K) δ 8.96 (1H, br s, H_5), 8.58 (1H, d, ^{3}J = 8.8 Hz $H_{13/14/15}$), 8.54 (1H, d, ^{3}J = 8.8, $H_{13/14/15}$), 8.34 (1H, dd, ^{3}J and ^{4}J = 8.3, 2.4 Hz, H_{4py}), 8.27 (1H, dd, ^{3}J and ^{4}J = 7.3, 1.0 Hz, H_{16}), 7.78 (1H, d, ^{3}J = 8.3 Hz, H_{3py}), 7.70 (1H, dd, ^{3}J = 7.3, 2.0 Hz, H_{17}), 7.66 (1H, dd, ^{3}J and ^{4}J = 8.8, 2.4 Hz, $H_{13/14/15}$), 7.56 (1H, d, ^{3}J = 7.3 Hz, H_{18}), 5.47 (1H, s, H_2), 3.41 (6H, s, H_1), 3.21 (2H, tr, ^{3}J = 7.3 $H_{7/11}$), 3.10 (6H, s, H_{19}), 2.89 (2H, tr, 3J = 6.8, $H_{7/11}$), 1.42 (4H, m, $H_{8/10}$). 1.24 (2H, m, H_9). ESI mass analysis m/z = 537.2 $[M+Na]^+$.

5.3.2 Synthesis of 2-formyl-5-(dansylcadaverine)-pyridine.

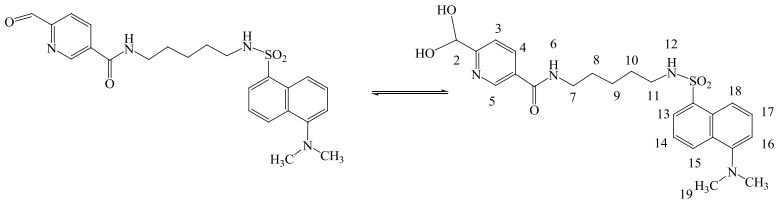

2-Dimethoxymethyl-5-(dansylcadaverine)-pyridine (0.5 mmol) was partially dissolved in 7 ml of THF and 3 ml of 1M HCl were added in 1 hour time at 0 °C. The mixture was stirred at room temperature and the reaction was monitored by analytical RP-HPLC every 18-22 h (from 0 to 100% of methanol in water in 40 min). The peak corresponding to the unprotected aldehyde (~ 2.5 min earlier than starting protected compound) appeared in the chromatogram after 24 hours, but the reaction was promoted by adding small quantities (~ 1 ml) of 1M HCl until the chromatogram showed the unprotected aldehyde as the main compound. 3 days were sufficient to have a complete reaction. The crude was purified by preparative RP-HPLC (from 0 to 100% of methanol in water in 70 min, 22 ml/min flow) obtaining pure compound with 73% yield.

^{1}H NMR (300 MHz, MeOD, 298 K) δ 8.89 (1H, d, ^{4}J = 2.2 Hz, H_{5py}), 8.53 (1H, d, ^{3}J = 8.8 Hz $H_{13/14/15}$), 8.36 (1H, d, ^{3}J = 8.8, $H_{13/14/15}$), 8.22 (1H, dd, ^{3}J and ^{4}J = 8.1, 2.2 Hz, H_{4py}), 8.19 (1H, dd, ^{3}J and ^{4}J = 7.3, 1.0 Hz, H_{16}), 7.71 (1H, d, ^{3}J = 8.1 Hz, H_{3py}), 7.56 (1H, dd, ^{3}J = 7.3, 1.1 Hz, H_{17}), overlapped 7.53 (1H, d, ^{3}J = 8.8, Hz, $H_{13/14/15}$), 7.26 (1H, d, ^{3}J = 7.3 Hz, H_{18}), 5.55 (1H, s, H_2), 3.18 (2H, m, $H_{7/11}$), 2.86 (6H, s, H_{19}), overlapped 2.83 (2H, tr, 3J = 6.8, $H_{7/11}$), 1.37 (4H, m, $H_{8/10}$). 1.22 (2H, m, H_9). ESI mass analysis m/z = 491.2 $[M+Na]^{+}$.

5.3.3 Synthesis of Ligand Ld.

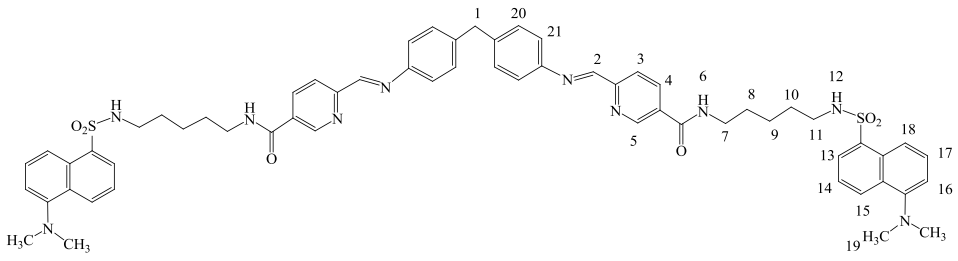

16.5 mg (0.08 mmol) of 4,4'-methylenedianiline were dissolved in 3 ml of ethanol and added drop wise (over 10 min time) to a stirring solution of 78 mg (0.16 mmol)

of 2-formyl-5-(dansylcadaverine)-pyridine in 5 ml of ethanol. Formation of yellow precipitate was immediately observed and the mixture was stirred overnight at room temperature. The yellow precipitate was collected by filtration, abundantly washed with ethanol and diethyl ether and dried under vacuum overnight, affording 58 mg of pure ligand (66% yield).

^{1}H NMR (400 MHz, d6-DMSO, 298 K) δ 9.07 (1H, d, ^{4}J = 2.4 Hz, H_{5py}), 8.68 (1H, t, ^{3}J = 5.9 Hz H_6), 8.66 (1H, s, H_2) 8.41 (1H, d, ^{3}J = 8.3 Hz, $H_{13/14/15}$), 8.32-8.28 (overlapped 1H, d, ^{3}J = 8.8, H_{4py}+ 1H, dd, ^{3}J and ^{4}J = 8.3, 2.2 Hz, H_{16}), 8.17 (1H, d, ^{4}J = 8.8 Hz, H_{3py}), 8.04 (1H, dd, ^{3}J = 8.3, 1.4 Hz, $H_{13/14/15}$), 7.83 (1H, t, ^{3}J = 5.9 Hz, H_{12}), 7.64-7.55 (2H, m, overlapped $H_{13/14/15}$+H_{17}), 7.31 (4H, s, $H_{20/21}$), 7.19 (1H, d, ^{3}J = 7.3 Hz, H_{18}), 3.98 (1H, s, H_1), 3.09 (2H, m, H_7), 2.77-2.75 (overlapped 6H, s, H_{19} + 2H, tr, ^{3}J = 6.8, H_{11}), 1.34 (4H, m, $H_{8/10}$). 1.17 (2H, m, H_9). ESI mass analysis m/z = 1121.7 $[M+Na]^+$.

5.3.4 Synthesis of dansylcadaverine-cylinder complex $[Fe_2(Ld)_3](BF_4)_4$.

32 mg (0.03 mmol) of Ligand Ld and 7 mg of $Fe(BF_4)_2$ were dissolved in 5 ml of methanol in N_2 atmosphere. Dark blue precipitate was observed within the first 5 min of reaction. The mixture was stirred (in N_2 atmosphere) in reflux for the first hour and at room temperature over night. The blue precipitate was collected by filtration, abundantly washed with methanol, ethanol and ether and dried overnight, affording 24 mg of pure complex (65% yield).

^{1}H NMR (400 MHz, CD_3CN, 298 K) δ 9.02 (1H, d, ^{4}J = 2.4 Hz, H_2), 8.63 (2H, overlapped H_{3py} + H_{4py}, ^{3}J = 8.0 Hz), 8.53 (1H, d, ^{3}J = 8.3 Hz, $H_{13/14/15}$), 8.27 (1H, d, ^{3}J = 7.3, H_{16}), 8.17 (1H, d, ^{4}J = 8.3 Hz, $H_{13/14/15}$), 7.74 (1H, br s, H_{5py}), 7.57 (2H, m, overlapped $H_{13/14/15}$+H_{17}), 7.24 (4H, d, ^{3}J = 7.5 Hz, H_{18}), 6.93 (1H, br, H_{20}), 5.86 (1H, t, ^{3}J = 7.3 Hz, H_{12}), 5.52 (1H, br, H_{21}), 4.02 (1H, s, H_1), 3.14 (2H, br m, H_7), 2.86 (6H, s, H_{19}), 2.78 (2H, br m, H_{11}), 1.33 (4H, m, $H_{8/10}$). 1.14 (2H, m, H_9). ESI mass analysis m/z = 852.2 $[Fe_2(Ld)_3]^{4+}$, 1165.3 $[Fe_2(Ld)_3(BF_4)]^{3+}$. UV-Vis (acetonitrile) λ_{max}(nm) = 595 (with a shoulder at 540), 334, 286, 247.

5.4 References.

(1) Hannon, M. J.; Moreno, V.; Prieto, M. J.; Moldrheim, E.; Sletten, E.; Meistermann, I.; Isaac, C. J.; Sanders, K. J.; Rodger, A. *Angewandte Chemie-International Edition* **2001**, *40*, 880-884.

(2) Childs, L. J.; Malina, J.; Rolfsnes, B. E.; Pascu, M.; Prieto, M. L.; Broome, M. L.; Rodger, P. M.; Sletten, E.; Moreno, V.; Rodger, A.; Hannon, M. J. *Chemistry-a European Journal* **2006**, *12*, 4919-4927.

(3) Meistermann, I.; Moreno, V.; Prieto, M. J.; Moldrheim, E.; Sletten, E.; Khalid, S.; Rodger, P. M.; Peberdy, J. C.; Isaac, C. J.; Rodger, A.; Hannon, M. J. *Proceedings of the National Academy of Sciences of the United States of America* **2002**, *99*, 5069-5074.

(4) Malina, J.; Hannon, M. J.; Brabec, V. *Nucleic Acids Research* **2008**, *36*, 3630-3638.

(5) Hampshire, A. J. R., D.A.; Broughton-Head, V.J.; Fox, K.R. *Methods* **2007**, *42*, 128-140.

(6) Veriot, G.; Dutasta, J. P.; Matouzenko, G.; Collet, A. *Tetrahedron* **1995**, *51*, 389-400.

(7) Rump, E. T.; Rijkers, D. T. S.; Hilbers, H. W.; de Groot, P. G.; Liskamp, R. M. J. *Chemistry-a European Journal* **2002**, *8*, 4613-4621.

(8) Kvedar, J. C.; Pion, I. A.; Bilodeau, E. B.; Baden, H. P.; Greco, M. A. *Biochemistry* **1992**, *31*, 49-56.

APPENDIX A

^{1}H-NMR spectra and 2D-COSY.

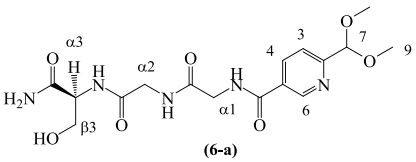

(6-a)

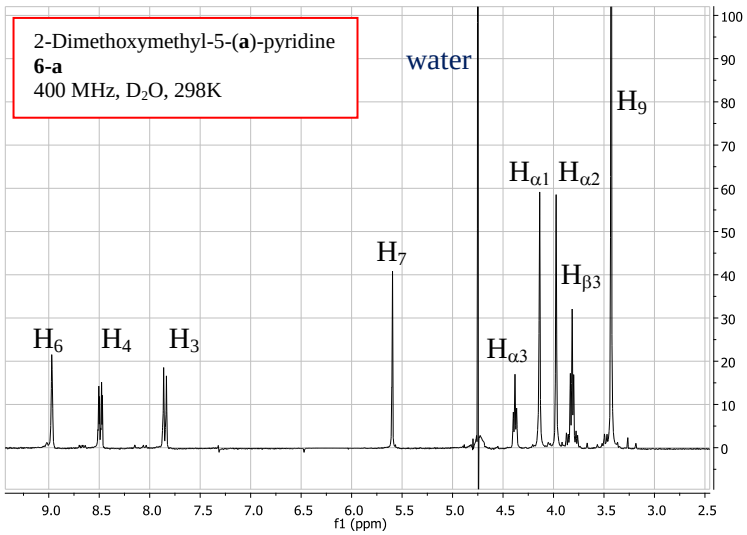

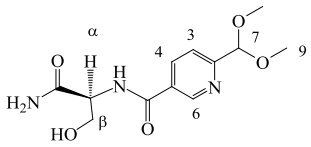

(6-b)

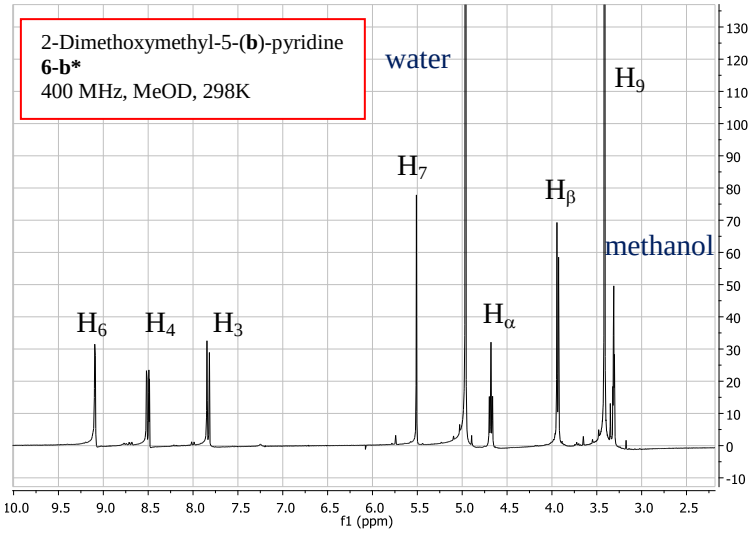

*Note: ^{1}H NMR spectrum of 2-Dimethoxymethyl-5-(**c**)-pyridine (compound **6-c**) is identical to the spectrum of **6-b**.

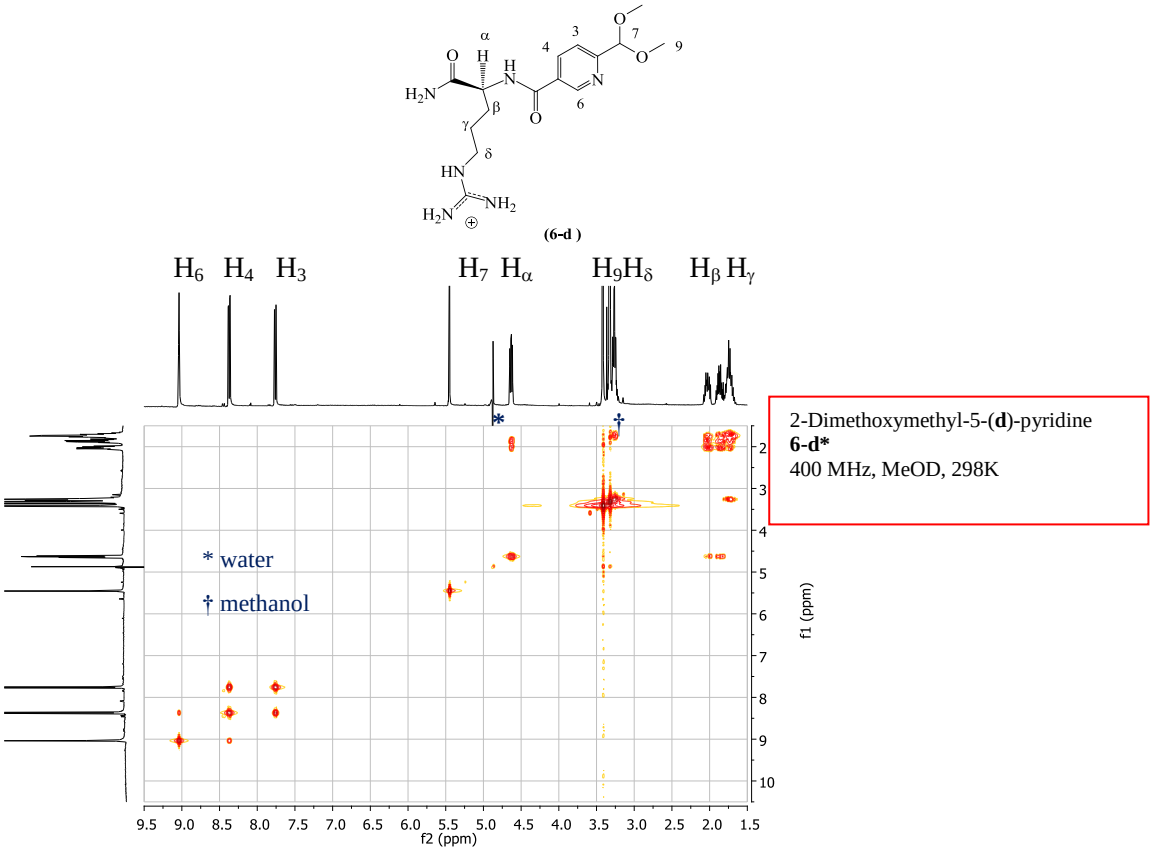

*Note: ^{1}H NMR spectrum of 2-Dimethoxymethyl-5-(**e**)-pyridine (compound **6-e**) is identical to the spectrum of **6-d**.

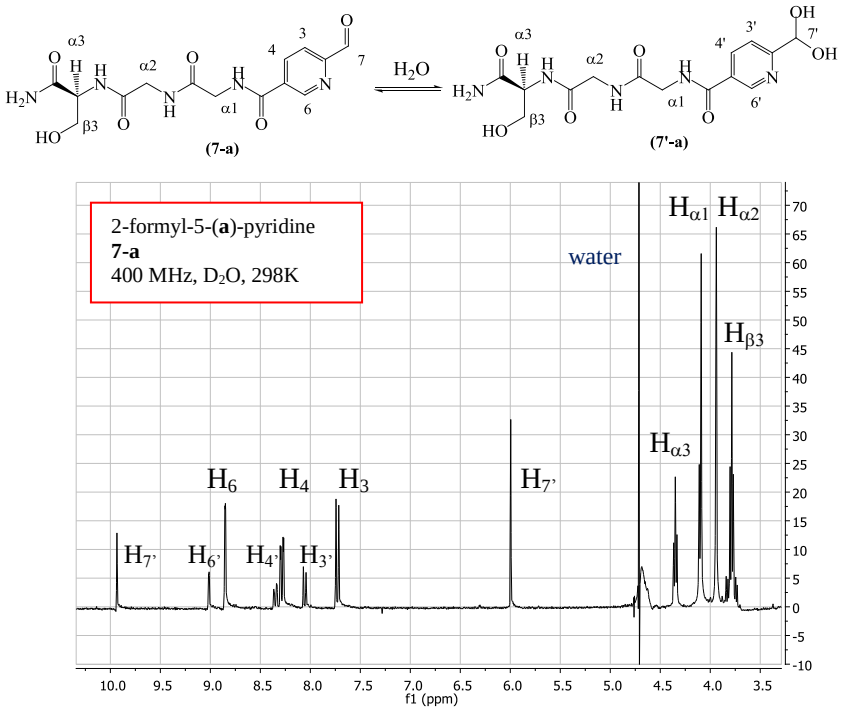

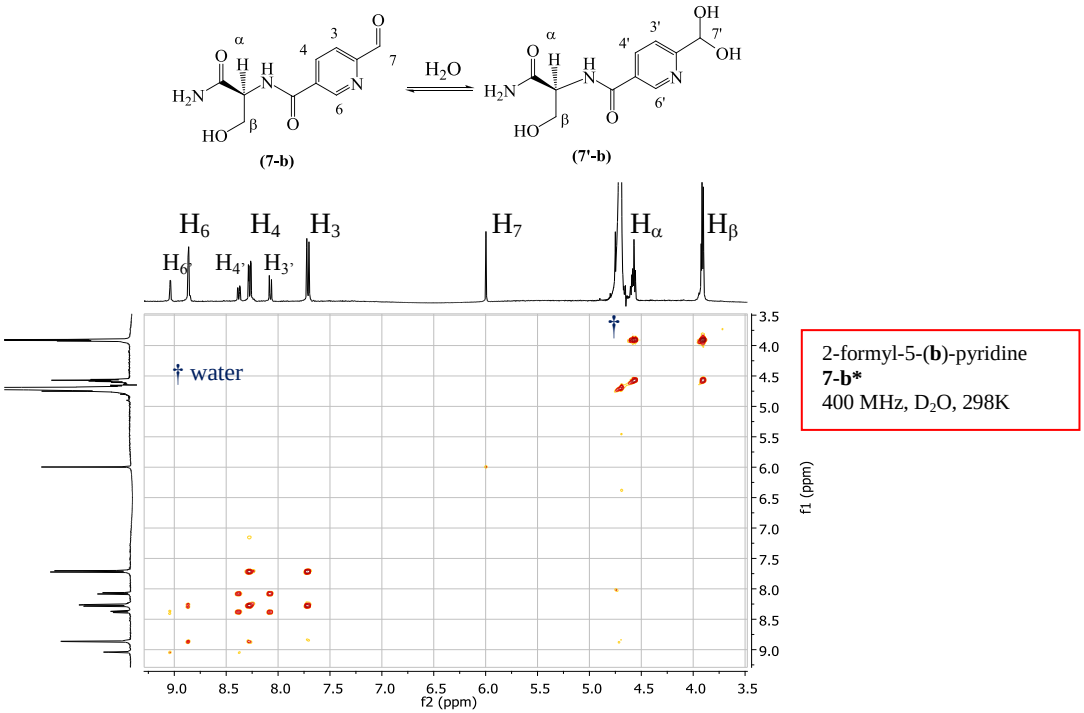

*Note: ^{1}H NMR spectrum of 2-formyl-5-(**c**)-pyridine (compound **7-c**) is identical to the spectrum of **7-b**.

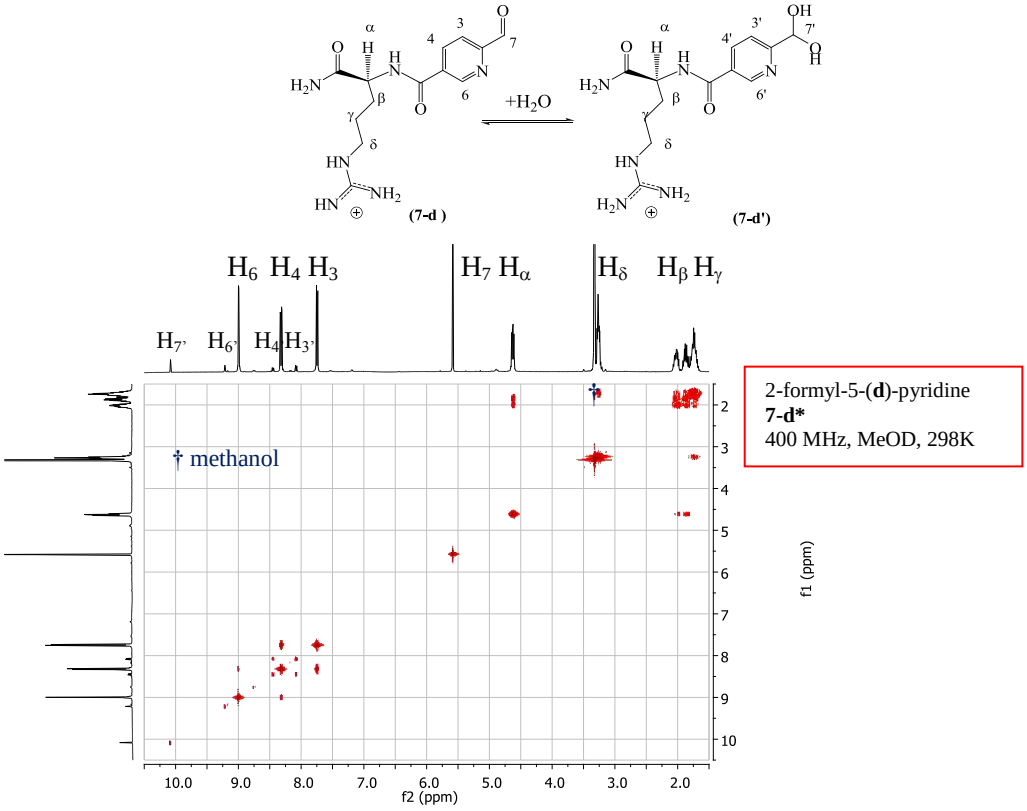

*Note: ^{1}H NMR spectrum of 2-formyl-5-(**e**)-pyridine (compound **7-e**) is identical to the spectrum of **7-d**.

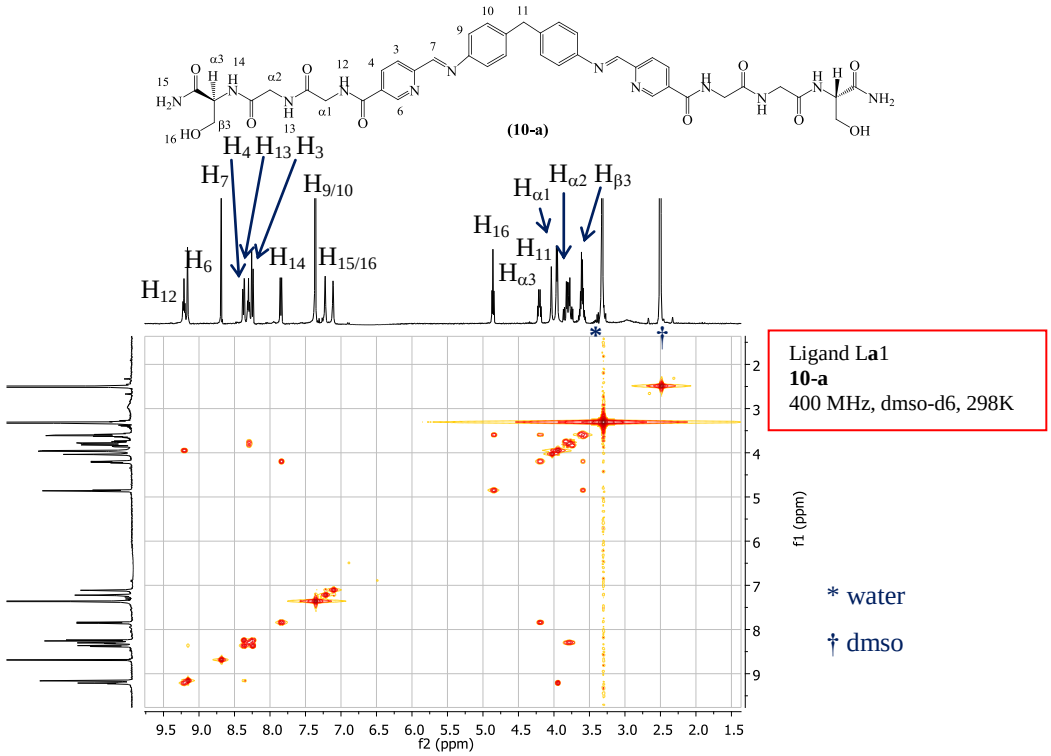

Ligand L**a**1
10-a
400 MHz, dmso-d6, 298K

* water

† dmso

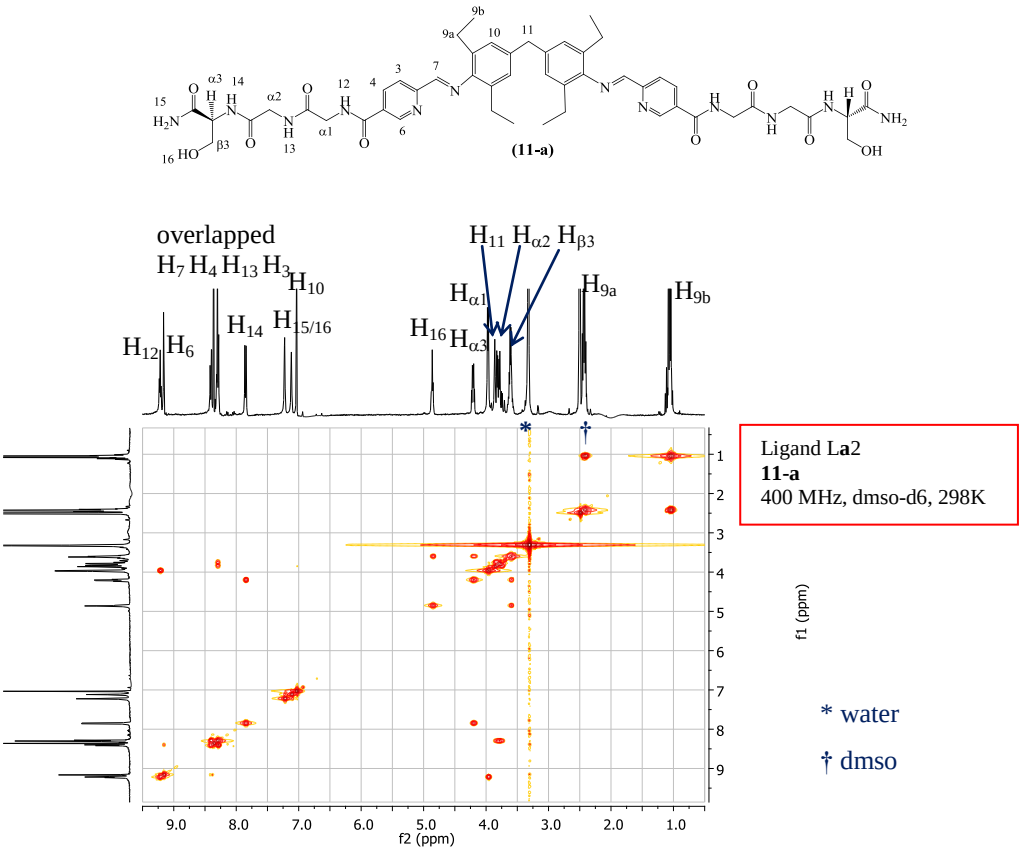

Ligand L**a**2
11-a
400 MHz, dmso-d6, 298K

* water

† dmso

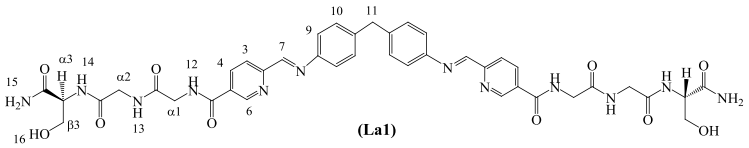

(La1)

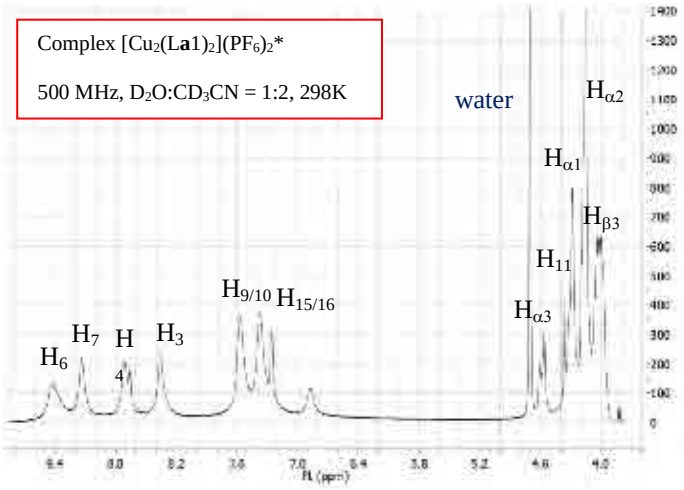

*Note: small paramagnetic impurities, most probably due to the presence of traces of Cu(II), might be the cause of the broadness of the signals. For this reason a 2D-COSY spectrum could not be registered for this complex and peaks were assigned upon comparison with the signals of the Ag(I) analogous complex ($[Ag_2(La1)_2](PF_6)_2$, see 2D-COSY spectrum below)

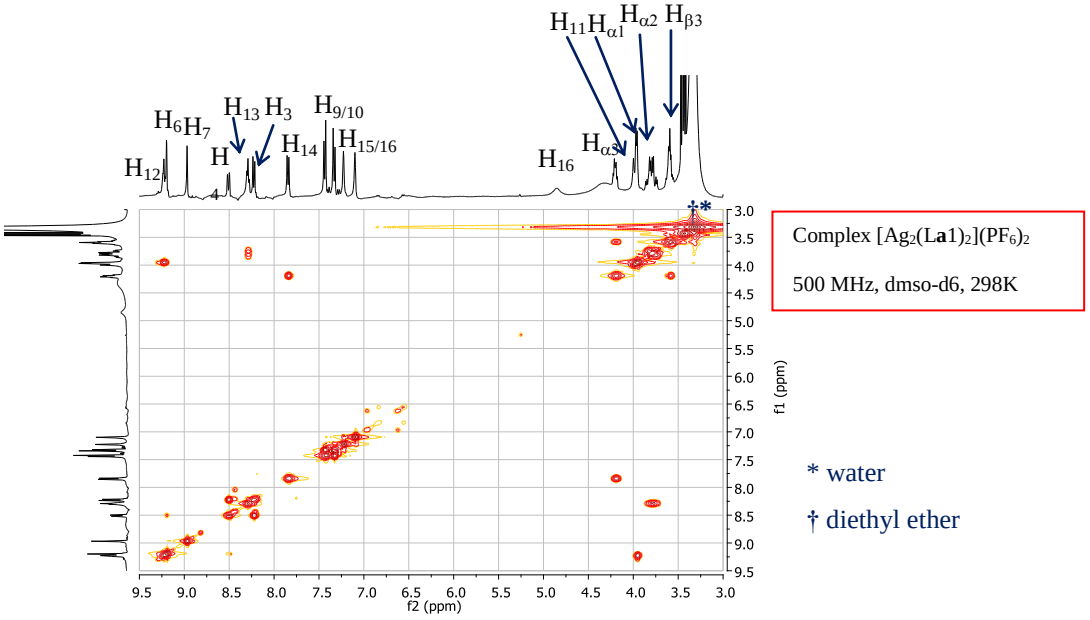

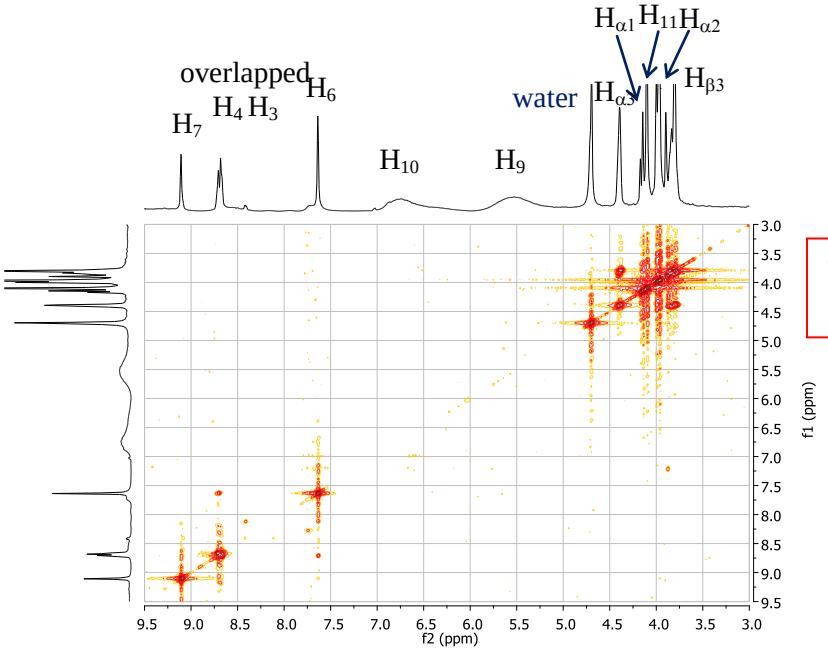

Complex $[Fe_2(L\mathbf{a}1)_3](Cl)_4$

500 MHz, D_2O, 298K

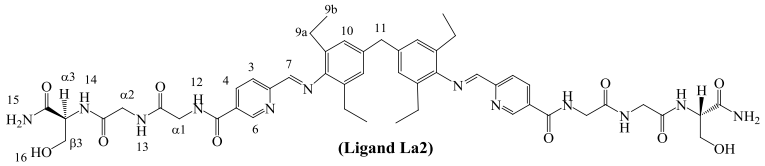

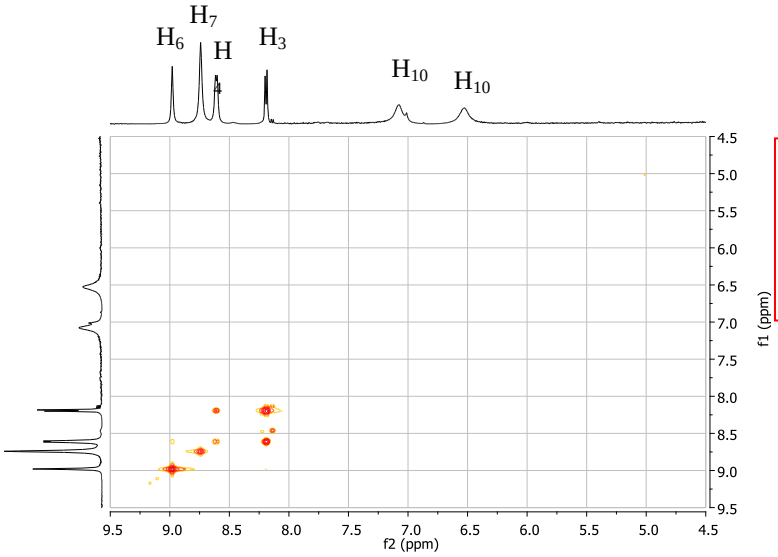

Complex $[Cu_2(L\mathbf{a}2)_2](PF_6)_2$

500 MHz, D_2O:CD_3CN = 1:3, 298K

<u>Downfield enlargement</u>

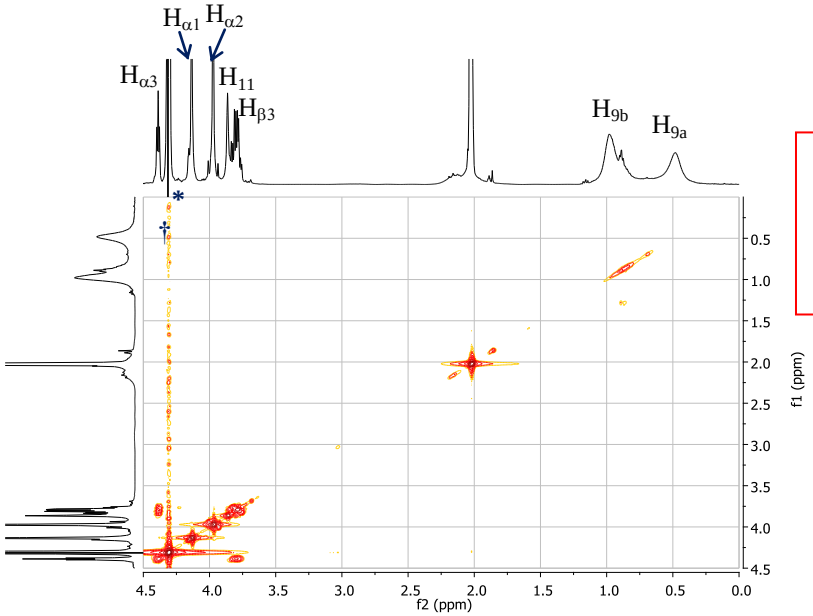

Complex $[Cu_2(La2)_2](PF_6)_2$

500 MHz, D_2O:CD_3CN = 1:3, 298K

Upfield enlargement

* water

† acetonitrile

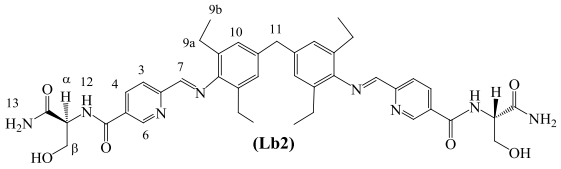

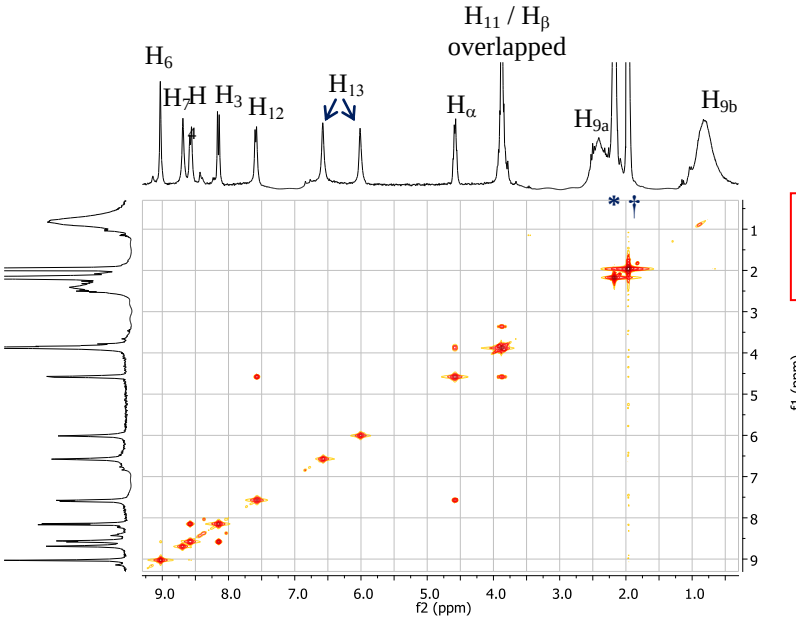

Complex $[Cu_2(Lb2)_2](PF_6)_2$

500 MHz, CD_3CN, 298K

* water

† acetonitrile

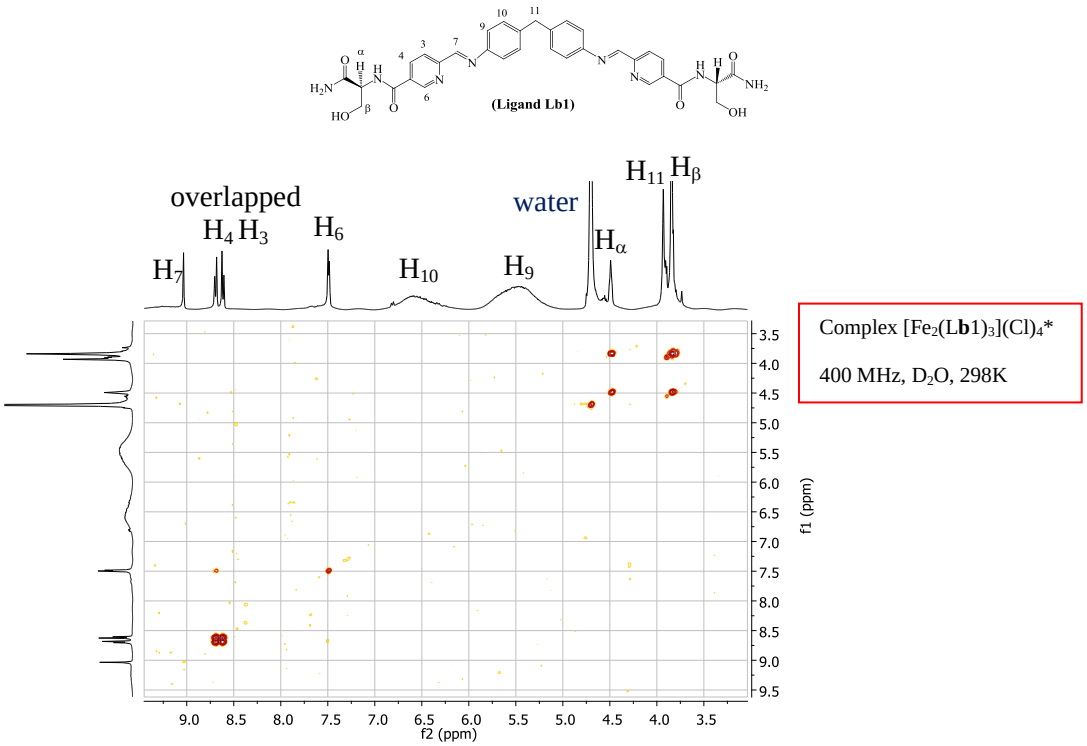

Complex $[Fe_2(L\mathbf{b}1)_3](Cl)_4$*

400 MHz, D_2O, 298K

*Note: ^1H NMR spectrum of complex $[Fe_2(L\mathbf{c}1)_3](Cl)_4$ (the analogous D-Ser conjugated cylinder) is identical to the spectrum of $[Fe_2(L\mathbf{b}1)_3](Cl)_4$ above.

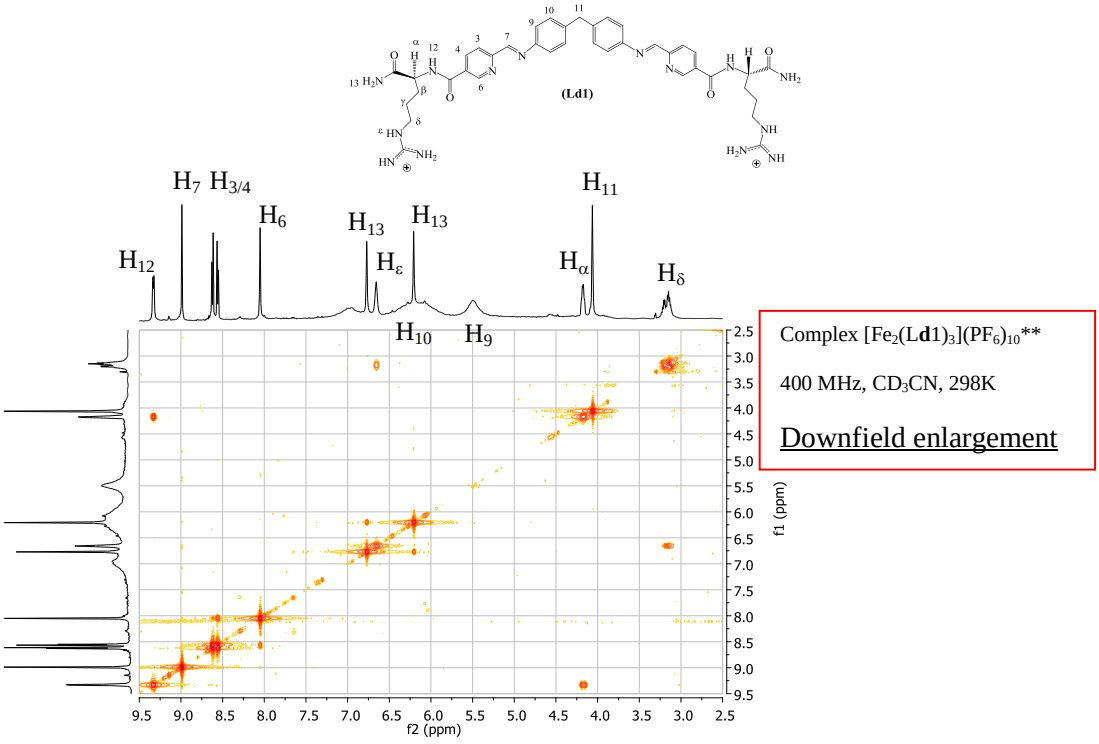

Complex $[Fe_2(L\mathbf{d}1)_3](PF_6)_{10}$**

400 MHz, CD_3CN, 298K

Downfield enlargement

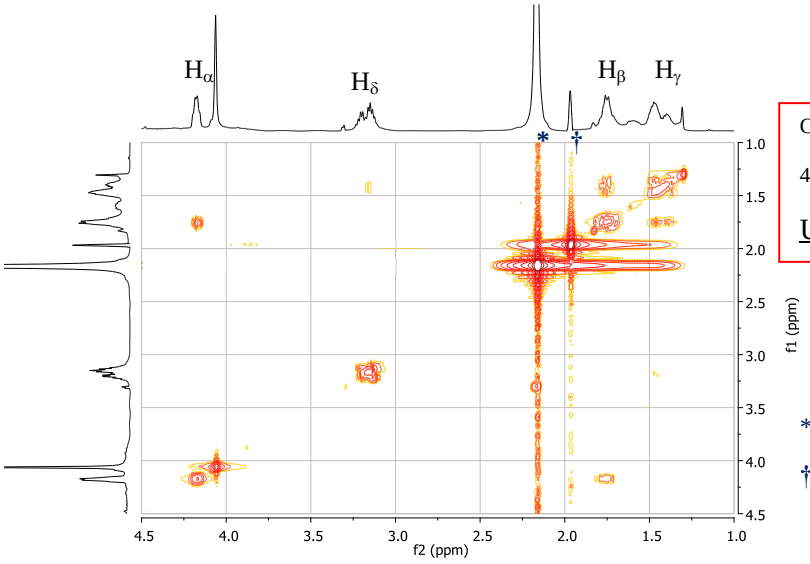

Complex $[Fe_2(L\mathbf{d}1)_3](PF_6)_{10}$**

400 MHz, CD_3CN, 298K

Upfield enlargement

* water

† acetonitrile

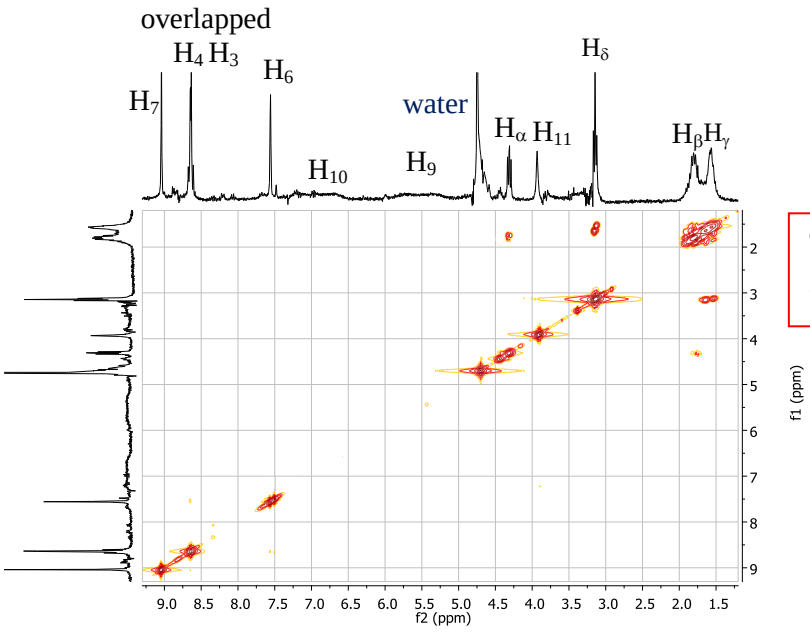

Complex $[Fe_2(L\mathbf{d}1)_3](Cl)_{10}$**

500 MHz, D_2O, 298K

**Note: ^{1}H NMR spectra of complex $[Fe_2(L\mathbf{e}1)_3]^{10+}$ (the analogous D-Arg conjugated cylinder), both in CD_3CN and D_2O, are identical to the spectra of $[Fe_2(L\mathbf{d}1)_3]^{10+}$ above.

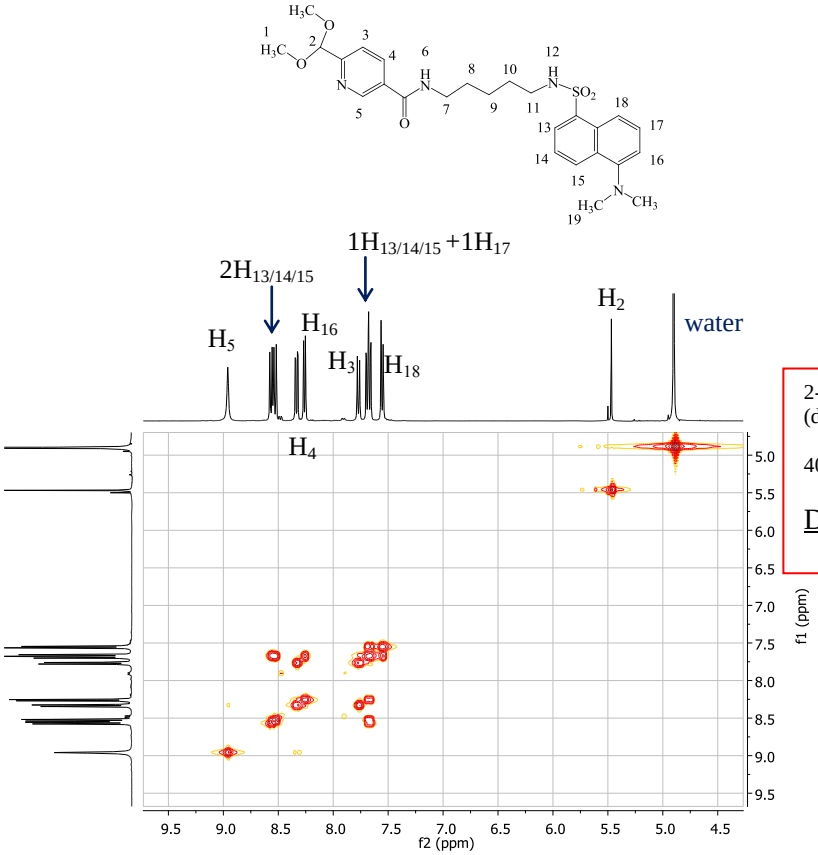

2-Dimethoxymethyl-5-(dansylcadaverine)-pyridine

400 MHz, MeOD, 298K

Downfield enlargement

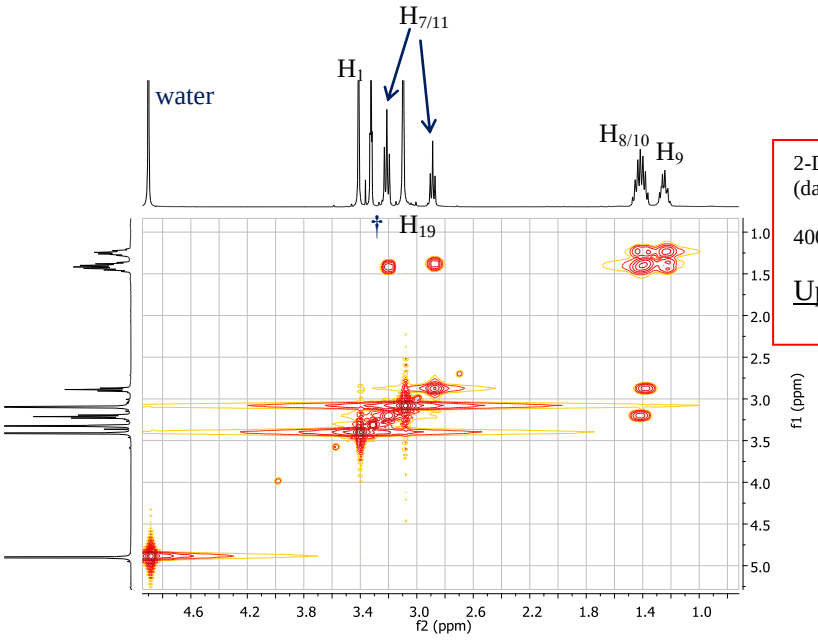

2-Dimethoxymethyl-5-(dansylcadaverine)-pyridine

400 MHz, MeOD, 298K

Upfield enlargement

† methanol

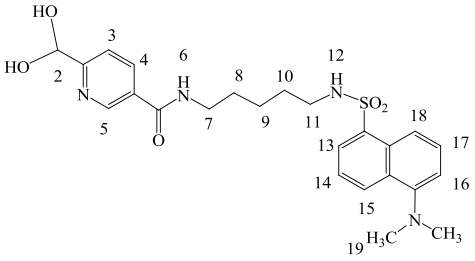

2-formyl-5-(dansylcadaverine)-pyridine

300 MHz, MeOD, 298K

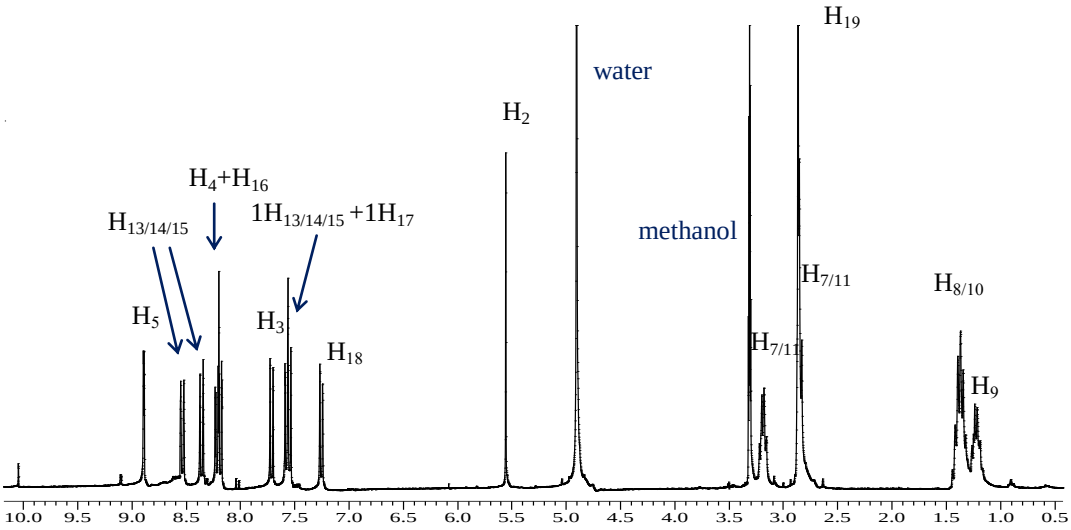

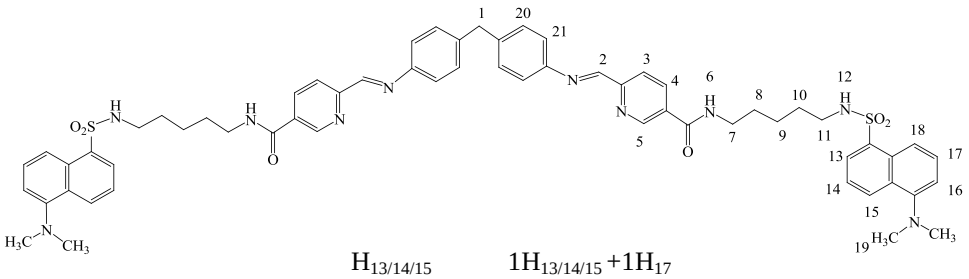

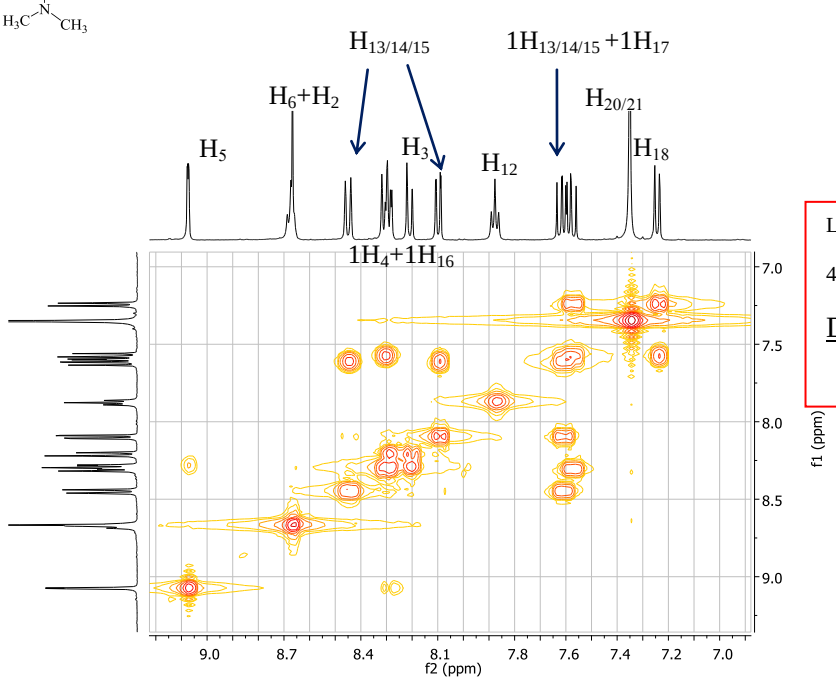

Ligand Ld

400 MHz, d6-dmso, 298K

Downfield enlargement

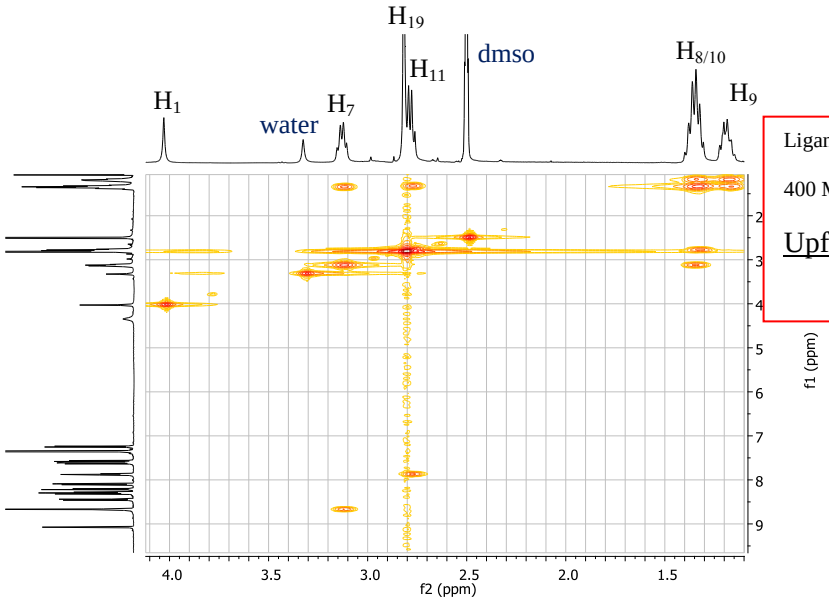

Ligand Ld

400 MHz, d6-dmso, 298K

Upfield enlargement

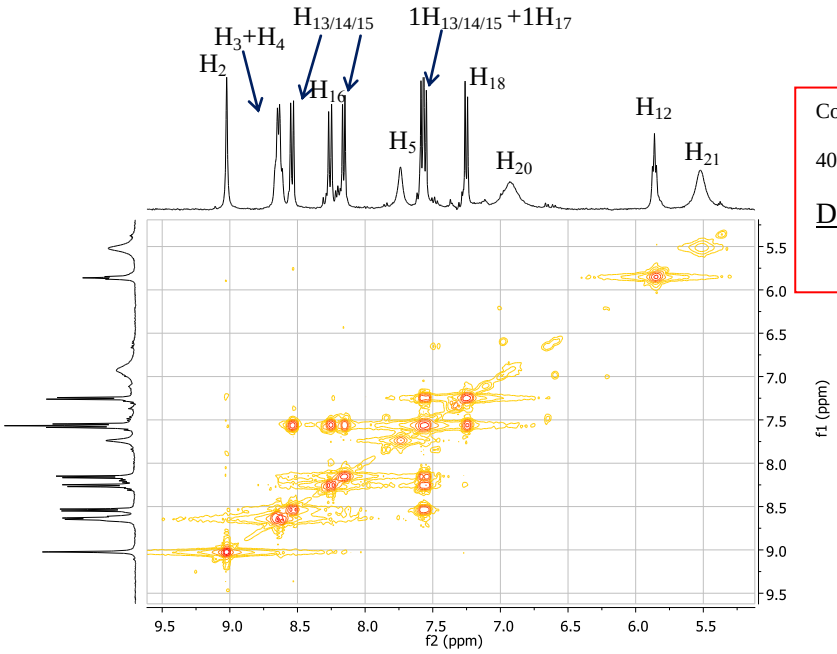

Complex $[Fe_2(Ld)_3](BF_4)_4$

400 MHz, CD_3CN, 298K

Downfield enlargement

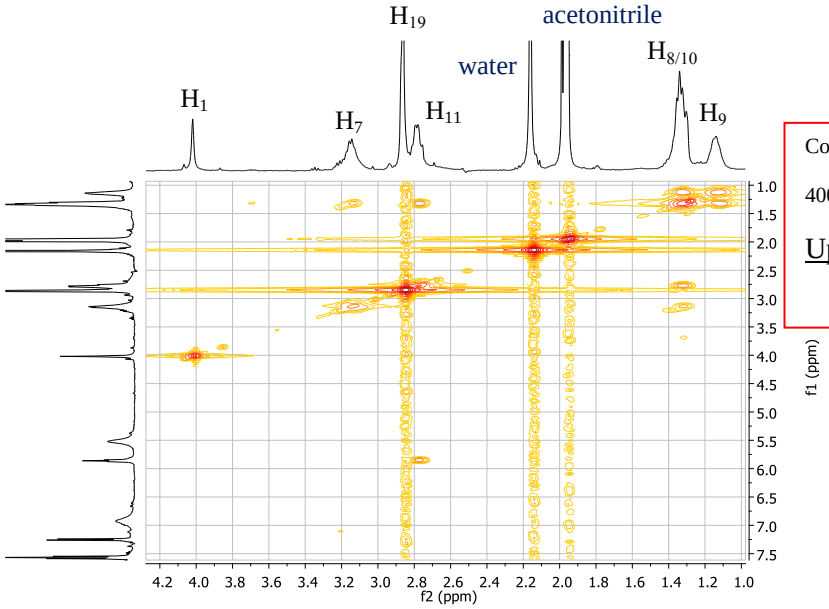

Complex $[Fe_2(Ld)_3](BF_4)_4$

400 MHz, CD_3CN, 298K

Upfield enlargement